FACULTY
OF
ELECTRICAL ENGINEERING

DOCTORAL THESIS

PILSEN, 2013   Ing. Jan Veleba

Faculty of Electrical Engineering

DOCTORAL THESIS

for achieving academic title 'Doctor' (Ph.D.) in the field of

Electric Power Engineering

Ing. Jan Veleba

Steady State Solution of Electric Power Systems with Accent on Fault Modelling

Supervisor: doc. Ing. Karel Noháč, Ph.D.
Date of state doctoral examination: 20.12.2010
Date of doctoral thesis submission: 31.5.2013

In Pilsen, 2013

Abstract: This thesis deals with steady-state load flow analysis of electric power systems. The problem is further combined with specialized procedures for maintaining numerical stability and high calculation speed of traditional load flow techniques (Gauss, Gauss-Seidel, Newton-Raphson, Fast-Decoupled, DC load flow), with robust codes for modelling on-load tap-changing (OLTC) transformers and with advanced approaches for evaluating steady-state voltage stability of electric power systems. With increasing system loadings, large numbers of uncontrollable renewable power sources being connected and deregulated market policies applied, the three above introduced topics seem to be of the highest priority nowadays. In this thesis, new methodologies are suggested for controlling voltage/reactive-power/active-power conditions using OLTC transformers and for evaluating reasonable voltage stability margins in distribution power systems. A specialized author-developed software tool in MATLAB environment is also designed and used for performing high number of practical studies related to presented areas of interest. For verification purposes, online optimization tool NEOS Server, free version of PowerWorld Simulator and free-to-use Power System Analysis Toolbox are applied to all performed case studies.

Keywords: Load flow analysis, bus admittance matrix, Gauss/Gauss-Seidel/Newton-Raphson/Fast-Decoupled/DC load flow method, on-load tap-changing transformers, voltage stability margin, shortest distance to voltage instability, continuation load flow analysis, predictor-corrector method, NEOS Server for Optimization, Power System Analysis Toolbox.

Anotace: Tato disertační práce se zabývá řešením ustáleného chodu elektrizačních soustav. Tato problematika je dále propojena se speciálními procedurami pro zajištění numerické stability a vysoké výpočtové rychlosti tradičních numerických metod (Gauss, Gauss-Seidel, Newton-Raphson, Fast-Decoupled, DC), s robustními kódy pro modelování transformátorů s přepínači odboček pod zatížením a s vyspělými technikami pro vyhodnocení napěťové stability elektrizačních soustav v ustáleném stavu. S rostoucím zatěžováním soustav, instalací velkého počtu neřiditelných obnovitelných zdrojů a zaváděním deregulovaných tržních principů se dnes stávají tato tři témata disertační práce obzvláště důležitými. V této práci jsou navrženy nové metodiky pro řízení napěťových poměrů a jalových/činných výkonů s použitím regulačních transformátorů a pro přesnější vyhodnocení rezervy napěťové stability v distribučních soustavách. Autorem byl také vytvořen specializovaný softwarový nástroj v prostředí MATLABu, s jehož pomocí byl proveden velký počet praktických případových studií týkajících se představené oblasti zkoumání. Pro ověření správnosti výsledků byl v případových studiích rovněž použit online optimalizační nástroj NEOS Server, volná verze programu PowerWorld Simulator a zdarma software Power System Analysis Toolbox.

Klíčová slova: Řešení chodu soustavy, admitanční matice, Gauss/Gauss-Seidelova/Newton-Raphsonova/Fast-Decoupled/DC metoda, regulační transformátory, rezerva napěťové stability, nejkratší vzdálenost do black-outu, continuation load flow analýza, prediktor-korektor metoda, NEOS Server for Optimization, Power System Analysis Toolbox.

Annotation: Diese Dissertation beschäftigt sich mit der Stabilitätsberechnung von elektrischen Netzen. Diese Problematik ist eng mit speziellen Prozeduren für Erhöhung der numerischen Stabilität, hoher Rechengeschwindigkeit der traditionellen numerischen Methoden (Gauss, Gauss-Seidel, Newton-Raphson, Fast-Decoupled, DC), mit robusten Algorithmen für das Modellieren von Transformatoren mit Stufenschaltern sowie mit hochentwickelten Techniken zur Auswertung der Spannungsstabilität in elektrischen Netzen verbunden. Die Lösung dieser derzeit sehr aktuellen Probleme gewinnt an Bedeutung, da die elektrischen Netze mit wachsender Belastung, massiven Installationen erneuerbarer Energiequellen und der Anwendung der deregulierten Marktprinzipen konfrontiert sind. In der vorliegenden Dissertation werden neue Regelungmethodiken für elektrischen Spannungen und Leistungen mittels der Regeltransformatoren und für die exakte Auswertung der Stabilitätsreserve in den Distributionsnetzen vorgeschlagen. Dazu wurde eine spezialisierte Software in MATLAB entwickelt, die auch für weitere praktische Aufgabenstellungen benutzt werden kann. Zur Resultätsverifizierung wurden verschiedene verfügbare Recheninstrumente benutzt - online Optimierungssoftware NEOS Server, Schulversion des Programs PowerWorld Simulator und Simulink-basierte Paket Power System Analysis Toolbox.

Keywords: Berechnung der Stabilität elektrischer Netze, Admittanzmatrix, Gauss/Gauss-Seidel/Newton-Raphson/Fast-Decoupled/DC Methode, Regeltransformatoren, Stabilitäts-reserve, die kürzeste Distanz zur Instabilität, Continuation Load Flow Analyse, Prediktor-Korrektor Methode, NEOS Server for Optimization, Power System Analysis Toolbox.

FOREWORD

This doctoral thesis was created during my Ph.D. study at the Department of Electric Power Engineering and Environmental Engineering, Faculty of Electrical Engineering, University of West Bohemia in Pilsen, Czech Republic.

The reasons for writing this thesis were to handle the problems related to present trends in power system operation and control. Due to increasing network loading, large installations of renewable power sources and deregulated market policies, abnormal network conditions may arise. Faults, such as under-/over-voltage scenarios and voltage instabilities, may occur and become a serious threat to power system operability. Moreover, numerical convergence of standard load flow methods can be significantly worsened in case of highly loaded networks.

First, the aim of this thesis was to develop reliable techniques for stabilizing and/or accelerating the load flow analysis in terms of iteration numbers and CPU times. Second, the focus was placed on developments of methodologies for controlling voltage/power conditions in the networks using on-load tap-changing transformers and other voltage-var devices. Third, the emphasis was put on developing methods for the evaluation of voltage stability margin of a system along with location of its weakest buses/branches/areas in terms of voltage stability and design of effective strategies for voltage stability improvement. Finally, the conclusions of this work should provide helpful directions for innovative power system control mechanisms when connected with Smart Grid concept, Smart Metering and Wide Area Measurement System technology.

This doctoral thesis was composed as a theoretical work with broad range of practical case studies performed by using the author-developed software tool and other professional or freeware programs. I honestly declare that this doctoral thesis was written in accord with common concepts for academic works. Author-developed software tool is subject to intellectual property and proprietary/author rights.

I would like to acknowledge doc. Ing. Karel Noháč, Ph.D. as my supervisor for his critical view to improve my doctoral thesis not only in technical but also in written and

formal way. Also, I appreciate technical background (hardware, software licences) and the possibilities for further personal development provided and offered by the Department.

I would like to acknowledge doc. Ing. Miloslava Tesařová, Ph.D., prof. dr. Ing. Rainer Haller, DrSc. and prof. doc. Ing. Jan Mühlbacher, CSc. for many useful advices, hints and guidance related to my dissertation topic.

Moreover, I would like to thank Prof. Malcolm Irving and Dr. Gary Taylor from Brunel Institute of Power Systems, Brunel University of West London, UK for their substantial support and the opportunity of visiting their lectures, tutorials and other discussions and meetings during my 10-month research stay at Brunel University in 2008-09.

Furthermore, I would admire to thank to excellent professionals and specialists in the field, namely to Ing. Miloslava Chladová, CSc., RNDr. Bohumil Sadecký, CSc., Ing. Ladislav Haňka (ČEPS, a.s.), to Ing. Richard Habrych, Ph.D. and Ing. Gabriela Jarolímková (EGÚ PRAHA Engineering, a.s.), to Ing. Petr Neuman, CSc. (NEUREG, s.r.o.) and to Maciej Fila MEng, MIET (Fundamentals Ltd, UK) for many useful highly-skilled ideas to the topic.

Many thanks also to my colleagues during the studies, namely to Ing. Jaroslav Bublík, Ing. Zaidan Mohamed Buhawa, Ph.D., Ing. Luboš Frank, Ing. Miroslav Hromádka, Ph.D., Ing. Petr Jindra, Ing. Veronika Královcová, Ing. Oldřich Kroupa, Ing. Aleš Krutina, Ing. Adam Kysela, Ing. Jana Liďáková, Ing. Viktor Majer, Ing. Lenka Raková, Ing. Jiří Polívka, Ing. František Rajský, Ph.D., Ing. David Rieger, Ing. Bc. Vladislav Síťař, Ing. Miroslav Šafařík, Ing. Vlastimil Šantín, Ph.D., Ing. Jaroslav Šnajdr and Ing. Josef Vaněk for maintaining a very friendly environment for academic and research activities at the Department.

Finally, many thanks to my sister Štěpánka and my parents for support and understanding during my study at the University.

In Pilsen, on 7th June 2013   Ing. Jan Veleba

Table of contents:

List of illustrations and tables:

List of employed abbreviations:

CLF	Continuation Load Flow
CP	Continuation Parameter
DC	Direct Current
F-D	Fast-Decoupled
G	Gauss
GUI	Graphic User Interface
G-S	Gauss-Seidel
NEOS	Network-Enabled Optimization System
N-R	Newton-Raphson
OLTC	On-Load Tap-Changing
OPF	Optimal Power Flow
OSFD	One-Shot Fast-Decoupled
OSGS	One-Shot Gauss-Seidel
PSAT	Power System Analysis Toolbox
SDVI	Shortest Distance to Voltage Instability
SimEPS	Steady-State Simulations of Electric Power Systems
STATCOM	Static Synchronous Compensator
SUT	State Update Truncation
SVC	Static Var Compensator
VSF	Voltage Sensitivity Factor
VSMI	Voltage Stability Margin Index

List of employed symbols:

$\bar{I}_i$, $\bar{V}_i$, $\bar{V}_{fi}$	phasor of injected current and of line-to-line/phase voltage in bus i
V_i, θ_i	voltage magnitude and phase angle in bus i
P_i, Q_i, $\bar{S}_i$	injected active/reactive/complex power in bus i
$\bar{V}_i^*$, $\bar{I}_i^*$, $\bar{S}_i^*$	complex conjugate bus voltage and injected current/power in bus i
$\underline{V}$, $\underline{I}$	column vectors of bus line-to-line voltages and injected currents
θ_{ik}	angular displacement between network buses i and k
$\underline{A}$, $\bar{A}_{ik}$ ($\bar{A}_{i,k}$)	bus admittance matrix of the network, its value on position i-k
P_{ik}, Q_{ik}, $\bar{I}_{ik}$	flow of the active/reactive power and the current from bus i to bus k
R_{ik}, X_{ik}	series resistance/reactance of the branch between buses i and k
G_{ik}, B_{ik}	series conductance/susceptance of the branch between buses i and k
G_{ik0}, B_{ik0}	shunt conductance/susceptance of the branch between buses i and k
$\bar{Z}_{ik}$, $\bar{Y}_{ik}$	series impedance/admittance of the branch between buses i and k
$\bar{Y}_{ik0}$	shunt admittance of the branch between buses i and k
$\bar{I}_u$, $\bar{I}_v$, $\bar{I}_w$	current flows via the windings of the two/three-winding transformer
$\bar{t}_{ik}$, t_{ik}, λ_{ik}	transformer tap settings (tap magnitude/angle) between buses i and k
$\bar{V}_{f0}$, $\bar{I}_0$, $\bar{Y}_i$	shunt voltage/current and admittances of a three-winding transformer
P_{Li}, Q_{Li}	active/reactive power load
$P_{Gi}^{(p)}$, $Q_{Gi}^{(p)}$	active/reactive power injected in PV bus i during iteration (p)
G_{shi}, B_{shi}	conductance/susceptance of the shunt device in bus i
P_{shi}, Q_{shi}	voltage-dependent active/reactive power injected by the shunt device
n, n_{PV}, n_{PQ}	total number of network buses, number of PV/PQ network buses
p_{max}, ε	maximum number of iterations, tolerance (convergence precision)
V_i^{sp}	specified voltage magnitude in the PV bus i
$\bar{V}_i^{corr}$	corrected voltage phasor value in the PV bus i after the scaling process
ΔP_i, ΔQ_i	active/reactive power mismatch for bus i
ΔP, ΔQ	column vector of active/reactive power mismatches
$\underline{H}$, $\underline{N}$, $\underline{J}$, $\underline{L}$	submatrices of the Jacobian matrix
$\underline{J}_x$, $\underline{J}_x^*$	Jacobian matrix of the system, singular Jacobian matrix
$\Delta\theta$, $\Delta V/V$	correction vectors of phase angles and voltage magnitudes
$\underline{B'}$, $\underline{B''}$	state matrices of the F-D method
$\underline{C}$	state matrix of the DC load flow method
$\underline{C'}$, $\underline{D}$	state matrix and ancillary vector for the modified DC load flow method

γ, m_{i1}, m_{i2}	acceleration and acceleration/retardation factors for the G-S method
$\overline{V}_{i\,acc}$, $V_{i\,acc}$, $\theta_{i\,acc}$	accelerated voltage phasor/magnitude/angle values in the G-S method
x	state vector, i.e. vector of state variables
Δx, Δx_T, DXT	computed/truncated state update vector, truncation limit value
$Q_{Gi\,\min}$, $Q_{Gi\,\max}$	lower/upper var limits in the PV bus i
M, M_i	difference var vector, difference var value for the PV bus i
n_t, Δt_{ik}	number of tap magnitude positions, step of the tap magnitude
n_λ, $\Delta \lambda_{ik}$	number of tap angle positions, step of the tap angle
$V_m^{t\,arg}$, $Q_{ki}^{t\,arg}$, $P_{ki}^{t\,arg}$	voltage/power target value for the transformer with V/Q/P control
$t_{ik\,\min}$, $t_{ik\,\max}$	lower/upper tap magnitude limits for the OLTC transformer
$\lambda_{ik\,\min}$, $\lambda_{ik\,\max}$	lower/upper tap angle limits for the OLTC transformer
y	active/reactive power flow control variable
Δy, $y^{t\,arg}$	power flow mismatch, power flow target value
n_{QP}	number of OLTC transformers for Q/P control
λ, $\lambda_{\max}$, $\lambda_{\max}^*$	network loadability factor, theoretical/practical maximum loadability
θ_0, V_0, λ_0	system state variables from the previous corrector step
K, e_k	vector of base-power generations/loads, supplementary vector
σ, σ_L, σ_U	actual/lower/upper step size value
dV, $d\theta$	tangent increments of state variables in the predictor step
VSMI_i, VSMI_{ik}	bus/branch voltage stability margin indices
VSF_i, $q_{reserve}$	bus voltage sensitivity factors, relative reactive power reserve
α, A, B	monitoring angle and coefficients of the step size evaluation function
S	system singularity hypersurface
P_{L0}, Q_{L0}, P_{G0}	initial active/reactive power load and active power generation
ρ_i, η_i, k_i	parameter/direction vector, distance to instability in loading scenario i
x_0, ρ_0, x_i^*, ρ_i^*	state/parameter vector for the initial stressing and the singular point
w_i	left eigenvector for zero real eigenvalue of the singular Jacobian
k_i^*, η_i^*	minimum distance to voltage instability, critical direction vector
$f(x)$, $g(x)$, $h(x)$	objective function, equality/inequality equations
P_{Loss}, Q_{Loss}	total active/reactive system losses
b_{li}, b_{ui}, F	lower/upper binary variables for the PV bus i, large positive constant
m_{ik}	integer tap position counter
$\Delta \lambda_{init}$, ε_{end}	initial step for loadability increase, ending convergence criterion

1. Current Situation, Motivation and Challenges

For decades, electric power systems have been developed and used for transmitting and distributing electrical energy from individual power sources to the customers. During this evolutional process, large interconnected power grids have been designed to fulfil both technical and economical criteria for secured, reliable and sustainable operation. Parallelly to this, standardized procedures for power system modelling and assessment during operational and fault states were based on the conventional load flow analysis.

Today's electric power systems are often operated rather close to their working limits due to gradational increase of power consumption and slow construction of new power plants, substations and transmission lines. Moreover, large amount of renewable sources is installed in both transmission/distribution networks changing their originally planned functions and inducing abnormal states. Also, deregulated market policies are implemented considering economical aspects rather than transfer capabilities of network branches. By all these factors, proper system operation can be seriously threatened. Historically, series of islanding/black-out incidents already occurred in the US (1998, 2003) and in Europe - e.g. in Sweden and Italy (both 2003) or Greece (2004). Czech Republic was also on the verge to system collapse due to high system loadings caused by increased generations from wind power plants in northern Germany (2006, 2008-09).

In past years, several strategies with possible solutions were designed:

1) Use of new computational techniques is needed for keeping high numerical stability of standard load flow methods when solving highly loaded systems. State estimation outputs are usually applied as more precise initial estimates.

2) Use of phase-shifting transformers is being intensively discussed also in Czech Republic. In other countries, these devices were already installed on the transmission level - e.g. in Italy, Austria, Slovenia, Poland and Belgium.

3) In the Smart Grid concept, installation of regulating transformers is being assessed also for medium/low voltage distribution networks to maintain proper voltage conditions under extreme weather conditions. Superior control system is to be used to optimize tap settings of all regulating transformers in real time with respect to actual loading and generation from renewable power sources.

4) Robust online monitoring of network operation is to be introduced including voltage stability criteria. Information about voltage-load sensitive network buses/areas with possible preventive/corrective actions are the key outputs of voltage stability analysis. Voltage stability criteria are being also included in contingency, reconfiguration and security constrained OPF analyses worldwide.

Along with nuclear moratorium, Germany proposes further increase of generation from wind and photovoltaic power sources to 47 GW and 50 GW by 2020, respectively.

2. Main Objectives of the Doctoral Thesis

Based on current problems with higher network loadings leading to potential voltage instability scenarios, the load flow analysis and related tasks for reliable network modelling are still worthy of scrutiny. Furthermore, the need for online evaluation of electric power system operation along with proposed strategies for fault prevention is actual in real power systems worldwide.

Key objectives of this doctoral thesis are further structured into three stand-alone thematic groups:

1) Optimization of conventional load flow methods

    a) to examine stability techniques for numerical enhancement of the Newton-Raphson method

    b) to accelerate numerical performance of the Gauss-Seidel method

    c) to apply vectorized Gauss method for faster load flow analysis

    d) to find better convergence setting of the Fast-Decoupled method for broad variety of test power systems

    e) to design the improved version of the DC method for better approximate load flow solutions

2) Optimization of network operation using voltage/power-controlled devices

    f) to develop reliable procedures for regulating transformers with V/Q/P control and logics for regulated buses with var limits in individual load flow methods

    g) to analyze possible cooperation of regulating transformers, synchronous condensers, generators and switched shunt inductor/capacitor banks for optimized operation of islanded distribution networks in the Smart Grid concept (in terms of voltage/var conditions)

3) Development and testing of techniques for voltage stability analysis

    h) to design iterative algorithms for fast and accurate voltage stability analysis

    i) to develop methodologies for locating voltage-weak network areas and for suitable preventive/corrective actions in terms of voltage stability

    j) to apply advanced procedures for finding the minimum distance to voltage instability for highly loaded electric power systems

    k) to evaluate whether the loading increase with constant power factor is sufficiently robust for voltage stability assessment or whether another approach has to be applied instead

To meet the targets above, author's original computing tool is to be realized in MATLAB environment for providing full-scale outputs of individual types of load flow analysis and for designing better system operation during high loading and voltage instability scenarios. Accent is to be placed especially on producing correct and reliable solutions with minimized iteration numbers and CPU times for possible real-time analyses.

In this respect, the topic of this doctoral thesis is still up-to-date and may further develop the state-of-the-art mechanisms for electric power system operation and control.

3. Fundamental Load Flow Analysis

Load flow analysis is the set of calculations providing basic perspective on current operational state of an electric power system [1], [2], [3], [4], [5], [6], [7], [8], [9], [10], [16], [17], [20], [22]. The outputs are primarily the voltage and angle conditions, secondary the bus active/reactive power injections, branch power flows and losses, percentage loadings, power factors and total system losses. Therefore, overall behaviour of the network during both normal and abnormal steady states can be obtained.

The following simplifications are to be made without threatening the precision of the simulations. First, only sinusoidal behaviour of currents and voltages is expected for steady-state analyses. Therefore, symbolic-complex method is used for expressing all active and passive variables in the form of phasors. Second, a generic 3-phase power system is assumed to be linear and balanced containing identical parameters for all network phases. Thus, it can be modelled as a single-phase equivalent circuit. Third, system parameters are constant at given frequency. Then, individual network elements can be represented by the same equivalent circuit in physical or per units.

Starting with Ohm's law and both Kirchhoff's laws, the node voltage method is the most suitable for expressing the system's nodal equations. Lower numbers of network buses and parameters are needed. Shunt parameters and branches along with tap settings in tap-changing transformers do not complicate the model. From this follows that only admittances of each network element must be applied using a respective Pie-element equivalent scheme.

Each bus i of the network represents a substation, consumption point, generator, superior network, etc. It is definitely determined by so-called active variables – either by phasors of an injected current and line-to-line bus voltage ($\bar{I}_i$, $\bar{V}_i$) or by line-to-line voltage magnitude V_i, voltage phase angle θ_i and both active and reactive power injections P_i, Q_i – see Fig. 3-1.
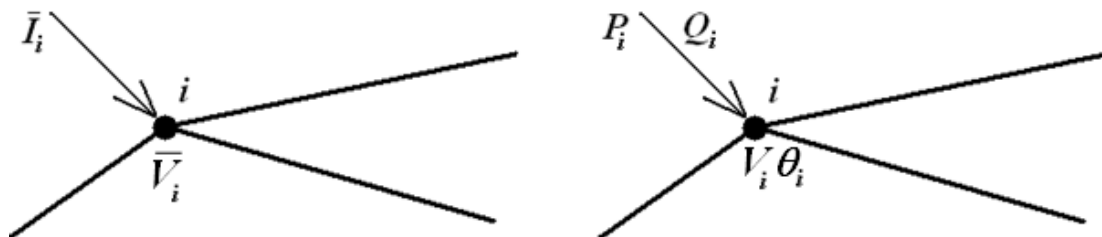
Fig. 3-1: Mathematical description of bus i in the network

Mutual dependence between these quantities is shown in Eqn. (3-1) below.

$$\bar{S}_i = P_i + jQ_i = \sqrt{3}\bar{V}_i\bar{I}_i^* \;\; \rightarrow \;\; \bar{I}_i = \frac{P_i - jQ_i}{\sqrt{3}\bar{V}_i^*} \tag{3-1}$$

Injected bus currents/powers comprise the sum of all currents/powers flowing in or out of a particular bus. Then, the net current/power can be either delivered into the bus ("+"

sign) or demanded ("-" sign). This sign convention is further used for building system's nodal equations.

Three types of network buses can be introduced for load flow analysis [1], [2], [3], [4], [5], [8], [9], [10], [11], [12], [18], [20], [22]. For each of them, two of active variables above must be provided while remaining two will be calculated.

- a PQ bus - represents a consumption point in the network
  - net active and reactive power is specified
  - both voltage magnitude and phase angle is to be calculated

- a PV bus - constitutes a connection point of a generator/synchronous condenser
  - active power and voltage magnitude is given
  - phase angle and reactive power for voltage control is to be calculated
  - lower/upper var limits constrain the reactive power generation

- slack bus - a fictitious bus responsible for total power losses of the network
  - a PV bus with the highest voltage level (largest active power generation, broadest var range) is often chosen
  - alternatively, a PQ bus with the connection to a superior system can be used
  - voltage magnitude and phase angle is specified
  - active/reactive powers are to be computed

Input data for the load flow analysis include network topology with impedances/admittances of all network elements (power lines, transformers, inductors, capacitors, etc.), transformer tap settings and controls. Net active powers in PQ and PV buses, net reactive powers in PQ buses, voltage magnitudes in PV buses (with respective upper/lower var limits) and complex voltage value in the slack bus must be also specified.

3.1 Bus Admittance Matrix

The matrix expression below is used for describing voltage and current conditions in each network bus – see Eqn. (3.1-1).

$$\sqrt{3}\underline{\overline{I}} = \underline{\overline{A}} \cdot \underline{\overline{V}} \tag{3.1-1}$$

where: $\underline{\overline{I}}$ - column $[n, 1]$ vector of complex net injected currents to each bus

$\underline{\overline{V}}$ - column $[n, 1]$ vector of complex line-to-line bus voltages

$\underline{\overline{A}}$ - square $[n, n]$ bus admittance matrix n - total number of network buses

Each of n complex nodal equations (Eqn. 3.1-1) can be re-written into its real/imaginary components containing two unknown active variables (according to the bus type). Thus, total number of $2n$ equations for $2n$ unknown variables is obtained (necessary condition for a unique solution) [1], [2], [3], [4], [5], [6], [9], [10], [11], [12], [16], [17], [20].

A simplified network section (see Fig. 3.1-1) is further used for deriving the bus admittance matrix $\underline{\overline{A}}$. For both power lines and two-winding transformers, series and shunt admittances of a Pie-element are computed from given passive parameters as shown in Eqn. (3.1-2) below. Note: For each transformer, the shunt susceptance value is negative.
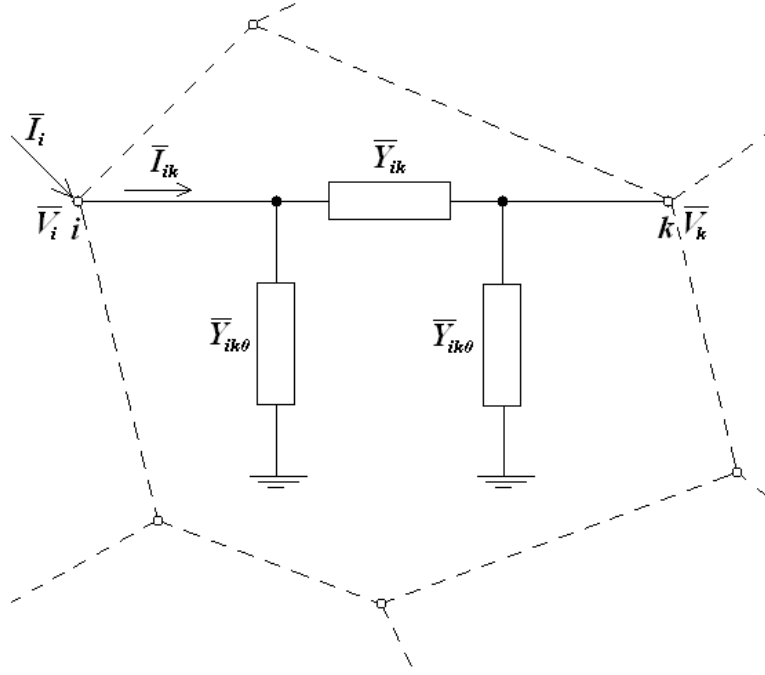
Fig. 3.1-1: Network section for building the bus admittance matrix [20]

$$\overline{Y}_{ik} = \frac{1}{\overline{Z}_{ik}} = \frac{1}{R_{ik} + jX_{ik}} = \frac{R_{ik}}{R_{ik}^2 + X_{ik}^2} - j\frac{X_{ik}}{R_{ik}^2 + X_{ik}^2} = G_{ik} + jB_{ik}$$

(3.1-2)

$$\overline{Y}_{ik0} = G_{ik0} + jB_{ik0}$$

As shown in Eqn. (3.1-3), total injected current $\overline{I}_i$ into a generic bus i is equal to the sum of all branch currents $\overline{I}_{ik}$ flowing from bus i to the defined subset of network buses.

$$\overline{I}_i = \sum_{\substack{k=1 \\ k \neq i}}^{n} \overline{I}_{ik}$$

(3.1-3)

The following applies for the branch current $\overline{I}_{ik}$ flowing from bus i to bus k:

$$\sqrt{3}\,\overline{I}_{ik} = \overline{V}_i\overline{Y}_{ik0} + (\overline{V}_i - \overline{V}_k)\overline{Y}_{ik} = \overline{V}_i(\overline{Y}_{ik0} + \overline{Y}_{ik}) - \overline{V}_k\overline{Y}_{ik}$$

(3.1-4)

Using Eqns. (3.1-3) and (3.1-4), total injected current $\overline{I}_i$ is:

$$\sqrt{3}\,\overline{I}_i = \overline{V}_i\sum_{\substack{k=1 \\ k \neq i}}^{n}(\overline{Y}_{ik0} + \overline{Y}_{ik}) - \sum_{\substack{k=1 \\ k \neq i}}^{n}\overline{V}_k\overline{Y}_{ik}$$

(3.1-5)

For network bus i, relevant nodal equation (3.1-1) can be re-written as follows:

$$\sqrt{3}\,\overline{I}_i = \overline{A}_{i1}\overline{V}_1 + \overline{A}_{i2}\overline{V}_2 + ... + \overline{A}_{ii}\overline{V}_i + ... + \overline{A}_{ik}\overline{V}_k + ... + \overline{A}_{in}\overline{V}_n$$

(3.1-6)

When comparing Eqns. (3.1-5) and (3.1-6), individual on-/off-diagonal elements of the bus admittance matrix can be derived.

$$\overline{A}_{ii} = \sum_{\substack{k=1 \\ k \neq i}}^{n}(\overline{Y}_{ik0} + \overline{Y}_{ik}) \qquad \overline{A}_{ik} = -\overline{Y}_{ik}$$

(3.1-7)

Terms self-admittance or driving point admittance are used for on-diagonal elements of the bus admittance matrix. Off-diagonal elements are usually called mutual or transfer admittances.

During topology changes, the bus admittance matrix does not have to be calculated again since only several matrix elements are to be modified. Below, element updates are shown for switching off (left) and switching on (right) the branch between buses i and k.

$$\overline{A}_{i,k-new} = \overline{A}_{k,i-new} = 0 \qquad\qquad \overline{A}_{i,k-new} = \overline{A}_{k,i-new} = -\overline{Y}_{ik}$$

$$\overline{A}_{i,i-new} = \overline{A}_{i,i-old} - \overline{Y}_{ik0} - \overline{Y}_{ik} \qquad \overline{A}_{i,i-new} = \overline{A}_{i,i-old} + \overline{Y}_{ik0} + \overline{Y}_{ik} \qquad (3.1\text{-}8)$$

$$\overline{A}_{k,k-new} = \overline{A}_{k,k-old} - \overline{Y}_{ik0} - \overline{Y}_{ik} \qquad \overline{A}_{k,k-new} = \overline{A}_{k,k-old} + \overline{Y}_{ik0} + \overline{Y}_{ik}$$

Majority of networks is highly sparse since only some connections between individual system buses are made. Thus, large number of off-diagonal elements in the bus admittance matrix is zero (no connection, infinite impedance) and the bus admittance matrix is sparse. Moreover, it is symmetrical when only power lines or transformer with nominal tap settings are connected. Also, it is usually diagonally dominant and contains general complex values.

In the bus admittance matrix, network topology along with all passive bus/branch parameters can be transparently encoded. When being assembled, usual procedure is to update relevant four elements of the matrix for each passive network element - power lines (also in parallel), two-/three-winding transformers, shunt compensators. For latter three, updating process of the bus admittance matrix is further presented.

3.2 Inclusion of Two-Winding Transformers

Two various power systems (marked as *I* and *II*) connected by a two-winding transformer with complex tap ratio $\overline{t}_{ik}$ are considered – see Fig. 3.2-1. Network *I* contains buses 1, 2, … i, … q; network *II* includes buses $q+1, q+2$, … k, … n. Based on sign convention, branch current flowing out from bus i (marked as $\overline{I}_u$) must have negative sign, while branch current flowing into bus k (marked as $\overline{I}_v$) positive sign. Currents $\overline{I}_1$, $\overline{I}_2$, … $\overline{I}_n$ are the net injected currents into network buses 1, 2, … n.

Both networks *I* and *II* can be mathematically described by nodal equations – see Eqns. (3.2-1) and (3.2-2).
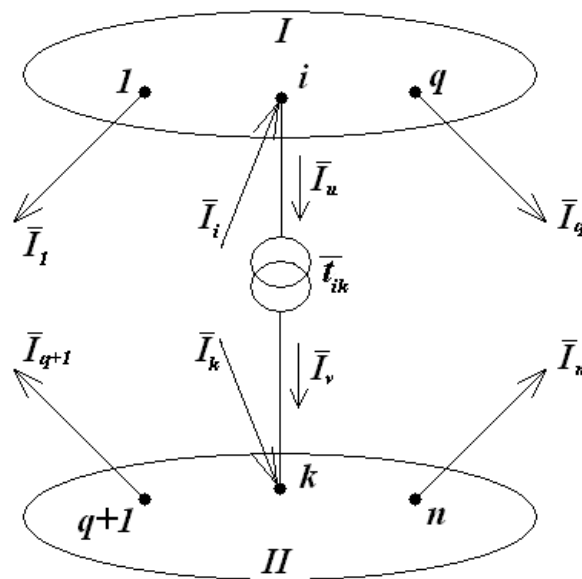
Fig. 3.2-1: Two networks connected by a two-winding transformer [20]

$$\sqrt{3}\begin{bmatrix} \overline{I}_1 \\ \vdots \\ \overline{I}_i - \overline{I}_u \\ \vdots \\ \overline{I}_q \end{bmatrix} = \begin{bmatrix} \overline{A}_{1,1} & \cdots & \overline{A}_{1,i} & \cdots & \overline{A}_{1,q} \\ \vdots & & \vdots & & \vdots \\ \overline{A}_{i,1} & \cdots & \overline{A}_{i,i} & \cdots & \overline{A}_{i,q} \\ \vdots & & \vdots & & \vdots \\ \overline{A}_{q,1} & \cdots & \overline{A}_{q,i} & \cdots & \overline{A}_{q,q} \end{bmatrix} \cdot \begin{bmatrix} \overline{V}_1 \\ \vdots \\ \overline{V}_i \\ \vdots \\ \overline{V}_q \end{bmatrix} \tag{3.2-1}$$

$$\sqrt{3}\begin{bmatrix} \overline{I}_{q+1} \\ \vdots \\ \overline{I}_k + \overline{I}_v \\ \vdots \\ \overline{I}_n \end{bmatrix} = \begin{bmatrix} \overline{A}_{q+1,q+1} & \cdots & \overline{A}_{q+1,k} & \cdots & \overline{A}_{q+1,n} \\ \vdots & & \vdots & & \vdots \\ \overline{A}_{k,q+1} & \cdots & \overline{A}_{k,k} & \cdots & \overline{A}_{k,n} \\ \vdots & & \vdots & & \vdots \\ \overline{A}_{n,q+1} & \cdots & \overline{A}_{n,k} & \cdots & \overline{A}_{n,n} \end{bmatrix} \cdot \begin{bmatrix} \overline{V}_{q+1} \\ \vdots \\ \overline{V}_k \\ \vdots \\ \overline{V}_n \end{bmatrix} \tag{3.2-2}$$

Unknown branch currents $\overline{I}_u$, $\overline{I}_v$ can be computed from the equivalent circuit of a two-winding transformer – see Fig. 3.2-2.
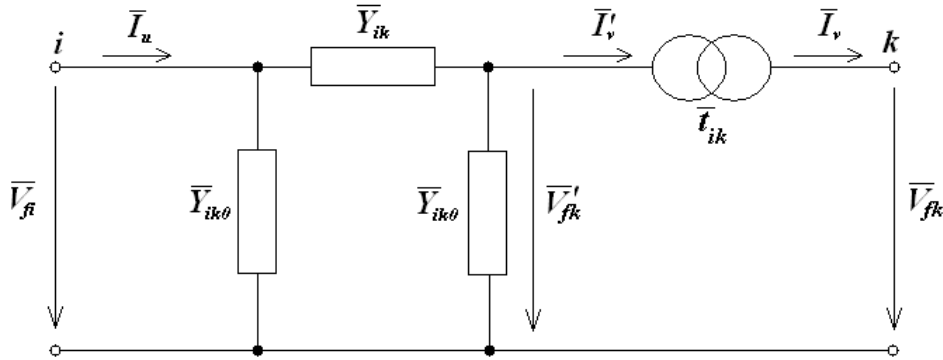
Fig. 3.2-2: Equivalent circuit of a two-winding transformer – in detail [20]

Formulas for both branch currents must contain only the functions of bus voltages $\overline{V}_{fi}$ and $\overline{V}_{fk}$. Current $\overline{I}_u$ can be expressed as follows:

$$\overline{I}_{ik} = \overline{Y}_{ik}\left(\overline{V}_{fi} - \overline{V}'_{fk}\right) + \overline{V}_{fi}\overline{Y}_{ik0} \tag{3.2-3}$$

For the complex tap ratio applies:

$$\overline{V}'_{fk} / \overline{V}_{fk} = \overline{t}_{ik} \tag{3.2-4}$$

Using both these formulas, final relation for branch current $\overline{I}_u$ can be obtained:

$$\overline{I}_u = \left(\overline{Y}_{ik} + \overline{Y}_{ik0}\right)\overline{V}_{fi} - \overline{t}_{ik}\overline{Y}_{ik}\overline{V}_{fk} \tag{3.2-5}$$

Equality of complex powers is valid for an ideal transformer:

$$3\overline{V}_{fk}\overline{I}_v^* = 3\overline{V}'_{fk}\overline{I}'^*_v \tag{3.2-6}$$

Current $\overline{I}'_v$ can be specified as follows:

$$\overline{I}'_v = \overline{Y}_{ik}\left(\overline{V}_{fi} - \overline{t}_{ik}\overline{V}_{fk}\right) - \overline{t}_{ik}\overline{V}_{fk}\overline{Y}_{ik0} \tag{3.2-7}$$

Using Eqns. (3.2-4), (3.2-6) and (3.2-7), final formula for branch current $\overline{I}_v$ is found.

$$\overline{I}_v = \overline{t}^*_{ik}\overline{Y}_{ik}\overline{V}_{fi} - t^2_{ik}\left(\overline{Y}_{ik} + \overline{Y}_{ik0}\right)\overline{V}_{fk} \tag{3.2-8}$$

In the matrix form, both branch currents are expressed as shown below.

21

$$\begin{bmatrix} \overline{I}_u \\ \overline{I}_v \end{bmatrix} = \begin{bmatrix} \overline{Y}_{ik} + \overline{Y}_{ik0} & -\overline{t}_{ik}\overline{Y}_{ik} \\ -\overline{t}_{ik}^*\overline{Y}_{ik} & -t_{ik}^2\left(\overline{Y}_{ik} + \overline{Y}_{ik0}\right) \end{bmatrix}\begin{bmatrix} \overline{V}_{fi} \\ \overline{V}_{fk} \end{bmatrix}$$

(3.2-9)

When combining Eqns. (3.2-1), (3.2-2) and (3.2-9), final matrix form of nodal equations including a two-winding transformer connected between buses i and k is as follows.

$$\sqrt{3}\begin{bmatrix} \overline{I}_1 \\ \vdots \\ \overline{I}_i \\ \vdots \\ \overline{I}_q \\ \overline{I}_{q+1} \\ \vdots \\ \overline{I}_k \\ \vdots \\ \overline{I}_n \end{bmatrix} = \begin{bmatrix} \overline{A}_{1,1} & \cdots & \overline{A}_{1,i} & \cdots & \overline{A}_{1,q} & 0 & \cdots & 0 & \cdots & 0 \\ \vdots & & \vdots & & \vdots & \vdots & & \vdots & & \vdots \\ \overline{A}_{i,1} & \cdots & \overline{A}_{i,i}+\overline{Y}_{ik}+\overline{Y}_{ik0} & \cdots & \overline{A}_{i,q} & 0 & \cdots & -\overline{t}\,\overline{Y}_{ik} & \cdots & 0 \\ \vdots & & \vdots & & \vdots & \vdots & & \vdots & & \vdots \\ \overline{A}_{q,1} & \cdots & \overline{A}_{q,i} & \cdots & \overline{A}_{q,q} & 0 & \cdots & 0 & \cdots & 0 \\ 0 & \cdots & 0 & \cdots & 0 & \overline{A}_{q+1,q+1} & \cdots & \overline{A}_{q+1,k} & \cdots & \overline{A}_{q+1,n} \\ \vdots & & \vdots & & \vdots & \vdots & & \vdots & & \vdots \\ 0 & \cdots & -\overline{t}^*\overline{Y}_{ik} & \cdots & 0 & \overline{A}_{k,q+1} & \cdots & \overline{A}_{k,k}+t^2\left(\overline{Y}_{ik}+\overline{Y}_{ik0}\right) & \cdots & \overline{A}_{k,n} \\ \vdots & & \vdots & & \vdots & \vdots & & \vdots & & \vdots \\ 0 & \cdots & 0 & \cdots & 0 & \overline{A}_{n,q+1} & \cdots & \overline{A}_{n,k} & \cdots & \overline{A}_{n,n} \end{bmatrix} \cdot \begin{bmatrix} \overline{V}_1 \\ \vdots \\ \overline{V}_i \\ \vdots \\ \overline{V}_q \\ \overline{V}_{q+1} \\ \vdots \\ \overline{V}_k \\ \vdots \\ \overline{V}_n \end{bmatrix}$$

Fig. 3.2-3: Final matrix form of network nodal equations (a two-winding transformer) [20]

As shown above, only four elements of the bus admittance matrix (positions ii, ik, ki, kk) must be modified during the updating process for each two-winding transformer. When the tap ratio of a two-winding transformer is modified, the entire bus admittance matrix does not need to be computed again since only three elements can be re-calculated for obtaining the updated bus admittance matrix. Note: All transformer parameters must be re-calculated to the primary side (bus i). Parameters of remaining system elements are calculated on their nominal voltage levels.

In professional load flow programs (e.g. PowerWorld Simulator [69]) and other freeware tools (MATPOWER [70], Power System Analysis Toolbox [71]), alternative equivalent scheme for a two-winding transformer is used. Corresponding Pie element is connected to the to-bus side (bus k), while an ideal transformer with the off-nominal tap settings is closer to the from-bus side (bus i). This poses no problems for derived formulas above only when dealing with fixed tap transformers with nominal tap settings. For off-nominal and tap-changing transformers, however, serious differences in results appear. Therefore, the unification with this new equivalent transformer model was made - see Chapter 7.

3.3 Inclusion of Three-Winding Transformers

Updating process of the bus admittance matrix for each three-winding transformer connected to the network can be derived similarly as for two-winding transformers. Three different power systems (marked as *I*, *II* and *III*) interconnected by a three-winding transformer with complex tap ratios $\overline{t}_{ik}$, $\overline{t}_{il}$ are considered − see Fig. 3.3-1. Network *I* contains buses 1, 2, … i, … q, while networks *II* and *III* include buses q+1, q+2, … k, … r

and $r+1$, $r+2$, ... l, ... n, respectively. Branch currents $\bar{I}_u$, $\bar{I}_v$ and $\bar{I}_w$ are treated as any other net injected currents to a generic network bus (i.e. identical sign convention applied).
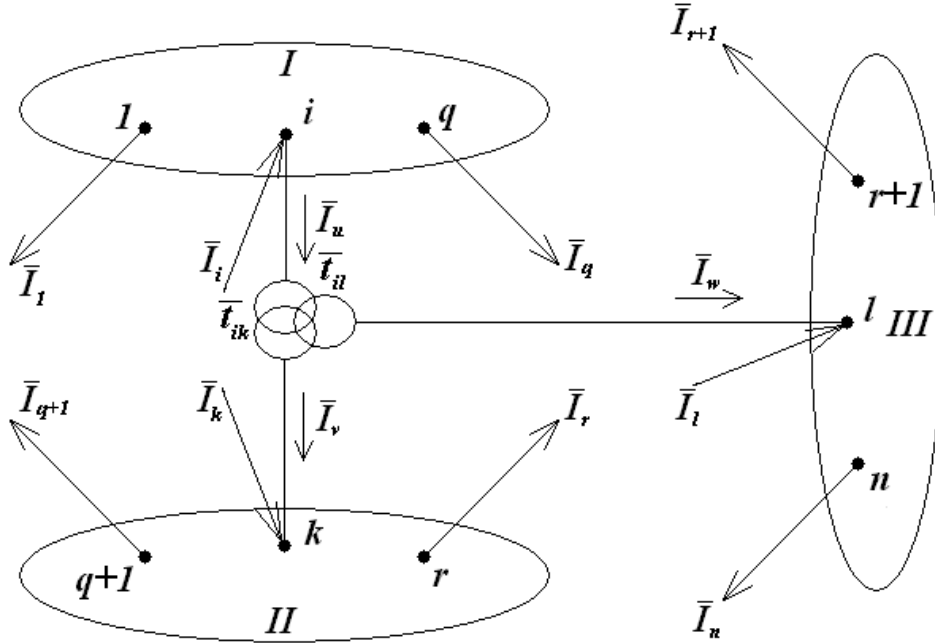
Fig. 3.3-1: Three networks interconnected by a three-winding transformer

In Eqns. (3.3-1), (3.3-2) and (3.3-3), individual power systems are described by nodal equations.

$$\sqrt{3}\begin{bmatrix} \bar{I}_1 \\ \vdots \\ \bar{I}_i - \bar{I}_u \\ \vdots \\ \bar{I}_q \end{bmatrix} = \begin{bmatrix} \bar{A}_{1,1} & \cdots & \bar{A}_{1,i} & \cdots & \bar{A}_{1,q} \\ \vdots & \ddots & \vdots & \ddots & \vdots \\ \bar{A}_{i,1} & \cdots & \bar{A}_{i,i} & \cdots & \bar{A}_{i,q} \\ \vdots & \ddots & \vdots & \ddots & \vdots \\ \bar{A}_{q,1} & \cdots & \bar{A}_{q,i} & \cdots & \bar{A}_{q,q} \end{bmatrix} \begin{bmatrix} \bar{V}_1 \\ \vdots \\ \bar{V}_i \\ \vdots \\ \bar{V}_q \end{bmatrix} \qquad (3.3\text{-}1)$$

$$\sqrt{3}\begin{bmatrix} \bar{I}_{q+1} \\ \vdots \\ \bar{I}_k + \bar{I}_v \\ \vdots \\ \bar{I}_r \end{bmatrix} = \begin{bmatrix} \bar{A}_{q+1,q+1} & \cdots & \bar{A}_{q+1,k} & \cdots & \bar{A}_{q+1,r} \\ \vdots & \ddots & \vdots & \ddots & \vdots \\ \bar{A}_{k,q+1} & \cdots & \bar{A}_{k,k} & \cdots & \bar{A}_{k,r} \\ \vdots & \ddots & \vdots & \ddots & \vdots \\ \bar{A}_{r,q+1} & \cdots & \bar{A}_{r,k} & \cdots & \bar{A}_{r,r} \end{bmatrix} \begin{bmatrix} \bar{V}_{q+1} \\ \vdots \\ \bar{V}_k \\ \vdots \\ \bar{V}_r \end{bmatrix} \qquad (3.3\text{-}2)$$

$$\sqrt{3}\begin{bmatrix} \bar{I}_{r+1} \\ \vdots \\ \bar{I}_l + \bar{I}_w \\ \vdots \\ \bar{I}_n \end{bmatrix} = \begin{bmatrix} \bar{A}_{r+1,r+1} & \cdots & \bar{A}_{r+1,l} & \cdots & \bar{A}_{r+1,n} \\ \vdots & \ddots & \vdots & \ddots & \vdots \\ \bar{A}_{l,r+1} & \cdots & \bar{A}_{l,l} & \cdots & \bar{A}_{l,n} \\ \vdots & \ddots & \vdots & \ddots & \vdots \\ \bar{A}_{n,r+1} & \cdots & \bar{A}_{n,l} & \cdots & \bar{A}_{n,n} \end{bmatrix} \begin{bmatrix} \bar{V}_{r+1} \\ \vdots \\ \bar{V}_l \\ \vdots \\ \bar{V}_n \end{bmatrix} \qquad (3.3\text{-}3)$$

Analogically, branch currents $\bar{I}_u$, $\bar{I}_v$, $\bar{I}_w$ must be derived from the equivalent circuit of a three-winding transformer – see Fig. 3.3-2.
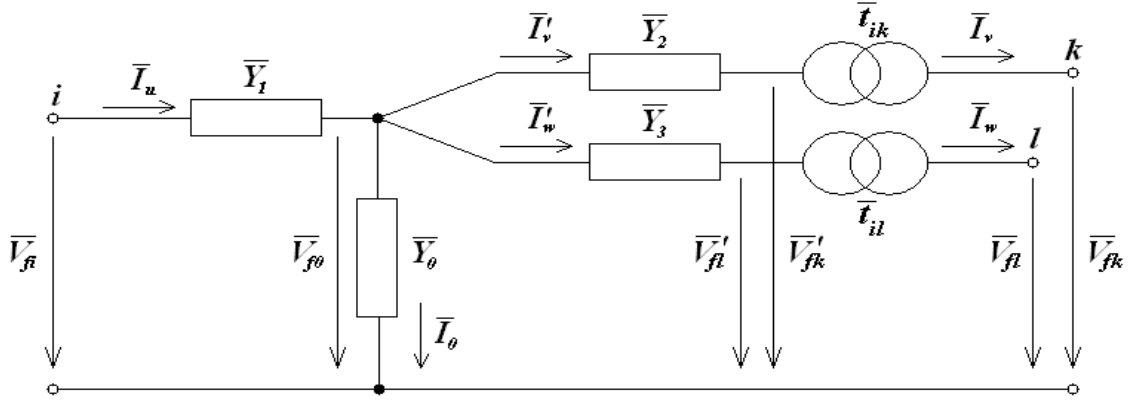
Fig. 3.3-2: Equivalent circuit of a three-winding transformer – in detail

For currents $\overline{I}_u$, $\overline{I}'_v$ and $\overline{I}'_w$, following formulas apply:

$$\overline{I}_u = \overline{Y}_1 \left(\overline{V}_{fi} - \overline{V}_{f0}\right) \quad \overline{I}'_v = \overline{Y}_2 \left(\overline{V}_{f0} - \overline{V}'_{fk}\right) \quad \overline{I}'_w = \overline{Y}_3 \left(\overline{V}_{f0} - \overline{V}'_{fl}\right) \tag{3.3-4}$$

Complex tap settings of both ideal transformers are defined as:

$$\overline{t}_{ik} = \frac{\overline{V}'_{fk}}{\overline{V}_{fk}} = \frac{\overline{I}^*_v}{\overline{I}'^*_v} \quad \overline{t}_{il} = \frac{\overline{V}'_{fl}}{\overline{V}_{fl}} = \frac{\overline{I}^*_w}{\overline{I}'^*_w} \tag{3.3-5}$$

The following equation is valid for the transformer common point.

$$\overline{I}_u = \overline{I}'_v + \overline{I}'_w + \overline{I}_0 \quad \text{where} \quad \overline{I}_0 = \overline{Y}_0 \overline{V}_{f0} \tag{3.3-6}$$

Using both Eqns. (3.3-4) and (3.3-5) in Eqn. (3.3-6), voltage $\overline{V}_{f0}$ can be determined.

$$\overline{V}_{f0} = \frac{\overline{Y}_1 \overline{V}_{fi} + \overline{t}_{ik} \overline{Y}_2 \overline{V}_{fk} + \overline{t}_{il} \overline{Y}_3 \overline{V}_{fl}}{\overline{Y}_1 + \overline{Y}_2 + \overline{Y}_3 + \overline{Y}_0} \tag{3.3-7}$$

Adding Eqns. (3.3-5) and (3.3-7) to each formula of Eqn. (3.3-4), final matrix-formed Eqn. (3.3-8) between branch currents $\overline{I}_u, \overline{I}_v, \overline{I}_w$ and bus voltages $\overline{V}_{fi}, \overline{V}_{fk}, \overline{V}_{fl}$ is obtained.

$$\begin{bmatrix} \overline{I}_u \\ \overline{I}_v \\ \overline{I}_w \end{bmatrix} = \frac{\begin{bmatrix} \overline{Y}_1\left(\overline{Y}_2 + \overline{Y}_3 + \overline{Y}_0\right) & -\overline{t}_{ik} \overline{Y}_1 \overline{Y}_2 & -\overline{t}_{il} \overline{Y}_1 \overline{Y}_3 \\ \overline{t}^*_{ik} \overline{Y}_1 \overline{Y}_2 & -t^2_{ik} \overline{Y}_2\left(\overline{Y}_1 + \overline{Y}_3 + \overline{Y}_0\right) & \overline{t}^*_{ik} \overline{t}_{il} \overline{Y}_2 \overline{Y}_3 \\ \overline{t}^*_{il} \overline{Y}_1 \overline{Y}_3 & \overline{t}_{ik} \overline{t}^*_{il} \overline{Y}_2 \overline{Y}_3 & -t^2_{il} \overline{Y}_3\left(\overline{Y}_1 + \overline{Y}_2 + \overline{Y}_0\right) \end{bmatrix}}{\overline{Y}_1 + \overline{Y}_2 + \overline{Y}_3 + \overline{Y}_0} \begin{bmatrix} \overline{V}_{fi} \\ \overline{V}_{fk} \\ \overline{V}_{fl} \end{bmatrix} \tag{3.3-8}$$

When assembled with Eqns. (3.3-1), (3.3-2) and (3.3-3), final form of nodal equations containing one three-winding transformer between buses i, k and l can be obtained – see Fig. 3.3-3. With very high accuracy, this model updates nine elements of the bus admittance matrix for each three-winding transformer connected to the network. However, more complicated input data structure is required. Alternative procedure is to handle three-winding transformers as one power line and two two-winding transformers. This model has no problem with additional input data concerning the fictitious branch elements. However, it is less accurate (only for non-zero $\overline{Y}_0$) and it also results in adding the common point of the transformer to the set of PQ buses where both voltage magnitudes and phase angles are to be eventually computed.

24

$$\sqrt{3}\begin{bmatrix} \overline{I}_1 \\ \vdots \\ \overline{I}_i \\ \vdots \\ \overline{I}_q \\ \overline{I}_{q+1} \\ \vdots \\ \overline{I}_k \\ \overline{I}_r \\ \overline{I}_{r+1} \\ \vdots \\ \overline{I}_l \\ \vdots \\ \overline{I}_n \end{bmatrix} = \begin{bmatrix} \overline{A}_{1,1} \cdots & \overline{A}_{1,i} & \cdots \overline{A}_{1,q} & 0 & \cdots & 0 & \cdots & 0 & 0 & \cdots & 0 & \cdots & 0 \\ \vdots & \vdots & \vdots & & & \vdots & & \vdots & \vdots & & \vdots & & \vdots \\ \overline{A}_{i,1} \cdots \overline{A}_{i,i} + \dfrac{\overline{Y}_1(\overline{Y}_2+\overline{Y}_3+\overline{Y}_0)}{\overline{Y}_1+\overline{Y}_2+\overline{Y}_3+\overline{Y}_0} \cdots \overline{A}_{i,q} & & & 0 & \cdots & -\dfrac{\overline{t}_{ik}\overline{Y}_1\overline{Y}_2}{\overline{Y}_1+\overline{Y}_2+\overline{Y}_3+\overline{Y}_0} & \cdots & 0 & 0 & \cdots & -\dfrac{\overline{t}_{il}\overline{Y}_1\overline{Y}_3}{\overline{Y}_1+\overline{Y}_2+\overline{Y}_3+\overline{Y}_0} & \cdots & 0 \end{bmatrix}\begin{bmatrix} \overline{V}_1 \\ \vdots \\ \overline{V}_i \\ \vdots \\ \overline{V}_q \\ \overline{V}_{q+1} \\ \vdots \\ \overline{V}_k \\ \overline{V}_r \\ \overline{V}_{r+1} \\ \vdots \\ \overline{V}_l \\ \vdots \\ \overline{V}_n \end{bmatrix}$$

Fig. 3.3-3: Final matrix form of network nodal equations (a three-winding transformer)

Even for high numbers of three-winding transformers (also with negligible shunt admittances) located in real networks, both accuracy and calculation speed should not significantly suffer using the latter procedure. Therefore, this methodology is further applied for modelling three-winding transformers in load flow and other analyses.

3.4 Inclusion of Shunt Compensators

For shunt inductors/capacitors and superior power systems connected to a generic bus i of the system, the bus admittance matrix can be easily updated – see Eqn. (3.4-1). Shunt susceptance for inductors and capacitors is negative and positive, respectively. Shunt conductance is usually non-zero only for superior grids.

$$\overline{A}_{ii} = \overline{A}_{ii} + G_{shi} + jB_{shi} \tag{3.4-1}$$

When modelling series inductors and capacitors, a generic Pie equivalent circuit can be employed with no resistance and shunt elements defined.

3.5 Load Flow as a Nonlinear Problem

At this moment, the bus admittance matrix is determined for all electric power systems and can be employed for the load flow analysis. When investigating nodal equations, it can be seen that unknown bus voltages are on both sides of Eqn. (3.1-1) – on the right-hand side directly in the unknown vector of bus line-to-line voltages, on the left-hand side inside the vector of net injected currents (in their complex conjugate forms). Due to this strong nonlinearity of nodal equations, load flow solution cannot be obtained using standard analytical procedures for majority of power systems. Only two- and several three-bus networks can be computed analytically. In remaining cases, numerical (iterative) techniques must be applied [1], [2], [3], [4], [5], [6], [7], [8], [9], [10], [11], [12], [14], [16], [17], [18], [20], [22].

4. Numerical Methods in the Load Flow Analysis

Generally, each numerical method starts with an initial (scalar or vector) estimate which should be close to the unknown solution. This estimate is used in individual procedures of the iterative process for the computation of a new (updated) estimate. At the end of every iteration, values of both new and old estimates are mutually compared. If their difference falls below a specified tolerance value, the solution is found with required accuracy. This can be expected for well-behaving problems, where fast numerical convergence occurs. In slowly-converging and diverging cases, however, the infinite loop of iterations must be stopped by specifying the maximum number of iterations.

Historically, several numerical methods were developed for solving the load flow problem. Individually, they were designed and applied with respect to their specific features such as code complexity, calculation speed, memory requirements, level of precision, etc.

4.1 Gauss and Gauss-Seidel Iterative Methods

First historically applied numerical procedures for ac load flow analysis were the Gauss (G) and the Gauss-Seidel (G-S) methods [1], [2], [3], [4], [5], [8], [9], [12]. In general, both methods use specific iterative formulas for calculating new values of each state variable of the problem - see Eqns. (4.1-1) and (4.1-2), respectively.

$$x_i^{(p+1)} = f\left(x_1^{(p)}, x_2^{(p)}, ..., x_{i-1}^{(p)}, x_i^{(p)}, x_{i+1}^{(p)}, ..., x_n^{(p)}\right) \tag{4.1-1}$$

$$x_i^{(p+1)} = f\left(x_1^{(p+1)}, x_2^{(p+1)}, ..., x_{i-1}^{(p+1)}, x_i^{(p)}, x_{i+1}^{(p)}, ..., x_n^{(p)}\right) \tag{4.1-2}$$

The G method employs old values of unknown variables (i.e. from the previous iteration p) to obtain new values in current iteration $p+1$. However, the update process is performed only at the end of the current iteration. In the G-S algorithm, a newly computed value is immediately used for the calculation of remaining estimates in the current iteration. In other words, the newest values of state variables are always employed (e.g. values of $x_1^{(p+1)}$ and $x_2^{(p+1)}$ along with old values of remaining variables for the computation of $x_3^{(p+1)}$). Therefore, the G-S method provides faster convergence with less iteration numbers needed for obtaining the solution with desired accuracy. Moreover, the G-S method has lower memory requirements since old values are not stored but just simply replaced by new estimates. However, the G method is easier to be programmed. Especially in today's computing tools, the vectorized version of the G method can lead to faster solutions (even with significantly higher iteration numbers).

Using Eqns. (3-1) and (3.1-1), a special iterative algorithm for the G-S method can be derived - see Eqn. (4.1-3). By this formula, complex line-to-line voltage in a generic network bus i can be newly estimated. For all network PQ buses, Eqn. (4.1-3) is used directly.

$$\overline{V}_i^{(p+1)} = \frac{1}{\overline{A}_{ii}}\left[\frac{P_i - jQ_i}{\overline{V}_i^{(p)*}} - \sum_{k=1}^{i-1}\overline{A}_{ik}\overline{V}_k^{(p+1)} - \sum_{k=i+1}^{n}\overline{A}_{ik}\overline{V}_k^{(p)}\right] \tag{4.1-3}$$

However, the reactive power is unknown for PV buses and hence it must be computed in advance. From Eqn. (4.1-3), the formula for the reactive power injection can be derived when balancing total var generation and load - see Eqn. (4.1-4).

$$Q_i^{(p)} = -\mathbf{Im}\left\{ \overline{V}_i^{(p)*}\left[\sum_{k=1}^{i-1} \overline{A}_{ik}\overline{V}_k^{(p+1)} + \sum_{k=i}^{n} \overline{A}_{ik}\overline{V}_k^{(p)} \right] \right\} = Q_{Gi}^{(p)} + Q_{Li} \tag{4.1-4}$$

When applying both Eqns. (4.1-4) and (4.1-3), new complex voltage value can be obtained for each PV bus. However, the voltage magnitude is different from the initially specified value V_i^{sp}. Therefore, the scaling process must be performed to maintain the pre-set voltage magnitude - see Eqn. (4.1-5).

$$\left[\overline{V}_i^{(p+1)} \right]^{corr} = V_i^{sp} \times \overline{V}_i^{(p+1)} / V_i^{(p+1)} \tag{4.1-5}$$
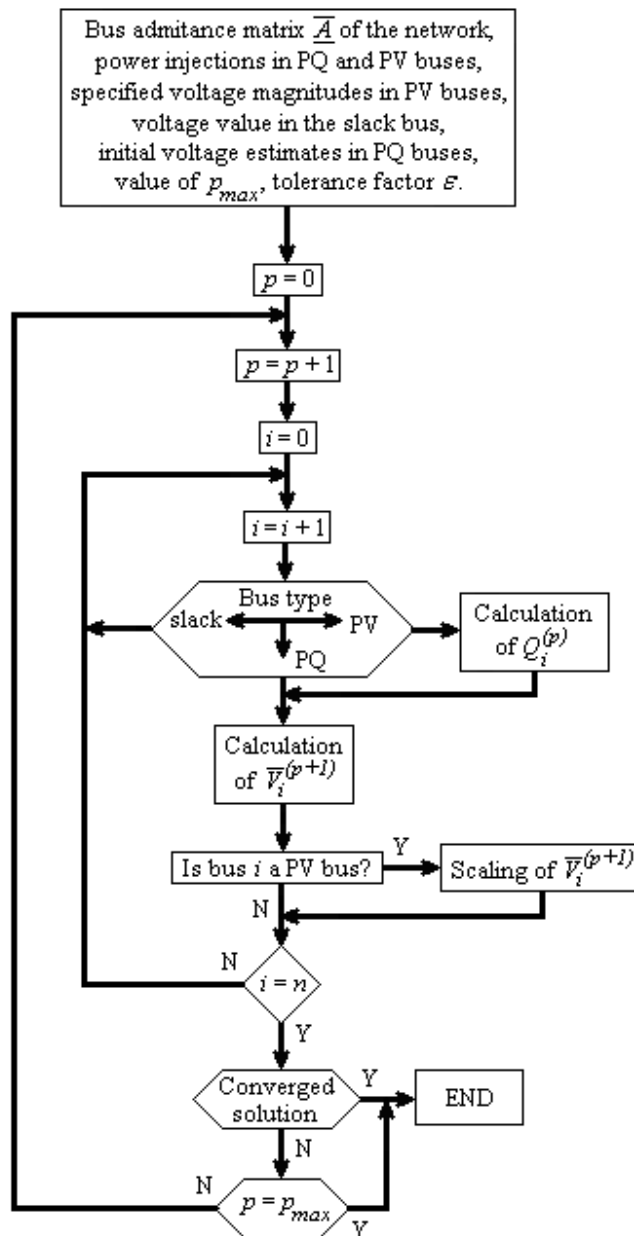
Fig. 4.1-1: Numerical procedure of the G-S algorithm - flow chart [20]

The most important task is to set suitable initial estimates for voltage magnitudes and voltage angles. When badly chosen, higher number of iterations may be needed or even divergence can occur. Referred to as the flat start, initial start points of 1.0 pu are usually used for all voltages in PQ buses (i.e. uniform voltage magnitudes). Another possibility is to apply the slack start where the voltage magnitude in the slack bus is used as the starting estimate. Nevertheless, the phase angle in the slack bus should be applied for all network buses as the initial guess.

The entire iterative process is as follows (Fig. 4.1-1). At the beginning, the bus admittance matrix is created from all network passive parameters and its topology. Next, Eqn. (4.1-3) is used directly for PQ buses or in combination with Eqns. (4.1-4) and (4.1-5) for PV buses in the first iteration. Then, the iteration is completed and both the convergence and divergence conditions are evaluated - see Eqns. (4.1-6) and (4.1-7).

$$\max_i \frac{\left|V_i^{(p+1)} - V_i^{(p)}\right|}{V_i^{(p)}} \le \varepsilon \qquad \max_i \left|\theta_i^{(p+1)} - \theta_i^{(p)}\right| \le \varepsilon \tag{4.1-6}$$

$$p \ge p_{\max} \tag{4.1-7}$$

If none of the conditions above is met, the iterative process continues for finding a good-converging solution with desired accuracy (tolerance factor ε) or for reaching the maximum number of iterations. In case of voltage mismatches, permitted tolerance value ε should be less than 10^{-6} pu to obtain reliable level of solution accuracy for all types of power systems. Alternative approach is to compare newly calculated power mismatches. Then, proper tolerance value should be between 0.005 and 0.01 pu to receive relatively exact load flow results. Maximum number of iterations should be set usually between 500 iterations for small-/medium-sized power systems, 5000 iterations for larger non-distribution networks and even 15000 iterations for distribution grids. For the G method, even tens of thousand iterations must be applied due to lower convergence speed. In case of PV buses with limited var generations or on-load tap-changing transformers, even higher maximum iteration numbers must be applied.

The advantages and disadvantages of the G and G-S methods are as follows:

+ code simplicity and high reliability

+ low computational, storage and CPU time requirements per iteration

- high total iteration numbers needed, only linear rate of convergence

- strong dependence of iteration numbers and CPU times on network size

- convergence problems for distribution and sparsely-meshed networks

Due to their simplicity, however, both of these methods are well used for educational purposes and still provided in many commercial and free load flow softwares (e.g. in [69], [70], [71]).

4.2 Newton-Raphson Method

More advanced numerical technique for the load flow analysis is the Newton-Raphson (N-R) method [1], [2], [3], [4], [5], [6], [8], [9], [10], [11], [12]. For the load flow

analysis, it is usually applied in its real form [1], [2], [3], [4], [5], [12]. For the derivation of the so-called power mismatch vector, Eqns. (3-1) and (3.1-6) are used first.

$$\overline{S}_i^* = P_i - jQ_i = \sqrt{3}\,\overline{I}_i\,\overline{V}_i^* = \left(\sum_{k=1}^{n}\overline{A}_{ik}\overline{V}_k\right)\overline{V}_i^* \tag{4.2-1}$$

When separating real and imaginary parts, relations for active/reactive power injections into bus i can be obtained - see Eqn. (4.2-2).

$$P_i = V_i\sum_{k=1}^{n}V_k\left(G_{ik}\cos\theta_{ik} + B_{ik}\sin\theta_{ik}\right)$$

$$\text{Note: } \theta_{ik} = \theta_i - \theta_k \tag{4.2-2}$$

$$Q_i = V_i\sum_{k=1}^{n}V_k\left(G_{ik}\sin\theta_{ik} - B_{ik}\cos\theta_{ik}\right)$$

Note: For real and imaginary components of the on-/off-diagonal admittance elements applies: $\mathrm{Re}\{\overline{A}_{ii}\} = G_{ii}$, $\mathrm{Re}\{\overline{A}_{ik}\} = G_{ik}$, $\mathrm{Im}\{\overline{A}_{ii}\} = B_{ii}$, $\mathrm{Im}\{\overline{A}_{ik}\} = B_{ik}$.

Active and reactive power mismatches in bus i are then simply obtained.

$$\Delta P_i = P_i - V_i\sum_{k=1}^{n}V_k\left(G_{ik}\cos\theta_{ik} + B_{ik}\sin\theta_{ik}\right)$$

$$\Delta Q_i = Q_i - V_i\sum_{k=1}^{n}V_k\left(G_{ik}\sin\theta_{ik} - B_{ik}\cos\theta_{ik}\right) \tag{4.2-3}$$

Power mismatches are obtained from the specified power injections and powers computed using the most recent values of state variables. When calculated, the power mismatches represent the solution accuracy in the current iteration. Thus, their values are decreasing rapidly to zero when approaching the solution. Both mismatch equations (4.2-3) are applied for each PQ bus while only the former is used for each PV bus. For a system of n buses and n_{PV} PV buses, only $(2n - n_{PV} - 2)$ equations must be built for the N-R method. Unknown variables are voltage magnitudes for the PQ buses and phase angles for all non-slack network buses. Thus, the number of state variables is equal to the number of mismatch equations.

Power mismatches can be further linearized using the Taylor series expansion around the current operating point (initial guess or new estimate). Higher-order terms (i.e. 1<) are neglected for obtaining simplified system of linear equations. This model remains highly accurate only for small changes of state variables from their initial guesses or estimates. Approximated (linearized) equations can be re-written into the relevant vector-matrix form with respect to the type of network bus - see Eqn. (4.2-4).

$$\begin{bmatrix}\Delta P^{(p-1)} \\ \Delta Q^{(p-1)}\end{bmatrix} = \begin{bmatrix}\underline{H}^{(p-1)} & \underline{N}^{(p-1)} \\ \underline{J}^{(p-1)} & \underline{L}^{(p-1)}\end{bmatrix} \cdot \begin{bmatrix}\Delta\theta^{(p)} \\ \dfrac{\Delta V^{(p)}}{V^{(p-1)}}\end{bmatrix} \tag{4.2-4}$$

Left vector in Eqn. (4.2-4) is often referred to as correction vector or state update vector since it contains unknown corrections (or updates) of individual state variables in the current iteration. Right matrix is called Jacobian or Jacobi matrix and consists of four submatrices $\underline{H}$, $\underline{N}$, $\underline{J}$ and $\underline{L}$ - see Eqn. (4.2-5). Corrections of voltage magnitudes ΔV are usually replaced by $\Delta V/V$. However, this change does not numerically affect the calculation

but simplifies the formulas for computing individual Jacobian terms using the most recent values of state variables.

$$H_{ik} = \frac{\partial P_i}{\partial \theta_k} \quad N_{ik} = V_k \frac{\partial P_i}{\partial V_k} \quad J_{ik} = \frac{\partial Q_i}{\partial \theta_k} \quad L_{ik} = V_k \frac{\partial Q_i}{\partial V_k} \tag{4.2-5}$$

When the Jacobian is invertible, unknown correction vector can be obtained iteratively either by matrix inversion or by the method of successive elimination of Eqn. (4.2-4). Application of sparsity techniques including near-optimal ordering and triangular (LU) factorization is also favourable especially for larger highly-sparse cases. Using these procedures, this most computationally demanding step in the N-R method can be significantly upgraded [1], [3], [4], [5], [6], [7], [22]. The Jacobian is highly sparse because its elements are non-zero only when buses i and k of the network are mutually interconnected. In real power systems, each bus is connected on average to 4-5 other buses. Therefore, the sparsity of the Jacobian is usually higher than 98 percent for larger networks [7]. When sparsity techniques applied, the CPU time for typical load flow studies of 2000+ buses, 3000+ lines and 500+ transformers can be reduced markedly below one second. Moreover, node elimination (Kron reduction) can be also applied [3].

Note: The Jacobian is symmetrical in structure but not in value, e.g. element H_{ik} does not have to be exclusively on $(i-k)^{th}$ position of the matrix.

Using calculated corrections $\Delta\theta$ and $\Delta V/V$, updating process of phase angles and voltage magnitudes can be performed - see Eqn. (4.2-6).

$$\theta_i^{(p)} = \theta_i^{(p-1)} + \Delta\theta_i^{(p)} \quad V_i^{(p)} = V_i^{(p-1)} + \left(\frac{\Delta V_i^{(p)}}{V_i^{(p-1)}}\right)V_i^{(p-1)} \tag{4.2-6}$$

Then, reactive power injections in PV buses can be also updated - see Eqn. (4.2-7).

$$Q_i^{(p)} = V_i^{(p)} \sum_{k=1}^{n} V_k^{(p)} \left(G_{ik}\sin\theta_{ik}^{(p)} - B_{ik}\cos\theta_{ik}^{(p)}\right) = Q_{Gi}^{(p)} + Q_{Li} \tag{4.2-7}$$

When new power mismatches are computed, they can be used for the convergence evaluation. As for the G-S method, similar convergence criterion is applied - see Eqn. (4.2-8).

$$\max_{i} \left|\begin{matrix} \Delta P \\ \Delta Q \end{matrix}\right| \leq \varepsilon \quad \text{, where } \varepsilon \text{ is the precision index value (mostly } 10^{-6} \text{ pu)} \tag{4.2-8}$$

Thus, the entire process is repeated until the maximum of the mismatch vector falls below the permitted tolerance ε or until the maximum number of iterations p_{max} is reached.

The entire procedure of the N-R method for the load flow analysis is as follows - see Fig. 4.2-1. At the beginning, identical input parameters as in the G-S method must be defined. The active and reactive power mismatches are computed primarily with given initial values of state variables (flat start). Convergence criterion is not met, therefore the first iteration is started with the calculation of Jacobian. Then, the new correction vector is computed for the update of state variables θ and V. Next, the reactive power injections in all PV buses are re-calculated and new power mismatch vector is obtained. The entire

process is repeated for reaching the required solution accuracy or the maximum number of iterations.
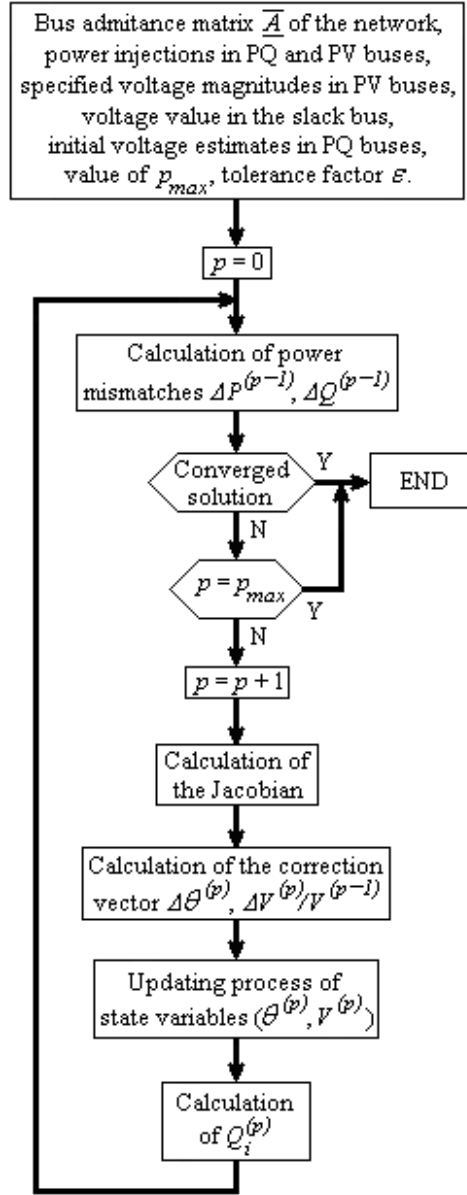
Fig. 4.2-1: Numerical procedure of the N-R algorithm - flow chart [20]

From Eqn. (4.2-5), the formulas for each element of submatrices $\underline{H}$, $\underline{N}$, $\underline{J}$ and $\underline{L}$ can be derived - see Eqns. 4.2-9 to 4.2-16.

$$H_{ii} = -\frac{\partial \Delta P_i}{\partial \theta_i} = \frac{\partial}{\partial \theta_i}\left(G_{ii}V_i^2 + V_i \sum_{\substack{k=1 \\ k \neq i}}^{n} V_k \left(G_{ik}\cos\theta_{ik} + B_{ik}\sin\theta_{ik} \right) \right) = -Q_i - B_{ii}V_i^2 \qquad (4.2\text{-}9)$$

$$N_{ii} = -V_i\frac{\partial \Delta P_i}{\partial V_i} = V_i\frac{\partial}{\partial V_i}\left(G_{ii}V_i^2 + V_i \sum_{\substack{k=1 \\ k \neq i}}^{n} V_k \left(G_{ik}\cos\theta_{ik} + B_{ik}\sin\theta_{ik} \right) \right) = P_i + G_{ii}V_i^2 \quad (4.2\text{-}10)$$

$$J_{ii} = -\frac{\partial \Delta Q_i}{\partial \theta_i} = \frac{\partial}{\partial \theta_i}\left(-B_{ii}V_i^2 + V_i\sum_{\substack{k=1 \\ k\neq i}}^{n} V_k\left(G_{ik}\sin\theta_{ik} - B_{ik}\cos\theta_{ik}\right)\right) = P_i - G_{ii}V_i^2 \quad (4.2\text{-}11)$$

$$L_{ii} = -V_i\frac{\partial \Delta Q_i}{\partial V_i} = V_i\frac{\partial}{\partial V_i}\left(-B_{ii}V_i^2 + V_i\sum_{\substack{k=1 \\ k\neq i}}^{n} V_k\left(G_{ik}\sin\theta_{ik} - B_{ik}\cos\theta_{ik}\right)\right) = Q_i - B_{ii}V_i^2 \quad (4.2\text{-}12)$$

$$H_{ik} = -\frac{\partial \Delta P_i}{\partial \theta_k} = V_iV_k\left(G_{ik}\sin\theta_{ik} - B_{ik}\cos\theta_{ik}\right) \quad (4.2\text{-}13)$$

$$N_{ik} = -V_k\frac{\partial \Delta P_i}{\partial V_k} = V_iV_k\left(G_{ik}\cos\theta_{ik} + B_{ik}\sin\theta_{ik}\right) \quad (4.2\text{-}14)$$

$$J_{ik} = -\frac{\partial \Delta Q_i}{\partial \theta_k} = -V_iV_k\left(G_{ik}\cos\theta_{ik} + B_{ik}\sin\theta_{ik}\right) = -N_{ik} \quad (4.2\text{-}15)$$

$$L_{ik} = -V_k\frac{\partial \Delta Q_i}{\partial V_k} = V_iV_k\left(G_{ik}\sin\theta_{ik} - B_{ik}\cos\theta_{ik}\right) = H_{ik} \quad (4.2\text{-}16)$$

Due to usually small angular displacements θ_{ik} in practical load flow studies, simplifications of trigonometric terms in Jacobian elements above are often applied to speed-up the load flow calculation [8], [18], [26].

$$\sin\theta_{ik} = \theta_{ik} - \frac{\theta_{ik}^3}{6} \approx \theta_{ik} \quad \cos\theta_{ik} = 1 - \frac{\theta_{ik}^2}{2} \quad (4.2\text{-}17)$$

Moreover, significant savings in calculation time can be achieved when calculating new Jacobian only in first two-three iterations of the numerical process where substantial changes of state variables are expected. For remaining iterations, the last computed inverse of the Jacobian is applied. Alternatively, the Jacobian can be updated only once per two or three iterations. However, more iterations may be needed to obtain the solution with desired accuracy. This procedure is often referred to as the Lazy N-R method [6].

The advantages and disadvantages of the N-R method are as follows:

+ quadratic rate of convergence

+ iteration numbers are independent of system size ($\approx$ 2-7 iterations needed)

+ low CPU time needed even for larger systems (higher than for G-S method)

+ partial derivatives of the Jacobian are useful for the sensitivity analysis

- iteration numbers visibly rise for var limits in PV buses or OLTC transformers

- 4-5 times higher memory/storage requirements than for the G-S method

- high sensitivity on initial state variable estimates

- strong uncertainty during the update process of state variables

Latter two disadvantages of the N-R method are very serious. Therefore, they are further discussed in detail.

Good behaviour of the N-R method is expected only when starting points are chosen near the physical solution. For highly loaded systems, where the voltages and angles are far from flat start values, divergence or convergence to unreasonable solutions may appear.

This is shown in Fig. 4.2-2, where the single-variable version of the N-R method is applied for solving a simple nonlinear problem with differently chosen start point. Then, the N-R method either a) converges to the physical solution, b) converges to a non-physical solution, c) converges with increased number of iterations or d) diverges.
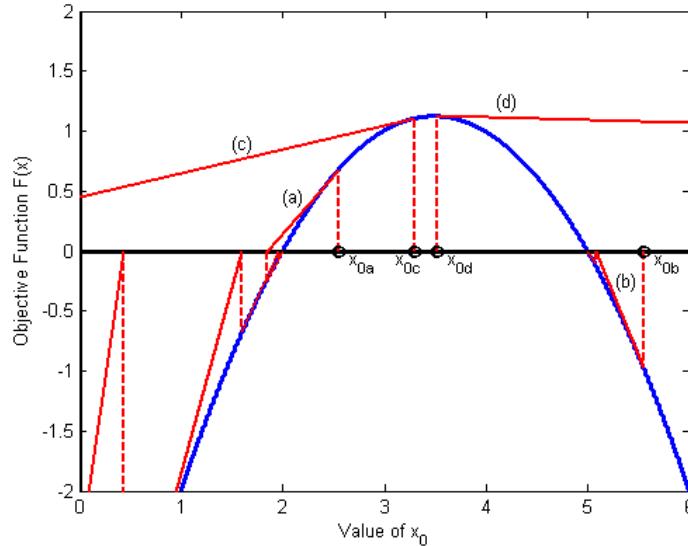
Fig. 4.2-2: Effects of different starting values on the N-R's convergence

For individual cases, it is very difficult to estimate the most suitable starting values ensuring the convergence to the physical solution. Once found useful initial values for one particular problem, they may show numerical instability for other cases. In load flow analysis, the regions of suitable initial values are fractals. In Fig. 4.2-3, fractal regions of a 2-bus power system are shown for different start points of V_2 and θ_2. Blue and green areas represent the convergence to the physical solution in less than 5 iterations and in 5-10 iterations. Convergence to other solutions and divergence are illustrated by magenta and cyan colours, respectively.
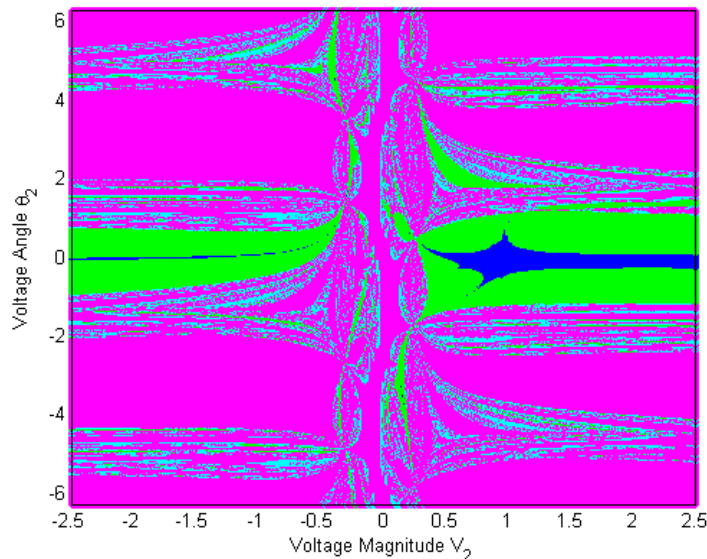
Fig. 4.2-3: Power-flow fractal regions of a 2-bus power system

33

During the updating process, the N-R method may behave also rather unstably. As can be seen in a pathological case of arctan function (Fig. 4.2-4), divergence behaviour can occur when employing full update in the second iteration (red lines). When using a partial update (magenta line) in the second iteration, convergence to the physical solution can be obtained.
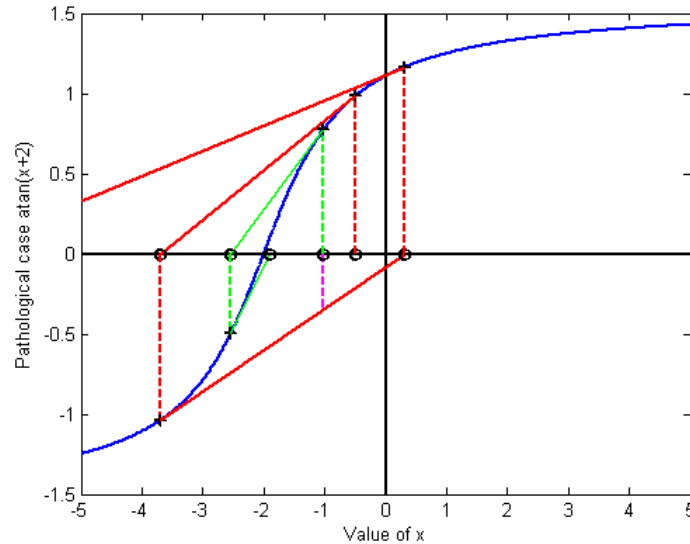
Fig. 4.2-4: Effects of full/partial updates on the N-R's convergence

Both the disadvantages of the N-R method are especially visible when solving highly sparse networks which are kept "on the edge" of their operating conditions (ill-conditioned systems). These networks are strongly sensitive on changes of state variables and are closely connected to the reactive power flows in the system. Moreover, power systems may be relatively close to the voltage collapse and may not to be solved due to the singularity of the Jacobian (see Chapter 8.1).

Note: Corrective strategies for N-R's convergence problems are suggested in [64].

Nowadays, the N-R method is still broadly used in power system centres for on-line controlling, contingency and optimal power flow studies, voltage stability and fault analyses, network planning, etc. Several modifications of the network topology are performed daily along with substantial changes in system loading in practical situations. Due to above mentioned numerical stability problems, the N-R method may not be able to perform the load flow analysis of such networks. Eventually, abnormal conditions can be reached threatening proper operation of the system.

4.3 Decoupled and Fast-Decoupled Load Flow Methods

As invented and first used in 1974 by B. Stott and O. Alsac [33], both of these numerical methods make the use of very strong dependences between voltage angles θ_i and active powers P_i and between the voltage magnitudes V_i and reactive powers Q_i [1], [2], [3], [4], [5], [8], [10], [11], [20], [65]. Changes of active/reactive power values by voltage magnitudes/angles remain insignificant. Based on this fact, submatrices $\underline{N}$ and $\underline{J}$ of the

Jacobian can be considered as zero and the load flow problem can be separated (decoupled) into two systems of equations. Significantly lower values of submatrices $\underline{N}$ and $\underline{J}$ are also caused by small values of angular displacements θ_{ik} and by small R/X ratios (in transmission networks).

In Eqn. (4.3-1), the iterative algorithm of the Decoupled method is shown.

$$\begin{bmatrix} \Delta P^{(p-1)} \\ \Delta Q^{(p-1)} \end{bmatrix} = \begin{bmatrix} \underline{H}^{(p-1)} & 0 \\ 0 & \underline{L}^{(p-1)} \end{bmatrix} \cdot \begin{bmatrix} \Delta \theta^{(p)} \\ \dfrac{\Delta V^{(p)}}{V^{(p-1)}} \end{bmatrix} \tag{4.3-1}$$

The decoupling itself can significantly speed-up the entire calculation process. To avoid calculating the elements of submatrices $\underline{H}$ and $\underline{L}$ iteratively, further simplifications were included. Angular displacements θ_{ik} are usually relatively close to zero. Moreover, the G_{ik} values are much lower than B_{ik} and Q_i negligible in comparison with B_{ii} (when in per units) in transmission networks.

$$\sin\theta_{ik} \approx 0 \quad \cos\theta_{ik} \approx 1 \quad G_{ik}\sin\theta_{ik} \ll B_{ik} \quad Q_i \ll B_{ii}V_i^2 \tag{4.3-2}$$

For small angular displacements (below 20 degrees), the error is less than 2 percent.

Also, the voltage magnitudes are usually very close to unity. Then, the modified elements of submatrices $\underline{H}$ and $\underline{L}$ can be computed.

$$H_{ii} = L_{ii} = -B_{ii}V_i^2 \quad H_{ik} = L_{ik} = -B_{ik}V_iV_k \tag{4.3-3}$$

Then, the iterative algorithm of the Fast-Decoupled (F-D) method is as follows:

$$\begin{aligned} \Delta P^{(p-1)}/V^{(p-1)} &= \underline{B}'^{(p-1)}\Delta\theta^{(p)} \\ \Delta Q^{(p-1)}/V^{(p-1)} &= \underline{B}''^{(p-1)}\Delta V^{(p)} \end{aligned} \tag{4.3-4}$$

Power mismatches are calculated using their exact definitions, no approximations are used. Matrices $\underline{B}'$ and $\underline{B}''$ of order $n_{PQ} + n_{PV}$ and n_{PQ} contain only constant susceptances B_{ii} and B_{ik} (with a negative sign) which can be taken directly from the bus admittance matrix $\underline{A}$. Therefore, the matrices (along with their inverses) can be computed only once at the beginning of the numerical process and used iteratively. However, full building of these matrices is recommended when implementing even further simplifications.

In matrix $\underline{B}'$:

      - to neglect all shunt compensation devices (even in Pie branch elements)

      - to use only nominal tap ratios

In matrix $\underline{B}''$:

      - to set zero tap angles to all transformers with complex tap settings

Furthermore, better performance of the F-D method can be achieved when neglecting series branch resistances either in matrix $\underline{B}'$ or $\underline{B}''$. This modification is often referred to as XB and BX versions of the F-D method, respectively. In [35], experimental results of the BX version are presented providing generally better convergence rate than by using the XB version. Moreover, it is also assumed that the XB version could have problems with high R/X ratios when solving distribution load flow cases. Therefore, further changes in

the structure of matrices $\underline{B}'$ and $\underline{B}''$ with respect to particular R/X ratio of each network branch were performed and tested in [66].

However, own testings of both XB and BX versions of the F-D method were performed in this thesis showing better performance of the former one. Also, higher numerical stability was maintained for distribution networks. Results are provided in a separated part of this thesis.
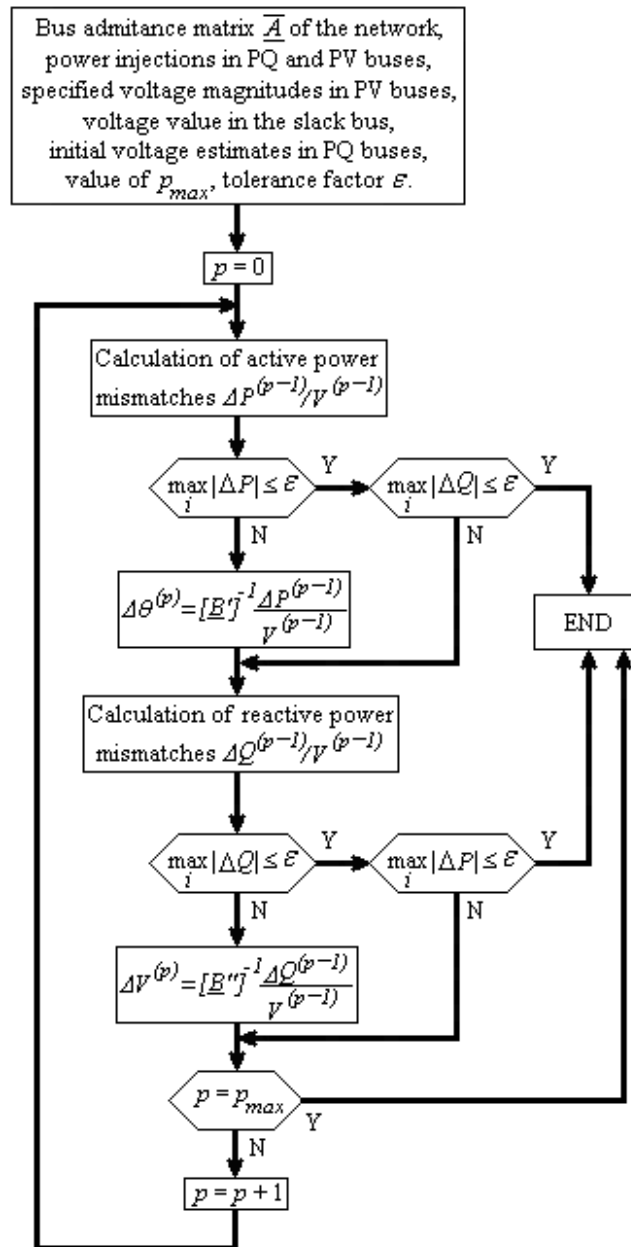
Fig. 4.3-1: Numerical procedure of the F-D algorithm - flow chart [8], [62]

The entire numerical process of the F-D method is divided into half-iterations - see Fig. 4.3-1. First, new values of voltage angles are computed using only active power mismatches ΔP with voltage magnitudes from the previous iteration. Then, new values of voltage magnitudes are obtained from only reactive power mismatches ΔQ and updated

voltage angle values. In other words, the latest solution estimates are always applied. The speed of convergence in P and Q half-iterations may be significantly different. Therefore, it is suitable to perform the check for convergence separately.

When incorporating PV buses with var limits into matrix $\underline{B}'$, this matrix would be modified always when any of PV buses hits its var limit. Thus, it is necessary to update this matrix iteratively for the calculation of voltage magnitude corrections.

The advantages and disadvantages of the F-D method are as follows:

+ convergence speed is comparable with the N-R method

+ numerically stable and reliable, less sensitive on initial voltage estimates

+ CPU requirements per iteration are 3-4 times lower than for the N-R method

+ storage requirements are about 40 percent lower than for the N-R method

+ partial derivatives can be used for sensitivity studies

- convergence rate decreases, it is only linear when approaching the solution

- higher iteration numbers needed, dependent on network size and PV buses

- convergence problems for ill-conditioned and some highly loaded systems

Due to the advantages above, the F-D method is the most suitable algorithm for performing checks for network instability, optimization studies, contingency calculations and on-line control of large-scale power systems.

4.4 DC Load Flow Analysis

When searching only for approximate solutions, the DC load flow analysis may be favoured [1], [3], [5], [12], [20]. The DC (lossless) load flow is the linearized approximation of the load flow problem. It considers voltage magnitudes equal to unity, fully neglects serious conductances for transmission power systems and assumes angular displacements near zero - see Eqns. (4.4-1) and (4.4-2). From these preconditions follows that the DC load flow method provides highly inaccurate results for distribution networks.

$$X_{ik} \gg R_{ik} \; \rightarrow \; G_{ik} = \frac{R_{ik}}{R_{ik}^2 + X_{ik}^2} \approx 0 \quad B_{ik} = -\frac{X_{ik}}{R_{ik}^2 + X_{ik}^2} = -\frac{1}{X_{ik}} \tag{4.4-1}$$

$$\theta_{ik} \approx 0 \qquad \rightarrow \qquad \cos\theta_{ik} \approx 1 \qquad \sin\theta_{ik} \approx \theta_{ik} \tag{4.4-2}$$

For active power branch flows and bus injections in per units, following formulas apply. Element j marks all network buses which are directly connected to bus i.

$$P_{ik} \approx \frac{\theta_{ik}}{X_{ij}} \quad \rightarrow \quad P_i = \sum_j \frac{\theta_{ik}}{X_{ij}} \tag{4.4-3}$$

In relevant matrix form, the algorithm of the DC load flow is presented in Eqn. (4.4-4). The slack bus must be excluded from the system of equations, otherwise the $\underline{C}$ matrix cannot be inverted.

$$[P] = [\underline{C}][\theta] \text{, where } C_{ii} = \sum_j \frac{1}{X_{ij}}, \; C_{ij} = -\frac{1}{X_{ij}} \tag{4.4-4}$$

The $Q - V$ equations are completely removed and the iterative approach is replaced by a simple one-step calculation of voltage angles in all network buses.

In this thesis, advanced version of the DC load flow method was developed to include given voltage magnitudes in PV buses and in the slack bus for the calculation of voltage angles. Moreover, it also considers actual tap magnitudes and angles for each transformer in the network. When developed from Eqn. (4.4-4), final mathematical formula is as follows.

$$[P] = [\underline{C}'][\theta] + [D] \tag{4.4-5}$$

Matrix $\underline{C}'$ and column vector D are built parallelly for each network branch (line, transformer) between buses i and k - see Eqn. (4.4-6).

$$
\begin{aligned}
C_{ii}' &= C_{ii}' + \frac{V_i V_k}{t_{ik} X_{ik}} & C_{ik}' &= C_{ik}' - \frac{V_i V_k}{t_{ik} X_{ik}} & D_i &= D_i - \frac{V_i V_k \lambda_{ik}}{t_{ik} X_{ik}} \\
C_{kk}' &= C_{kk}' + \frac{V_i V_k}{t_{ik} X_{ik}} & C_{ki}' &= C_{ki}' - \frac{V_i V_k}{t_{ik} X_{ik}} & D_k &= D_k + \frac{V_i V_k \lambda_{ik}}{t_{ik} X_{ik}}
\end{aligned} \tag{4.4-6}
$$

Eqn. (4.4-6) can be also used for lines since their tap magnitudes and angles are equal to 1.0 pu and 0.0 rad, respectively.

Using the DC load flow method, the calculation itself is very fast. CPU time reductions of order 100 are often observed. Despite only approximate solutions produced, the DC load flow is frequently used for basic analysis of electric power systems in order to screen all examined load flow cases and choose those which deserve further attention (e.g. during contingency analysis).

5. Numerical Improvements of Individual Load Flow Algorithms

Using specialized procedures, the focus is primarily placed on possible iteration and CPU time reductions of the G-S method and numerical stabilization capabilities of the N-R method. Great improvements in numerical performance of both methods are expected.

5.1 Improvements of the Gauss-Seidel Numerical Behaviour

For large-scale power systems and networks with high R/X ratios, the G-S method usually converges to the physical solution with inevitably increased numbers of iterations. One approach is to employ the R/X modification rules [65] for performing slight changes of high R/X rates in large distribution networks. In this way, better values of passive parameters can be obtained for avoiding divergence or slow-converging performance of the G-S method. Another approach lies in the use of special acceleration techniques for reducing numbers of iterations and CPU times. Investigation of the latter area was further performed in this thesis.

First procedure [1] may increase the rate of convergence using repeated iterative calculation of complex voltages. In other words, each complex voltage will be calculated twice in the current iteration for each PQ and PV network bus. This approach is very simple and it may have substantial positive impacts on total numbers of iterations needed.

Second procedure for considerable reduction of iteration numbers is the successive over-relaxation method [2]. This technique applies an acceleration factor γ to calculate new (accelerated) voltage values for each network bus - see Eqn. (5.1-1).

$$\overline{V}_{i\,acc}^{(p)} = \overline{V}_i^{(p-1)} + \gamma\left(\overline{V}_i^{(p)} - \overline{V}_i^{(p-1)}\right)$$
(5.1-1)

Value of γ must be chosen within the interval between 1.0 (no acceleration) and 2.0 (divergence). Its optimal value cannot be determined and reliably used for all load flow cases since varying from system to system. Badly estimated values may eventually lead to poor convergence or divergence. Only empirically found sub-optimal values from broad range of load flow studies can be efficiently employed. Proposed value is usually between 1.3 and 1.7, minimum numbers of iterations are often observed around 1.6 [2], [3], [4], [5], [31]. Above this point, highly stressed G-S method needs significantly more iterations. Therefore, the value of 1.6 is well recommended for iteration reduction. When observing slow convergence thereafter, the value of γ must be slightly decreased.

Third technique [22] describes the use of an acceleration and a retardation factor for effective reduction of total iteration numbers. In this thesis, presented algorithm was further improved by the acceleration of voltage magnitudes and voltage angles separately for all PQ and PV network buses - see Eqn. (5.1-2).

$$
\begin{aligned}
m_{i1} &\begin{cases} > 1.0 & if \quad \left(V_i^{(p+1)} - V_i^{(p)}\right) \times \left(V_i^{(p)} - V_i^{(p-1)}\right) \geq 0 \\ \leq 1.0 & if \qquad\qquad otherwise \end{cases} \\
m_{i2} &\begin{cases} > 1.0 & if \quad \left(\theta_i^{(p+1)} - \theta_i^{(p)}\right) \times \left(\theta_i^{(p)} - \theta_i^{(p-1)}\right) \geq 0 \\ \leq 1.0 & if \qquad\qquad otherwise \end{cases}
\end{aligned}
$$
(5.1-2)

Acceleration and retardation factors are represented by computed coefficients in Eqn. (5.1-2) with values above and below unity, respectively. When obtained, accelerated voltage magnitudes and angles can be obtained - see Eqn. (5.1-3).

$$V_{i\,acc}^{(p+1)} = V_i^{(p)} + m_{i1}\left(V_i^{(p+1)} - V_i^{(p)}\right) \quad \theta_{i\,acc}^{(p+1)} = \theta_i^{(p)} + m_{i2}\left(\theta_i^{(p+1)} - \theta_i^{(p)}\right) \tag{5.1-3}$$

Higher storage requirements are required for saving voltage values always from previous two iterations.

The essence of this procedure is graphically demonstrated in Fig. 5.1-1. If monotonous behaviour of the numerical process appears, acceleration factor should be used to speed-up the calculation (left). Otherwise, retardation factor must be applied to avoid possible numerical oscillations (right).
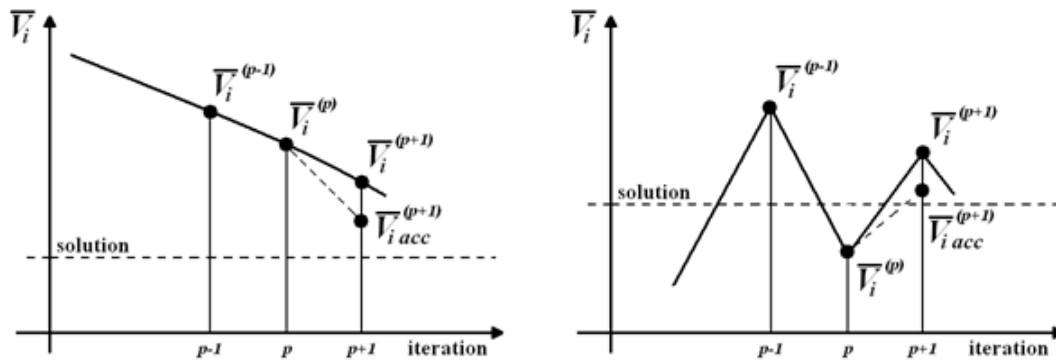
Fig. 5.1-1: Performance of the G-S method by acceleration and retardation factors [22]

Unfortunately, optimal combination of values for acceleration/retardation factors was not published in [22]. In this thesis, robust testing on broad variety of power systems was performed to find optimal factors for the best convergence behaviour of the G-S method.

5.2 Improvements of the Newton-Raphson Numerical Behaviour

To handle strong dependence of the N-R method on initial estimates, other than flat start guesses must be applied in case of ill-conditioned and slow-converging power systems. Therefore, the use of start point estimation methods is usually preferred to find better start values of state variables for the entire numerical process. The most powerful are the One-Shot F-D (OSFD) and One-Shot G-S (OSGS) methods [5], [65]. These procedures are located in the pre-processing part of the N-R method where a limited number of their iterations is applied before switching to standard N-R method. Currently, the One-Shot F-D algorithm is successfully employed in commercial software package PowerWorld Simulator [69].

In the N-R method, high uncertainty of the updating process can be significantly reduced in many ways. In [27], [28], power mismatch minimization approach is introduced. In this procedure, optimal value of the relaxation factor is calculated and used iteratively in the updating process to multiply computed corrections of state variables. With its value between 0.0 (no update) and 1.0 (full update), the mean power mismatch value can be minimized. For ill-conditioned networks, however, relaxation factor values can be iteratively

pushed close to zero producing only approximate solutions. Also, more complicated code and higher memory/CPU requirements must be considered.

Despite being usually neglected, alternative approach is to include the second order Taylor series expansion of power mismatch functions (i.e. the Hessian matrix) into the numerical process of the N-R method [30]. However, this method is very time-consuming even with sparsity techniques employed.

For this thesis, another highly effective and less time-demanding approach was adopted for iterative modification of correction vectors [65]. Due to quadratic convergence of the N-R method, significant changes in values of state variables are usually observed in adjacent iterations. Rarely, they may eventually result in divergence or convergence to a non-physical solution. Therefore, correction values should be curtailed when too high in absolute values. However, slightly increased iteration numbers (and CPU times) may be necessary. Therefore, compromise limit values for V and θ should be applied. Presented technique implements the continuous state update truncation (SUT) function (Fig. 5.2-1) to limit state variable corrections according to their currently computed value.
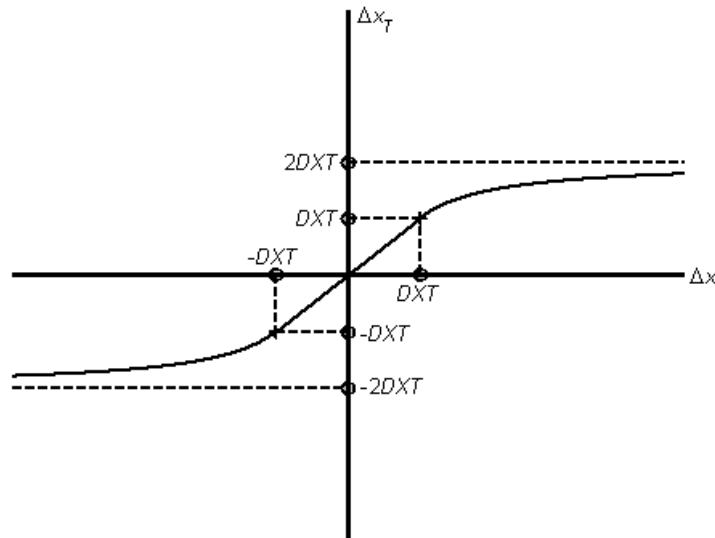
Fig. 5.2-1: State update truncation function [65]

In Eqn. (5.2-1), the relation between computed Δx and truncated Δx_T values is shown. This may represent more straightforward and effective way instead of placing two fixed limit values for both groups of state variables.

$$\Delta x_T = \begin{cases} \Delta x & if \ |\Delta x| < DXT \\ 2\mathrm{sgn}(\Delta x)DXT - \dfrac{DXT^2}{\Delta x} & if \ |\Delta x| \geq DXT \end{cases} \tag{5.2-1}$$

In [65], DXT values of 0.2 pu and 1.5 radians were used for corrections of voltage magnitudes and angles, respectively. In this thesis, extensive testing was performed for finding optimal DXT values for producing physical load flow solutions in highly reduced numbers of iterations.

6. PV Buses with Limited Var Generations in the Load Flow Analysis

In real power systems, voltage-controlling devices such as generators, synchronous condensers, static var systems and shunt inductors/capacitors can produce only constrained amount of reactive power. Their var limits $Q_{Gi\,\min}, Q_{Gi\,\max}$ are set to relevant values in accordance with their operation capabilities and continuous/discrete nature.

Voltage regulator is connected to each voltage-controlled bus maintaining the voltage magnitude at the pre-set value and the reactive power within the interval. If it fails to hold their values on the targets (due to system conditions), the particular PV bus must be switched to PQ bus with relevant var limit value exceeded. In the load flow analysis, such iterative switching may be correct only partially since unnecessarily higher numbers of PV buses must be switched to PQ. Therefore, specialized PV-PQ bus-type switching logics must be applied in individual load flow methods to maximize the numbers of devices which can still maintain their voltage-control abilities.

6.1 PV-PQ Bus-Type Switching Logic for the Gauss-Seidel Method

Above described logic of the voltage regulator is often adopted and used [1], [4], [10], [22]. In [1], the activation of this logic is considered at every iteration of the numerical process. In [22], its execution is proposed only at the end of the entire load flow simulation. Thus, the entire load flow analysis must be performed repetitively from the beginning in case of exceeding any of var limits defined.

As the contribution to the topic, more reliable logic was developed in this thesis. Proposed logic consists of two main sections, which are activated only when converging behaviour of the G-S method is obtained. In the former section, difference value M_i is found for each PV bus i exceeding one of its var limits - see Eqn. (6.1-1).

$$M_i = \begin{cases} Q_{Gi} - Q_{Gi\,\max} & if \quad Q_{Gi} > Q_{Gi\,\max} \\ Q_{Gi\,\min} - Q_{Gi} & if \quad Q_{Gi} < Q_{Gi\,\min} \end{cases} \tag{6.1-1}$$

In the latter section, only one PV bus with the greatest difference value is switched permanently to PQ. Such PV bus will be referred to as pathological PV bus - see Eqn. (6.1-2). Note: In previously presented logic, all PV buses exceeding their var limits were considered as pathological PV buses.

$$Q_{Gi} = \begin{cases} Q_{Gi\,\max} & if \quad Q_{Gi} > Q_{Gi\,\max} \quad AND \quad M_i = \max(M) \\ Q_{Gi\,\min} & if \quad Q_{Gi} < Q_{Gi\,\min} \quad AND \quad M_i = \max(M) \end{cases} \quad and \quad PV \rightarrow PQ \tag{6.1-2}$$

In this developed logic, each PV bus currently exceeding its var limit is either a PV bus affected by pathological PV buses or one of them directly. Under convergence criterion applied, this logic switches each pathological PV bus to PQ until all var generations are within the limits.

Due to convergence criterion, higher iteration numbers are required. However, such cautious approach must be taken for obtaining reliable and accurate solutions. If the criterion is too strict, correct load flow results are obtained with highly increased total

iteration numbers needed. When too relaxed, though, inaccurate solutions may be computed. Finally, compromise value of about 1-2 magnitudes higher than chosen precision index ε was suggested. Increase of iteration numbers should be significantly decreased using one of presented acceleration techniques with optimized factors.

Note: Commercial software PowerWorld Simulator [69] does not obtain any useful bus-type switching logic in its G-S method.

In this thesis, testing of this logic is performed on broad range of larger networks with high numbers of PV buses to show its numerical performance (reliability, accuracy).

6.2 PV-PQ Bus-Type Switching Logic for the Newton-Raphson Method

Robust and flexible logic for the N-R method [5], [11] contains the direct switching from PV to PQ (as in voltage regulators) - see Eqn. (6.2-1).

$$Q_{Gi} = \begin{cases} Q_{Gi\max} & if \quad Q_{Gi} > Q_{Gi\max} \\ Q_{Gi\min} & if \quad Q_{Gi} < Q_{Gi\min} \end{cases} \quad and \quad PV \rightarrow PQ \tag{6.2-1}$$

Moreover, it applies the reverse switching mechanism for converting some of switched PV buses back when certain conditions satisfied - see Eqn. (6.2-2).

$$V_i = V_i^{sp} \quad if \qquad \begin{matrix} Q_{Gi} = Q_{Gi\max} \ AND \ V_i > V_i^{sp} \\ OR \\ Q_{Gi} = Q_{Gi\min} \ AND \ V_i < V_i^{sp} \end{matrix} \quad and \quad PQ \rightarrow PV \tag{6.2-2}$$

Both logics are activated iteratively due to fast convergence rate of the N-R method, i.e. no convergence criterion applied.
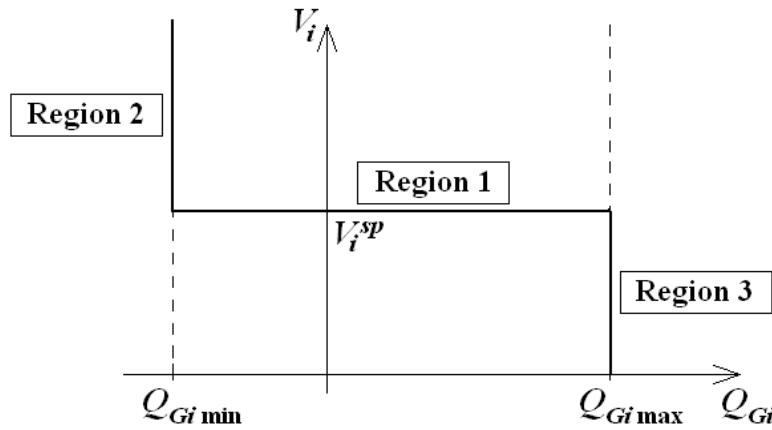
Fig. 6.2-1: Three operating regions for PV buses with limited var generations

Reverse switching logic corresponds to relatively strong dependence between voltage magnitudes and reactive powers. When the reactive power for PV bus i is constrained by its upper var limit and newly computed voltage magnitude V_i is higher than V_i^{sp}, the reactive power could probably move back into the permitted var region in case of restoring the pre-set voltage magnitude V_i^{sp}. This is the necessary condition for switching the PQ bus back to PV. This could analogically work also for PV buses kept on lower var limits with voltage magnitudes below V_i^{sp}. Therefore, only three situations (Regions 1/2/3) can

occur when dealing with PV buses in the load flow analysis – see Fig. 6.2-1. In remaining cases, reverse logic is used to switch particular PQ bus back to PV (Region 1). In [34], these cases are referred to as unstable branches, they are depicted by dashed lines in Fig. 6.2-1.

This logic is very straightforward, highly reliable and with potentially low or medium impact on total iteration numbers. However, authors in [34] draw attention to possible danger of bus type identification divergence consisting in repeated switching from PV to PQ back and forth without producing the solution. However, this logic is safely applied in commercial software package PowerWorld Simulator [69].

Note: This logic can be reliably used also for the F-D method [33]. However, another procedure [42] applies sensitivity factors to iteratively correct voltage magnitudes in PV buses with an exceeding var limit for reducing the var generation mismatch to zero.

In this thesis, comprehensive testing of this logic is accomplished on broad range of larger systems with high numbers of PV buses to show its performance in both the N-R and F-D methods. Comparison with the G-S method is also provided.

7. On-Load Tap-Changing Transformers in the Load Flow Analysis

From practical point of view, following types of on-load tap-changing (OLTC) transformers are often used in practice [1], [3], [6], [8], [13], [75].

- Transformers with variable tap magnitude for voltage control in the control (usually secondary-side) bus or in some remote network bus
- Transformers with variable tap magnitude for reactive power flow control to the secondary-side bus
- Transformers with variable tap phase shift for active power flow control to the secondary-side bus, so-called phase-shifting transformers

Note: Both symmetrical and asymmetrical types of phase-shifting transformers are normally employed. The former modify tap phase shifts while tap magnitudes remain unity (MW control). The latter change both tap magnitudes and angles (voltage/MW control). In this thesis, only symmetrical phase-shifting transformers are modelled.

For OLTC transformers, unknown taps must be included to both sets of output state variables and nonlinear load flow equations of the system [1], [2], [3], [4], [5], [6], [7], [8], [10], [12], [17], [18], [19], [36], [37], [38], [39], [40], [41], [65], [66]. Additional input data required are: starting tap settings, lower/upper tap limits, lower/upper V/Q/P limits, control bus number (PQ bus type, for voltage control only) and the tap step value. Lower/upper V/Q/P limits are needed to determine the target value which has to be maintained by changing the taps. Minimum/maximum or mean limit value is usually applied.

In professional and free load flow tools [69], [70], [71], alternative equivalent scheme of a two-winding transformer is mostly used for modelling off-nominal and OLTC transformers.
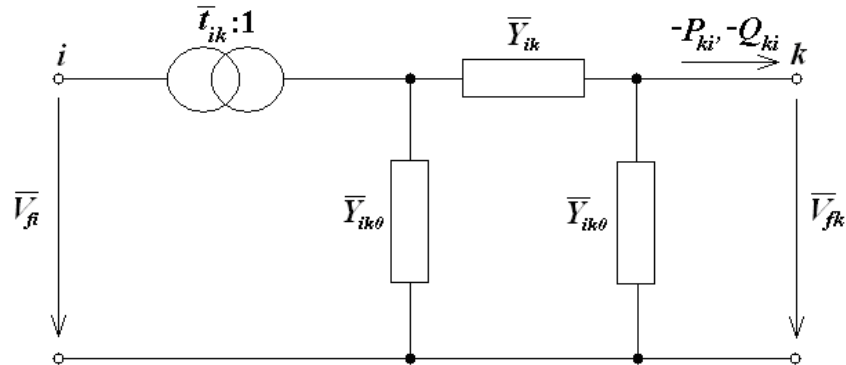
Fig. 7-1: Alternative equivalent circuit of a two-winding transformer

Comparing this circuit with the one in Fig. 3.2-2, only indices i and k are switched term $\bar{t}_{ik}$ is substituted with term $1/\bar{t}_{ik}$. Thus, the updating process of the bus admittance matrix is then performed as follows.

$$\overline{A}_{ii} = \overline{A}_{ii} + \left(\overline{Y}_{ik} + \overline{Y}_{ik0}\right)/t_{ik}^2 \qquad \overline{A}_{ik} = \overline{A}_{ik} - \overline{Y}_{ik}/\bar{t}_{ik}^*$$
$$\overline{A}_{ki} = \overline{A}_{ki} - \overline{Y}_{ik}/\bar{t}_{ik} \qquad \overline{A}_{kk} = \overline{A}_{kk} + \overline{Y}_{ik} + \overline{Y}_{ik0}$$

(7-1)

For the alternative equivalent circuit (Fig. 7-1), secondary-side/remote voltage magnitudes and reactive/active power flows are inversely related to tap magnitude or angle change. In other words, their values decrease with increasing tap magnitude and tap angle. Active/reactive power flows can be further derived for voltage/flow control.

$$P_{ik} = (G_{ik} + G_{ik0})(V_i / t_{ik})^2 - V_i V_k / t_{ik} [G_{ik} \cos(\theta_{ik} - \lambda_{ik}) + B_{ik} \sin(\theta_{ik} - \lambda_{ik})]$$

$$Q_{ik} = -(B_{ik} + B_{ik0})(V_i / t_{ik})^2 + V_i V_k / t_{ik} [B_{ik} \cos(\theta_{ik} - \lambda_{ik}) - G_{ik} \sin(\theta_{ik} - \lambda_{ik})]$$

$$P_{ki} = (G_{ik} + G_{ik0})V_k^2 - V_i V_k / t_{ik} [G_{ik} \cos(\lambda_{ik} - \theta_{ik}) + B_{ik} \sin(\lambda_{ik} - \theta_{ik})]$$

$$Q_{ki} = -(B_{ik} + B_{ik0})V_k^2 + V_i V_k / t_{ik} [B_{ik} \cos(\lambda_{ik} - \theta_{ik}) - G_{ik} \sin(\lambda_{ik} - \theta_{ik})]$$

(7-2)

In the numerical process, optimal taps (magnitudes/angles) are found for each OLTC transformer to hold its selected active variable as close as possible to its target. Calculated tap settings are continuous, while real taps are discrete multiples of the tap step and constrained by the minimum/maximum tap limit. Therefore, immediately after finding all taps during the analysis, they must be corrected to their nearest physical values, set fixed and some more iterations must be performed to reconverge with desired accuracy.

For each OLTC transformer, relevant positions in the bus admittance matrix must be iteratively modified by newly calculated taps - see Eqn. (7-3).

$$\overline{A}_{ii} = \overline{A}_{ii} + (1/t_{ik-new}^2 - 1/t_{ik-old}^2)(\overline{Y}_{ik} + \overline{Y}_{ik0})$$

$$\overline{A}_{ik} = \overline{A}_{ik} + (1/\overline{t}_{ik-old}^* - 1/\overline{t}_{ik-new}^*)\overline{Y}_{ik}$$

$$\overline{A}_{ki} = \overline{A}_{ki} + (1/\overline{t}_{ik-old} - 1/\overline{t}_{ik-new})\overline{Y}_{ik}$$

(7-3)

When adjusting both taps (OLTC transformers) and vars (PV buses with limited var generation) concurrently, numerical instability may appear. Then, it is recommended to block tap adjustments until the voltage magnitude correction with vars is calculated.

For discretely operating taps, the degree of freedom is increased and multiple generally correct solutions may be obtained by individual numerical algorithms especially for larger networks with high number of OLTC transformers. Among these solutions, the solution with the lowest total V/Q/P error should be taken as the best available solution.

Note: In professional package PSS®E 32 [74], advanced level of heuristic is used when solving load flow problems with OLTC transformers - e.g. tap movement deceleration factors for reducing the number of tap changes, adjustment threshold for the maximum tap change, etc.). In computational tool PowerWorld [69], tap-dependent voltage/MVAr/MW sensitivities are applied for the load flow analysis with OLTC transformers.

For real OLTC transformers, resistance and leakage reactance values vary with the tap settings activated due to certain winding portion being added or removed by the tap changer. Then, so-called impedance correction table provided by the manufacturer is included into the set input data and the bus admittance matrix is modified by both newly calculated taps and relevant passive parameters [4], [12], [36], [69], [74]. However, such precise modelling of OLTC transformers is not usually necessary.

Note: Voltage control in a remote network bus substitutes so-called line drop compensation [4], [74].

In case of parallelly operated OLTC transformers for voltage control, maximum difference of ±(1-2) tap positions is permitted to prevent circulating flows, higher losses and overloadings. As in practice, the Master-Slave method [46], [74] is usually applied in the load flow analysis. One of parallel transformers is marked as the Master, while the remaining ones as the Slaves. When a new tap is computed for the Master, this tap is automatically forced upon his Slaves. Thus, all these transformers have always identical taps during the iterative process. Note: About 50 % of new OLTC transformers in the U.S. are installed in parallel. Only 10 % of them are controlled by the Master-Slave method. The rest is operated by the Minimum Circulating Current method. Both of these methods are reliable when being used for more than 50 years [46].

7.1 Modelling of OLTC Transformers in the Gauss-Seidel Method

Due to relatively slow convergence of the G-S method, preferred strategy [11] is to calculate approximate number of tap positions to be passed iteratively for each OLTC transformer based on its V/Q/P error. This technique is applied only in the region of convergence to avoid its false actions in the flat start or directly after activating the PV/PQ bus-type switching logic. Note: Approach [11] seems to be more robust and faster compared to broadly used stepping technique [8], [13], [38] where changes of maximum ±1 tap step are performed at every iteration for voltage control. For MVAr/MW control, the stepping technique is not applied at all.

For voltage control, the entire process is as follows:

1) The calculation is initiated with starting tap ratios.

2) If pre-set convergence level reached, new numbers of tap step positions are computed directly. Note: Symbol $'^R'$ denotes the rounding process to the closest integer, bus m is a generic control bus (secondary-side or remote).

$$n_t = \left[\frac{V_m^{(p)} - V_m^{t\,arg}}{V_m^{(p)} \Delta t_{ik}} \right]^R \tag{7.1-1}$$

3) New tap ratio is obtained by:

$$t_{ik}^{(p+1)} = t_{ik}^{(p)} + n_t \Delta t_{ik} \tag{7.1-2}$$

4) Check on tap limits is performed.

$$t_{ik}^{(p+1)} = \begin{cases} t_{ik\,max} & if \quad t_{ik}^{(p+1)} > t_{ik\,max} \\ t_{ik\,min} & if \quad t_{ik}^{(p+1)} < t_{ik\,min} \\ t_{ik}^{(p+1)} & if \quad otherwise \end{cases} \tag{7.1-3}$$

5) Bus admittance matrix is updated by new taps, next iteration begins.

For MVAr/MW controls, partial derivatives of reactive/active power flows with respect to tap magnitudes/angles must be included, respectively.

$$\frac{\partial(-Q_{ki})}{\partial t_{ik}} = \frac{V_i V_k}{t_{ik}^2} \left[B_{ik} \cos(\lambda_{ik} - \theta_{ik}) - G_{ik} \sin(\lambda_{ik} - \theta_{ik}) \right] \tag{7.1-4}$$

$$\frac{\partial(-P_{ki})}{\partial \lambda_{ik}} = \frac{V_i V_k}{t_{ik}} \left[B_{ik} \cos(\lambda_{ik} - \theta_{ik}) - G_{ik} \sin(\lambda_{ik} - \theta_{ik}) \right] \tag{7.1-5}$$

Then, the MVAr/MW control mechanism is as continues:

1) The calculation is initiated with starting tap ratios.

2) If pre-set convergence level reached, new numbers of tap step positions are computed based on current MVAr/MW power flows and respective sensitivities.

$$n_t = \left[\frac{\left(-Q_{ki}^{(p)}\right) - \left(-Q_{ki}^{t\,arg}\right)}{\left[\partial\left(-Q_{ki}\right)/\partial t_{ik}\right]\Delta t_{ik}} \right]^R \quad \text{or} \quad n_\lambda = \left[\frac{\left(-P_{ki}^{(p)}\right) - \left(-P_{ki}^{t\,arg}\right)}{\left[\partial\left(-P_{ki}\right)/\partial \lambda_{ik}\right]\Delta \lambda_{ik}} \right]^R \tag{7.1-6}$$

3) New tap ratio (magnitude/angle) is obtained by:

$$t_{ik}^{(p+1)} = t_{ik}^{(p)} - n_t \Delta t_{ik} \quad \text{or} \quad \lambda_{ik}^{(p+1)} = \lambda_{ik}^{(p)} - n_\lambda \Delta \lambda_{ik} \tag{7.1-7}$$

4) Check on tap limits is performed.

$$t_{ik}^{(p+1)} = \begin{cases} t_{ik\,max} & if \ \ t_{ik}^{(p+1)} > t_{ik\,max} \\ t_{ik\,min} & if \ \ t_{ik}^{(p+1)} < t_{ik\,min} \\ t_{ik}^{(p+1)} & if \ \ otherwise \end{cases} \quad \text{or} \quad \lambda_{ik}^{(p+1)} = \begin{cases} \lambda_{ik\,max} & if \ \ \lambda_{ik}^{(p+1)} > \lambda_{ik\,max} \\ \lambda_{ik\,min} & if \ \ \lambda_{ik}^{(p+1)} < \lambda_{ik\,min} \\ \lambda_{ik}^{(p+1)} & if \ \ otherwise \end{cases} \tag{7.1-8}$$

5) Bus admittance matrix is updated by new taps, next iteration begins.

In this thesis, this voltage/MVAr/MW control methodology was further developed by controlling both OLTC transformers and PV buses with limited var generations together (identical pre-set convergence level applied). Using the proposed logic (see Chapter 6.1), only the transformer/PV bus with the greatest tap/var error is permanently switched to fixed/PQ mode with its tap/var value adjusted to the exceeded limit. This rather cautious approach is reliable but significantly increases total iteration numbers needed for convergence. This was the reason for optimizing the settings of acceleration/retardation factors (see Chapter 5.1) for faster numerical performance of the G-S method.

This methodology, however, brings also two serious problems: 1) When the sensitivities in Eqns. (7.1-1) and (7.1-6) are significantly higher than power errors in the numerators, rounding process may lead to stable tap settings even if the V/Q/P errors are still relatively large. Therefore, high sensitivities surprisingly produce no change in tap settings. 2) Oscillations between two tap settings may arise when none of them provides satisfiable V/Q/P value compared to respective target.

In this thesis, improved procedure with artificially excited tap oscillations is proposed and further tested. In case of voltage control, tap positions are moved in relevant directions by 1 when zero tap changes are computed but voltage errors are still larger than tap steps. For MVAr/MW control, identical process is performed when relevant MVAr/MW errors are above applied constant 0.005 pu. In some cases, these modifications automatically cause oscillations between two adjacent tap positions. Repeated jumps between individual tap settings are monitored including respective tap values and V/Q/P errors. When exceeding selected number of jumps (value of 12 applied), the tap setting with smaller target error is selected and such transformer is permanently switched to fixed-tap mode. Number of jumps for remaining oscillating OLTC transformer are then counted again from zero. This procedure will be definitely highly sensitive on network size and number of OLTC transformers, however, iteration numbers should be significantly pushed down using the proper acceleration technique.

Note: In commercial software PSS®E [74], no MVAr/MW control is realized in the G-S method. For these types of control, tap settings are assumed to be fixed.

7.2 Modelling of OLTC Transformers in the Newton-Raphson Method

Suitable approach, so-called the direct method, is to include one additional constraint for each OLTC transformer to load-flow equations and to the Jacobian [3], [5], [6], [8], [37], [38], [39], [40], [41], [74]. Based on control type, this constraint is as follows - see Eqn. (7.2-1). Note: Bus m is a generic control bus (secondary-side or remote).

$$V_m^{(p)} = V_m^{t\,arg}, \quad \left(-Q_{ki}^{(p)}\right) = \left(-Q_{ki}^{t\,arg}\right), \quad \left(-P_{ki}^{(p)}\right) = \left(-P_{ki}^{t\,arg}\right) \tag{7.2-1}$$

In the matrix form [5], [8], load-flow equations including the taps of OLTC transformers and relevant constraints are shown - see Eqn. (7.2-2).

$$\begin{bmatrix} \underline{H} & \underline{N} & | & x\partial P/\partial x \\ \underline{J} & \underline{L} & | & x\partial Q/\partial x \\ ---- & ---- & + & ---- \\ \partial y/\partial\theta & V\partial y/\partial V & | & x\partial y/\partial x \end{bmatrix}^{(p-1)} \begin{bmatrix} \Delta\theta \\ \Delta V/V \\ -- \\ \Delta x/x \end{bmatrix}^{(p)} = \begin{bmatrix} \Delta P \\ \Delta Q \\ -- \\ \Delta y \end{bmatrix}^{(p-1)} \tag{7.2-2}$$

For MVAr/MW control, flow mismatch Δy is defined.

$$\Delta y^{(p-1)} = y^{t\,arg} - y^{(p-1)} \tag{7.2-3}$$

Control variable y represents the active/reactive power flow, variable x is then the new state variable (tap magnitude/angle) for each OLTC transformer. For MVAr and MW controls, the correction vector contains the terms $\Delta t_{ik}/t_{ik}$ and $\Delta\lambda_{ik}$, respectively. If variable x exceeds its limit, respective row and column in Eqn. (7.2-2) is removed. Thus, two scenarios occur during the calculation:

1] Tap setting is inside its limits. Then, the tap ratio is the state variable while the voltage/flow value is kept constant. With the slack bus No. 1, vector of state variables is shown below:

$$[\theta_2,...\theta_n, V_2,...V_{m-1}, t_{ik}, V_{m+1},...V_n]^T, \quad [\theta_2,...\theta_n, V_2,...V_n, t_{ik}]^T, \quad [\theta_2,...\theta_n, V_2,...V_n, \lambda_{ik}]^T \tag{7.2-4}$$

2] Tap setting exceeds its limit. Then, the tap ratio is set fixed and the voltage/flow is the variable to be computed by the original set of load-flow equations. With the slack bus No. 1, vector of state variables is as follows:

$$[\theta_2, \theta_3,...\theta_n, V_2, V_3,...V_n]^T \tag{7.2-5}$$

For voltage control, an OLTC transformer is connected between buses i and k (bus i is the tap bus, bus k is the controlled bus). Control bus m is either identical to bus k or any other bus further in the network. Both the row and the column with variable x and y are excluded from Eqn. (7.2-2). If the tap remains within its limits, $\Delta V_m/V_m$ is replaced by $\Delta t_{ik}/t_{ik}$ in the state update vector. Formulas in Eqn. (7.2-2) are as follows:

$$N_{im} = -t_{ik}\partial\Delta P_i/\partial t_{ik} = t_{ik}\partial P_{ik}/\partial t_{ik} =$$
$$= -2(G_{ik} + G_{ik0})(V_i/t_{ik})^2 + V_iV_k/t_{ik}[G_{ik}\cos(\lambda_{ik} - \theta_{ik}) - B_{ik}\sin(\lambda_{ik} - \theta_{ik})] \tag{7.2-6}$$

$$N_{km} = -t_{ik}\partial\Delta P_k/\partial t_{ik} = t_{ik}\partial P_{ki}/\partial t_{ik} = V_iV_k/t_{ik}[G_{ik}\cos(\lambda_{ik} - \theta_{ik}) + B_{ik}\sin(\lambda_{ik} - \theta_{ik})] \tag{7.2-7}$$

$$L_{im} = -t_{ik} \partial \Delta Q_i / \partial t_{ik} = t_{ik} \partial Q_{ik} / \partial t_{ik} =$$
$$= 2(B_{ik} + B_{ik0})(V_i / t_{ik})^2 - V_i V_k / t_{ik} [B_{ik} \cos(\lambda_{ik} - \theta_{ik}) + G_{ik} \sin(\lambda_{ik} - \theta_{ik})] \tag{7.2-8}$$

$$L_{km} = -t_{ik} \partial \Delta Q_k / \partial t_{ik} = t_{ik} \partial Q_{ki} / \partial t_{ik} = V_i V_k / t_{ik} [G_{ik} \sin(\lambda_{ik} - \theta_{ik}) - B_{ik} \cos(\lambda_{ik} - \theta_{ik})] \tag{7.2-9}$$

In both submatrices $\underline{N}$ and $\underline{L}$, remaining rows in column m must be set to zero.

For MVAr control, an OLTC transformer is connected between buses i and k (bus i is the tap bus). Respective formulas in Eqn. (7.2-2) are as continues:

$$\Delta y = (-Q_{ki}^{t\,\mathrm{arg}}) - (B_{ik} + B_{ik0})V_k^2 + V_i V_k / t_{ik} [B_{ik} \cos(\lambda_{ik} - \theta_{ik}) - G_{ik} \sin(\lambda_{ik} - \theta_{ik})] \tag{7.2-10}$$

$$\partial y / \partial \theta_i = -V_i V_k / t_{ik} [B_{ik} \sin(\lambda_{ik} - \theta_{ik}) + G_{ik} \cos(\lambda_{ik} - \theta_{ik})] \tag{7.2-11}$$

$$\partial y / \partial \theta_k = V_i V_k / t_{ik} [B_{ik} \sin(\lambda_{ik} - \theta_{ik}) + G_{ik} \cos(\lambda_{ik} - \theta_{ik})] \tag{7.2-12}$$

$$V_i \partial y / \partial V_i = V_i V_k / t_{ik} [G_{ik} \sin(\lambda_{ik} - \theta_{ik}) - B_{ik} \cos(\lambda_{ik} - \theta_{ik})] \tag{7.2-13}$$

$$V_k \partial y / \partial V_k = 2(B_{ik} + B_{ik0})V_k^2 - V_i V_k / t_{ik} [B_{ik} \cos(\lambda_{ik} - \theta_{ik}) - G_{ik} \sin(\lambda_{ik} - \theta_{ik})] \tag{7.2-14}$$

$$t_{ik} \partial y / \partial t_{ik} = V_i V_k / t_{ik} [B_{ik} \cos(\lambda_{ik} - \theta_{ik}) - G_{ik} \sin(\lambda_{ik} - \theta_{ik})] \tag{7.2-15}$$

Remaining formulas needed are those derived in Eqns. (7.2-6) - (7.2-9).

For MW control, an OLTC transformer is connected between buses i and k (bus i is the tap bus). The formulas in Eqn. (7.2-2) are as follows:

$$\Delta y = (-P_{ki}^{t\,\mathrm{arg}}) + (G_{ik} + G_{ik0})V_k^2 - V_i V_k / t_{ik} [G_{ik} \cos(\lambda_{ik} - \theta_{ik}) + B_{ik} \sin(\lambda_{ik} - \theta_{ik})] \tag{7.2-16}$$

$$\partial y / \partial \theta_i = V_i V_k / t_{ik} [G_{ik} \sin(\lambda_{ik} - \theta_{ik}) - B_{ik} \cos(\lambda_{ik} - \theta_{ik})] \tag{7.2-17}$$

$$\partial y / \partial \theta_k = V_i V_k / t_{ik} [B_{ik} \cos(\lambda_{ik} - \theta_{ik}) - G_{ik} \sin(\lambda_{ik} - \theta_{ik})] \tag{7.2-18}$$

$$V_i \partial y / \partial V_i = V_i V_k / t_{ik} [G_{ik} \cos(\lambda_{ik} - \theta_{ik}) + B_{ik} \sin(\lambda_{ik} - \theta_{ik})] \tag{7.2-19}$$

$$V_k \partial y / \partial V_k = -2(G_{ik} + G_{ik0})V_k^2 + V_i V_k / t_{ik} [G_{ik} \cos(\lambda_{ik} - \theta_{ik}) + B_{ik} \sin(\lambda_{ik} - \theta_{ik})] \tag{7.2-20}$$

$$\partial y / \partial \lambda_{ik} = V_i V_k / t_{ik} [B_{ik} \cos(\lambda_{ik} - \theta_{ik}) - G_{ik} \sin(\lambda_{ik} - \theta_{ik})] \tag{7.2-21}$$

$$\partial P_i / \partial \lambda_{ik} = \partial P_{ik} / \partial \lambda_{ik} = V_i V_k / t_{ik} [G_{ik} \sin(\lambda_{ik} - \theta_{ik}) + B_{ik} \cos(\lambda_{ik} - \theta_{ik})] \tag{7.2-22}$$

$$\partial P_k / \partial \lambda_{ik} = \partial P_{ki} / \partial \lambda_{ik} = V_i V_k / t_{ik} [G_{ik} \sin(\lambda_{ik} - \theta_{ik}) - B_{ik} \cos(\lambda_{ik} - \theta_{ik})] \tag{7.2-23}$$

$$\partial Q_i / \partial \lambda_{ik} = \partial Q_{ik} / \partial \lambda_{ik} = V_i V_k / t_{ik} [G_{ik} \cos(\lambda_{ik} - \theta_{ik}) - B_{ik} \sin(\lambda_{ik} - \theta_{ik})] \tag{7.2-24}$$

$$\partial Q_k / \partial \lambda_{ik} = \partial Q_{ki} / \partial \lambda_{ik} = -V_i V_k / t_{ik} [B_{ik} \sin(\lambda_{ik} - \theta_{ik}) + G_{ik} \cos(\lambda_{ik} - \theta_{ik})] \tag{7.2-25}$$

For MVAr/MW control, all other positions in an extra row/column must be zero.

This methodology maintains highly sparse structure of the extended Jacobian. For n_{QP} number of OLTC transformers with MVAr/MW control, there are in total two matrices of sizes $[n_{QP}; 2n]$ and $[2n; n_{QP}]$ and one diagonal matrix of size n_{QP}. Due to majority of their positions being zero, they can be also sparsely defined. In submatrices of the extended Jacobian, rows/columns for the slack and PV buses must be excluded similarly as in the original Jacobian. The entire calculation process with OLTC transformers is as follows:

1) At iteration $p = 0$, controlled bus voltages for all OLTC transformers with voltage control are set to their targets. Initial tap magnitudes and angles are defined.

2) Iteration number is increased by one. Both the mismatch vector and Jacobian are computed (Eqn. 7.2-2) using original or modified formulas.

3) State update vector is calculated and the updating process of all state variables is accomplished. For x, updated value is obtained as follows.

$$t_{ik}^{(p)} = t_{ik}^{(p-1)} + \left(\frac{\Delta t_{ik}^{(p)}}{t_{ik}^{(p-1)}} \right) t_{ik}^{(p-1)} \qquad \lambda_{ik}^{(p)} = \lambda_{ik}^{(p-1)} + \Delta \lambda_{ik}^{(p)} \qquad (7.2\text{-}26)$$

4) Check for tap limits is performed. In case of a limit violation, such OLTC transformer is switched to be fixed, its controlled voltage/power is released and relevant changes in the Jacobian will be done.

5) Updating process of the bus admittance matrix is performed. Entire procedure continues from 2) until required convergence precision is obtained.

6) After reaching required convergence level, all tap magnitudes/angles are set fixed to their nearest physical values by the rounding process and several additional iterations are needed for the solution to re-converge.

Higher CPU times and iteration numbers are needed for numerical convergence. Numerical instability can even appear due to combined control by OLTC transformers and PV buses with var limits. Therefore, the priority mechanism is usually applied where blocking tap adjustments until the voltage magnitudes with vars are corrected. Alternatively, updated taps are calculated only when certain convergence level is reached [5], [68].

Note: Similar approach for modelling OLTC transformers in the N-R method is described in [67]. Rounding and reconvergence are included, var limits in PV buses omitted.

In [68], applied methodology in this thesis is evaluated as aggressive for pushing the regulated taps too often out of their limits and forcing the transformers to be permanently switched to be fixed. Instead, sensitivity approach is proposed for fast but gentle tap changes in the network. Moreover, special acceleration coefficients are employed to prevent tap oscillations and mutual influences among individual OLTC transformers. Similar techniques are also applied in the F-D method [11], [43], [44], [45], [56]. In [5], [33], so-called local feedback process recommends to use sensitivities of y only when reaching sufficient level of convergence to prevent oscillatory/divergence behaviour. One of these sensitivity techniques is also applied in professional software PowerWorld Simulator [69].

In this thesis, upgraded N-R method with algorithms for OLTC transformers for voltage/flow control has been developed. 1] The One-Shot F-D method is used for estimating better starting values for all non-control buses. 2] No priority mechanisms were applied due to escalated complexity of the code. 3] The rounding process to closest tap positions was avoided preferring rather continuous model of OLTC transformers (e.g. electronic transformers). 4] Suitable DXT values for taps were found and added into the SUT procedure for stabilizing the numerical performance. 5] Reverse logics for switching OLTC transformers back from the fixed to regulated mode were also proposed under certain conditions. However, so-called bus-type identification divergence was often observed. Therefore, this logic was not used in the final version of the code. 6] Master-Slave logics for two or more parallel OLTC transformers were applied.

The N-R method must be upgraded to a level, where networks with/without OLTC transformers can be safely examined with only slightly increased CPU time requirements.

8. Steady-State Voltage Stability Modelling and Assessment

Steady-state voltage stability is defined as the capability of the system to withstand a small disturbance without abandoning a stable operating point [4], [5], [9], [25], [59]. Voltage stability problems are bound with long distances between reactive power sources and loads, low source voltages, severe topology changes and low level of var compensation. Voltage collapse is not connected only with undervoltage scenarios since it may arise even during nominal voltage conditions. Moreover, variety of practical situations can lead to voltage collapse, e.g. tripping of parallelly connected line during the fault or reaching the var limit of a synchronous condenser/generator. Subsequent var reduction for voltage support is followed by higher branch currents, further voltage drops and var losses until the black-out occurs. This may occur in seconds to tens of minutes.

To prevent voltage collapse scenarios, e.g. shunt capacitors/inductors, series capacitors, SVCs, synchronous condensers and STATCOMs are applied. Furthermore, under voltage load shedding of low-priority loads [5], reconfigurations (connecting parallel lines/transformers/cables), power transfer limitations and activations of new generating units at most critical network areas are also used. OLTC transformers should be blocked during low voltage stability scenarios since each tap position corresponds to an increase of the load which eventually leads to higher branch losses and further voltage drops [4], [5], [47], [59]. These negative effects of OLTC actions are also presented in many studies with voltage stability margin calculation from synchrophasor measurements [57], [58].

8.1 Conventional Numerical Calculation of the Voltage Stability Problem

When increasing the loading (or loadability factor λ) of the system, its bus voltages slowly decrease due to the lack of reactive power. At the critical point (called singular or saddle-node bifurcation), characterized by maximum loadability factor λ_{max} and critical bus voltages, the system starts to be unstable and voltage collapse appears. From this point on, only lower loadings with voltage values lead to the solution. Note: Term bifurcation simply relates to the fact, that from the singular point there are two different voltage magnitudes for each network loading - the upper (stable) and the lower (unstable).

The dependence between bus voltage magnitudes and λ is graphically represented by the nose (V-P) curve. Unfortunately, the base-case position of the system operating point on the V-P curve is not known along with its distance from the voltage collapse (so-called voltage stability margin). Thus, the location of the singular point must be reliably found during the analysis.

Note: Values of λ_{max} and critical voltages are theoretical since they do not reflect voltage/flow limits of network buses/branches. When included, real maximum loadability λ_{max}^* can be found as the maximum value for keeping all network buses and branch loadings within the limits. Moreover, available var reserve must be also evaluated for individual points on the V-P curve.

Voltage stability is a dynamic problem, however, it can be described using the symbolic-complex method when system parameters move slowly. Thus, even approximate analytical solution can be obtained for 2-bus equivalent models of larger networks (Thévenin's equivalent) where the load flow equations loose strong nonlinearity and become linear.

More suitable approach for finding λ_{max} is to apply the Cycled N-R method for the base-case load flow analysis (i.e. for λ = 1.0). When obtaining current position on the V-P curve, network loading (i.e. loads/generations in selected network buses) is increased in defined manner by a certain step and the load flow is computed repetitively along with a new position on the V-P curve. This process continues in an infinite loop until the singular point is reached. However, total iteration numbers in each V-P step are gradually increasing so that when close to the singular point, the Cycled N-R method fails to converge. This relates to the fact, that Jacobian $\underline{J}_x$ becomes singular (i.e. $\det \underline{J}_x^* \approx 0$) and its inverse matrix cannot be computed.

For speeding up the calculation, variable step change is applied. When obtaining the divergence of the Cycled N-R method, the step size is simply divided by two and the calculation for the current V-P point is repeated until the convergence is achieved. If the current step size value reaches the pre-set minimum value, the calculation is stopped. Note: The Cycled N-R method enables the completion of the stable V-P part only. Unstable part including the singular point cannot be examined. Also, higher CPU requirements prevent this method to be employed for larger networks.

8.2 Continuation Load Flow Analysis

Continuation Load Flow (CLF) analysis [4], [7] suitably modifies conventional load flow equations to become stable also in the bifurcation point and therefore it is capable of drawing both upper/lower parts of the V-P curve. It uses a two-step predictor/corrector algorithm along with the new unknown state variable called continuation parameter (CP).

Predictor is a tangent extrapolation of the current operation point estimating approximate position of the new point on the V-P curve - see Eqn. (8.2-1).

$$
\begin{bmatrix} \theta \\ V \\ \lambda \end{bmatrix}^{predicted} = \begin{bmatrix} \theta_0 \\ V_0 \\ \lambda_0 \end{bmatrix} + \sigma \begin{bmatrix} & \vdots & \\ \underline{J}_x & \vdots & K \\ & \vdots & \\ \dots & \dots & \dots & \dots \\ & e_k & \end{bmatrix}^{-1} \begin{bmatrix} 0 \\ \vdots \\ 0 \\ 1 \end{bmatrix} \tag{8.2-1}
$$

Vector K contains base-case power generations and loads. Variables θ_0, V_0, λ_0 define the system state from the previous corrector step. Vector e_k is filled with zeros and certain modifications [4], [7] are implemented for selected CP in each network bus k at the current point on the V-P curve. Remaining elements in Eqn. (8.2-1) are the newly computed Jacobian $\underline{J}_x$ and step size σ of the CP.

Tangent predictor is relatively slow [5], anyway shows good behaviour especially in steep parts of the V-P curve. Note: The norm of tangent increments dV and $d\theta$ can be also used as an additional index for saddle-node proximity prediction. Unlike tangent predictor, secant predictor is simpler, computationally faster and behaves well in flat parts of the V-P curve. Close to the singular point and at sharp corners where a generator exceeds its var limit, however, it computes new predictions too far from the exact solution. This may eventually lead to serious convergence problems in the next corrector step.

Note: When the sharp corner arise straight in the singular point, it is called the limit-induced bifurcation point and contains no Jacobian singularities.

Corrector is the standard N-R algorithm for correcting state variables from the predictor step to satisfy load flow equations. Due to one extra parameter λ, additional Eqn. (8.2-2) must be included for keeping the value of the CP constant in the current corrector step. This condition makes the final set of equations non-singular even at the bifurcation point.

$$x_k - x_k^{predicted} = 0 \quad , \quad x = \begin{cases} \lambda & if \quad \text{CP} \ is \ \lambda \\ V & if \quad \text{CP} \ is \ V \end{cases} \tag{8.2-2}$$

Difference between both types of predictors and the entire process of the predictor/corrector algorithm is graphically demonstrated in Fig. 8.2-1. Horizontal/vertical corrections are performed with respect to chosen CP type.
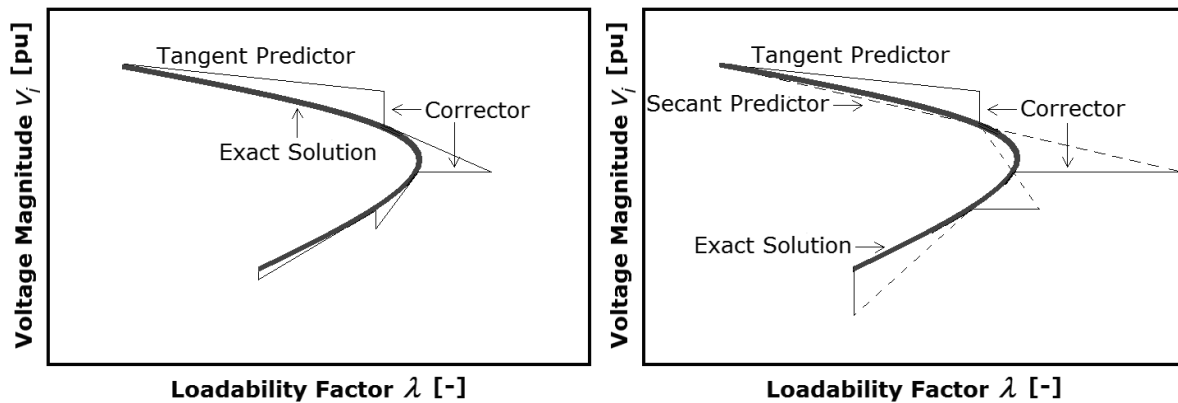
Fig. 8.2-1: Predictor/corrector mechanism for CLF analysis

As the CP, state variable with the highest rate of change must be chosen (i.e. λ and V in flat and steep parts of the V-P curve, respectively). When the process starts diverging, parameter σ must be halved or parameter CP must be switched from λ to V.

Step size should be carefully increased to speed-up the calculation when far from the singular point or decreased to avoid convergence problems when close to the peak. Step size modification based on the current position on the V-P curve (i.e. as a function of the line slope for previous two corrected points on the V-P curve) is recommended in [60]. This approach belongs to so-called rule-based or adaptive step size control algorithms.

Note: It is impossible to automatically presume that all PV buses will be switched to PQ in the bifurcation point. Many buses may still preserve their var compensation ability due to broad var limits or low local transfers of reactive power.

For comprehensive voltage stability analysis, several voltage stability margin indices were developed in the literature for finding the most critical buses/branches/areas of the system. In these regions, preventive or remedial actions should be taken.

Voltage stability margin indices (VSMI) [25], [59], [60] express percentage distance of base-case bus voltage magnitudes from their critical values - see Eqn. (8.2-3). Those buses with very low absolute VSMI values are too close to the voltage collapse.

$$\text{VSMI}_i = \left(V_{i\,(\lambda=1)} - V_{i\,(\lambda=\lambda_{\max})}\right)/V_{i\,(\lambda=\lambda_{\max})} \times 100\% \qquad (8.2\text{-}3)$$

Similar indices for branch angular displacements can be also defined [25]. Comparing base-case and critical angular values, the formula is as follows.

$$\text{VSMI}_{ik} = \left(\theta_{ik\,(\lambda=\lambda_{\max})} - \theta_{ik\,(\lambda=1)}\right)/\theta_{ik\,(\lambda=\lambda_{\max})} \times 100\% \qquad (8.2\text{-}4)$$

Relative reactive power reserve [53] should be also assessed at every point on the V-P curve - see Eqn. (8.2-5).

$$q_{reserve} = 1 - \sum_i^{PV} Q_{Gi} \Big/ \sum_i^{PV} Q_{Gi\,\max} \qquad (8.2\text{-}5)$$

VSMI values show the voltage proximities to the collapse point without any dynamics. Therefore, voltage-load bus sensitivities or voltage sensitivity factors (VSF) [4], [25] can be calculated - see Eqn. (8.2-6). Elements dV are the voltage increments computed by the tangent predictor in the singular point or its close vicinity.

$$\text{VSF}_i = dV_i \Big/ \sum_{k=1}^{n} dV_k \qquad (8.2\text{-}6)$$

In this thesis, collective evaluation of all these voltage stability indices and sensitivity factors is proposed for comprehensive voltage stability assessment of the power system. Individual factors/indices show only one half of the information needed. When combined, clearer picture about the system status can be seen. For example, voltage stability is especially critical for each bus with very low VSMI value but very high VSF value. Such buses and those with negative sensitivities (unstable operation) should be corrected in the first place.

Today, the CLF analysis still remains very popular for high-speed solving of voltage stability studies. Due to its reliable numerical behaviour, it is often included into the N-R method providing stable solutions even for ill-conditioned load flow cases. Moreover, it is applied in foreign control centres for N-1 on-/off-line contingency studies with frequencies of 5 and 60 minutes [5], respectively.

8.3 Properties of Author-Developed Codes in MATLAB Environment

Both Cycled N-R and CLF procedures were developed in MATLAB environment for providing fundamental examination of medium-sized and larger power systems in terms of steady-state voltage stability. Several key aspects of these codes are discussed below.

1] Predictor: Despite of computationally more complex algorithm, tangent predictor was used for finding reliable estimations of new V-P points especially around the singular point. Applied in the CLF algorithm only.

2] Corrector: First, corrector step is used at the start of the CLF program to find the base-case point for further calculations. Due to possible weak numerical stability at this point (for badly-scaled power systems), the OSFD procedure is implemented to the standard N-R method for providing more stable solutions and thus preventing numerical divergence. Moreover, voltage truncation (SUT algorithm) is also included into the state update process at every N-R's iteration. Both were also applied to the Cycled N-R algorithm to increase the loading range, for which the stable load flow solutions can be obtained (i.e. closer proximity to singular point can be reached).

3] Step size: Largest-load PQ network bus is chosen for computing the angle α between the horizontal and the line interconnecting two adjacent V-P points. Based on this, the step size evaluation function is applied - see Fig. 8.3-1.

$$\sigma = \begin{cases} \sigma_L & for & |\alpha| \geq \pi/8 \\ \sigma_U & for & |\alpha| \leq \pi/32 \\ A/\sin^2 \alpha + B & otherwise \end{cases} \qquad (8.3\text{-}1)$$

Upper and lower step limit constants σ_U and σ_L define the step size for the flat part of the V-P curve and for close vicinity to the singular point, respectively.
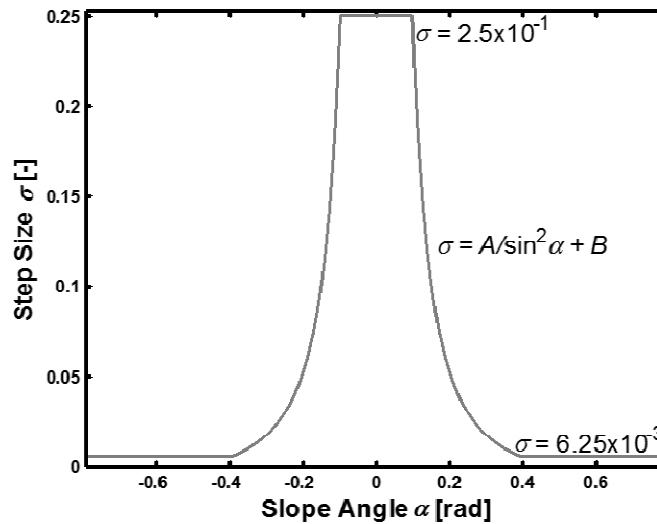
Fig. 8.3-1: Step size evaluation function

For the Cycled N-R algorithm, this is a rather too complex concept of step size control. Therefore, only a single step size is chosen at the start and a simple step-cutting technique (dividing by 2) is applied in case of divergence.

4] Ending criterion: Only stable part of the V-P curve (incl. exact singular point calculation) is computed by CLF code. Thus, if the computed value of λ begins to decrease, the process is stopped. For Cycled N-R code, the calculation is terminated when the step size falls below a certain small value (1×10^{-8}). For each load flow case, maximum number of iterations and permitted tolerance for convergence is set to 20 and 1×10^{-8}, respectively.

5] Calculation speed and accuracy: For excessively accurate voltage stability solutions, σ_U and σ_L values of 2.5×10^{-2} and 6.25×10^{-4} are used in the CLF algorithm. Rather

compromise values of 5×10⁻² and 1×10⁻² are also used to obtain fast and fairly accurate solutions for any of tested power systems. For Cycled N-R algorithm, initial step size of 2.5×10⁻² is chosen as sufficient.

6] Code versatility: Both Cycled N-R and CLF procedures are programmed so that the user directly specifies an arbitrary group of network buses for load/generation increase. From this set of buses, only those non-slack buses with non-zero active power loads/generations are activated for the analysis. Two scenarios can be activated by the user. a) L scenario increases both P/Q loads in selected PQ/PV buses with constant power factor (i.e. with identical increase rate). b) L+G scenario increases both P/Q loads in selected PQ/PV buses and P generations in selected PV buses (with identical increase rate). In both scenarios, more pessimistic constant var limits in PV buses were used.

7] Code limitations: a) Only identical increase rate is applied. However, implementing user-defined increase rates for each load/generation would not pose any serious problem. Only slightly more time-spending input data preparation by the user would be needed. b) Voltage and power flow limits were not considered for the evaluation of real maximum loadability λ^*_{max}.

8] Sparse programming: Sparsity techniques along with smart vector/matrix programming are used in both Cycled N-R and CLF codes to greatly decrease the CPU time.

9] Outputs: Theoretical value of λ_{max} and $V - \lambda$ data outputs for V-P curves are computed and graphically projected. Also, var reserve for each V-P point is calculated and stored along with all VSMI/VSF index values. Respective values of λ for switching some of PV buses permanently to PQ are also recorded. Finally, singularity type (saddle-node/limit-induced bifurcation) is determined for each network bus.

8.4 Shortest Distance to Voltage Instability

Voltage stability margin, i.e. the distance to voltage instability, is usually evaluated by stressing the system loading in certain predefined manner (with constant power factor, most probable scenario based on historical/forecasted data). However, it is also important to determine such loading pattern for all non-slack network buses, which results in the minimum stability margin. Then, such set of MW/MVAr bus increments has the minimum vector sum and causes the Jacobian to be singular when added to the base-case system loading.

One of the methods [4] is further explained on a simple 2-bus power system containing the PQ bus No. 2 with connected initial P/Q load. The aim is to find such loading scenario for P_{L2} and Q_{L2} which leads to minimum distance to black-out. In a P-Q 2D plane (see Fig. 8.4-1), initial loading (P_{L0}, Q_{L0}) can be projected. Curve S connects the load cases for which the Jacobian is singular and voltage instability occurs. All points inside the area and out of it represent stable and unstable voltage conditions, respectively. Note: For higher-dimensional cases, curve S turns to a general hypersurface.

Principle of the method is to increase the load from initial conditions in some chosen direction until voltage instability appears (point ①). The normal to curve S in this point

(vector η_1) is determined representing the new direction for initial load change. Thus, the system is stressed again from initial conditions with new loading scenario η_1 and new point ② on the curve S is reached. Loading scenario is updated by computing the normal to curve S (η_2). The process is iteratively repeated until convergence to the solution (shortest distance to instability) is obtained (point ⑤). In such case, the normal is exactly parallel to applied loading scenario direction. This method seems to be relatively simple and fast-converging.
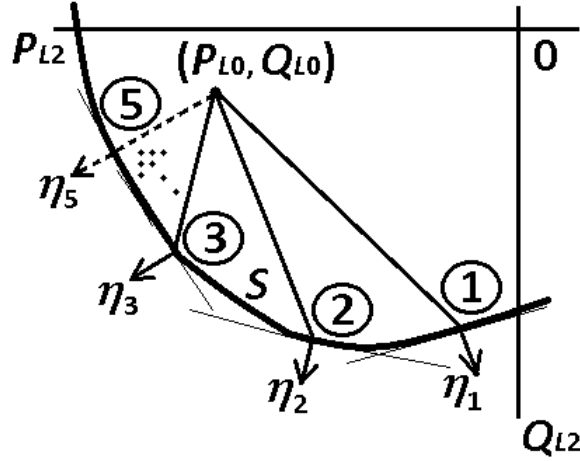
Fig. 8.4-1: Principle of the method

For an arbitrarily large power system, mathematical model of this method considers the increase of active/reactive power loads in PQ buses and active power generations in PV buses. Then, the N-R's Jacobian $\underline{J}_x$, state vector $x = [\theta; V]$ and parameter vector $\rho = [P; Q]$ have identical sizes, i.e. $n_{PQPV} = 2n_{PQ} + n_{PV}$. Note: Increase of active/reactive power loads and active power generations is considered only in those buses where real loads/generations are physically connected. The entire procedure is as follows:

1) The system is activated for initial load/generation stressing, i.e. i = 0. As the initial load/generation stressing, direction vector η_i with constant power factor (or equal increase rate) is recommended. Direction vector η_i is then normalized, i.e. $| \eta_i | = 1$.

2) The system is stressed from the initial system operating point (x_0, ρ_0) incrementally along a chosen direction η_i. Load/generation increase is defined as:

$$\rho_i = \rho_0 + k_i \eta_i \qquad (8.4\text{-}1)$$

3) Stressing is stopped when reaching the voltage stability singular point (x_i^*, ρ_i^*). The system in on the surface S and the Jacobian $\underline{J}_x$ is close to be singular. It applies:

$$\rho_i^* = \rho_0 + k_i \eta_i \qquad (8.4\text{-}2)$$

4) Distance to voltage instability k_i can be evaluated by the norm.

$$k_i = | \rho_i^* - \rho_0 | \qquad (8.4\text{-}3)$$

5) If the difference between two newly computed values of k_i falls below a pre-set convergence criterion (1×10^{-8}), the procedure is stopped and the shortest distance to voltage instability k_i^* is found. Otherwise, continue with step 6).

6) The left eigenvector w_i corresponding to zero real eigenvalue of singular matrix $\underline{J}_x^*$ is obtained. Index i is increased by 1 and the new direction vector η_i is calculated.

$$\eta_i = w_i \quad \text{and} \quad |\eta_i| = 1 \tag{8.4-4}$$

7) Move back to 2).

Using this procedure, the shortest distance to voltage instability k_i^* can be found. For such a point applies:

$$\rho_i^* = \rho_0 + k_i^* \eta_i^* \tag{8.4-5}$$

Minimum load/generation increases ($k_i^* \eta_i^* = \rho_i^* - \rho_0$) are also obtained for all network buses providing the most critical loading scenario for reaching the singular point.

For this methodology, several key ideas must be kept in mind. 1] Hypersurface S is to be completely smooth. However, this is not valid for PV buses with var limits. Therefore, possible actions of bus-type switching logics must be prevented. 2] Hypersurface S in the parameter space has an unknown shape. Therefore, only a local minimum dependent on the initial direction of load/generation stressing can be found. Therefore, an experienced guess based on measured/forecasted network operation should be employed to obtain a reasonable critical scenario. 3] Only the generators are assumed to be connected to PV buses, i.e. no loads in PV buses are considered.

To deal with all these problems, more robust approach must be applied instead of this rather simpler methodology, e.g. using particle swarm optimization [55].

In this thesis, the above describe optimization method was programmed and applied for load-only power systems (distribution networks, grids with no PV buses) using the modified Cycled N-R method. The goal was to provide sufficiently reliable and fast solutions since no professional softwares provide this type of voltage stability analysis and only a few pieces of literature are devoted to this problem.

9. Application of NEOS Server for Optimization on Load Flow Analyses

Conventional load flow methods may have serious problems to reliably perform load flow analysis when it is combined with many other tasks. An alternative lies in the use of optimization software packages which eventually can represent more straightforward and flexible approach without any visible drawbacks. Also, they can be used as verification tools to standard load flow techniques and methodologies.

In this thesis, the focus is placed on non-commercial optimization software package NEOS Server for Optimization [72]. NEOS (Network Enabled Optimization System) contains about 65 different solvers capable to deal with broad variety of problems including binary/integer variables and nonlinearities. For each examined problem, the user chooses appropriate solver and formulate the problem in the input data file using the specific text format (e.g. AMPL [21]). Then, such file is submitted to the NEOS Server through the e-mail/web interface. Then, the problem is sent to one of available Server's remote workstations where the entire optimization process is performed. When the optimal (or locally optimal) solution is found, the results are sent back to the NEOS Server and they can be seen on the Server's webpage or they can be delivered to the user's e-mail address. Note: In case of infeasible solutions obtained, the user is also informed about the analysis to make possible modifications to the input data file or solver settings.

NEOS solvers are free of charge but some of them may have limited use. According to the NEOS Server FAQ [72], time limits for solving each problem are set to 8 hours for linear and nonlinear optimization problems and 48 hours for problems containing integer variables. Other limitations, such as memory restrictions and maximum size of an input data file allocated, must be also taken into account by the user.

Problem simulations can be delayed significantly due to the fact that many other users are using NEOS Server in the same time, i.e. the queue of all the running or waiting jobs is already full. Total number of jobs running concurrently is approximately 7 while the queue capacity is around 35. Besides, each solver offers only a limited number of jobs being analyzed together in real time. Therefore, the new sent problem may be rejected during the peak times because of reasons above.

Regardless, the NEOS is rather robust programming tool for broad variety of optimization problems and its free use makes it even more attractive for many different research areas.

In this thesis, the challenge was to effectively define necessary input data structures about any analyzed power system for available NEOS solvers in AMPL format. Load flow, voltage/power control and voltage stability optimization problems were designed and further developed.

9.1 Load Flow Optimization Problem

In general, the load flow problem is a nonlinearly constrained, large-scale, static, non-convex optimization task [23] with both binary/continuous variables - Eqn. (9.1-1).

$$\text{minimize } f(x) \quad \text{subject to}: \quad g(x)=0, \quad h_l \le h(x) \le h_u, \quad x_l \le x \le x_u. \tag{9.1-1}$$

Function $f(x)$ is an objective function whose value has to be optimized. Vector $g(x)$ represents active/reactive power balance equations for each network bus - see Eqn. (9.1-2). All remaining equations, such as branch power flows, var injections from generation/compensation units and total power losses are included in vector $h(x)$ - see Eqns. (9.1-3) - (9.1-5), respectively. Unknown vector x comprises voltage magnitudes/angles in all system buses.

Balance equations confirm the 1st Kirchhoff's law validity for generators, loads and compensation devices on one side and power flows on the other.

$$0 = -P_{Gi} - P_{Li} - P_{shi} + \sum_{\substack{k=1 \\ k \ne i}}^{n} P_{ik} \qquad 0 = -Q_{Gi} - Q_{Li} - Q_{shi} + \sum_{\substack{k=1 \\ k \ne i}}^{n} Q_{ik} \tag{9.1-2}$$

Branch power flows represent both-side active/reactive power flows in the line/transformer between network buses i and k. In Eqn. (9.1-3), only one-side power flows through a line are shown.

$$P_{ik} = (G_{ik} + G_{ik0})V_i^2 - V_i V_k G_{ik} \cos(\theta_i - \theta_k) - V_i V_k B_{ik} \sin(\theta_i - \theta_k)$$
$$Q_{ik} = -(B_{ik} + B_{ik0})V_i^2 + V_i V_k B_{ik} \cos(\theta_i - \theta_k) - V_i V_k G_{ik} \sin(\theta_i - \theta_k) \tag{9.1-3}$$

Shunt power flows express active/reactive power flows from shunt compensators and supergrids connected to bus i. Signs correspond to the power flow direction.

$$P_{shi} = -G_{shi} V_i^2 \qquad Q_{shi} = +B_{shi} V_i^2 \tag{9.1-4}$$

Total power losses can be also included. Note: Loads are presented by corresponding negative value.

$$P_{Loss} = \sum_{i=1}^{n} (P_{Gi} + P_{Li} + P_{shi}) \qquad Q_{Loss} = \sum_{i=1}^{n} (Q_{Gi} + Q_{Li} + Q_{shi}) \tag{9.1-5}$$

All bus/branch input parameters and variables must be fully specified analogically as in the conventional load flow analysis, i.e. according to the bus/branch type. For individual variables, reasonable lower/upper limits must be carefully determined to ensure sufficient degree of freedom during the optimization process. Otherwise, the problem can be evaluated as unfeasible.

Var limits in PV buses are included using two additional binary variables (b_{li}, b_{ui}) expressing the voltage/var conditions for each PV bus - see Eqns. (9.1-6) and (9.1-7). Note: Parameter F is an arbitrarily large positive scalar constant (e.g. equal to 100 pu).

$$-F b_{ui} + V_i^{sp} \le V_i \le V_i^{sp} + F b_{li} \tag{9.1-6}$$

$$Q_{Gi\,min} + b_{ui}(Q_{Gi\,max} - Q_{Gi\,min}) \le Q_{Gi} \le Q_{Gi\,max} + b_{li}(Q_{Gi\,min} - Q_{Gi\,max}) \tag{9.1-7}$$

Based on the PV/PQ bus type-switching logic in the N-R method (Fig. 6.2-1), a particular PV bus i can be either still capable of voltage control ($b_{ui} = b_{li} = 0$) or one of the limits must be exceeded ($b_{ui} = 1$, $b_{li} = 0$ or $b_{ui} = 0$, $b_{li} = 1$). Combination $b_{ui} = b_{li} = 1$ leads to logical nonsense and thus, additional condition must be applied - see Eqn. (9.1-8).

$$b_{li} + b_{ui} \le 1 \tag{9.1-8}$$

Introduced binary variables are added to the set of expected outputs of the problem. For the load flow analysis, the sum of all PV-to-PQ-switched PV buses must be minimized to maintain voltage-var control ability. Therefore, the objective function is as follows - see Eqn. (9.1-9).

$$f(x) = \sum_{i}^{PV} (b_{li} + b_{ui})$$

(9.1-9)

Constraints in Eqns. (9.1-6) - (9.1-8) can be applied also to buses with unlimited var generations and even to systems without any PV buses (e.g. distribution networks). In such cases, random PQ bus must be converted into an equivalent PV bus as follows.

$$P_{Li}, Q_{Li} \quad \rightarrow \quad P_{Gi} = P_{Li}, \quad Q_{Gi\,\min} = Q_{Gi\,\max} = Q_{Li}, \quad V_i^{sp} = 1.0 \,\text{pu}$$

(9.1-10)

Due to identical var limits for this artificially defined PV bus, it will be permanently switched to the originally defined PQ bus. Thus, the objective function above can be safely used also for load flow cases with no PV buses.

9.2 Voltage and Reactive/Active Power Control Optimization Problem

OLTC transformers for voltage and power flow control can be also included to the load flow optimization problem. For each such transformer connected between buses i and k, tap limits with voltage/power targets and tap steps must be added to the set of input parameters. Final tap setting along with integer tap position counter m belong to the outputs of the optimization process - see Eqn. (9.2-1).

$$t_{ik} = m_{ik} \Delta t_{ik} \quad \text{or} \quad \lambda_{ik} = m_{ik} \Delta \lambda_{ik}$$

(9.2-1)

For each group of parallel OLTC transformers for voltage control, the equality constraint between their tap magnitudes is also defined.

Final voltage/power values must be kept as close as possible to their targets. Thus, the objective function containing the total V/Q/P quadratic error must be minimized - see Eqn. (9.2-2).

$$f(x) = \sum_{LTC\_V} \left(V_m - V_m^{t\,\text{arg}}\right)^2 + \sum_{LTC\_Q} \left(-Q_{ki} + Q_{ki}^{t\,\text{arg}}\right)^2 + \sum_{LTC\_P} \left(-P_{ki} + P_{ki}^{t\,\text{arg}}\right)^2$$

(9.2-2)

Note: Different approach, defining the load flow optimization task with OLTC transformers as a complementarity problem, is introduced in [38].

9.3 Voltage Stability Optimization Problem

In the load flow optimization problem, initial values for active/reactive power loads and active power generations in PV buses are defined as input parameters while the loadability factor $\lambda_{\max}$ and all critical values (i.e. voltage magnitudes/angles, power flows and injections) as the output variables. With respect to higher loading scenarios and much higher critical values of active system variables, limits for voltage magnitudes, phase angles, power injections, flows and losses must be significantly broader than for conventional load flow analysis. Lower/upper var limits for PV buses are considered constant for the entire analysis. Note: When setting the limits for voltage magnitudes properly, value of either $\lambda_{\max}$ or $\lambda_{\max}^*$ can be eventually obtained.

All load flow equality and inequality constraints are used also for the voltage stability optimization problem. Additional condition must be used for load/generation increase with constant power factor.

$$P_{Li} = \lambda P_{L0i} \quad Q_{Li} = \lambda Q_{L0i} \quad P_{Gi} = \lambda P_{G0i} \tag{9.3-1}$$

As the objective function, loadability factor must be maximized to find the singular point - see Eqn. (9.3-2).

$$f(x) = \lambda \tag{9.3-2}$$

Using the above problem definition, V-P curves and voltage collapse indicators (such as voltage-load sensitivities) cannot be provided. Nevertheless, these optimization (direct) methods [5] may be more straightforward and flexible than the CLF analysis for locating the bifurcation point of the examined power system.

9.4 Input Data Preparation - the AMPL Builder

For majority of available NEOS solvers in AMPL format, two input text files are needed - Model file and Commands file. The Model file is always required, since it contains all the necessary information describing the problem. The Commands file is optional, i.e. the calculation is still performed but without showing the results found. It can be used to a) display the results and/or b) modify the solver settings.

a) solve; display _varname, _var;

b) option solvername_options "fun_name1 = value1";

Load flow optimization problems pose increased burden for the user to prepare the input data file for each tested network with all necessary information and in required format. Input data volume is rather high even for smaller systems which makes the preparation very laborious. In this thesis, specialized program - the AMPL Builder - was created in MATLAB environment for converting load flow input data into AMPL format. Significant time savings can be achieved without a danger of manually created errors by the user. In Tab. 9.4-1, the volume of input data is demonstrated for broad range of tested systems. File size and preparation time are presented for standard load flow analysis. The latter was clocked at Pentium Dual-Core CPU 2.80 GHz - 1.96 GB RAM computer station.

Tab. 9.4-1: Demonstration of input data volume for NEOS solvers

case	buses	PV buses	branches	parameters	variables	constraints	text lines	size [B]	time [s]
IEEE9	9	2	9	50	62	66	234	13,018	0.2085
IEEE14	14	4	20	109	123	131	419	23,187	0.3283
IEEE30	30	5	41	200	243	253	752	42,774	0.5258
IEEE57	57	6	80	387	457	469	1369	80,032	1.0210
IEEE118	118	53	186	970	1155	1261	3442	194,944	2.2968
IEEE300	300	68	411	2163	2481	2617	7317	456,779	5.6017

The AMPL Builder was designed to make its use very simple and convenient also for larger power systems. Using AMPL Builder, the input data file for selected NEOS Solvers can be compiled within several seconds.

10. Author-Developed Tool for Load Flow Analyses - SimEPS v. 3.0

To accomplish all the targets of this doctoral thesis, programming tool SimEPS (Steady-State Simulations of Electric Power Systems) has been developed by the Author in MATLAB environment. It is mainly focused on load flow analysis (with var limits and OLTC transformers), voltage stability analysis (with var limits) and shortest distance to voltage instability (SDVI) analysis of test power systems. For this purpose, optimized and sparsely programmed iterative load flow methods and other codes were designed. Input data can be inserted in both per/physical units. Outputs can be stored in graphical/text format.

1] Load flow analysis

For the load flow analysis, the tool contains the G/G-S/N-R/F-D/DC load flow algorithms (SimEPS_G.m, SimEPS_GS.m, SimEPS_NR.m, SimEPS_FD.m and SimEPS_DC.m). Acceleration or stability techniques along with maximum iteration numbers and convergence tolerances can be selected by the user before starting the calculation.

As graphical outputs (SimEPS_Graph.m), voltage magnitudes, phase angles, bus types, var generations, tap magnitudes and tap angles can be iteratively drawn. Latter two are available for both G/G-S methods while only tap magnitudes can be plotted for the N-R method (V control only). In the F-D method, no algorithms for OLTC transformers were realized due to different programming strategy to be taken. Additionally, network scheme can be also projected along with maximum convergence error obtained iteratively.

As text outputs (SimEPS_Writer.m), final voltage/power bus conditions are saved along with branch power flows, losses, currents, power factors and loadings. For compensation devices, their final injections and loadings are stored as well. For OLTC transformers, final tap magnitudes/angles and total V/Q/P error value are also recorded. Total system generations, loads and losses are computed mostly for the comparison purposes with other methods. Understandably, only phase angles, branch active power flows and branch active power losses are the reasonable outputs of the DC load flow method. Remaining variables such as voltages, reactive powers, injections from shunt compensators, total system losses and slack bus injections are highly inaccurate.

For archival purposes, complete record is generated including the day and time of the record, overview of the tested network, number of iterations needed, CPU time taken and final mismatch value. Furthermore, limit violations (under-/over- voltages, branch over-/under- loadings, shunt compensator overloadings) are also highlighted.

2] Voltage stability analysis

For this task, both Cycled N-R (SimEPS_CNR.m) and CLF (SimEPS_CLF.m) methods can be applied. Tolerance value and maximum number of iterations are fixed while the set of buses for load/generation increase, one of L/L+G scenarios and the step size value(s) can be selected. Stable part of the V-P curve can be drawn only.

As graphical outputs (SimEPS_VS_Graph.m), network scheme, V-P curves for all network buses, var reserve and VSMI/VSF indices can be projected. The VSF indices are available only for the CLF algorithm.

As text outputs (SimEPS_VS_Writer.m), the day and time of the study along with the network overview is stored for archival purposes. Chosen scenario (L, L+G), set of buses, step size(s), number of stable V-P points, total CPU time and theoretical maximum loadability values are saved. Bus voltage magnitudes, phase angles and var injections for the base case and the singular point are also included along with the singularity type (saddle-node, limit-induced) of each network bus and loadability values for which a particular PV bus was switched to PQ. Also, the VSMI/VSF indices are sorted according to size and recorded.

3] SDVI analysis

In the SDVI analysis, the PQ-only networks can be solved using the modified version of the Cycled N-R method (SimEPS_SDVI.m). Set of buses for load increase and the initial step size value are to be selected by the user, while the tolerance, maximum number of iterations and of stable V-P points are set fixed.

As graphical outputs (SimEPS_SDVI_Graph.m), network scheme with distances to instability, total MW/MVAr loadings and critical MW/MVAr bus increments can be plotted.

As text outputs (SimEPS_SDVI_Writer.m), the day and time of the study with the network overview is stored for archival purposes. Set of buses, initial step size, total CPU time and the SDVI value are saved. Initial MW/MVAr network loading along with distances to instability, maximum MW/MVAr network loadings and minimum real eigenvalues of the critical Jacobian are recorded for every loading scenario. For each bus, critical MW/MVAr increments leading to voltage instability are included in tabular form as well.

4] AMPL Builder

For comparison purposes, AMPL Builder (AMPL_Builder_v3.m) is also incorporated into SimEPS to generate input data of the load flow analysis (also with V/Q/P control) and the voltage stability analysis for online optimization package NEOS Server for Optimization.

10.1 Input Data Format in Per Units for SimEPS Software

Tool SimEPS is operated in MATLAB environment through its main graphical user interface (SimEPS.m). It is usefully created for interactive and user-friendly loading of input data (in physical/per units), selection of computational procedures, projection of graphical outputs and saving of text/numerical/graphical outputs. It is designed for active switching between individual graphical figures and multiple launching of the analysis. Also, it includes complete Help section as the guide for new users of this tool.

To be applicable for a broad range of problems, rather complex input data format was developed in both physical/per units. Unfortunately, high demands on the user for creating the input data file with all necessary information are noticeable.

In per units, the input data file must contain four mandatory matrices (M0, M1, M2, M4) and three supplementary matrices M3, M5_1 and M5_2. Matrix M0 consists of a brief description of the load flow case (i.e. the name of the network, the source from which it was taken, etc.). Data in this matrix are used only for archival purposes.

Matrix M1 contains 17 columns for each network branch (line/transformer):
- column 1   ...   branch number (1, 2, ...)
- column 2   ...   branch type

0	–	power lines
1	–	transformers with fixed tap ratios
2, 3, -1	–	OLTC transformers for V/Q/P control

- column 3   ...   from-bus (tap-bus) number
- column 4   ...   to-bus (Z-bus) number
- column 5   ...   control-bus number (for the OLTC transformer with V control)
- column 6   ...   series resistance of the branch (in pu)
- column 7   ...   series reactance of the branch (in pu)
- column 8   ...   total shunt conductance of the branch (in pu)
- column 9   ...   total shunt susceptance of the branch (in pu)
- column 10   ...   tap ratio (in pu, on tap-bus side, 0 – for power lines)
- column 11   ...   tap angle (in degrees, usually zero)
- column 12   ...   minimum tap limit for OLTC transformers (in pu)
- column 13   ...   maximum tap limit for OLTC transformers (in pu)
- column 14   ...   tap step for OLTC transformers (in pu)
- column 15   ...   minimum V/Q/P value (in pu)
- column 16   ...   maximum V/Q/P value (in pu)
- column 17   ...   branch loading limit (in A for lines, in VA for transformers)

Matrix M2 contains total of 15 columns for each network bus:
- column 1   ...   bus number (1, 2, ...)
- column 2   ...   bus type (1 – slack bus, 2 – PQ bus, 3 – PV bus)
- column 3   ...   nominal voltage level in the bus (in kV)
- column 4   ...   active load in the bus (in pu, negative for the load)
- column 5   ...   reactive load in the bus (in pu, negative for the load)
- column 6   ...   voltage magnitude (in pu, pre-set value or initial estimate)
- column 7   ...   voltage angle (in degrees, for the slack bus may be non-zero)
- column 8   ...   minimum var limit (in pu, for PV buses only)
- column 9   ...   maximum var limit (in pu, for PV buses only)
- column 10   ...   active power generation (in pu, for PV buses only)
- column 11   ...   reactive power generation (in pu, for PV buses, set to zero)
- column 12   ...   conductance of the shunt compensation device (in pu)
- column 13   ...   susceptance of the shunt compensation devices (in pu)
- column 14   ...   minimum voltage limit (in pu, for archival purposes only)
- column 15   ...   maximum voltage limit (in pu, for archival purposes only)

Matrix M3 contains 4 columns to describe graphical position of each network bus:
- column 1   ...   bus number (1, 2, ...)
- column 2   ...   x-coordinate (zero is on the left of the monitor)
- column 3   ...   y-coordinate (zero is on the top of the monitor)
- column 4   ...   type of the bus (1 – horizontal, 2 – vertical)

Matrix M4 consists of bus names in the string data format. These names are used in the output data file for listing bus/branch outputs.

Both matrices M5_1 and M5_2 include additional data to those in matrix M3 for network visualization. When drawing the scheme, each bus is represented by either horizontal or vertical thick busbar with 20 connection points. Each connection point is used only for connecting one branch or bus device (generator, load, etc.). This concept is suitable especially for parallel network branches. Therefore, matrix M5_1 contains connection points for both sending/receiving buses of each network branch. Matrix M5_2 specifies connection points for adding synchronous generators/condensers, loads, compensation devices and superior networks to each network bus.

Creating of matrices M5_1 and M5_2 is rather laborious for the user. Therefore, specialized program (SimEPS_Optimizer.m) was created for filling these two matrices with proper values in much easier and faster way. Then, drawing process of the network scheme is performed automatically by SimEPS. However, some manual corrections are still needed.

10.2 Input Data Format in Physical Units for SimEPS Software

Due to different input data format for some systems, physical units were also included. In physical units, similar five matrices M00, M11, M22, M33 and M44 must be defined. Matrices M00 and M44 have the same structure and content as for the per-unit system. Equivalent matrices to matrices M5_1 and M5_2 are not considered.

Matrix M11 contains 9 columns of data for each line of the network:
- column 1   ...   branch number (1, 2, …)
- column 2   ...   from-bus number
- column 3   ...   to-bus number
- column 4   ...   series resistance (in Ω/km)
- column 5   ...   series reactance (in Ω/km)
- column 6   ...   shunt susceptance (in S/km)
- column 7   ...   shunt conductance (in S/km)
- column 8   ...   length of the line (in km)
- column 9   ...   current loading limit of the line (in A)

Matrix M22 consists of 17 columns for each network bus:
- column 1   ...   bus number (1, 2, …)
- column 2   ...   bus type (same as for the per-unit system)
- column 3   ...   nominal voltage level in the bus (in kV)
- column 4   ...   active load in the bus (in W, negative for the load)
- column 5   ...   reactive load in the bus (in VAr, negative for the load)
- column 6   ...   voltage magnitude (in V, pre-set value or initial estimate)
- column 7   ...   voltage angle (in degrees, for the slack bus may be non-zero)
- column 8   ...   x-coordinate (zero is on the left of the monitor)
- column 9   ...   y-coordinate (zero is on the top of the monitor)
- column 10   ...   minimum var limit (in VAr, for PV buses only)
- column 11   ...   maximum var limit (in VAr, for PV buses only)
- column 12   ...   active power generation (in W, for PV buses only)
- column 13   ...   reactive power generation (in VAr, for PV buses, set to zero)

- column 14 ... conductance of the shunt compensation device (in S)
- column 15 ... susceptance of the shunt compensation device (in S)
- column 16 ... minimum voltage limit (in pu, for archival purposes only)
- column 17 ... maximum voltage limit (in pu, for archival purposes only)

Matrix M33 includes 11 columns for describing each transformer in the network:
- column 1 ... transformer number (1, 2, ...)
- column 2 ... Z-bus number
- column 3 ... tap-bus number
- column 4 ... nominal apparent power (in VA)
- column 5 ... nominal primary voltage level (in V)
- column 6 ... short-circuit voltage (in %)
- column 7 ... no-load current (in %)
- column 8 ... short-circuit power losses (in W)
- column 9 ... no-load power losses (in W)
- column 10 ... nominal tap setting (ratio btw. primary/secondary voltages)
- column 11 ... tap angle (in degrees)

Note: OLTC transformers are not specified in the physical-unit system.

During the analyses, physical data are always converted into the per-unit system due to faster numerical convergence. Base power of 100 MVA is always applied.

10.3 Graphical Demonstration of SimEPS Software

Selected graphical outputs of SimEPS are provided - see Figs. 10.3-1 to 10.3-5.
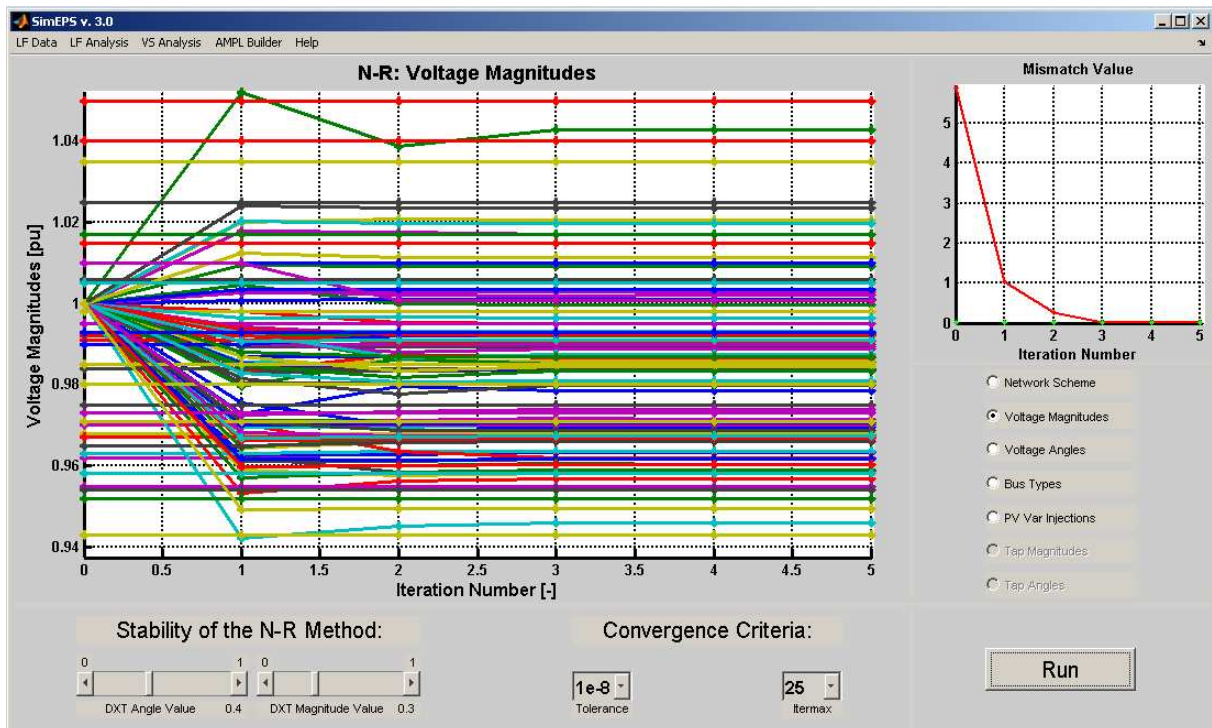
Fig. 10.3-1: Load flow analysis using the N-R method (SUT only) - the IEEE 118-bus system (voltage magnitudes)

68
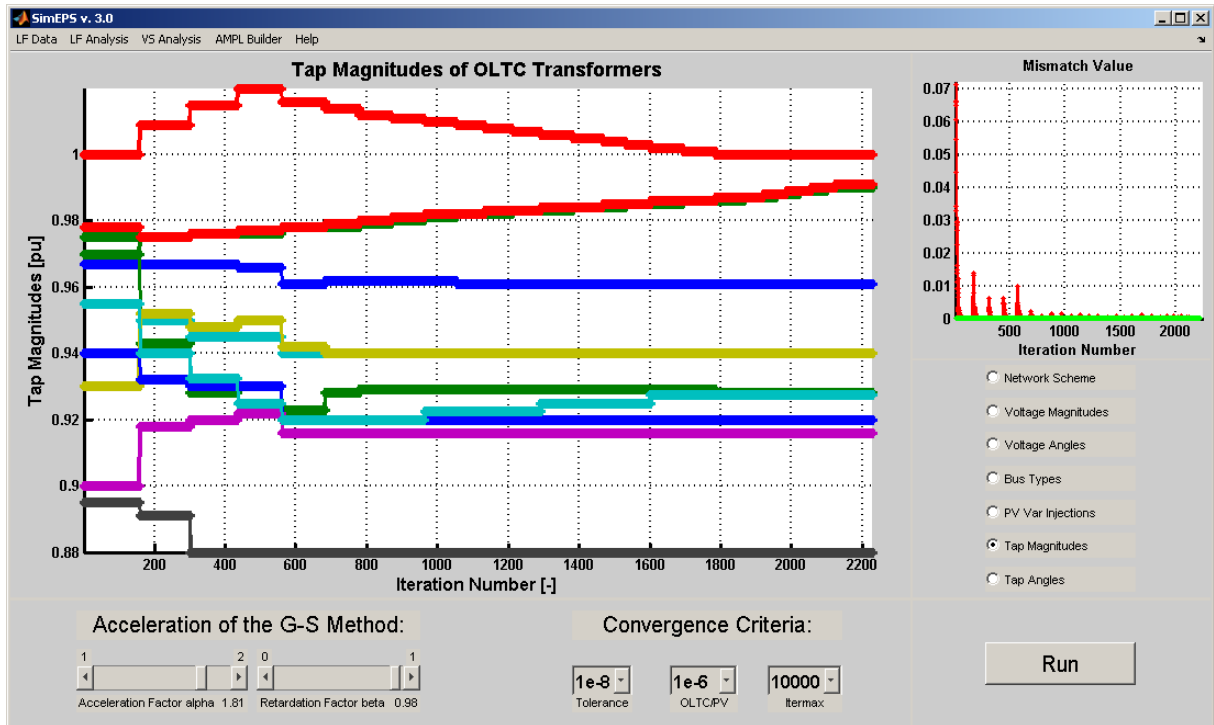
Fig. 10.3-2: V/Q/P control analysis using the G-S method (accel./ret. factors) - the IEEE 57-bus system (tap magnitudes)

Note: Each of plotted graphical outputs can be intentionally zoomed for providing more detailed information about the load flow study.
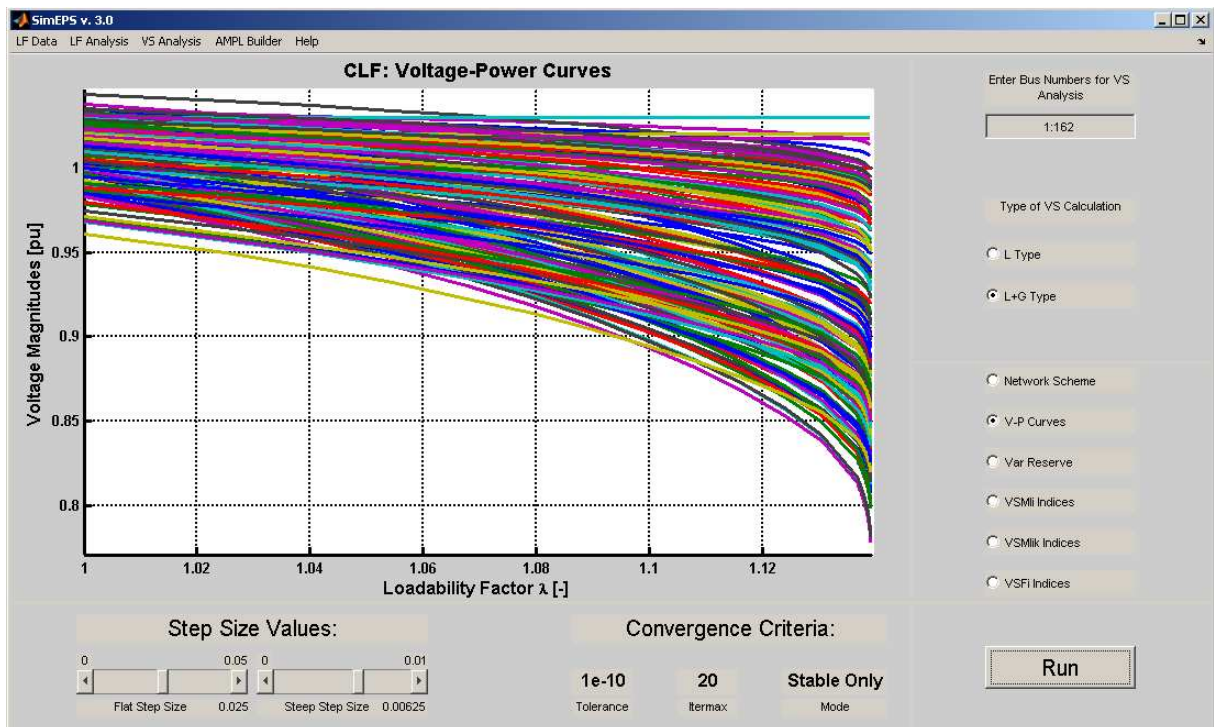
Fig. 10.3-3: Voltage stability analysis using the CLF method (L+G, all network buses) - the IEEE 162-bus system (voltage-power curves)
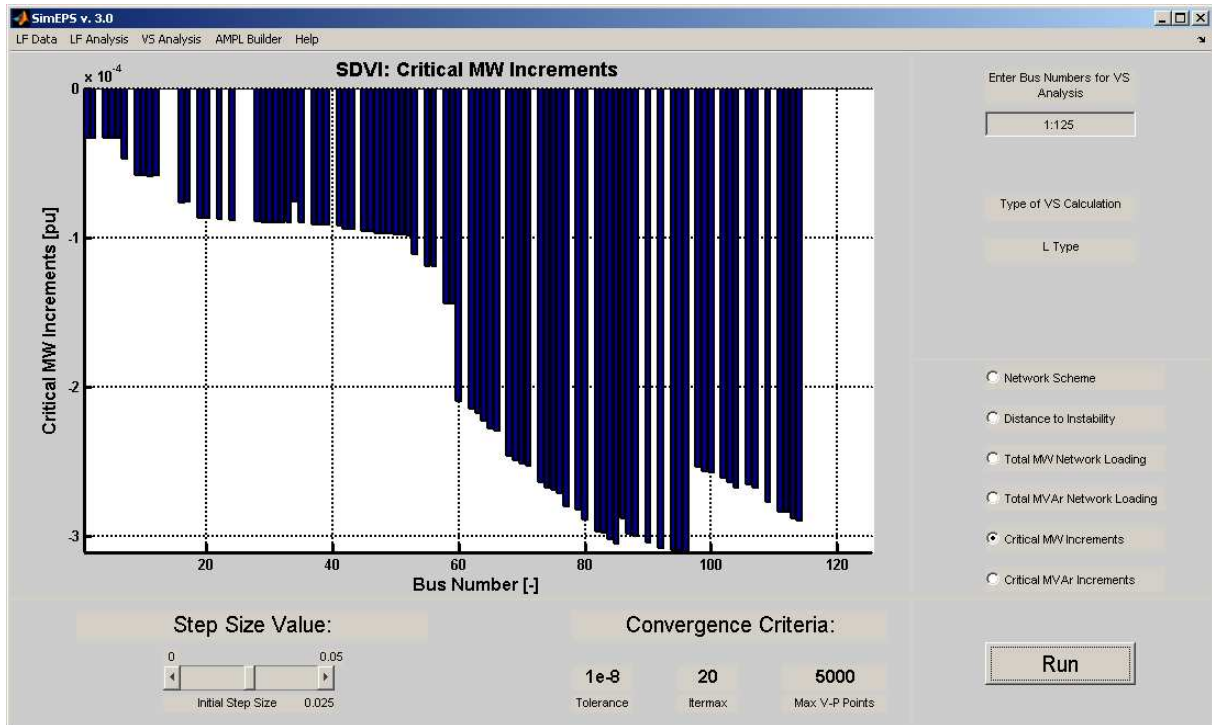
Fig. 10.3-4: Shortest distance to voltage instability analysis (all network buses)- the IEEE 125-bus system (critical MW increments)
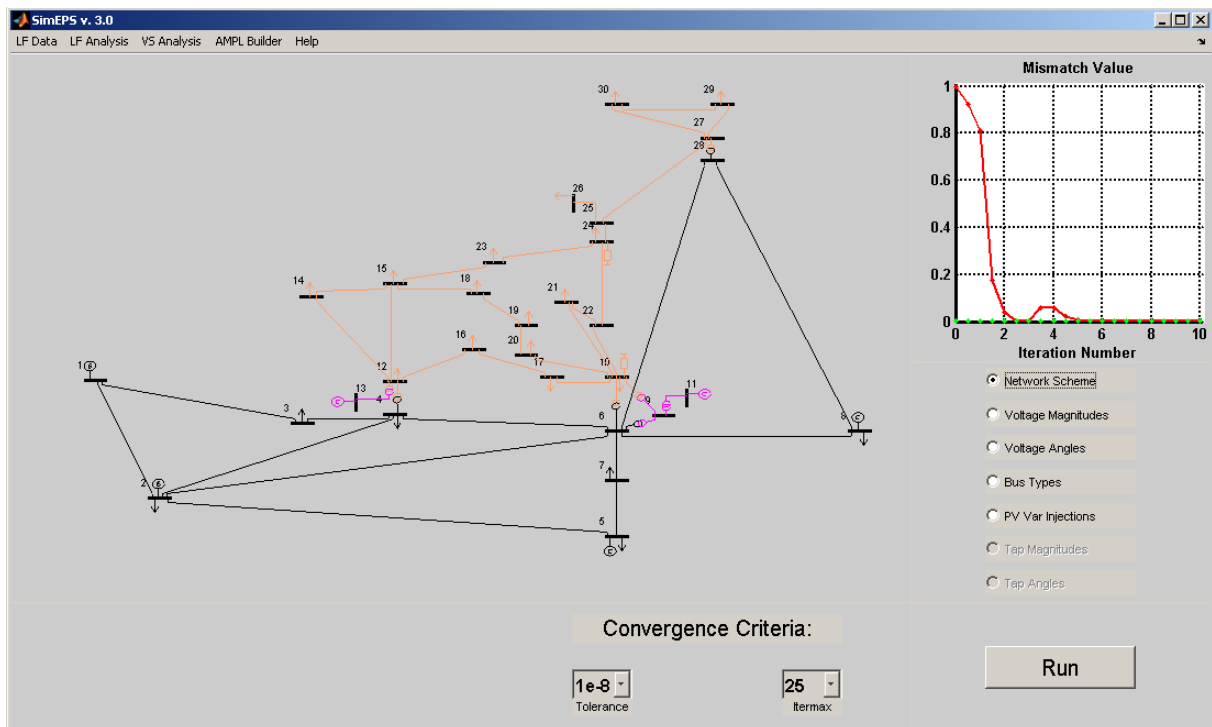
Fig. 10.3-5: Network scheme of the IEEE 30-bus system (solved by XB-type F-D method)

Due to limited extent of this doctoral thesis, full demonstration of SimEPS software will be available during its academic defence. However, some of load flow studies in following chapters of this dissertation work already contain several graphical extracts from older version of SimEPS.

11. Optimization and Testing of Conventional Load Flow Methods

When developing the codes for individual load flow methods in MATLAB environment, important part was to apply smart programming using sparsity techniques and other related functions and approaches.

In electric power systems, every bus is hardly connected to all remaining network buses. From this fact, analyzed load flow problems are highly sparse and therefore, proper sparse programming must be included to reduce computation times. In Tab. 11.1-1, sparsity levels for selected test power systems are shown.

Tab. 11.1-1: Sparsity of the Jacobian for selected test power systems

case	all elements	non-zero elements	sparsity [%]
IEEE14	784	144	81.633
IEEE30	3600	388	89.222
IEEE57	12996	718	94.475
IEEE118	55696	1149	97.937
IEEE300	360000	3858	98.928
EPS734	2155024	8463	99.607
EPS3120	38937600	40512	99.896

To reduce computation time, 1) maximum number of for/while-cycles must be replaced by their vectorized versions, 2) maximum number of if-conditions must be cancelled by defining suitable pointers (function 'find' proved to be sufficient enough), 3) smart matrix indexing (function 'sub2ind') along with direct assembling of sparse matrices (function 'sparse') must be used, 4) fundamental programming rules are to be applied such as the use of pre-defined sizes of matrices/vectors and simpler load flow formulas with identical precision level or the elimination of useless mathematical operations (matrix/vector transpositions, etc.). With these rules applied, significant CPU time savings can be obtained in MATLAB environment.

In this testing session, optimization of both G-S and N-R methods in terms of iteration/CPU reduction and numerical stabilization is provided in Chapters 11.1 and 11.2, respectively. In these two chapters, only half-sparsity techniques were applied since the primary goal was to improve their convergence properties in the first place. Comprehensive testing of G/G-S, N-R, F-D and DC load flow methods on broad range of test power systems is performed with smart programming applied - see Chapters 11.3 to 11.6. If not stated otherwise, all the testings were performed at IntelCore i3 CPU 2.53 GHz/3.8 GB RAM station.

11.1 Testing of Acceleration Techniques for the Gauss-Seidel Method

Acceleration technique with both acceleration/retardation factors was presented in Chapter 5.1. However, settings of both factors was not provided in available literature. The only information provided was that the acceleration factor value should be in interval between 1.0 (no acceleration) and 2.0 (divergence) while the retardation factor value in interval between 0.0 (divergence) and 1.0 (no acceleration). Unfortunately, this gives relatively large space of possible acceleration/retardation factor combinations.

Therefore, the task was to find optimized values of these factors to achieve the greatest reduction of iterations and CPU times. A set of 27 well-behaving test power systems between 3 and 162 buses was examined with permitted convergence tolerance of 10^{-8} pu. In Fig. 11.1-1, acceleration/retardation factor optimization process is demonstrated. For each factor combination, inverted sum of total iteration numbers needed for all analyzed systems is illustrated on the vertical axis.
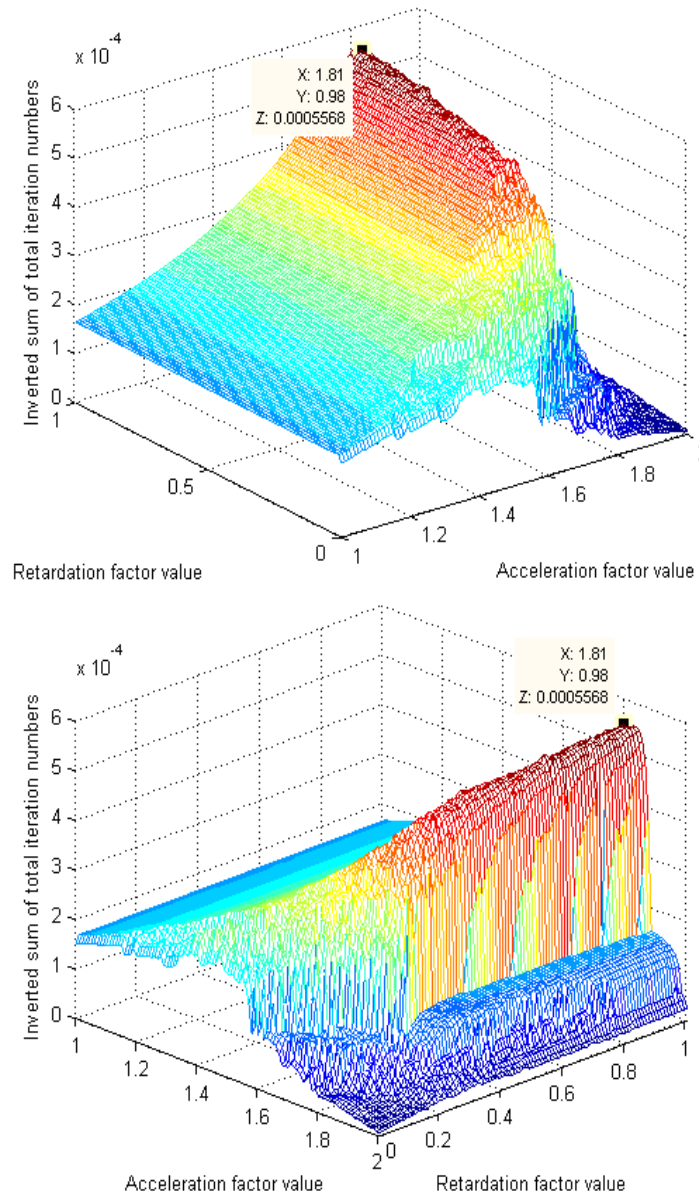
Fig. 11.1-1: Optimization of acceleration/retardation factors - 3D mesh diagram (2 viewpoints)

From Fig. 11.1-1 follows that the most suitable settings of acceleration/retardation factors is [1.81; 0.98]. In case of too stressed operation of the G-S method, the setting of [1.75; 1] is proposed instead for much safer convergence behaviour. Above optimal factor values are also influenced by the selected set of tested networks. However, this effect is expected to be only fractional.

In the evaluation process, the set of 28 real power systems was tested by each acceleration algorithm with permitted tolerance of 10^{-8} pu and maximum iteration number of 25000. Procedure No. 1 is the original G-S method without any acceleration techniques applied. Procedure No. 2 is the algorithm with repeated calculation of bus voltage values. Procedure No. 3 is the technique with acceleration factors (value of 1.6 applied). Procedure No. 4 is the algorithm with optimized settings of acceleration/retardation factors, i.e. with values of 1.81 and 0.98. In Figs. 11.1-2 and 11.1-3, total iteration numbers and CPU times per iteration are shown for each test power system (marked with a star), respectively.
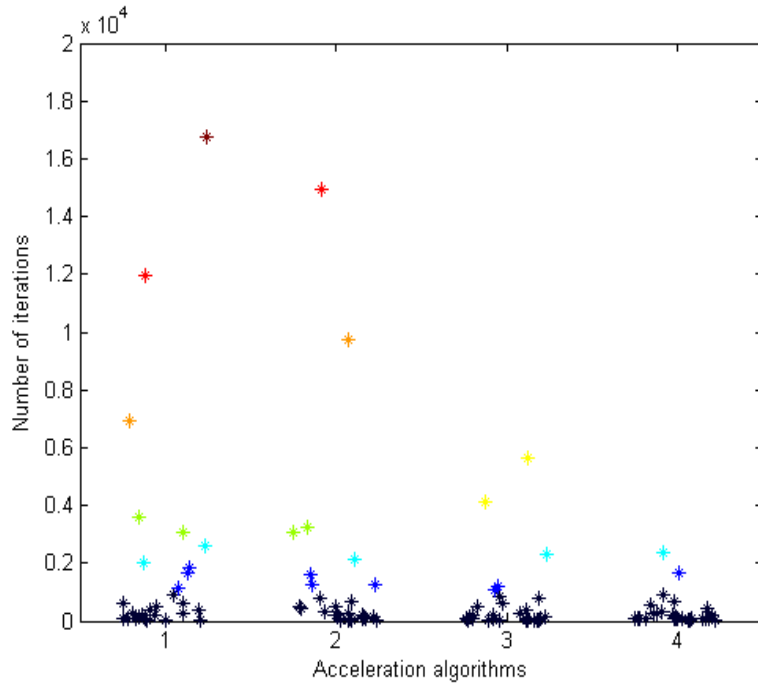
Fig. 11.1-2: Comparison of individual acceleration techniques - total iteration numbers
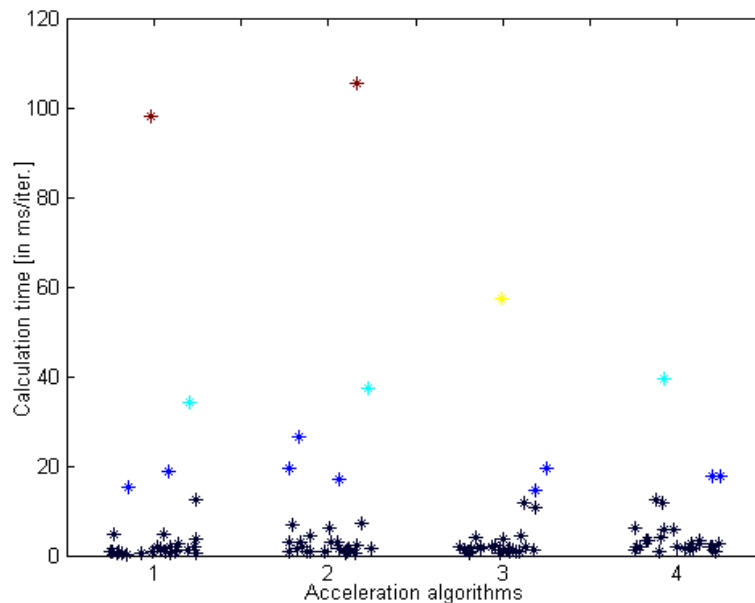
Fig. 11.1-3: Comparison of individual acceleration techniques - CPU times per iteration

The following conclusions apply (percentages are median values). Compared to original G-S method:

1) technique No. 2 provided only 20 % reduction of iteration numbers but 52 % increase of CPU times per iteration

2) technique No. 3 reduced iteration numbers by 66 % while the CPU time per iteration increase was only by 6 %

3) technique No. 4 decreased total iteration numbers by 73 % but increased the CPU time per iteration by 77 %

Also, algorithms No. 1, No. 3 and No. 4 were further tested on 28 test distribution networks between 7 and 794 buses to observe their numerical behaviour. In Fig. 11.1-4, total iteration numbers (left) and total CPU times (right) are transparently shown. These simulations were performed at Intel Core Quad CPU 3.00 GHz - 64bit/8 GB RAM station.
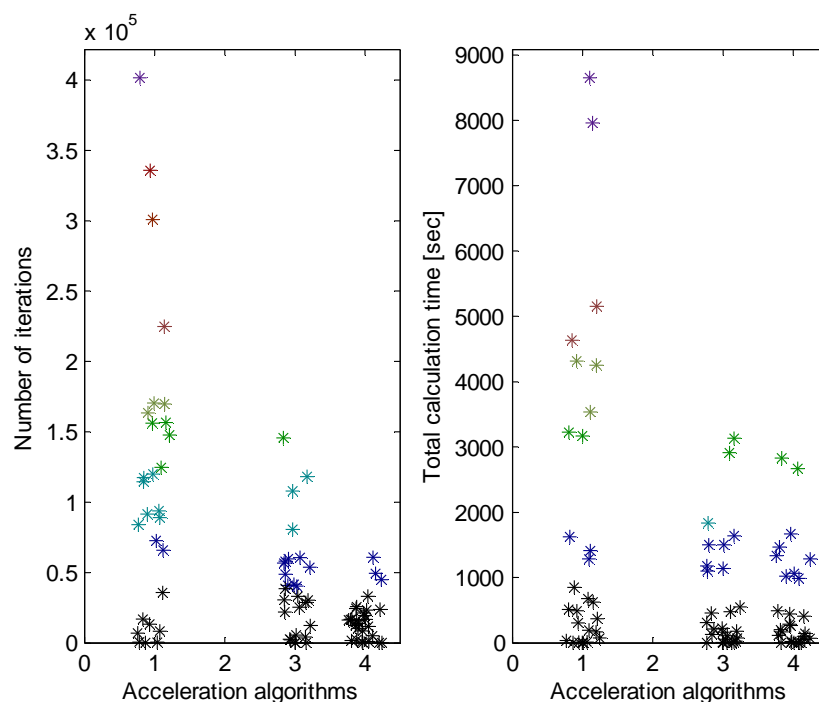
Fig. 11.1-4: Comparison of acceleration techniques for solving distribution networks

In conclusion, from all performed simulations follows that acceleration algorithm No. 3 should be used for all non-distribution load flow cases up to 25 buses. For larger (or distribution) networks say up to 300 buses, acceleration algorithm No. 4 with optimized settings of acceleration/retardation factors should be employed instead. For larger networks, the G-S method is not suitable at all due to very high CPU times.

According to my personal opinion, it is still worthy to use the G-S method in off-line load flow studies but only with acceleration procedures No. 3 and No. 4 and their optimized settings. Optimized setting of acceleration/retardation factors found during the simulations above seems to be highly effective for further applications of the G-S method (PV buses with var limits, OLTC transformers for V/Q/P control, etc.).

11.2 Testing of Stability Techniques for the Newton-Raphson Method

For the N-R method, various stability techniques (see Tab. 11.2-1) were tested to primarily avoid non-convergent behaviour and to perform reliable results. Secondary target was to achieve the solution with minimum iteration numbers and shortest CPU times.

Tab. 11.2-1: Overview of tested stability algorithms

procedure	description
No. 1	original N-R code
No. 2	SUT algorithm only
No. 3	OSFD algorithm + V-updates only
No. 4	OSFD algorithm + V-updates only + SUT
No. 5	OSGS algorithm + V-updates only + SUT
No. 6	Power Mismatch Minimization procedure with relaxation factors

Procedure No. 1 is the original N-R code without any stability technique applied. For the SUT algorithm, searching for best available combination of $\theta/V\ DXT$ values was performed. As the result, original DXT value of 1.5 radians for $\Delta\theta$ [65] was changed to 0.3 radians while the DXT value of 0.2 pu was found sufficient for ΔV. In some cases, One-Shot algorithms with θ-updates surprisingly caused numerical instability of the N-R method. Therefore, both OSFD and OSGS algorithms were used with V-updates only. Moreover, combined operation of One-Shot techniques and the SUT algorithm was tested. Finally, the Power Mismatch Minimization approach with relaxation factors was included [27].

The following six networks (A-F) with convergence problems were tested by each of procedures above - see Tab. 11.2-2. In Tabs. 11.2-3 and 11.2-4, total iteration numbers and CPU times per iteration are presented for each load flow case and technique applied.

Tab. 11.2-2: Overview of analyzed test power systems

case	description
A	Reduced Mato Grosso System, Brazil (11-bus)
B	Simplified Czech Transmission System (56-bus)
C	Simplified 14-Gen SE Australian System (59-bus)
D	South England Power System (61-bus)
E	Power System of Iowa, US (145-bus)
F	Simplified Scottish System, UK (629-bus)

Tab. 11.2-3: Total iteration numbers

case	stability algorithm					
	No. 1	No. 2	No. 3	No. 4	No. 5	No. 6
A	5*	6	5	7	8	7*
B	11	6	5	5	5	6
C	50**	30*	18*	9	6	8
D	50**	50**	5	5	5	5
E	50**	8	50**	8	8	10
F	8*	7	4	4	7	10

* convergence to a non-physical solution ** divergence

Tab. 11.2-4: Total CPU times per iteration in milliseconds

case	stability algorithm			
	No. 1	No. 4	No. 5	No. 6
A	14.6	13.4	11.7	19.4
B	71.5	89.5	86.4	95.4
C	73.2	84.5	90.4	102.9
D	75.1	101.1	98.9	118.7
E	425.2	480.5	472.6	592.2
F	9,791.6	11,653.6	10,114.6	12,753.1

As shown above, the most reliable stability algorithms were procedures No. 4 and No. 5. Remaining procedures had serious problems with finding correct solutions, i.e. convergence to non-physical solutions or divergence was often observed. From these two procedures, the former produces solutions with minimum iteration numbers but higher CPU times (mean increase of 16.5 %). The latter needs more iterations to converge but less CPU time (mean increase of 11.8 % only).

Broad range of 50 real test power systems between 3 and 2746 buses was examined by each stability algorithm - see Fig. 11.2-1. Green stars represent load flow cases with the convergence to physical solutions while blue and red stars highlight those with the divergence and the convergence to non-physical solutions, respectively. Physical solutions were verified using PowerWorld Simulator (GSO version 13) [69] or MATPOWER (version 4.0b4) [70].
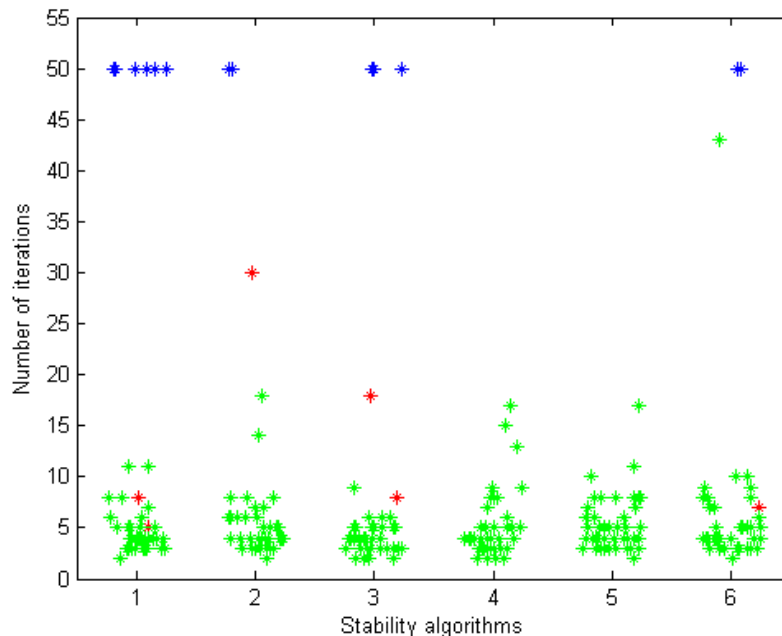
Fig. 11.2-1: Comparison of tested stability algorithms

Again, procedures No. 4 and No. 5 showed the best numerical performance with reliable results, lowest iteration numbers, only small CPU time increase and relatively simple modification of the original N-R method. From these two procedures, the former behaved better in both iteration numbers and CPU times.

Further notes about stability procedure No. 4:

1) For the OSFD algorithm, matrix $\underline{B}''$ was computed directly from respective elements of the bus admittance matrix. XB and BX versions of the F-D method were not tested.

2) SUT algorithm may increase total iteration numbers for systems with higher loading conditions. Rarely, even 15 to 20 iterations can be necessary for obtaining correct results.

3) When producing non-physical solutions or diverging, it is recommended to slightly change both DXT values. The N-R method will then be more stressed or relaxed and correct solutions can be obtained.

Based on the results, the OSFD algorithm with V-updates and in combination with the SUT procedure is applied in the original N-R method. Using this procedure, all load flow studies (well-behaving, ill-conditioned, distribution, etc.) are performed in this thesis.

11.3 Testing of Gauss/Gauss-Seidel Load Flow Methods

In this chapter, both G and G-S methods were examined on broader range of test power systems including the PV buses with var limits. The G method was implemented for its easier programming since it can be vectorized to behave very fast even for larger systems. However, it has slower rate of convergence and no acceleration technique can be applied. The G-S method was upgraded by optimized acceleration and acceleration/retardation factor values, respectively. In both G/G-S methods, sparse matrix indexing for only non-zero elements of the bus admittance matrix was also included. Proposed PV/PQ bus-type switching logic was applied with convergence criterion 1×10^{-6}. Overall precision index of 1×10^{-10} and 1×10^{-8} was used for the G and G-S method along with maximum iteration number of 20000 and 500000, respectively.

In Tab. 11.3-1, non-distribution and well-conditioned networks were tested by the G method and the G-S method with optimized acceleration factors. For mutual comparison, total active/reactive system losses were assessed.

Tab. 11.3-1: Comparison of G/G-S methods for solving medium-sized networks

case	solution		G method		G-S method	
	ΔP	ΔQ	iter	time [s]	iter	time [s]
IEEE9II	0.050633	-0.771009	825	0.2808	68	0.0624
EPS11III	0.086393	-15.149000	219	0.0468	31	0.0156
IEEE14I	0.133930	0.301220	378	0.078001	57	0.0312
EPS15I	0.129830	-0.176810	537	0.1092	80	0.0312
EPS16I	0.150120	0.274840	989	0.1872	166	0.078
EPS17I	0.939790	5.052600	1670	0.3432	276	0.1248
EPS23I	0.182970	-1.192800	657	0.1404	113	0.078
IEEE24I	0.512470	-0.951320	737	0.156	123	0.078001
IEEE26I	0.157640	0.847570	387	0.078001	64	0.0468
IEEE30I	0.175520	0.330390	1089	0.2184	191	0.156
IEEE39I	0.415910	-0.644420	3146	0.6708	522	0.5304
IEEE57I	0.278640	0.063280	1173	0.2652	189	0.2808
EPS61I	0.746880	4.238800	3224	0.7488	633	0.99841
IEEE118I	1.324900	-5.176200	3083	0.90481	805	2.5272
IEEE162I	1.629600	-4.408100	6929	2.3712	1061	4.4928
IEEE300I	4.089900	-3.936700	30741	14.118	5610	45.895

In Tab. 11.3-2, broad range of distribution networks was examined by the G method and the G-S method with optimized acceleration/retardation factors. Note: All simulations were executed at Intel Core Quad CPU 3.00 GHz - 64bit/8 GB RAM station.

Tab. 11.3-2: Comparison of G/G-S methods for solving larger distribution networks

case	solution		G method		G-S method	
	ΔP	ΔQ	iter	time [s]	iter	time [s]
EPS114I	0.000860	0.004355	259456	61.605	11793	32.183
EPS125I	0.002070	0.006673	49311	12.355	2239	7.2852
EPS128I	0.001937	0.012682	23667	5.8344	1040	3.4476
EPS133I	0.000656	0.002378	130424	31.933	5054	17.503
EPS137I	0.001098	0.010219	279853	68.859	12325	37.986
EPS167I	0.001078	0.001151	399300	104.55	16788	63.992
EPS246I	0.000751	-0.001260	229886	66.503	10358	54.366
EPS272I	0.001342	-0.000979	345054	109.28	13744	93.959
EPS304I	0.000680	-0.002442	200998	58.282	8546	46.285
EPS323I	0.002034	0.014323	378686	132.1	16564	134.16
EPS361I	0.018824	0.153962	385432	138.56	16673	162.33
EPS366I	0.001495	0.005390	358593	131.74	16054	146.44
EPS392I	0.001154	0.003627	1218289	403.75	49480	348.13
EPS535I	0.001576	0.000676	551470	249.09	23809	331.49
EPS558I	0.001898	0.002458	1403910	660.79	60773	898.91
EPS682I	0.002429	0.007376	457303	238.88	19383	346.85
EPS706I	0.001926	-0.001932	750113	379.89	33185	570.12
EPS707I	0.002382	0.002383	550832	293.61	24535	456.19
EPS760I	0.003096	0.007251	497753	284.12	21199	441.3
EPS791I	0.002311	-0.002726	1097293	648.98	45129	976.6
EPS794I	0.002165	-0.007427	549943	319.9	23408	507.53

By both iterative methods, identical results were obtained for each load flow study. These solutions were later successfully compared to those from the N-R and F-D methods. Properties of both methods are further demonstrated by solving the IEEE 300-bus power system with var limits. Bus voltage magnitudes/angles, bus types and var injections in PV buses are iteratively shown in Figs. 11.3-1 to 11.3-8, respectively. Note: Blue dots in Figs. 11.3-5 and 11.3-6 show the bus-type switching from PV to PQ.
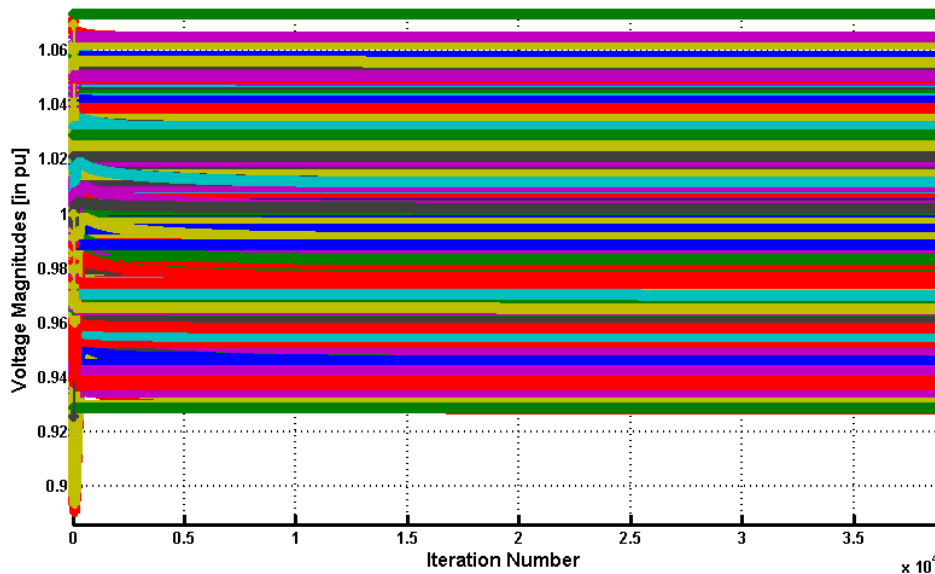
Fig. 11.3-1: IEEE 300-bus power system - voltage magnitudes (G method)
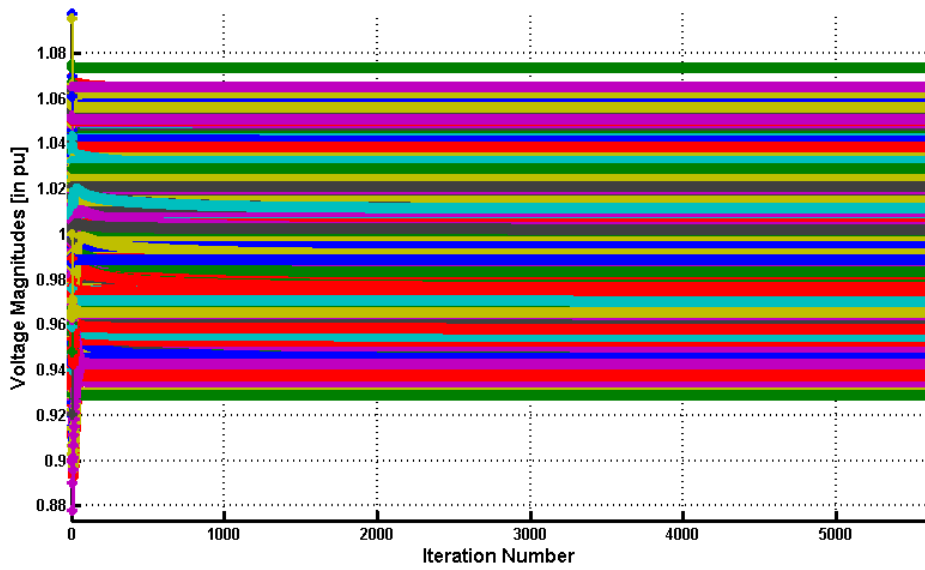
Fig. 11.3-2: IEEE 300-bus power system - voltage magnitudes (G-S method)
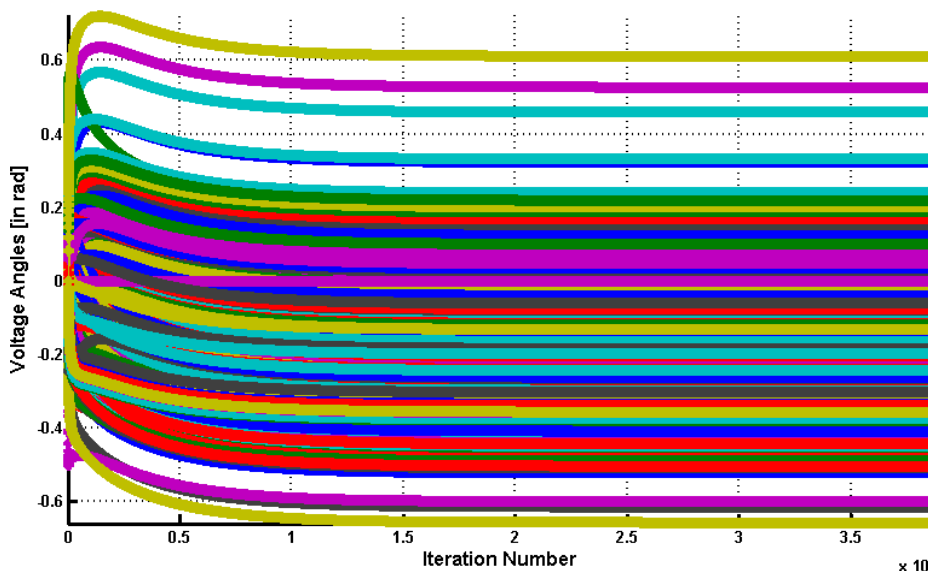
Fig. 11.3-3: IEEE 300-bus power system - voltage angles (G method)
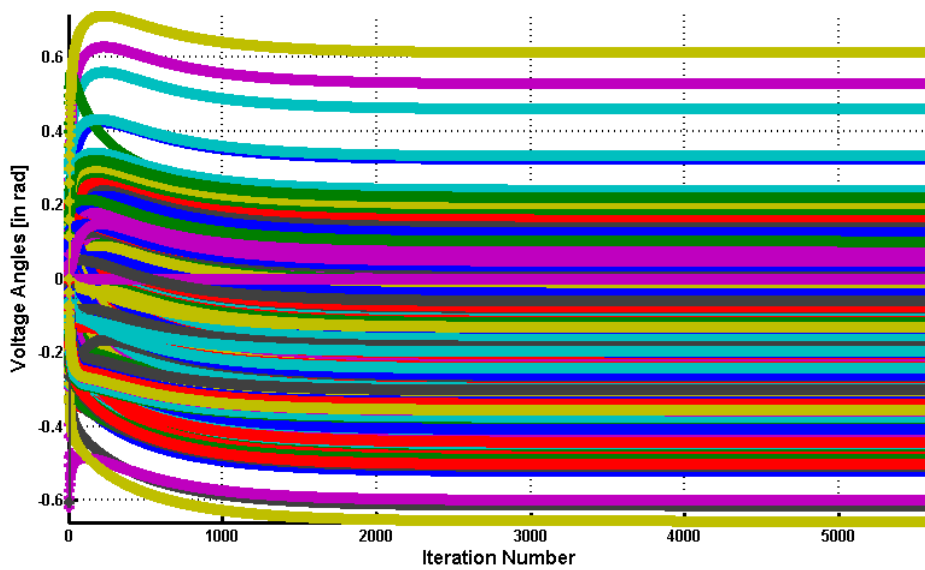
Fig. 11.3-4: IEEE 300-bus power system - voltage angles (G-S method)
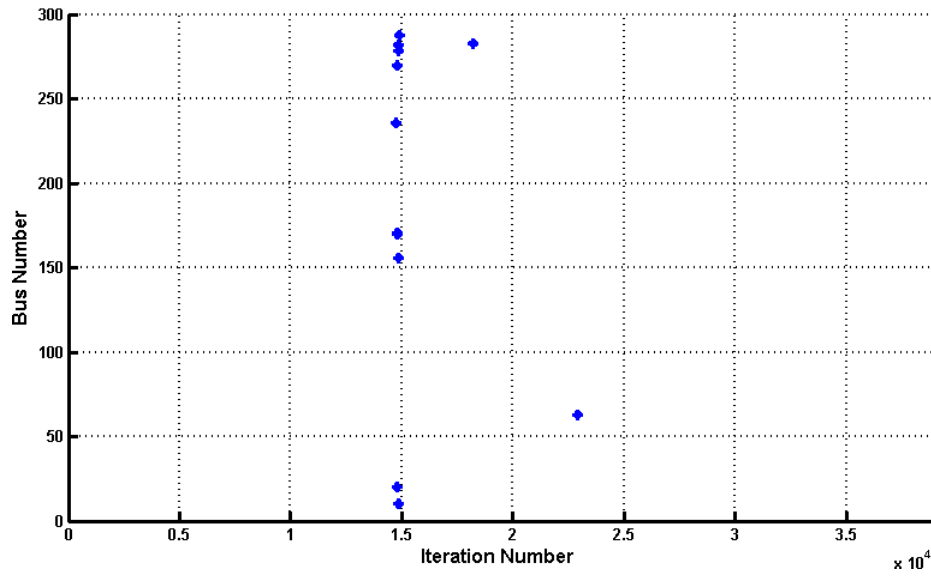
Fig. 11.3-5: IEEE 300-bus power system - bus type switching (G method)
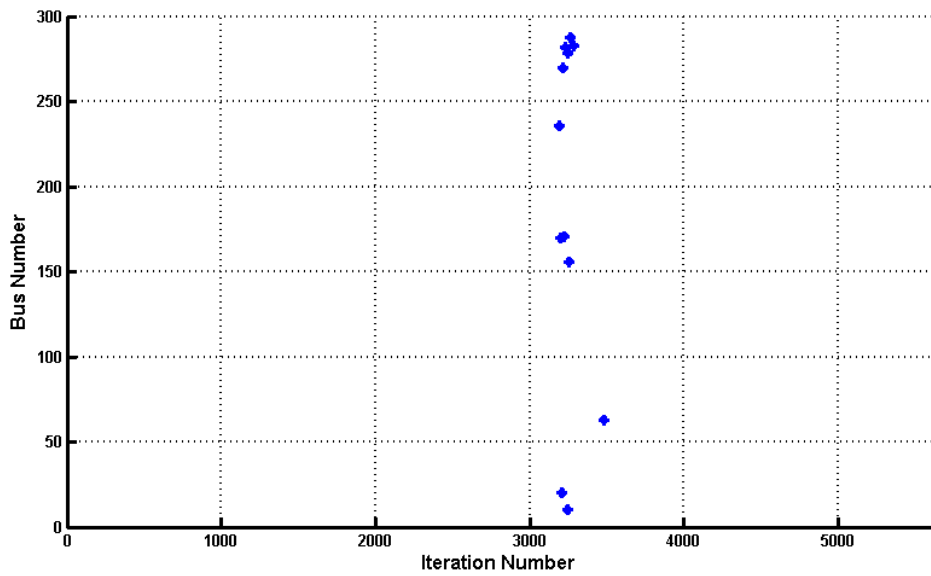
Fig. 11.3-6: IEEE 300-bus power system - bus type switching (G-S method)
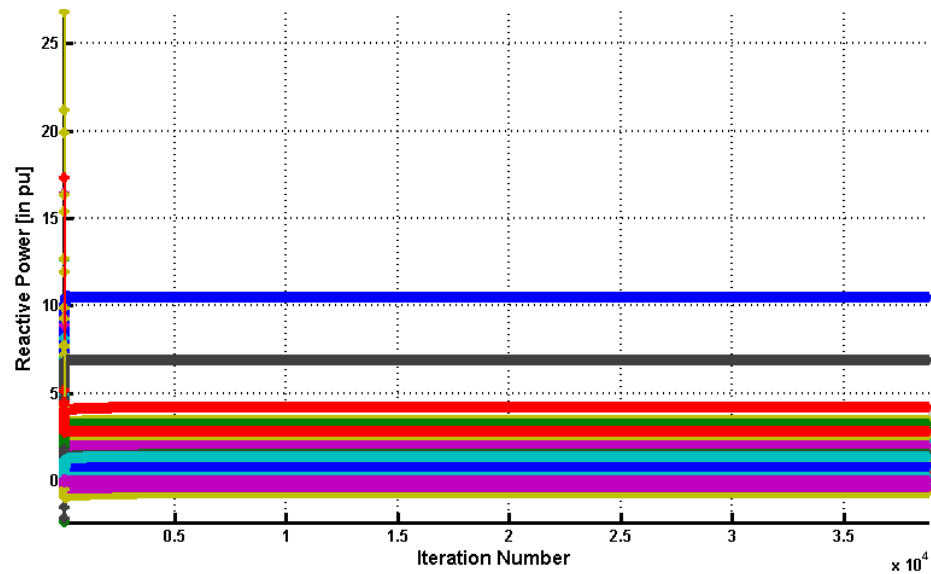
Fig. 11.3-7: IEEE 300-bus power system - reactive power injections (G method)
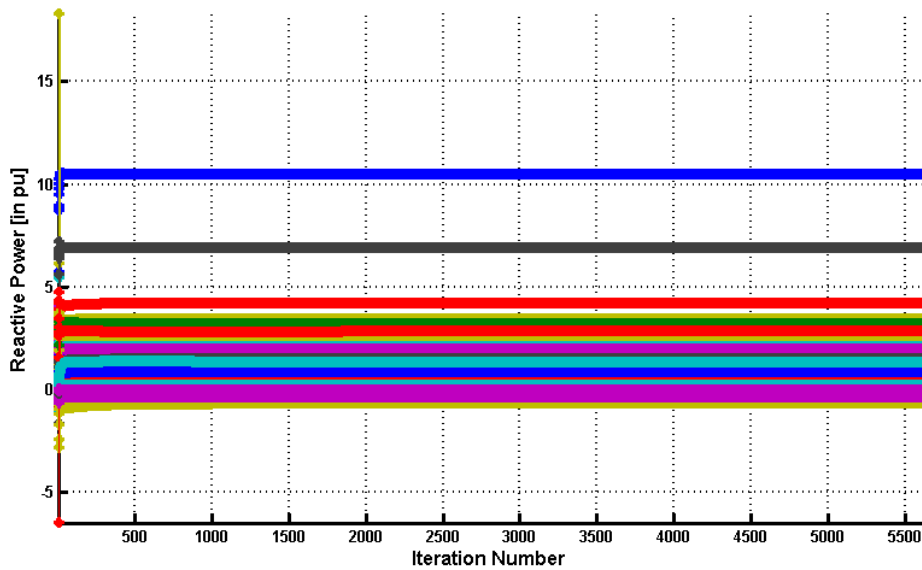
Fig. 11.3-8: IEEE 300-bus power system - reactive power injections (G-S method)

The dependence of both G/G-S methods on network size and number of PV buses with var limits is clearly observed in performed simulations. Therefore, their use is limited for non-distribution and well-behaving networks up to 300 buses. For larger systems, the G method needs higher iteration numbers but it is still significantly faster than the G-S method.

11.4 Testing of Newton-Raphson/Fast-Decoupled Load Flow Methods

In this chapter, the N-R method with applied OSFD/SUT algorithms and both XB/BX versions of the F-D method were tested with permitted tolerances of 1×10^{-8} and 1×10^{-7}, respectively. Proper PV-PQ bus-type switching logics were applied for both methods.

As for G/G-S methods, identical set of test power systems with var limits in PV buses was examined. Results for medium-sized and well-behaving, distribution, ill-conditioned and larger networks are shown in Tabs. 11.4-1 to 11.4-4, respectively. For all load flow cases, the same results were obtained. Due to MATLAB's insensitivity to clock precise calculation lengths, CPU times were truncated by MATLAB to closest checkpoints (function 'cputime'). Thus, the times seem to be suspiciously identical for smaller and medium-sized networks.

Tab. 11.4-1: Comparison of N-R/F-D methods for medium-sized and well-behaving systems

case	solution		N-R method		F-D method (XB)		F-D method (BX)	
	ΔP	ΔQ	iter	time [s]	iter	time [s]	iter	time [s]
IEEE9I	0.049547	-0.8012	4	0.0156	7.0	0.0156	6.5	0.0156
EPS11III	0.086392	-15.1486	3	0.0156	9.0	0.0156	10.0	0.0156
IEEE14I	0.133933	0.301224	4	0.0156	7.0	0.0156	9.0	0.0156
EPS15I	0.129832	-0.17681	4	0.0156	11.0	0.0156	10.5	0.0156
EPS16I	0.150124	0.274843	4	0.0156	16.0	0.0156	15.5	0.0156
EPS23I	0.182971	-1.19279	3	0.0156	6.5	0.0156	6.0	0.0156
IEEE24I	0.512464	-0.95132	4	0.0156	7.5	0.0156	8.0	0.0156
IEEE26I	0.157641	0.847571	4	0.0156	12.5	0.0156	12.5	0.0156
IEEE30I	0.175519	0.330387	4	0.0156	9.0	0.0156	9.0	0.0156
IEEE39I	0.415922	-0.64442	5	0.0156	9.0	0.0156	8.5	0.0156
IEEE57I	0.278638	0.06328	4	0.0156	8.5	0.0156	8.5	0.0312
IEEE118I	1.324914	-5.17617	4	0.0156	9.0	0.0156	9.0	0.0156
IEEE162I	1.629586	-4.40806	6	0.0312	14.0	0.0156	15.0	0.0156
IEEE300I	4.089965	-3.93666	7	0.0468	14.0	0.0312	13.5	0.0312

Tab. 11.4-2: Comparison of N-R/F-D methods for larger distribution networks

case	solution		N-R method		F-D method (XB)		F-D method (BX)	
	ΔP	ΔQ	iter	time [s]	iter	time [s]	iter	time [s]
EPS114I	0.000860	0.004355	2	0.0156	6.5	0.0156	12.5	0.0156
EPS128I	0.001937	0.012682	3	0.0156	8.5	0.0156	11.0	0.0156
EPS133I	0.000656	0.002378	3	0.0156	11.5	0.0156	13.5	0.0156
EPS246I	0.000751	-0.001260	2	0.0156	6.0	0.0156	14.0	0.0156
EPS272I	0.001342	-0.000979	2	0.0156	7.0	0.0156	10.0	0.0156
EPS304I	0.000680	-0.002442	2	0.0156	6.5	0.0156	13.5	0.0312
EPS361I	0.018824	0.153962	4	0.0156	10.0	0.0156	14.0	0.0156
EPS366I	0.001495	0.005390	2	0.0156	6.5	0.0156	13.5	0.0312
EPS396I	0.000677	-0.004430	2	0.0156	6.5	0.0156	13.5	0.0156
EPS535I	0.001576	0.000676	2	0.0156	6.5	0.0156	13.5	0.0312
EPS558I	0.001898	0.002458	3	0.0312	6.5	0.0156	12.5	0.0624
EPS682I	0.002429	0.007376	3	0.0312	7.5	0.0156	13.5	0.0312
EPS706I	0.001926	-0.001932	2	0.0156	6.5	0.0156	14.5	0.0780
EPS760I	0.003096	0.007251	3	0.0312	7.0	0.0156	12.5	0.0312
EPS791I	0.002311	-0.002726	2	0.0312	7.5	0.0312	14.5	0.0312
EPS794I	0.002165	-0.007427	3	0.0312	7.5	0.0156	13.5	0.0312

Tab. 11.4-3: Comparison of N-R/F-D methods for ill-conditioned systems

case	solution		N-R method		F-D method (XB)		F-D method (BX)	
	ΔP	ΔQ	iter	time [s]	iter	time [s]	iter	time [s]
EPS11I	0.548902	-0.138043	6	0.0156	25.0	0.0156	23.0	0.0156
EPS11II	0.839751	9.078277	8	0.0156	12.0	0.0156	10.5	0.0156
EPS17I	0.939792	5.052564	5	0.0156	13.5	0.0156	12.5	0.0156
EPS43I	0.028018	-14.075661	5	0.0156	40.0	0.0312	41.0	0.0312
EPS59I	7.300444	32.077480	16	0.0312	12.5	0.0156	12.0	0.0156
EPS59III	6.322038	27.447944	7	0.0156	12.0	0.0156	12.0	0.0156
EPS59IV	2.395374	-16.057423	10	0.0156	12.5	0.0156	11.0	0.0156
EPS59V	4.627153	6.540490	14	0.0312	12.0	0.0156	11.5	0.0156
EPS61I	0.746899	4.238759	5	0.0156	11.5	0.0156	11.5	0.0156
IEEE145I	-18.298883	167.967914	8	0.0312	19.0	0.0312	22.5	0.0312

Tab. 11.4-4: Comparison of N-R/F-D methods for larger networks

case	solution		N-R method		F-D method (XB)		F-D method (BX)	
	ΔP	ΔQ	iter	time [s]	iter	time [s]	iter	time [s]
EPS629II	1.592025	-71.481763	5	0.0468	20.0	0.0468	16.5	0.0468
EPS734II	2.117157	-75.734587	5	0.0624	20.0	0.0780	19.0	0.0468
EPS2383I	7.360204	8.226186	7	0.2808	23.5	0.1560	24.5	0.2964
EPS2736I	3.259748	-30.717082	8	0.4056	17.0	0.1404	19.0	0.2964
EPS2737I	1.562046	-40.179476	5	0.2340	14.0	0.1092	15.0	0.2340
EPS2746I	3.331831	-29.391248	10	0.4524	30.0	0.2340	33.0	0.4836
EPS2746II	5.135388	-17.641861	7	0.3120	21.0	0.1560	25.0	0.3744
EPS3012I	6.186859	-13.321250	6	0.2964	15.5	0.2340	18.5	0.2652
EPS3120I	5.357315	-15.632522	6	0.3120	18.0	0.2808	21.0	0.3276

The N-R method provided fast/correct solutions with rather low iteration numbers. The F-D method obtained reliable results even for distribution networks and systems where the N-R method needed stability techniques for finding the solution. The best algorithms were the N-R method with stability procedures and the XB version of the F-D method.

Properties of the N-R and XB-type F-D methods are illustrated on the IEEE 300-bus power system with var limits. Voltage magnitudes/angles, bus types and var injections in PV buses are shown in Figs. 11.4-1 to 11.4-8, respectively. Note: Blue and red dots in Figs. 11.4-5 and 11.4-6 show the bus-type switching from PV to PQ and from PQ to PV, respectively.
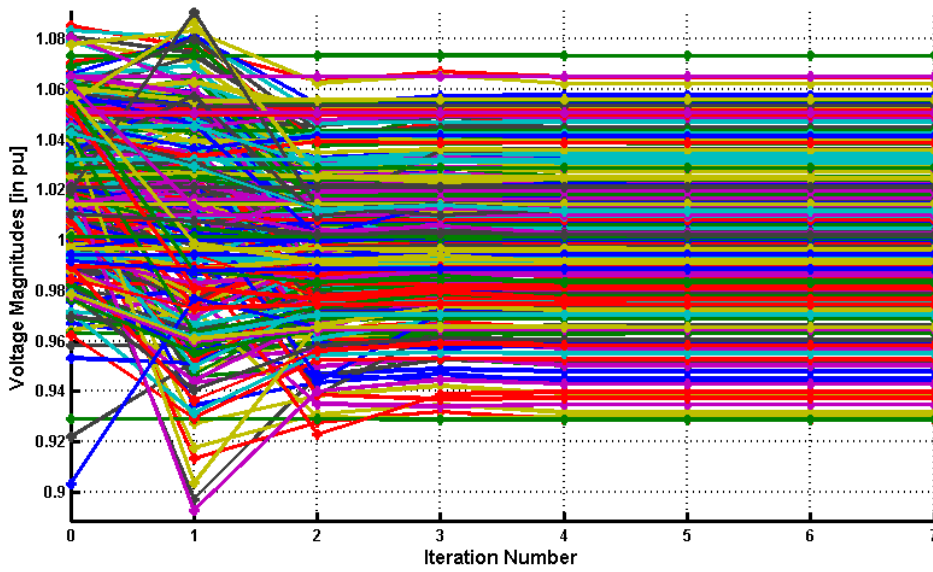
Fig. 11.4-1: IEEE 300-bus power system - voltage magnitudes (N-R method)
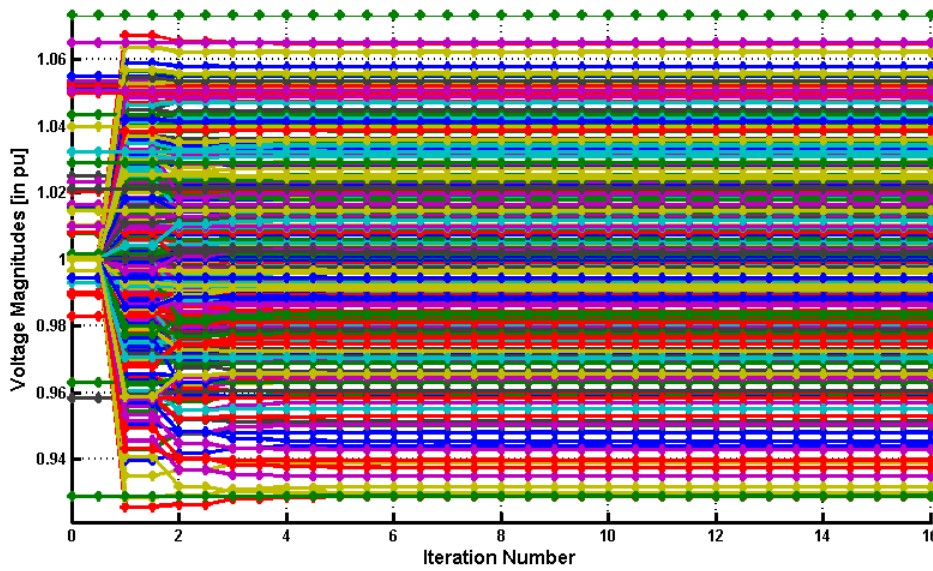
Fig. 11.4-2: IEEE 300-bus power system - voltage magnitudes (XB-type F-D method)
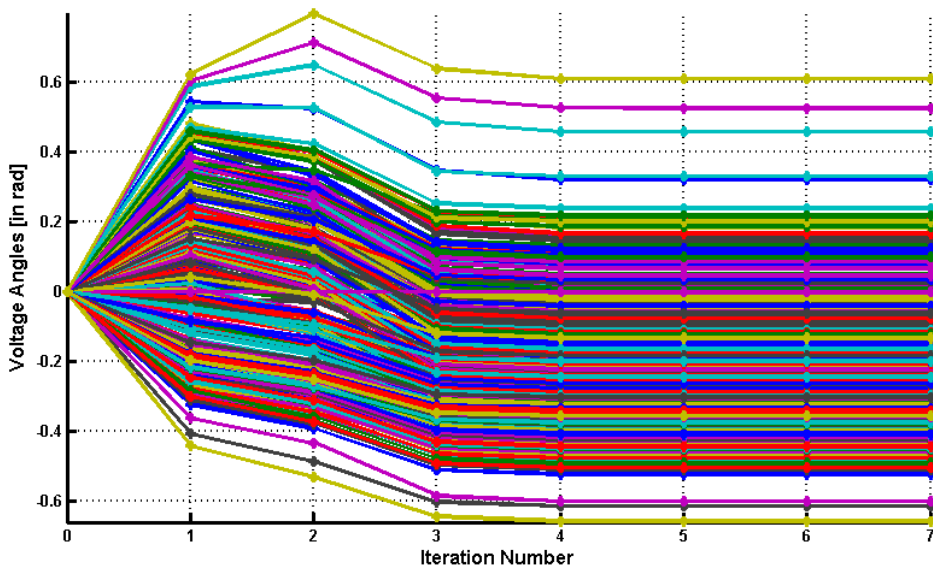
Fig. 11.4-3: IEEE 300-bus power system - voltage angles (N-R method)
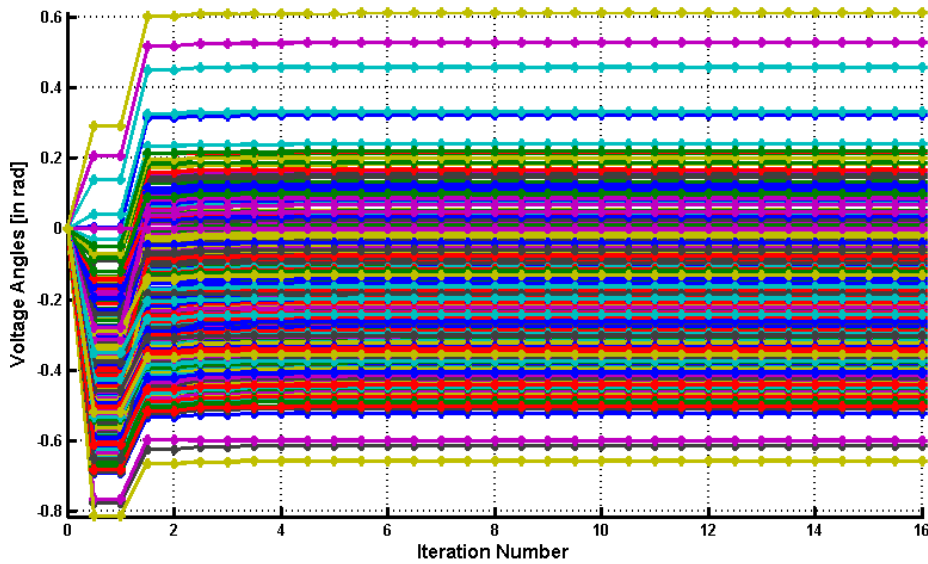
Fig. 11.4-4: IEEE 300-bus power system - voltage angles (XB-type F-D method)
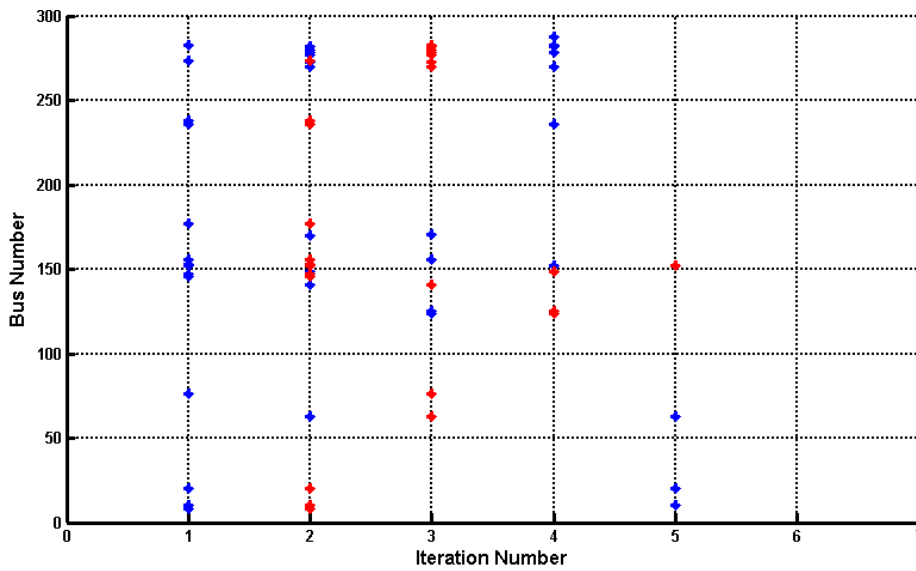
Fig. 11.4-5: IEEE 300-bus power system - bus type switching (N-R method)
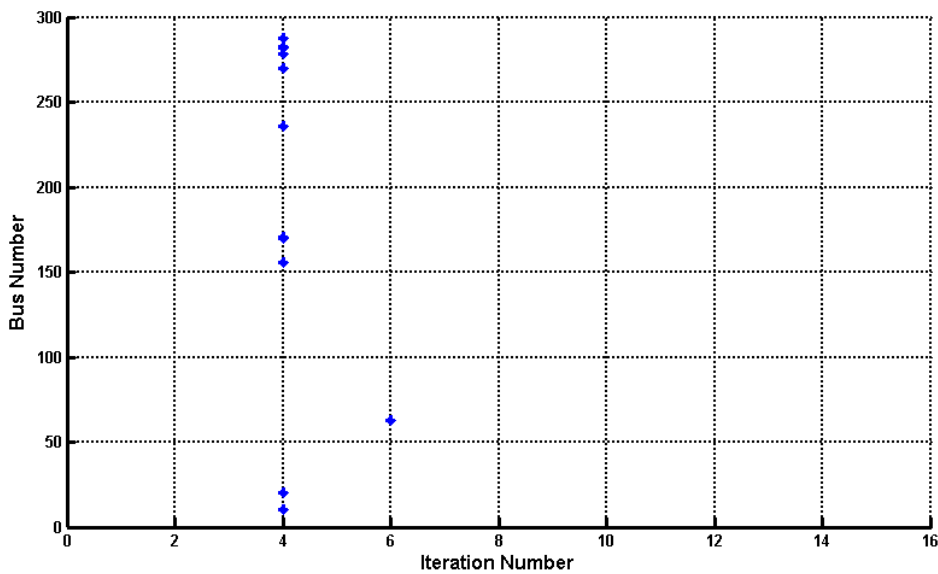
Fig. 11.4-6: IEEE 300-bus power system - bus type switching (XB-type F-D method)
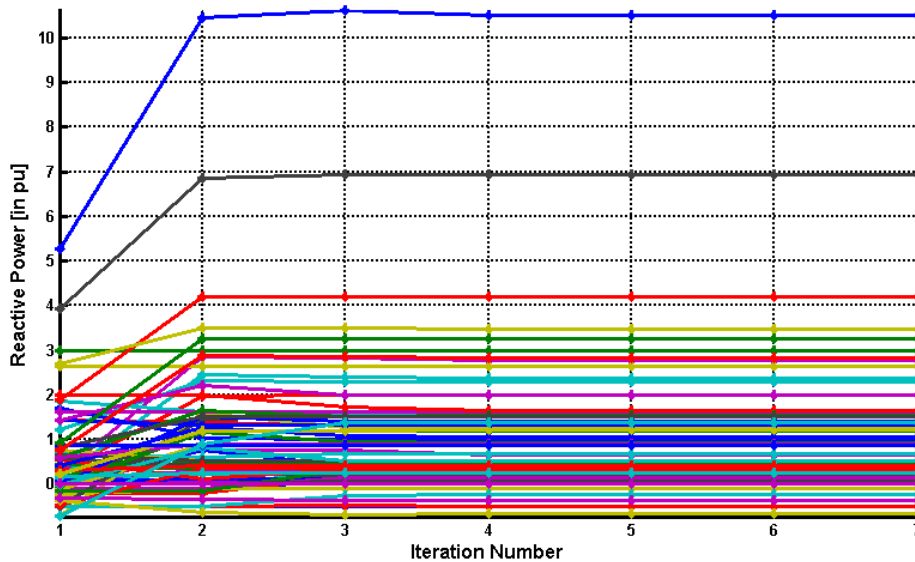
Fig. 11.4-7: IEEE 300-bus power system - reactive power injections (N-R method)
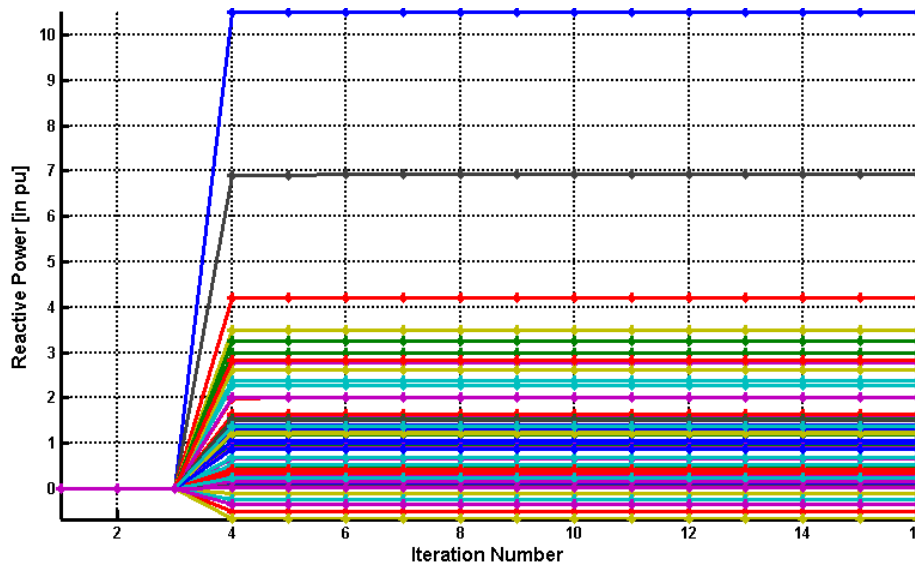
Fig. 11.4-8: IEEE 300-bus power system - reactive power injections (XB-type F-D method)

From all testings applies that both the N-R and F-D methods are highly advanced for the load flow analysis. The N-R method is further used also for more challenging tasks such as voltage/power control and voltage stability problems.

11.5 Testing of the DC Load Flow Method

In this chapter, both Basic and proposed Advanced versions of the DC load flow algorithm were tested on a set of well-behaving transmission power systems. Total active power losses were calculated and compared to those from the G-S and the N-R method. In Tab. 11.5-1, percentage result deviations from the accurate N-R's solution are shown along with their mutual comparison for both versions of the DC load flow algorithm. Possible solution improvement/degradation using the Advanced DC load flow method is provided in green/red colour, respectively.

Note: For ill-conditioned and distribution networks, the DC load flow method cannot be used for producing solutions significantly far from exact ones (if existing).

Tab. 11.5-1: Comparison of Basic/Advanced DC methods - total active power losses

case	N-R method	Basic DC	Advanced DC	Basic DC vs. N-R [%]	Advanced DC vs. N-R [%]	evaluation [%]
IEEE14I	0.1339	0.1761	0.1603	31.5	19.7	11.8
EPS15I	0.1278	0.1222	0.1199	4.4	6.2	-1.8
EPS16I	0.1495	0.1276	0.1267	14.7	15.3	-0.6
EPS17I	0.9398	0.8098	0.7944	13.8	15.5	-1.6
EPS23I	0.1830	0.1880	0.1845	2.8	0.9	1.9
IEEE24I	0.5125	0.6172	0.5842	20.4	14.0	6.5
IEEE26I	0.1577	0.1612	0.1539	2.2	2.4	-0.2
IEEE30I	0.1756	0.1805	0.1625	2.8	7.4	-4.6
IEEE39I	0.4159	0.4316	0.4340	3.8	4.4	-0.6
IEEE57I	0.2786	0.2514	0.2454	9.8	11.9	-2.2
EPS59I	7.3004	8.3976	8.3615	15.0	14.5	0.5
IEEE118I	1.3287	1.4323	1.4135	7.8	6.4	1.4
IEEE162I	1.6310	1.5651	1.5637	4.0	4.1	-0.1
IEEE300	4.0899	4.4377	4.3428	8.5	6.2	2.3
EPS734I	1.9698	1.8500	1.8534	6.1	5.9	0.2

From Tab. 11.5-1 it is not clear which of both methods is better for producing approximate load flow solutions in all examined cases. The Advanced DC load flow algorithm makes larger improvements in some studies than solution degradations in other ones. Degradation of results by the Advanced DC load flow method is usually small in the order of units only.

Note: For the N-R method, no var limits in PV buses were considered. If included, however, only negligible changes in values above would be obtained.

Comparison of voltage angles in each network bus was made by computing the total angular square difference - see Tab. 11.5-2. This value is the sum of square differences in bus voltage angles between the N-R method (exact solution) and selected version of the DC load flow method (approximate solution).

In Figs. 11.5-1 and 11.5-2, voltage angle square differences are projected for each bus of the IEEE 30-bus and IEEE-57-bus network, respectively. Red colour shows the exact solution of the N-R method while blue and green colours provide the results and deviations for the Basic and Advanced DC load flow methods, respectively.

Tab. 11.5-2: Comparison of Basic/Advanced DC methods - total angular square differences

case	Basic DC vs. N-R [-]	Advanced DC vs. N-R [-]
IEEE14I	0.0032	0.0003
EPS15I	0.0007	0.0009
EPS16I	0.0054	0.0053
EPS23I	0.0004	0.0003
IEEE24I	0.0067	0.0027
IEEE30I	0.0051	0.0009
IEEE57I	0.0048	0.0027
EPS59I	13.3738	13.2931
IEEE118I	0.2238	0.2587
IEEE300I	27.3114	27.2520
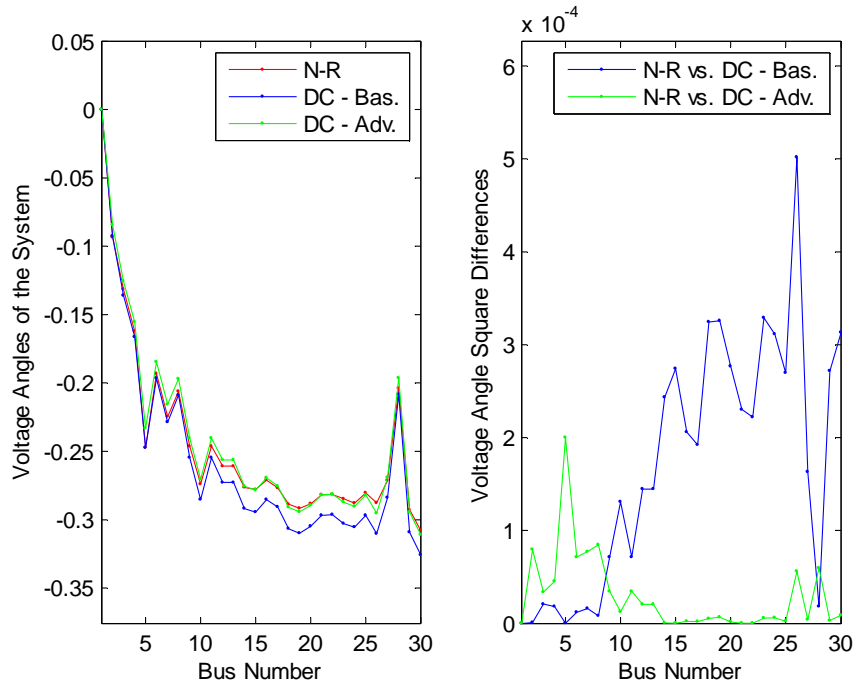
Fig. 11.5-1: Voltage angles and voltage angle square differences - the IEEE 30-bus system
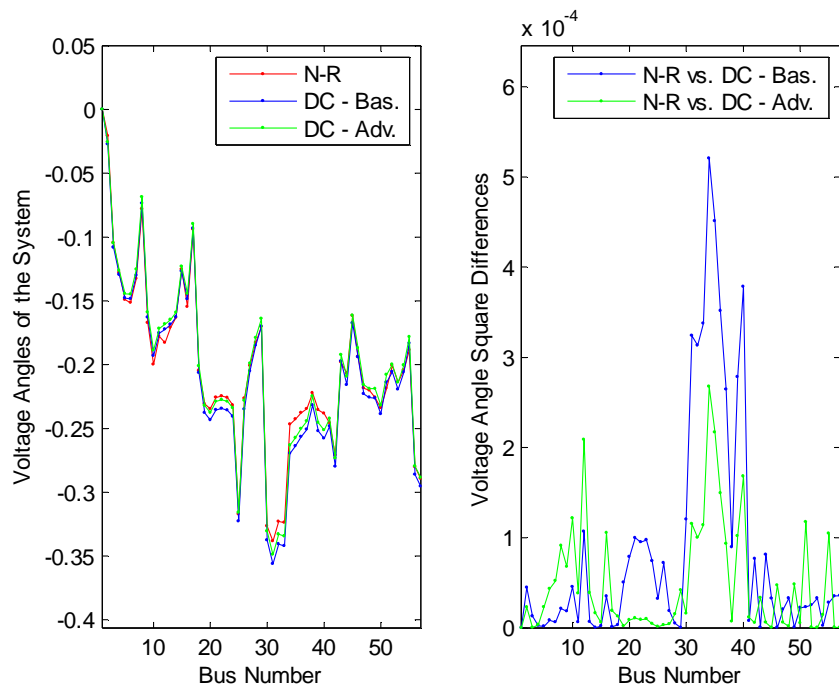
Fig. 11.5-2: Voltage angles and voltage angle square differences - the IEEE 57-bus system

The Advanced DC load flow method provided significantly better approximate solutions than the Basic DC load flow method. If worse solutions are obtained, such degradations of results are rather small. Therefore, proposed Advanced DC load flow technique should be used for fast and close-to-accurate load flow solutions. Otherwise, it is recommended to apply both DC load flow versions and select better solution for reducing computational errors to minimum.

87

12. Testing of Load Flow Methods with OLTC Transformers (V/Q/P)

In this testing session, the G/G-S and N-R methods are further tested for V/Q/P control by OLTC transformers - see Chapters 12.1 and 12.2, respectively. Check on properly programmed and tuned algorithms is performed in many load flow studies - see Tab. 12-1.

Tab. 12-1: Overview of modified IEEE test systems with OLTC transformers

case	number of PV buses	number of OLTC transformers for			number of transformers
		V-control	Q-control	P-control	
IEEE9ltc-1	2	1	2	0	3
IEEE9ltc-2	2	3	0	0	3
IEEE14ltc-1	4	2	1	1	5
IEEE24ltc-1	10	2	1	2	5
IEEE30ltc-1	5	1	1	2	7
IEEE30ltc-2	5	4	0	0	7
IEEE39ltc-1	9	3	0	0	13
IEEE57ltc-1	6	8	3	4	18
IEEE118ltc-1	53	1	3	5	11
IEEE300ltc-1	68	49	1	1	129
IEEE300ltc-2	68	49	0	0	129

In Chapter 12.3, practical situation with voltage/var control in an islanded distribution network with photovoltaic power plants is modelled by the N-R method. In detail, OLTC transformers for V-control along with generators, synchronous condensers and switched shunt capacitor/inductor banks are considered.

12.1 Testing of the G/G-S Methods for V/Q/P Control

To decrease total iteration numbers and CPU times in the G-S method, acceleration technique with optimized acceleration/retardation factors was applied. Without this algorithm, the use of the G-S method would be entirely impossible for dealing with OLTC transformers and PV buses with var limits concurrently.

In the simulations, original G and G-S methods with Basic algorithm for tap/var limits were tested - see Tab. 12.1-1. Moreover, original G-S method (Basic) and improved G-S method (Advanced) were also examined - see Tab. 12.1-2. Total active/reactive system losses and total V/Q/P square errors were evaluated for each tested network.

Tab. 12.1-1: Overview of tested G/G-S algorithms for solving V/Q/P control problems

case	G: Basic					G-S: Basic				
	ΔP [pu]	ΔQ [pu]	iter [-]	time [s]	VQP_err	ΔP [pu]	ΔQ [pu]	iter [-]	time [s]	VQP_err
IEEE9ltc-1	0.0594	-0.5051	3179	0.7488	9.06e-5	0.0594	-0.5051	526	0.2028	9.06e-5
IEEE9ltc-2	0.0507	-0.8012	1157	0.3276	1.37e-6	0.0507	-0.8012	193	0.0624	1.37e-6
IEEE14ltc-1	0.1378	0.3551	1858	0.4680	2.83e-5	0.1378	0.3551	557	0.2184	2.83e-5
IEEE24ltc-1	0.5302	-0.9917	2321	0.6240	1.49e-4	0.5302	-0.9917	548	0.3432	1.49e-4
IEEE30ltc-1	0.1783	0.3530	3119	0.9204	1.65e-5	0.1783	0.3530	438	0.3588	1.65e-5
IEEE30ltc-2	0.1765	0.3313	3334	0.8580	1.19e-6	0.1765	0.3313	535	0.4368	1.19e-6
IEEE39ltc-1	0.4164	-0.5413	4278	1.5600	1.26e-6	0.4164	-0.5413	262	0.2808	1.26e-6
IEEE57ltc-1	0.2779	0.0872	6848	1.7784	2.21e-4	0.2779	0.0872	2227	3.3384	2.22e-4
IEEE118ltc-1	1.7840	-3.5703	50388	13.4160	7.68e-3	1.7840	-3.5703	5560	17.4720	7.68e-3
IEEE300ltc-1	4.3141	-1.4478	63779	36.8160	3.86e-2	4.3141	-1.4478	8548	71.4170	3.86e-2
IEEE300ltc-2	4.3135	-1.4272	65519	34.8510	2.16e-2	4.3118	-1.4654	8476	70.9180	2.16e-2

Tab. 12.1-2: Overview of tested G-S algorithms for solving V/Q/P control problems

case	G-S: Basic					G-S: Advanced				
	ΔP [pu]	ΔQ[pu]	iter [-]	time [s]	VQP_err	ΔP [pu]	ΔQ[pu]	iter [-]	time [s]	VQP_err
IEEE9ltc-1	0.0594	-0.5051	526	0.2028	9.06e-5	0.0597	-0.4983	558	0.5148	2.59e-5
IEEE9ltc-2	0.0507	-0.8012	193	0.0624	1.37e-6	0.0507	-0.8012	178	0.1872	1.37e-6
IEEE14ltc-1	0.1378	0.3551	557	0.2184	2.83e-5	0.1380	0.3557	560	0.8268	7.48e-7
IEEE24ltc-1	0.5302	-0.9917	548	0.3432	1.49e-4	0.5307	-0.9887	579	1.3260	8.39e-5
IEEE30ltc-1	0.1783	0.3530	438	0.3588	1.65e-5	0.1783	0.3530	438	1.2948	1.65e-5
IEEE30ltc-2	0.1765	0.3313	535	0.4368	1.19e-6	0.1765	0.3313	538	1.5444	1.19e-6
IEEE39ltc-1	0.4164	-0.5413	262	0.2808	1.26e-6	0.4164	-0.5413	262	1.0140	1.26e-6
IEEE57ltc-1	0.2779	0.0872	2227	3.3384	2.22e-4	0.2779	0.0872	2130	12.4960	2.22e-4
IEEE118ltc-1	1.7840	-3.5703	5560	17.4720	7.68e-3	1.7954	-3.5007	8599	95.8160	2.83e-3
IEEE300ltc-1	4.3141	-1.4478	8548	71.4170	3.86e-2	4.3229	-1.3859	15390	428.4900	2.24e-2
IEEE300ltc-2	4.3118	-1.4654	8476	70.9180	2.16e-2	4.3118	-1.4654	8509	237.2200	2.16e-2

Note: All simulations in Tabs. 12.1-1 and 12.1-2 were performed at Intel Core Quad CPU 3.00 GHz - 64bit/8 GB RAM station.

Comparing total V/Q/P square errors, it can be seen that the G-S (Advanced) method provided either identical or better results than the G-S (Basic) method. In Tabs. 12.1-3 and 12.1-4, numbers of PV buses switched to PQ and final taps for both Basic and Advanced versions of the G-S method are shown for IEEE24ltc-1 and IEEE57ltc-1 systems, respectively.

Tab. 12.1-3: Overview of G-S algorithms for the IEEE 24-bus system with OLTC transformers

IEEE24ltc-1	G-S: Basic	G-S: Advanced
PV->PQ	1 2 18 21	1 2 18 21
t_{3-24}	1.0060	1.0060
λ_{9-11}	0.0628	0.0646
t_{9-12}	0.9620	0.9620
t_{10-11}	1.1000	1.1000
λ_{10-12}	-0.0646	-0.0663
VQP_err	1.49e-4	8.39e-5

Tab. 12.1-4: Overview of G-S algorithms for the IEEE 57-bus system with OLTC transformers

IEEE57ltc-1	G-S: Basic	G-S: Advanced
PV->PQ	8 9 12	8 9 12
t_{4-18-1}	0.9900	0.9900
t_{4-18-2}	0.9910	0.9910
$\lambda_{24-25-1}$	0.0018	0.0018
$\lambda_{24-25-2}$	0.0969	0.0969
t_{7-29}	0.9610	0.9610
t_{34-32}	0.9280	0.9280
t_{11-41}	0.9275	0.9275
t_{41-43}	1.0000	1.0000
t_{15-45}	0.9400	0.9400
t_{14-46}	0.9160	0.9160
t_{10-51}	0.9400	0.9400
t_{13-49}	0.8800	0.8800
λ_{40-56}	0.0279	0.0279
λ_{39-57}	0.0401	0.0401
t_{9-55}	0.9200	0.9200
VQP_err	2.22e-4	2.22e-4

Finally, the IEEE 300-bus system with OLTC transformers (IEEE300ltc-1) was solved by both G-S methods. Voltage, bus type and tap conditions are iteratively shown for both methods - see Figs. 12.1-1 to 12.1-8. Note: Different colours are used for voltages and taps.

89

Fig. 12.1-1: Voltage magnitudes of IEEE300ltc-1 power system - G-S (Basic) method
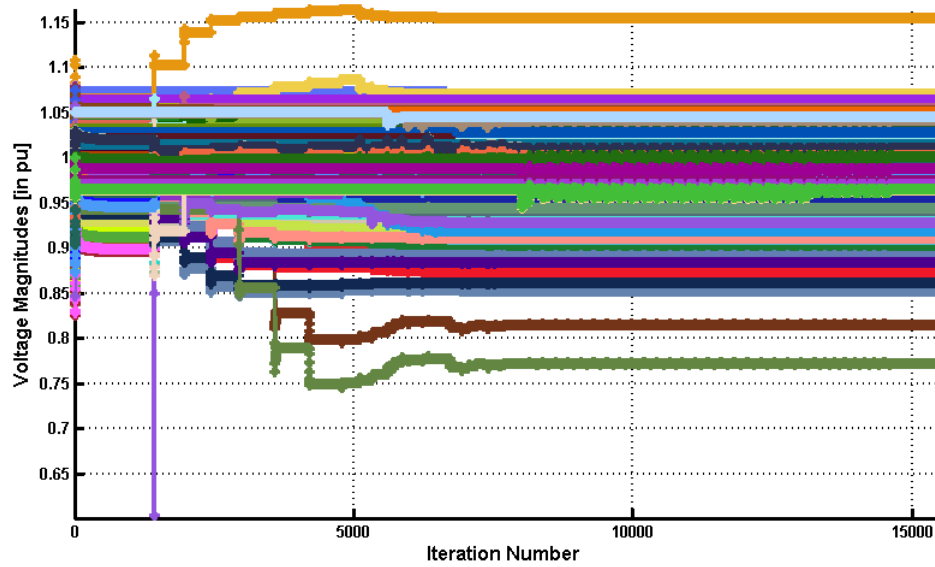
Fig. 12.1-2: Voltage magnitudes of IEEE300ltc-1 power system - G-S (Advanced) method
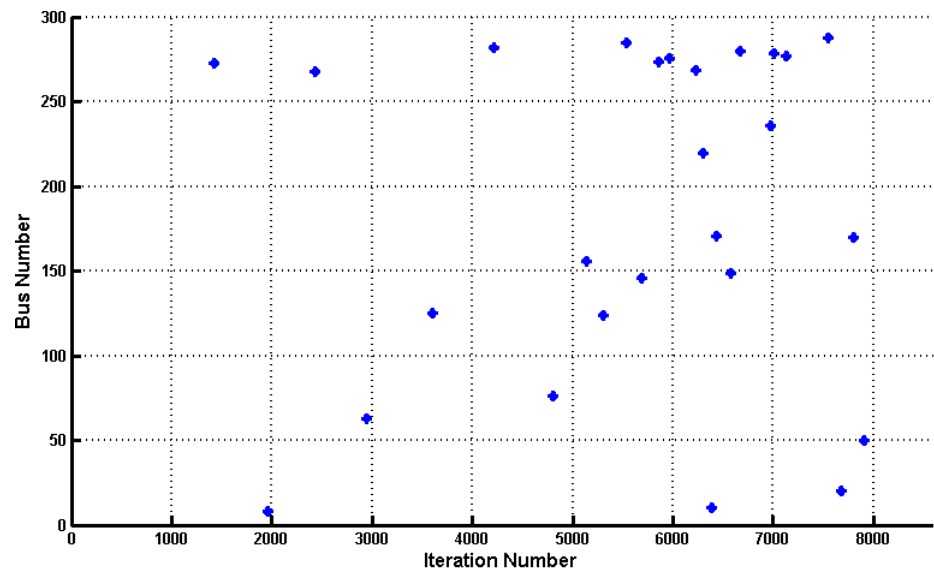
Fig. 12.1-3: Bus type conditions of IEEE300ltc-1 power system - G-S (Basic) method
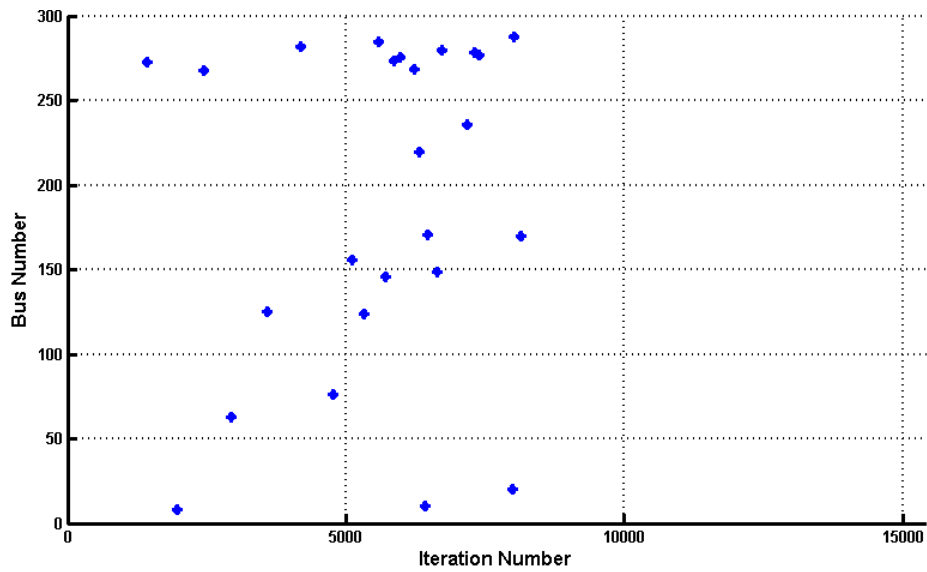
Fig. 12.1-4: Bus type conditions of IEEE300ltc-1 power system - G-S (Advanced) method
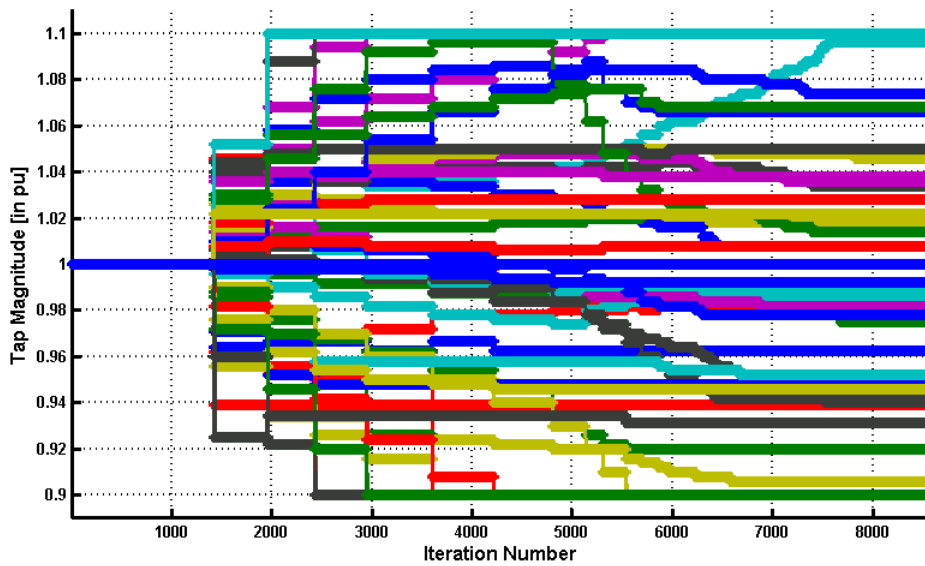
Fig. 12.1-5: Tap magnitudes of IEEE300ltc-1 power system - G-S (Basic) method
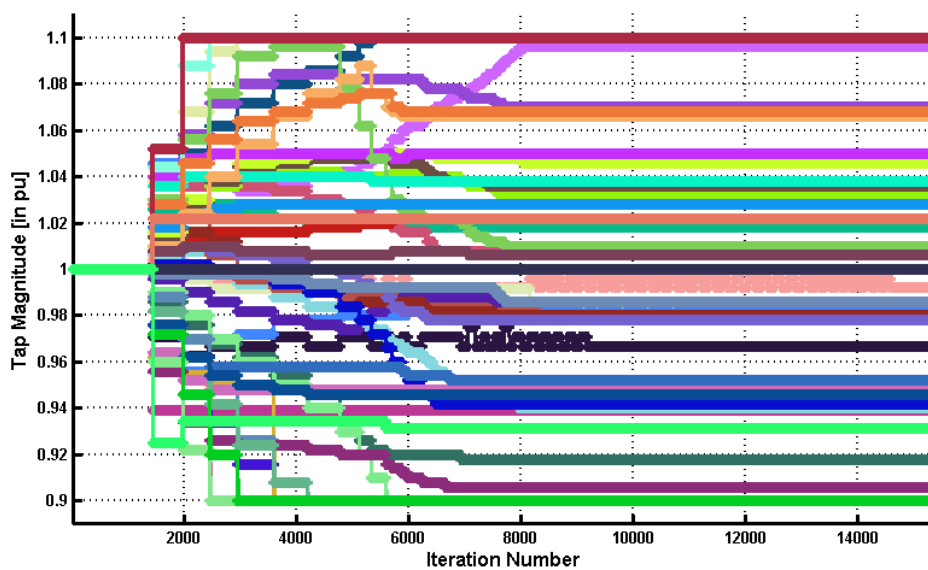
Fig. 12.1-6: Tap magnitudes of IEEE300ltc-1 power system - G-S (Advanced) method
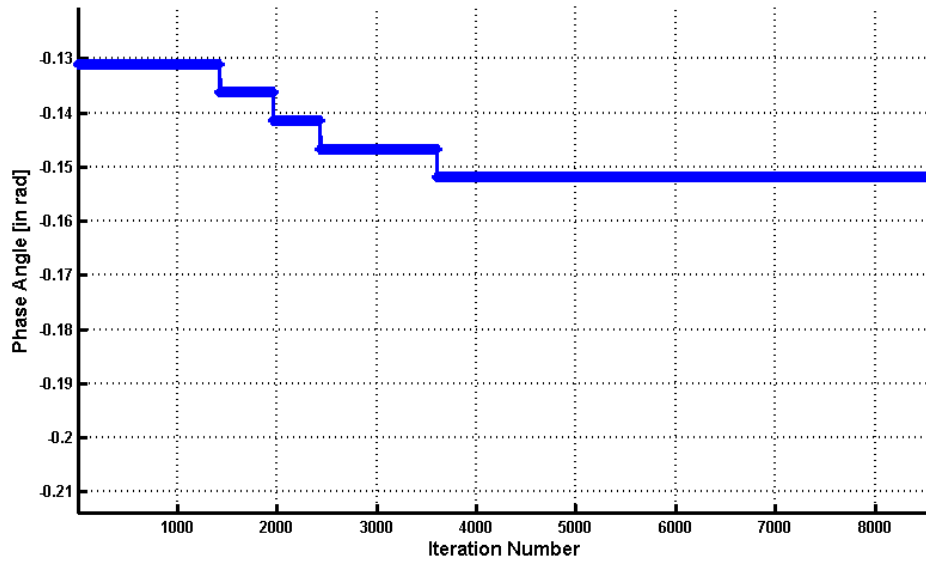
Fig. 12.1-7: Tap angles of IEEE300ltc-1 power system - G-S (Basic) method
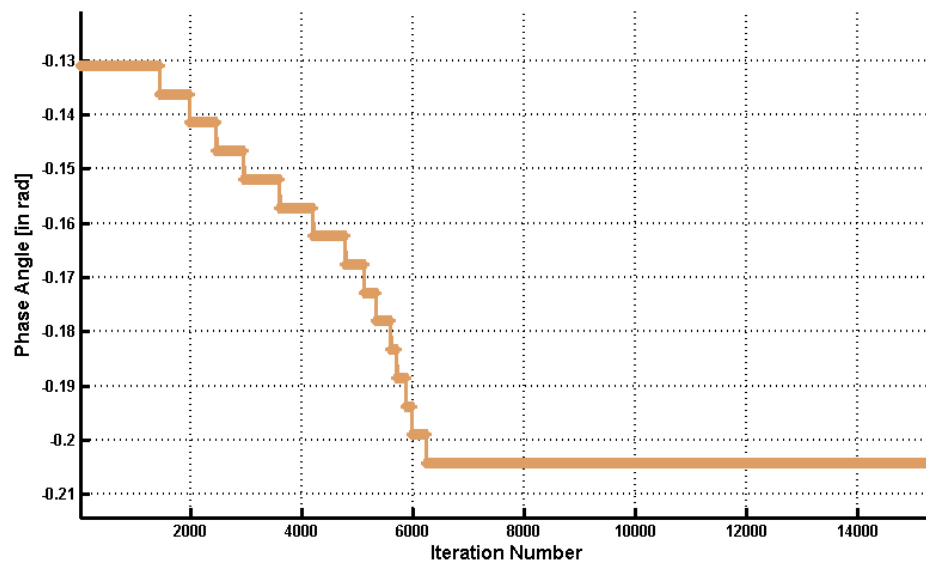
Fig. 12.1-8: Tap angles of IEEE300ltc-1 power system - G-S (Advanced) method

With clearly visible tap oscillations, the Advanced G-S method needed almost twice the number of the Basic G-S method for finding final results. However, only slight improvement of the V/Q/P square error value was achieved. In total, 26 and 25 PV buses were eventually switched to PQ for Basic and Advanced G-S method, respectively. During the tap oscillations, remaining tap magnitudes sufficiently converged so that these oscillating taps either converged to final tap settings by themselves or they were forcedly switched to fixed-tap mode when exceeding maximum number of jumps. Absolutely different final tap angles were obtained by individual G-S algorithms.

In conclusion, slightly better solutions of the Advanced G-S method are downgraded by significantly increased total iteration numbers and CPU times. Due to its more complex programming, the Basic G-S method is preferred to by applied in the author-developed computing tool. Also, the G method proved to be even more suitable offering highly accurate results with much less CPU times for larger load flow cases.

12.2 Testing of the N-R Method for V Control

Instead of the One-Shot F-D method, two iterations of the F-D method (XB-type) were implemented. It was observed that the N-R method is strongly affected by DXT settings of the SUT algorithm. To obtain reliable solutions, DXT values of 0.4/0.27/0.135 were applied for voltage magnitudes, voltage angles and tap magnitudes, respectively.

Only the V control by OLTC transformers was successfully tested using the N-R method. For Q/P controls, the concept was too unreliable and numerically unstable since the taps (magnitudes and angles) were always switched to their limits immediately after a few iterations. Thus, only systems IEEE9ltc-2, IEEE30ltc-2, IEEE39ltc-1 and IEEE300ltc-2 were tested - see Tab. 12.2-1. Detailed information about final tap settings for former three systems is shown in Tab. 12.2-2 where compared with the G/G-S methods.

Tab. 12.2-1: Overview of the tested N-R algorithm for solving V control problems

case	G-S (Basic) method with acc/ret factors					N-R method				
	ΔP [pu]	ΔQ [pu]	iter [-]	time [s]	VQP_err	ΔP [pu]	ΔQ [pu]	iter [-]	time [s]	VQP_err
IEEE9ltc-2	0.0507	-0.8012	193	0.2704	1.37e-6	0.0503	-0.7802	6	0.0728	5.34e-4
IEEE30ltc-2	0.1765	0.3313	535	1.9604	1.19e-6	0.1776	0.3382	3	0.0624	0.00e+0
IEEE39ltc-1	0.4164	-0.5413	262	1.1284	1.26e-6	0.4163	-0.5450	5	0.078	1.01e-6
IEEE300ltc-2	4.3118	-1.4654	8512	272.8717	2.16e-2	4.3466	-0.7990	10	0.1352	5.22e-2

Tab. 12.2-2: Overview of final tap settings produced by G/G-S/N-R algorithms

case	final tap settings		
	G method	G-S method	N-R method
IEEE9ltc-2	1.0280	1.0280	1.0238
	0.9740	0.9740	1.1000
	0.9960	0.9960	0.9874
IEEE30ltc-2	0.9420	0.9420	0.9169
	1.0060	1.0060	1.0036
	0.9620	0.9620	0.9539
	1.0020	1.0020	0.9922
IEEE39ltc-1	1.0000	1.0000	1.0800
	0.9960	0.9960	1.0800
	1.0120	1.0120	1.0131

The N-R code was realized for both the systems with/without OLTC transformers. For the code complexity evaluation, both older/newer versions (without/with OLTC algorithms) of the N-R method were compared in terms of CPU time requirements when solving the largest test systems (above 2000 buses) - see Tab. 12.2-3.

Tab. 12.2-3: CPU time requirements of the N-R method without/with OLTC algorithms

case	CPU time [s]		
	without OLTC algorithms	with OLTC algorithms	increase by [%]
EPS2383I	0.2808	0.3380	20.3704
EPS2736I	0.4056	0.4368	7.6923
EPS2737I	0.2340	0.2860	22.2222
EPS2746I	0.4524	0.5200	14.9425
EPS2746II	0.3120	0.3744	20.0000
EPS3012I	0.2964	0.3931	32.6248
EPS3120I	0.3120	0.3796	21.6667

From Tab. 12.2-3 follows that the maximum CPU time increase was about 33 percent. This gives enough information about the code complexity of V control by OLTC transformers in the N-R method.

For the IEEE300ltc-2 system, final tap settings produced by the G/G-S/N-R methods are shown in Fig. 12.2-1. Detailed outputs of voltage magnitudes, phase angles, bus types, var generations and tap magnitudes are further provided - see Figs. 12.2-2 to 12.2-6.
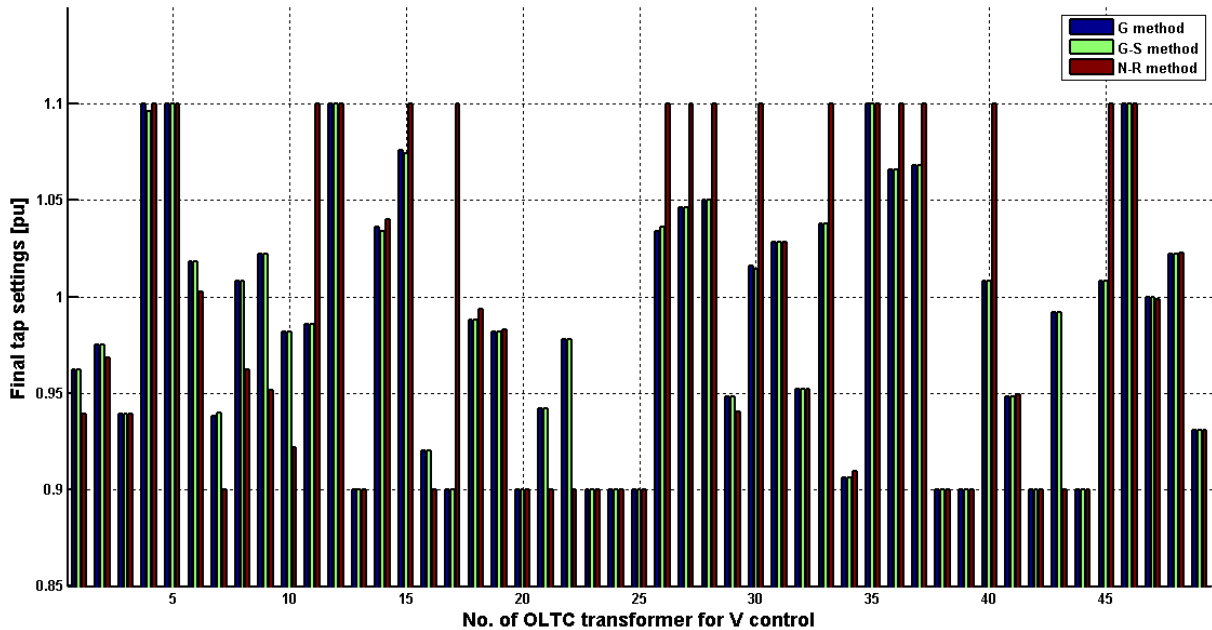
Fig. 12.2-1: Final tap settings by G/G-S/N-R algorithms for the IEEE300ltc-2 system

Fig. 12.2-1 demonstrates significant tap deviations between the G/G-S and N-R methods (total of 13 from all 49 cases). All three load flow methods switched 26 PV buses (of total 68) to PQ while G/G-S and N-R algorithms converted 15 and 33 OLTC transformers (of total 49) to fixed, respectively.
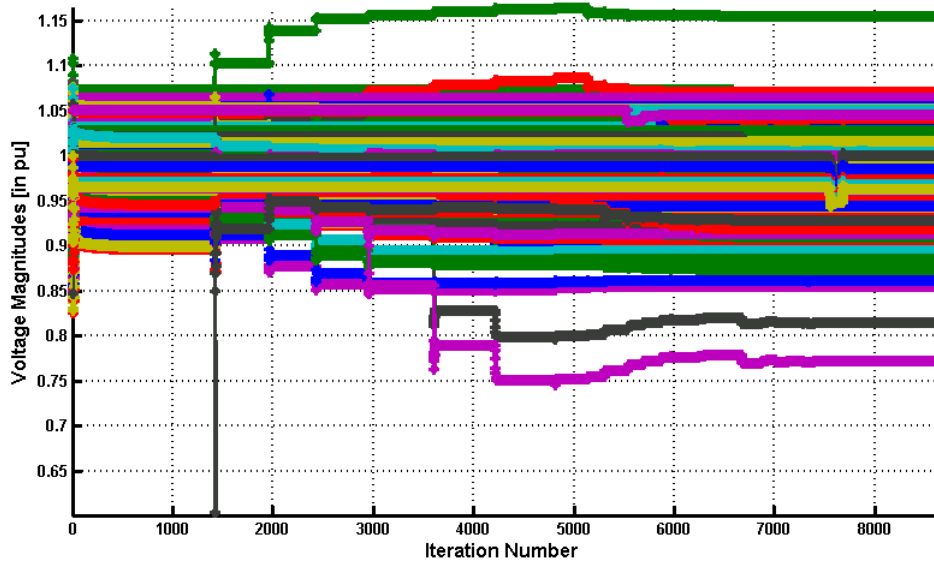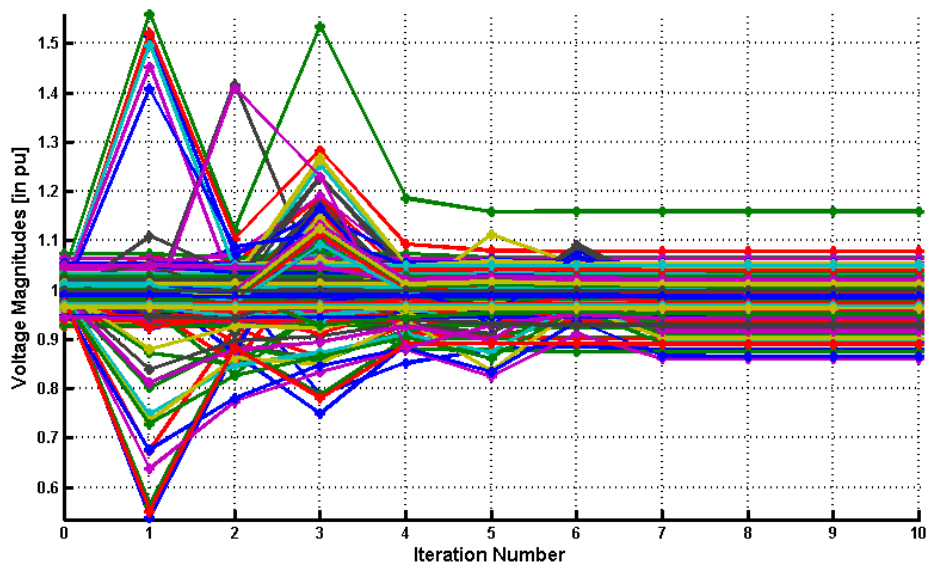

Fig. 12.2-2: Voltage magnitudes of IEEE300ltc-2 power system - N-R method
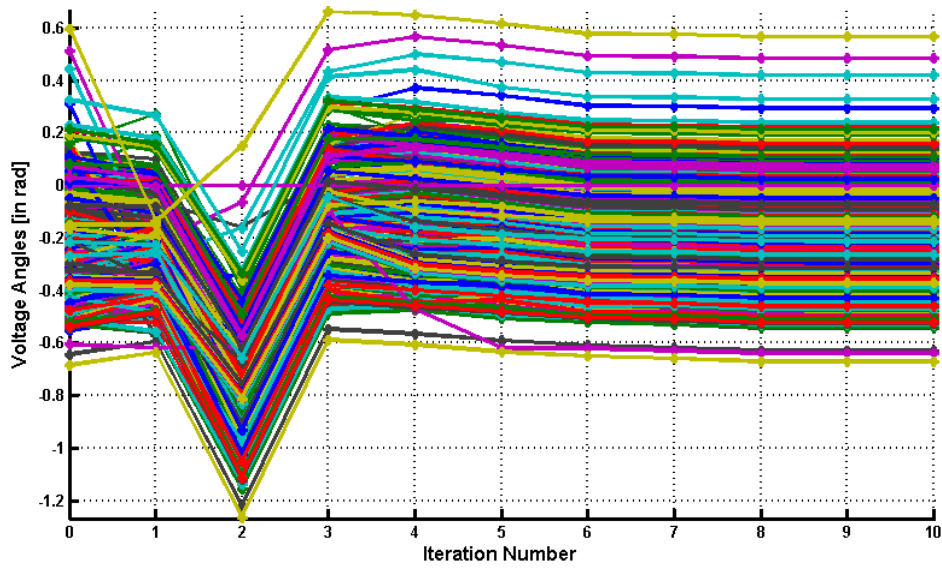
Fig. 12.2-3: Voltage angles of IEEE300ltc-2 power system - N-R method
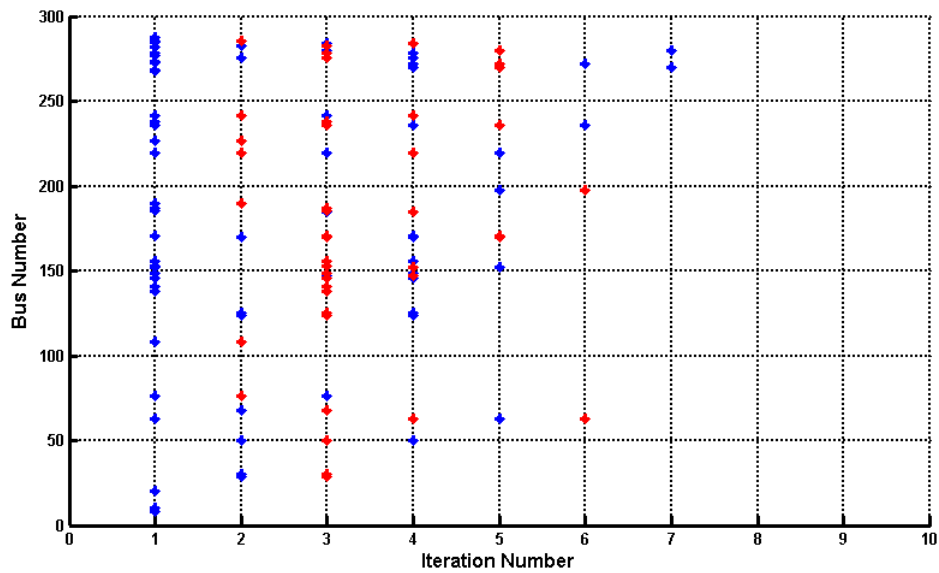
Fig. 12.2-4: Bus type conditions of IEEE300ltc-2 power system - N-R method
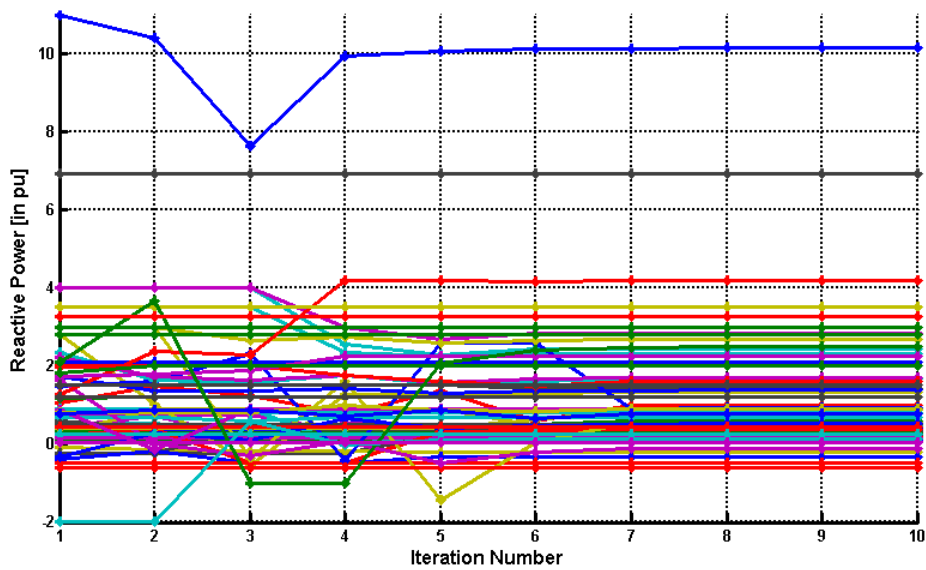
Fig. 12.2-5: Var injections of IEEE300ltc-2 power system - N-R method
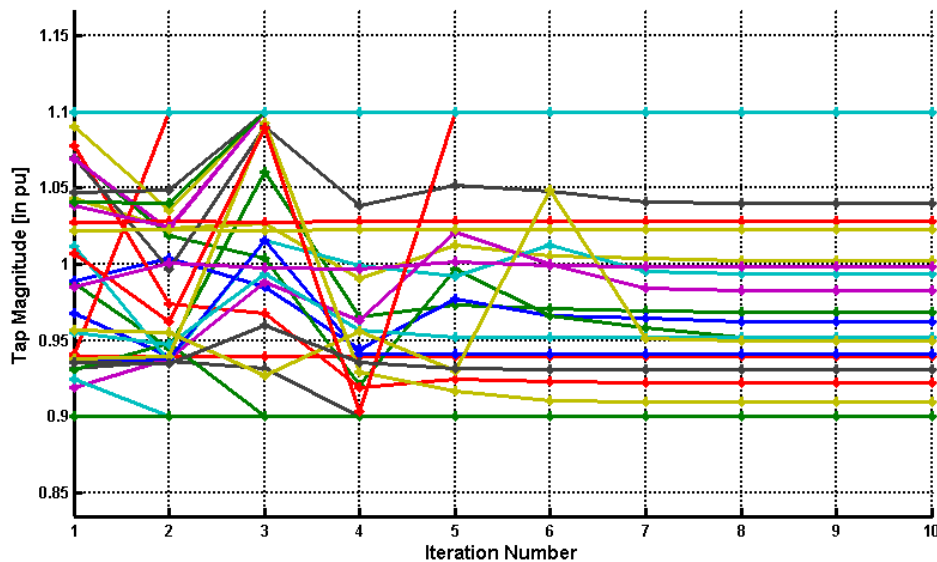
Fig. 12.2-6: Tap magnitudes of IEEE300ltc-2 power system - N-R method

The N-R method switches significantly more transformers to fixed than the G/G-S methods. Even with continuous tap settings, total V/Q/P error value is then often much higher. Thus, more work must be done for improving the codes of OLTC transformers for the N-R method to obtain better solutions. One possible way is to implement fair collaboration of the reverse switching logic for tap magnitudes/angles, priorities or convergence criteria and SUT settings. Another methodology is to apply tap sensitivities which should provide much gentle tap modifications in OLTC transformers.

12.3 Voltage Control in Islanded Distribution Networks - Winter Scenario

For testing various voltage control mechanisms, the modified version of IEEE 123-bus radial system [81] was employed: a) original 3-phase input data (loads, branch parameters) were averaged for only 1-phase analysis, b) switches were opened/closed according to instructions given, c) original frequency and voltage levels (60 Hz, 115/4.16/0.48 kV) in loads and branch parameters were replaced by those common in Czech Republic (50 Hz, 110/6/0.4 kV), d) several buses were cancelled for achieving islanded system operation, e) five photovoltaic power plants (Tab. 12.3-1) with relevant 6/0.4 kV fixed-tap transformers 150 kVA were connected, f) two additional isolation transformers 2 MVA were placed instead of original switches to worsen local voltage conditions and the distribution of reactive power.

Tab. 12.3-1: PV power plants for winter (undervoltage) scenario

bus	nominal power [kWp]
119	80
124	100
125	90
126	70
127	80

Steady-state model [63] of the photovoltaic cell with temperature and irradiation corrections is applied. Active power output includes the level of cloud formation (8-step scale: 0 - no cloudiness, 8 - full cloudiness), losses (3 to 12 %) and number of cells. Optimum

voltage for maximum power output is found by differentiating the active power formula, setting to zero and using the Newton method for solving the respective nonlinear equation. Photovoltaic power plants are considered as PQ power sources with power factor dependent on the active power generation. Reactive power is negative (i.e. consumed) for small irradiances and positive (i.e. delivered) for higher irradiances. Linearized P-Q dependence [54] was used for finding the actual reactive power of the power plant.

Average daytime temperature and clear-sky global irradiance data were obtained using specialized web application [78] for given locality in Czech Republic and the month December. In this month, the lowest active power generations are observed. Thus, photovoltaic sources would consume the maximum reactive power and significantly worsen voltage conditions of the system (i.e. December is the worst-case scenario for the undervoltage study). For voltage control, three OLTC isolation transformers (Tab. 12.3-2) were connected to improve voltage conditions in the most critical regions of the system. In remaining network sections, two synchronous condensers (SC), three capacitor banks (CB) and two generators (G) - possible waste incineration plant and biomass power plant - were included (Tab. 12.3-3). Note: For capacitor banks (modelled as PV buses), standard PV-PQ bus-type switching logic is to be applied along with the rounding process to closest integers (activated numbers of capacitor steps) when close to convergence.

Tab. 12.3-2: OLTC isolation transformers for undervoltage scenario

from-to bus	nominal power [kVA]	tap settings (min/max/step)	targeted voltage [pu]
018-021	2000	0.9/1.1/0.00625	0.96
013-115	3000	0.9/1.1/0.002	0.98
060-116	2000	0.9/1.1/0.008	0.96

Tab. 12.3-3: Voltage-controlled devices for undervoltage scenario

bus	type	active power [kW]	min/max var limits [kVAr]	specified voltage [pu]
008	G	-	-	0.95
076	G	2000	-350/650	0.95
044	SC	0	-75/150	0.94
101	SC	0	-50/100	0.96
064	CB	0	0/7x50	0.97
094	CB	0	0/6x100	0.96
110	CB	0	0/10x50	0.96

Secondary bus of every OLTC transformer was always selected for voltage control. Targeted/specified voltage values, var limits and tap settings were intentionally set for worsening voltage conditions in the system and forcing applied logics to higher activity.

Original active and reactive power loads from IEEE 123-bus radial system [81] were taken as maximum (peak) values for modelling the loads in individual network buses. Time-dependence of the loads was defined using power coefficients of normalized load diagrams (type 1-7, see [77]) for chosen month and day. For obtaining sufficiently smooth outputs of the entire simulation, both load consumptions and photovoltaic generations were recalculated to 5-minute interval data. System operation can be still taken as steady-state since all transients would be damped due to very short time constant of the network.
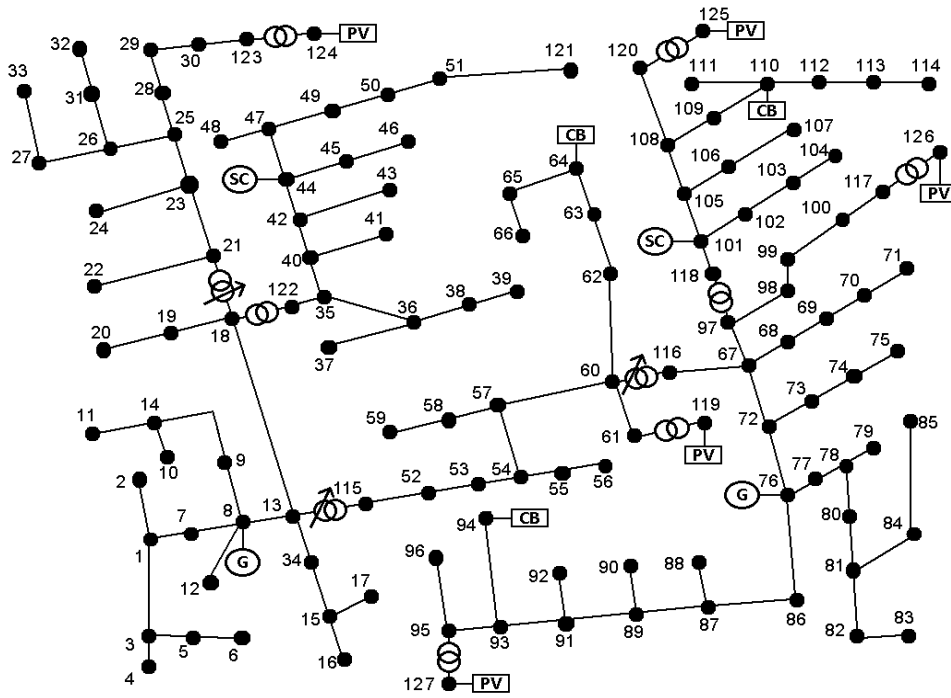
Fig. 12.3-1: Modified version of IEEE 123-bus radial network - undervoltage scenario

This situation (see Fig. 12.3-1) fairly matches the future isolated smart grid operation with large number of dispersed power sources and lack of reactive power when operated close to feasible voltage limits. Therefore, such systems are worthy to be simulated with focus on voltage conditions using conventional or novel voltage-control mechanisms.

For the simulation itself, a script in MATLAB was developed to solve all 277 load flow problems (from 1 am to 12 pm) by the N-R method with included OLTC algorithms for V control. High convergence speed was achieved by using the final solution from the previous time interval as the initial estimate for the subsequent one. No numerical problems were detected when dealing with both tap-/var- logics.

Optimal settings of tap changers and capacitor banks for keeping all system voltage magnitudes within permitted limits (or at the targets) in all time intervals are shown in Figs. 12.3-2 and 12.3-3.
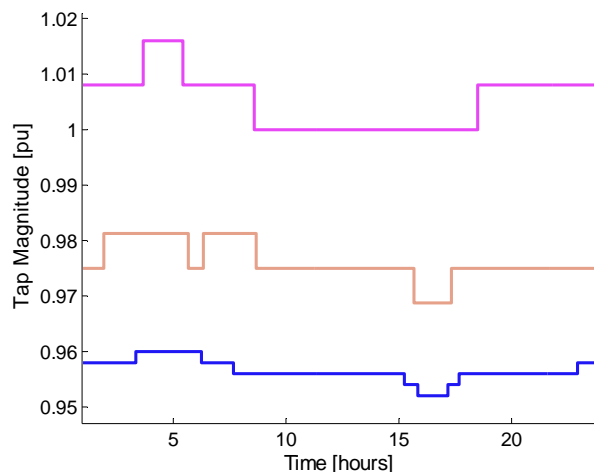
Fig. 12.3-2: Tap settings of OLTC transformers for V-control
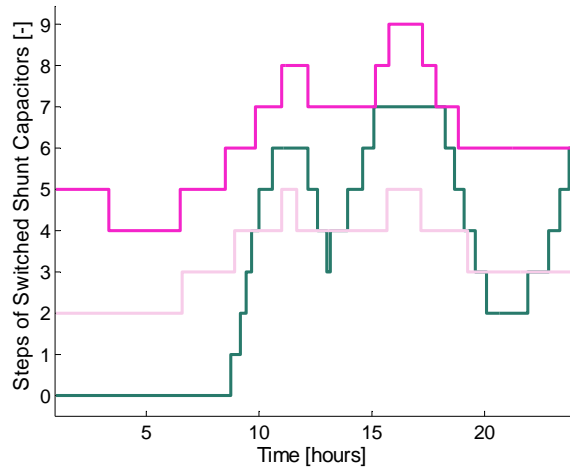
Fig. 12.3-3: Numbers of capacitor steps activated

Var generations from both discrete/continuous voltage-controlled devices are provided in Fig. 12.3-4. Note: Default base of 100 MVA was applied.
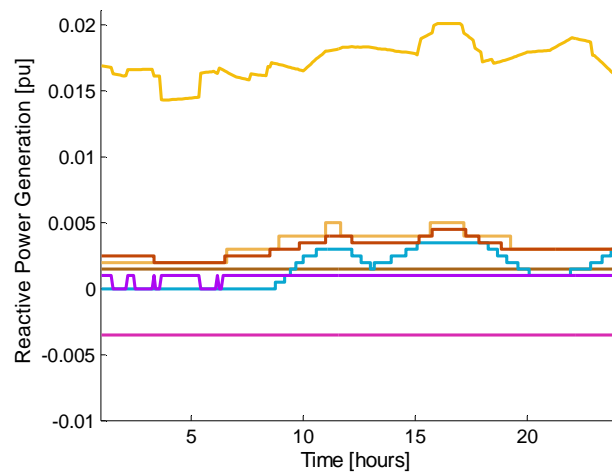
Fig. 12.3-4: Var generations by voltage-controlled devices

In Fig. 12.3-5, voltage conditions with applied voltage mechanism (right) are compared to those without activated OLTC transformers, synchronous condensers and capacitor banks (left).
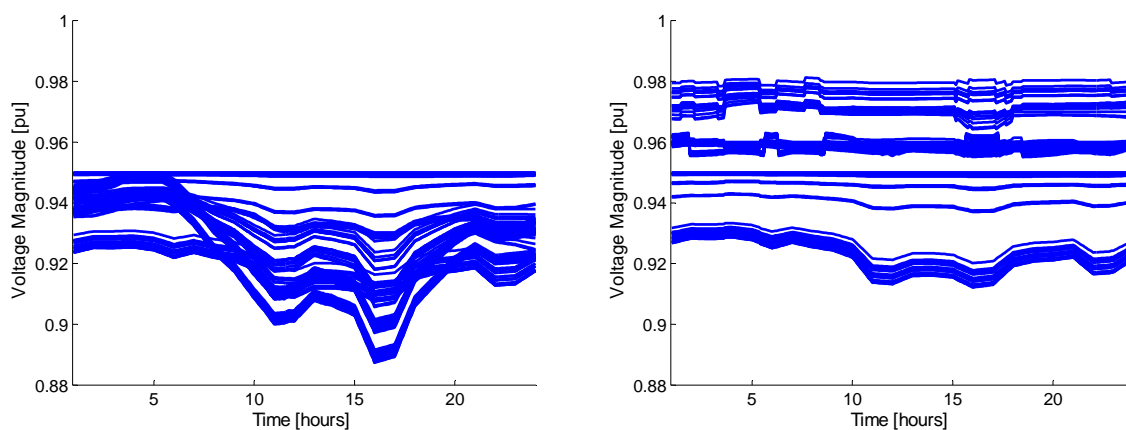
Fig. 12.3-5: Voltage conditions - without V control (left) and with V control (right)
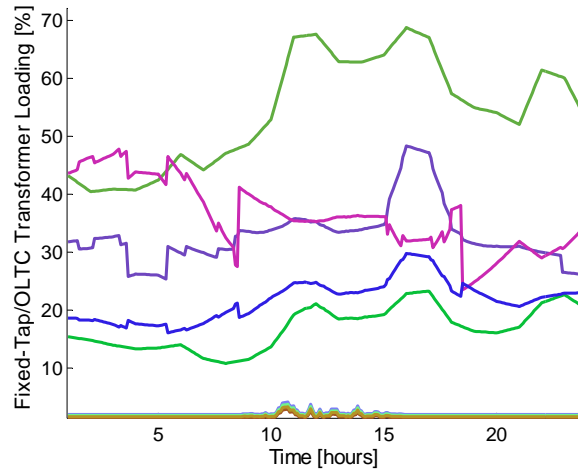
Fig. 12.3-6: MVA loadings of fixed-tap and OLTC transformers

During the entire simulation, loadings of all fixed-tap and OLTC transformers were kept in tolerable limits - see Fig. 12.3-6.
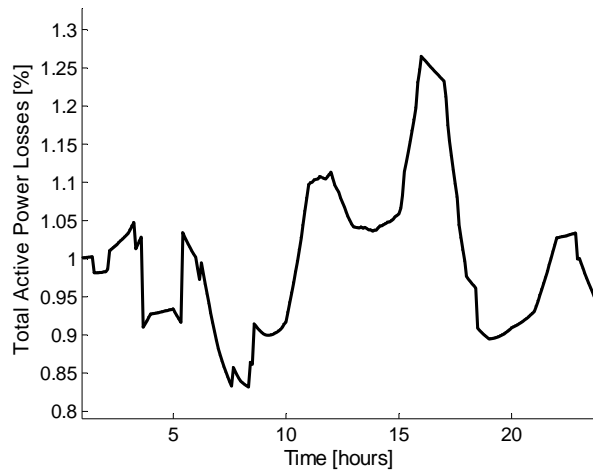
Fig. 12.3-7: Total active system losses

Total active power losses (Fig. 12.3-7) were calculated moving only between 0.832 and 1.265 percent. Active energy losses of 0.998 MWh were detected for the day-time operation.

12.4 Voltage Control in Islanded Distribution Networks - Spring Scenario

In the modified IEEE 123-bus distribution network, two additionally placed isolation transformers were replaced by original switches. Photovoltaic data for April give the highest active/reactive power generations. With zero cloudiness level, these sources could cause serious system overvoltages (i.e. April is the worst-case scenario for the overvoltage study).

Tab. 12.4-1: PV power plants for spring (overvoltage) scenario

bus	nominal power [kWp]
119	200
124	240
125	220
126	180
127	200

100

For the overvoltage study, three OLTC isolation transformers were connected along with two synchronous condensers (SC), five inductor banks (IB) and two generators (G) - see Tabs. 12.4-2 and 12.4-3, respectively. Note: Inductor banks are also modelled as PV buses, the PV-PQ bus-type switching logic and the rounding process to closest integer is applied.

Tab. 12.4-2: OLTC isolation transformers for overvoltage scenario

from-to bus	nominal power [kVA]	tap settings (min/max/step)	targeted voltage [pu]
018-021	2000	0.9/1.1/0.002	1.08
013-115	3000	0.9/1.1/0.005	1.08
060-116	2000	0.9/1.1/0.003	1.06

Tab. 12.4-3: Voltage-controlled devices for overvoltage scenario

bus	type	active power [kW]	min/max var limits [kVAr]	specified voltage [pu]
008	G	-	-	1.100
076	G	2000	-350/350	1.100
044	SC	0	-45/85	1.090
101	SC	0	-50/100	1.080
029	IB	0	14x-25/0	1.075
061	IB	0	12x-50/0	1.080
091	IB	0	20x-25/0	1.060
108	IB	0	14x-25/0	1.060
117	IB	0	12x-50/0	1.060
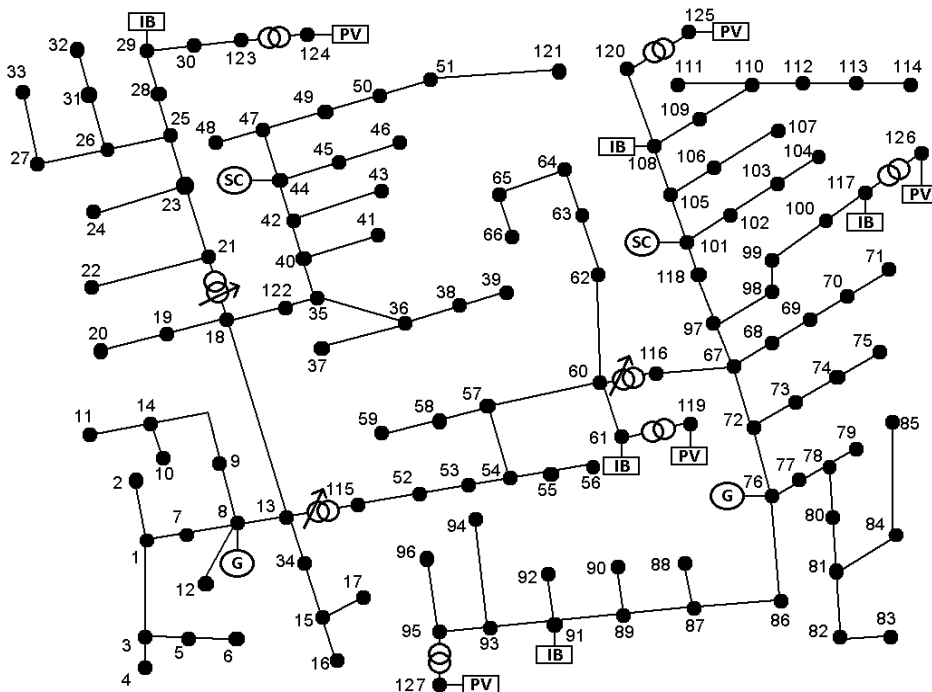
Fig. 12.4-1: Modified version of IEEE 123-bus radial network - overvoltage scenario

In Fig. 12.4-1, isolated smart grid operation with injections from PV power sources and the excess of reactive power is simulated when close to feasible voltage limits. Due to massive future use of electromobiles, there would be intentions to control the power factor also in ordinary households by individual compensation devices. Therefore, reactive power loads were also neglected for the entire study. With no numerical problems detected, identical script (see Chapter 12.3) was used to solve all load flow problems of this study.

Optimal settings of tap changers and inductor banks for keeping all system voltage magnitudes within permitted limits (or at the targets) in all time intervals are shown in Figs. 12.4-2 and 12.4-3, respectively. For var injections from V-controlled devices - see Fig. 12.4-4.
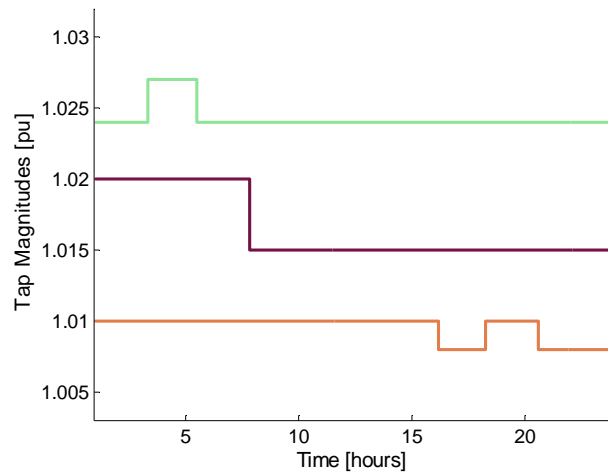
Fig. 12.4-2: Tap settings of OLTC transformers for V-control
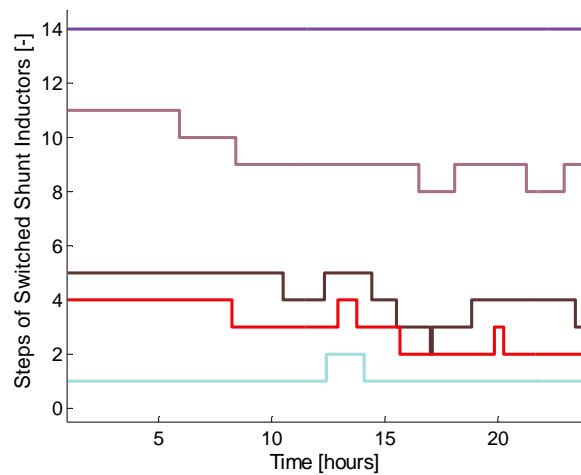
Fig. 12.4-3: Numbers of inductor steps activated
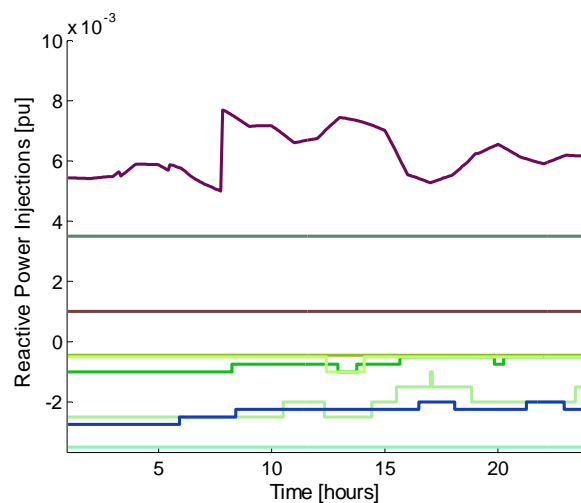
Fig. 12.4-4: Var generations by voltage-controlled devices

In Fig. 12.4-5, voltage conditions without/with applied voltage mechanism (left/right) are mutually compared. Loadings of all fixed-tap/OLTC transformers were kept in tolerable limits - see Fig. 12.4-6. For transformers of PV power plants, much higher loadings were seen.
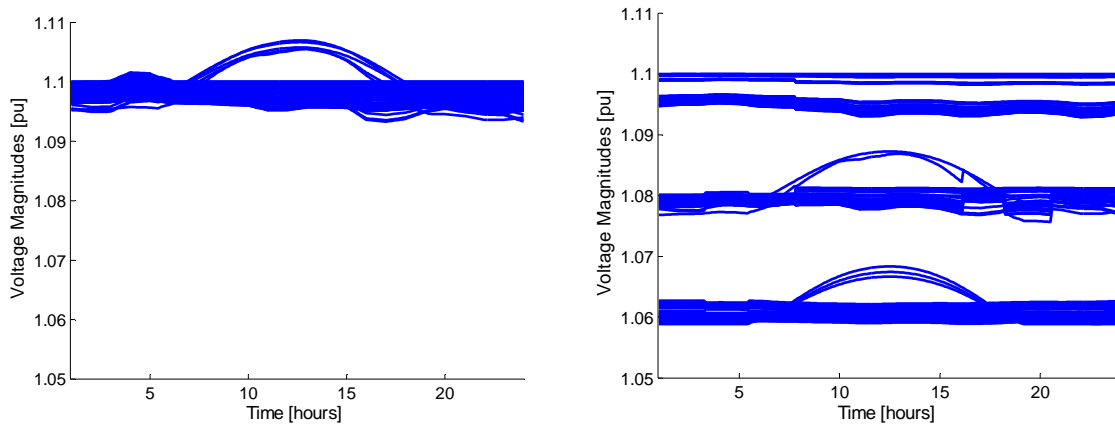
Fig. 12.4-5: Voltage conditions - without V control (left) and with V control (right)
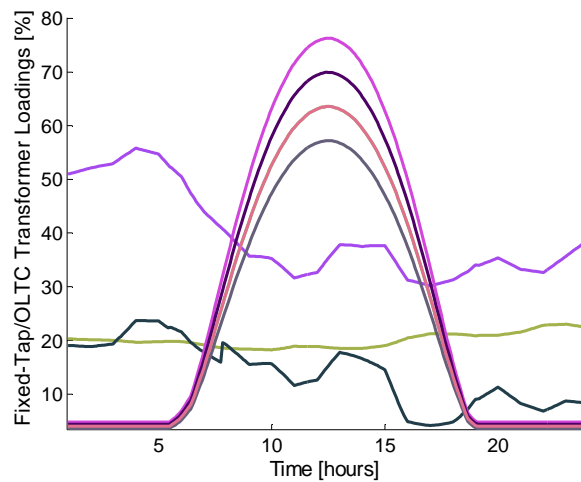
Fig. 12.4-6: MVA loadings of fixed-tap and OLTC transformers
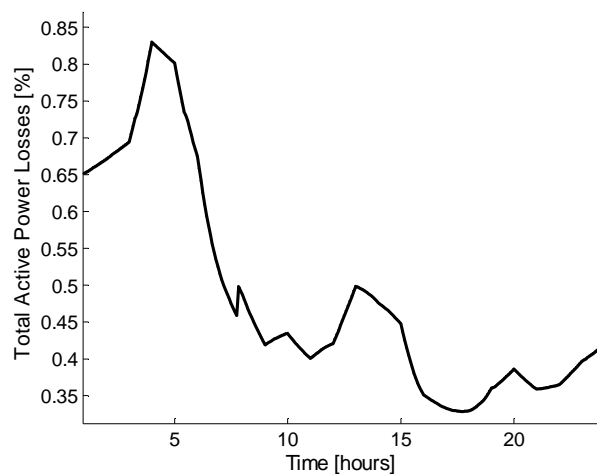
Fig. 12.4-7: Total active system losses

Total active power losses (Fig. 12.4-7) produced active energy losses of 0.328 MWh for the day-time operation.

13. Testing of Load Flow Methods in the Voltage Stability Analysis

In this testing session, both the Cycled N-R and CLF algorithms were tested on broad range of networks to find their compromise settings in terms of solution accuracy and calculation speed - see Chapter 13.1. Full voltage stability analysis of a highly loaded power system is then provided by the CLF algorithm - see Chapter 13.2. Fundamental testing of the Shortest Distance to Voltage Instability (SDVI) approach along with two practical case studies is presented in Chapters 13.3 to 13.5, respectively. All the testings were performed at IntelCore i3 CPU 2.53 GHz/3.8 GB RAM station.

13.1 Initial Testing of Cycled N-R and CLF Algorithms

Total number of 50 test power systems between 3 and 734 buses were analyzed using developed Cycled N-R and CLF algorithms in MATLAB environment. Identical increase rate was applied to all network buses (before filtering those with non-zero active power loads or generations). For both L and L+G scenarios, only stable part of the V-P curve was calculated with included var limits.

In Tab. 13.1-1, results of several test cases are shown for three different accuracy settings (see Chapter 8.3) in relevant rows, respectively.

1] CLF - highly accurate: $\sigma_U = 2.5 \times 10^{-2}$, $\sigma_L = 6.25 \times 10^{-4}$, $\varepsilon = 1 \times 10^{-10}$, $p_{max} = 20$

2] CLF - fair compromise: $\sigma_U = 5 \times 10^{-2}$, $\sigma_L = 1 \times 10^{-2}$, $\varepsilon = 1 \times 10^{-6}$, $p_{max} = 20$

3] Cycled N-R: $\Delta\lambda_{init} = 2.5 \times 10^{-2}$, $\varepsilon = 1 \times 10^{-8}$, $p_{max} = 20$, $\varepsilon_{end} = 1 \times 10^{-8}$

Presented results contain maximum loadabilities, numbers of stable V-P points and CPU times needed.

Tab. 13.1-1: Voltage stability solutions by Cycled N-R and CLF algorithms - L/L+G scenarios

case	scenario L			scenario L+G		
	λ_{max} [-]	points	time [s]	λ_{max} [-]	points	time [s]
IEEE9II	1.302632	331	0.5616	1.162053	215	0.3900
	1.302632	27	0.1404	1.162052	24	0.1248
	1.302632	23	0.4056	1.162053	20	0.4212
IEEE14	1.760331	658	1.2012	1.777995	506	0.9360
	1.760331	87	0.2340	1.777995	59	0.2028
	1.760331	43	0.5460	1.777995	45	0.6396
IEEE30	1.536905	854	1.9500	1.546751	726	1.6536
	1.536905	88	0.2808	1.546752	124	0.4212
	1.536905	37	0.6396	1.546751	37	0.6552
IEEE57	1.406778	891	2.9016	1.616845	399	1.3884
	1.406778	229	0.6864	1.616845	57	0.2652
	1.406778	27	0.8112	1.616845	37	0.8112
IEEE162	1.079959	1640	12.9169	1.138996	1185	9.3913
	1.079960	464	3.1044	1.138996	65	0.8112
	1.079960	13	1.7628	1.138996	16	1.8408
IEEE300	1.024573	8457	103.8655	1.058820	311	4.0092
	1.024573	529	7.0044	1.058819	94	1.4508
	1.024573	16	2.4180	1.058820	17	2.5584
EPS734II	3.104162	139	4.5864	3.104162	139	4.8360
	3.104083	46	1.8720	3.104083	46	1.8408
	3.104162	96	8.2369	3.104162	96	8.1745

As can be seen, exact solutions of maximum loadability were obtained for both of tested methods and each of the three accuracy settings. The first setting was definitely too much focused on producing exact results. Therefore, numbers of V-P points and CPU times were pushed often above 200 and 1 second, respectively. When using fair compromise setting, the maximum error for λ_{max} from all 50 test power systems was only 0.0185 percent, while numbers of V-P points and CPU times were decreased on average by 75.27 percent and 64.11 percent, respectively.

Cycled N-R code obtains highly accurate results and usually provides even better solutions than the CLF algorithm with compromise accuracy. Surprisingly, it always computes slightly higher maximum loadabilities than by the high-accurate CLF code which seems to be one visible drawback of the Cycled N-R method. Only low numbers of V-P points are needed for reaching close proximity to singular point. These numbers are well comparable to those needed for compromise CLF code. Unfortunately, each divergence case (between 22 and 28) significantly delays the entire computation process of the Cycled N-R method. Therefore, the Cycled N-R code suffers from being extremely time-dependent on computing each V-P point. When compared to the compromise CLF code, the CPU time needed by the Cycled N-R method is on average about 167 % higher. Therefore, the compromise CLF code seems to be the best method for providing fast and highly accurate voltage stability solutions.

Stable V-P curves of the IEEE 30-bus power system (L+G scenario) are computed by both Cycled N-R and CLF methods and shown in Figs. 13.1-1 and 13.1-2, respectively. For the CLF method, the V-P curves are extended to demonstrate numerical stability of this algorithm around the singular point. Fair compromise setting was applied with var limits included. Extension of V-P curves in the unstable region is provided for $0.97\lambda_{max} < \lambda < \lambda_{max}$.
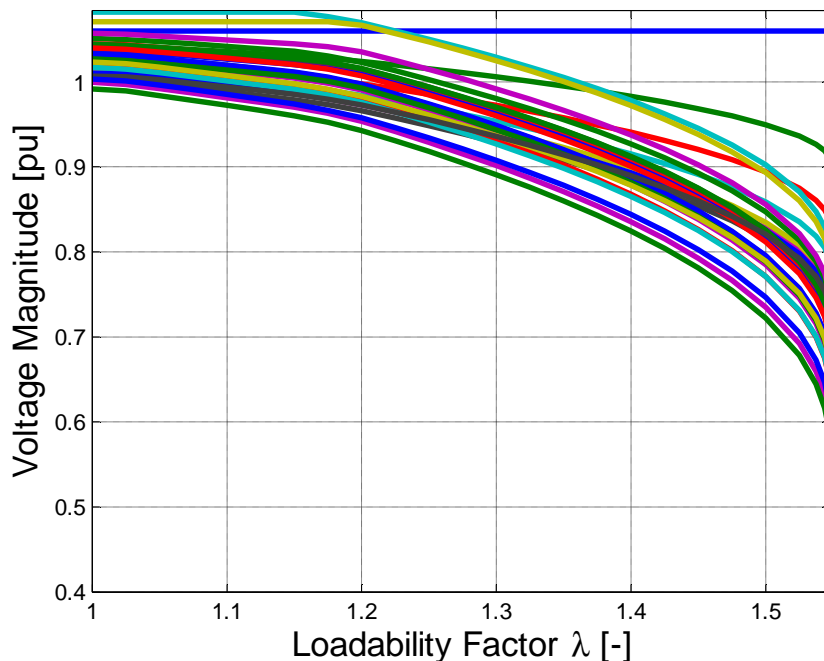
Fig. 13.1-1: V-P curves for the IEEE 30-bus power system (Cycled N-R method)
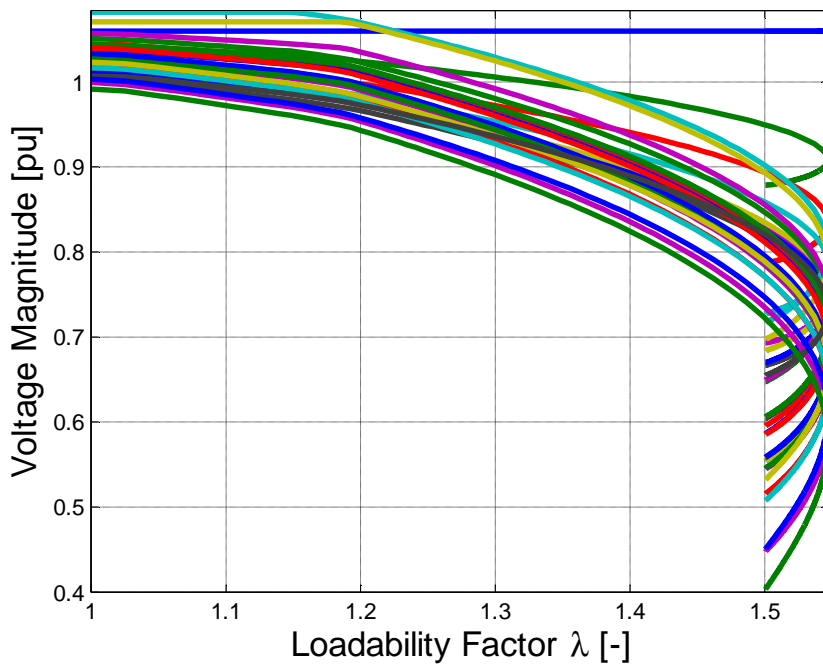
Fig. 13.1-2: Extended V-P curves for the IEEE 30-bus power system (CLF method)

As Tab. 13.1-1 indicates, applied version of the CLF method is still not applicable for real-time voltage stability assessments but it can be useful for off-line reliability, evaluation or planning studies of even larger and more complex power systems.

13.2 Comprehensive Voltage Stability Analysis of a 59-bus Test Network

The 59-bus test network is a simplified 14-generator model of the South-East Australian Power system [82]. It contains four highly meshed subsystems which are mutually interconnected via very few single or parallel lines. Thus, the behaviour of this system can be assumed as analogous to typical interstate operation of individual national power systems. From all six load flow cases A to F, peak load conditions (case C: total base-case generation/load of 25.43/24.8 GW) were selected as the most attractive for the voltage stability study. Due to high loadability and possible voltage problems, five shunt capacitors, four shunt inductors, two parallelly connected series capacitors and five static var compensators were connected in the base case. With very high loading and sparsely interconnected network sections, the system has the character of a typical ill-conditioned network. Neither G-S nor standard N-R method is able to provide base-case load flow solution. Therefore, the use of stability techniques in each corrector step was crucial.

Total of 41 buses were activated for load/generation increase (L+G scenario) with selected step size setting of $2.5 \times 10^{-2}/6.25 \times 10^{-3}$ to achieve fair compromise between the accuracy and the CPU time. Total number of 153 stable/unstable V-P points were calculated in less than 1.17 seconds. Found value of λ_{max} was 1.251775 [-] for which even all network buses remained inside their permitted ±10% tolerance. From this follows that proper network operation in next 10-15 years could be seriously threatened in terms of voltage stability due to gradual increase of system loading when no remedies are applied.

In Fig. 13.2-1, the V-P curves for PQ bus No. 43 and PV bus No. 46 are shown. For the latter, the selected PV bus maintained its voltage control capability up to loadability of approx. 1.2 [-]. Then, it was switched to PQ and a sharp point on the V-P curve emerged. Around loadability of 1.24 [-], another PV network bus was switched to PQ (i.e. second sharp point appeared). In the stable part of the V-P curve, five PV buses were switched to PQ (namely buses No. 5, 7, 32, 35 and 46) decreasing total number of 18 PV buses to 13.
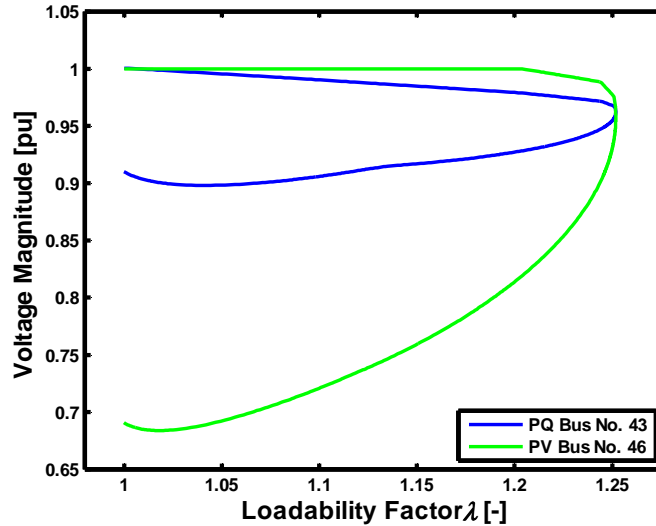
Fig. 13.2-1: V-P curves for selected PV/PQ network buses

In Fig. 13.2-2, relative reactive power reserve of the network is drawn. The decrease by approx. 63 percent between the base case and the singular point is clearly visible.
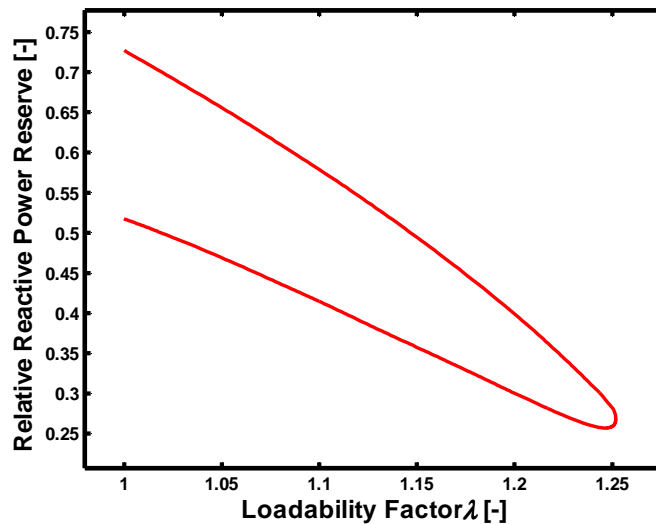
Fig. 13.2-2: Relative level of reactive power reserve

In Figs. 13.2-3 and 13.2-4, $VSMI_i$/$VSMI_{ik}$ indices are presented for each network bus/branch, respectively. In the former, blank columns belong to those PV buses (incl. the slack bus) which still provide voltage/var control. To distinguish voltage stable and unstable network buses, maximum $VSMI_i$ value was taken as the reference and all remaining buses

were compared to this value. Finally, buses No. 7, 39-42, 54-56 and 58 were found the most critical with $VSMI_i$ values below 2 %.
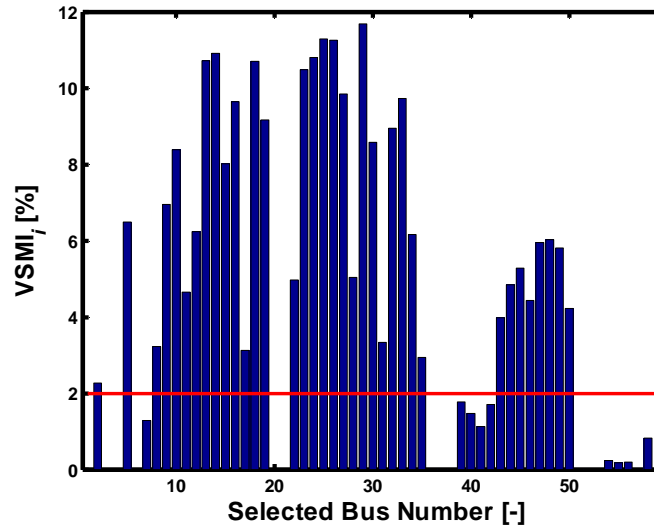
Fig. 13.2-3: Voltage stability margin indices - bus conditions

The most critical $VSMI_{ik}$ values were found for branches No. 5-7 (buses No. 2-28), 48-51 (buses No. 28-29 and 29-30), 64 (buses No. 41-42) and 146-147 (buses No. 24-30).
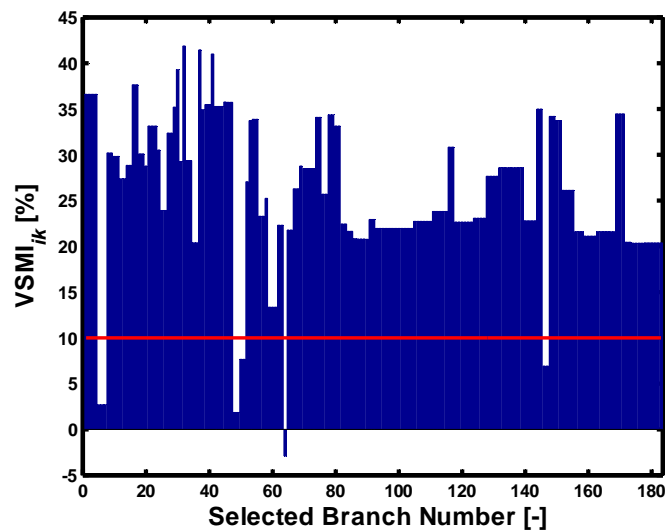
Fig. 13.2-4: Voltage stability margin indices - branch conditions

Finally, sensitivity study was performed to show voltage-load sensitive network areas. In these regions, protective measures should be applied to prevent/minimize the effects of possible voltage instabilities. The VSF_i values were calculated for each non-slack network bus using the dV vector of the predictor in close vicinity to the singular point. System buses with the highest VSF_i values are shown in Tab. 13.2-1.

Tab. 13.2-1: Highly voltage-load sensitive network buses

bus	48	47	49	44	46	50	35	45	7	43	42	39	40
VSF_i [-]	0.106	0.106	0.105	0.099	0.096	0.092	0.091	0.090	0.070	0.027	0.018	0.016	0.007

Network scheme along with highlighted voltage-weak areas (high VSF_i values) and critical buses/branches (low $VSMI_i$ and $VSMI_{ik}$ values) is shown in Fig. 13.2-5. Voltage-weak areas were structured in zones 1 (highest sensitivity) to 3 (high sensitivity) to easily locate the epicentre of possible voltage-sensitivity problems.
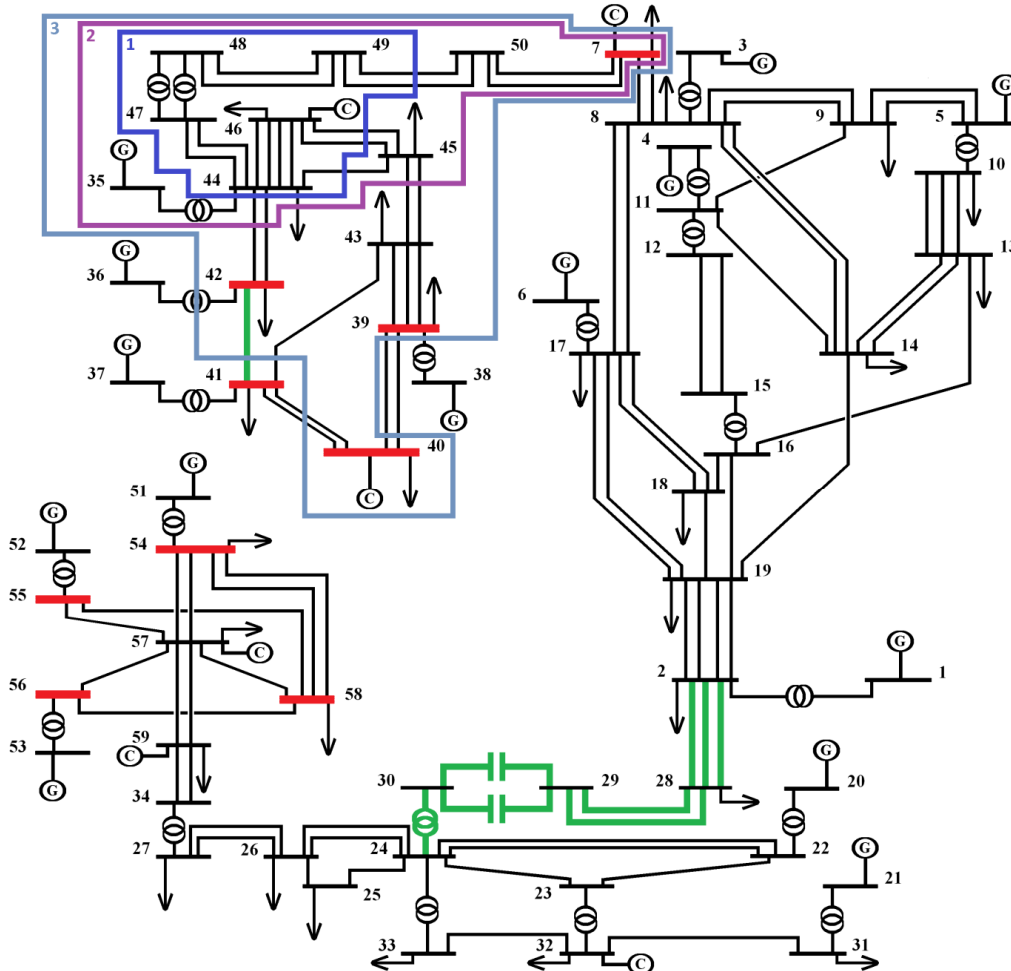
Fig. 13.2-5: Network scheme with highlighted critical buses/branches/areas

Individual corrective actions can be mostly applied only when approaching the singular point. They are meaningful only with respect to the region of viable voltage values and reasonable branch loadings. Proposed corrective process is to implement each corrective action individually, repeat the voltage stability analysis of the system, locate new weak system regions and activate the next suitable correction. Thus, multiple corrective strategies can be prepared. The most suitable would be the one with the best compromise between possible stability improvements and operational costs.

Following corrective strategies are proposed for improving the voltage stability: 1) Connect synchronous condensers/generators and/or apply load-shedding in critical buses located in weak network areas (i.e. those with lowest $VSMI_i$ and highest VSF_i values). 2) Use broader var limits and higher voltage magnitudes in PV buses inside or close to weak areas. 3) Disconnect all shunt inductors. 4) Activate synchronous condensers or switched shunt capacitors to buses with the lowest $VSMI_i$ values outside the highly sensitive regions.

For voltage stability study above, three different corrective scenarios are introduced.

Scenario I:

    - replace inductors in buses No. 48 - 50, 54 by shunt capacitors of the same size

    - increase var ranges in PV buses No. 3, 21, 46, 59 by 5, 15, 10 and 10 percent

Scenario II:

    - connect synchronous condenser to bus No. 48 (voltage 1.05 pu, vars: -2.5/2.5 pu)

    - increase var range in PV bus No. 7 by 20 percent

    - connect shunt capacitors to buses 14 (2.0 pu), 31 (3.0 pu) and 59 (2.0 pu)

Scenario III:

    - replace inductors in buses No. 48 - 50, 54 by shunt capacitors of the same size

    - connect synchronous condensers to buses No. 24 (voltage 1.00 pu) and No. 29 (voltage 1.01 pu), vars -2.0/4.0 pu

    - broaden var range in all PV buses by 35 percent

    - connect shunt capacitors to buses 41, 42, 46, 55, 56 and 58 (1.0 pu each)

In Tab. 13.2-2, both base-case and singular voltage conditions are presented along with the improvements of both theoretical/real maximum loadabilities, numbers of V-P points and CPU times. Note: Voltage limits of ±10 % were applied for the evaluation of λ_{max}^{*}, no flow limits were included.

Tab. 13.2-2: Effects of individual corrective scenarios I - III on system's voltage stability

corrective scenario	voltage conditions [pu]		improvement of λ_{max} [%]	improvement of λ_{max}^{*} [%]	number of V-P points	time [ms]
	base case	singular point				
I	0.9961 - 1.0942	0.8229 - 1.0731	4.93	0.35	44	358.8
II	0.9955 - 1.0923	0.8215 - 1.0536	5.81	2.09	45	359.9
III	0.9967 - 1.0985	0.7809 - 1.0785	10.68	1.87	69	483.6

Radical improvement of λ_{max} was also found, when replacing all shunt inductors by shunt capacitors of the same size and by activating unlimited var generations in PV buses. For such an imaginary case, base-case and singular voltage conditions were 0.9961 - 1.0942 pu and 0.7371 - 1.0716 pu, respectively. Improvements of theoretical/real maximum loadabilities were 14.55 and 3.61 percent. Understandably, implementing these changes would significantly increase both investment and operating costs of the network.

13.3 Initial Testing of the Shortest Distance to Voltage Instability Approach

The Shortest Distance to Voltage Instability (SDVI) approach was realized using the Cycled N-R method with incremental loading increase. The code was equipped with the convertor from physical to per units and with stability procedures (OSFD + SUT algorithms). Due to limited use of employed iterative method (see Chapter 8.4), the networks with PQ buses can be examined only. Then, non-slack PQ buses with non-zero active power load (i.e. L scenario) are activated for the analysis. All eigenvalues with relevant left eigenvectors are computed at the end of each loading scenario, the real eigenvalue with minimum magnitude is found and used to determine the next loading increase direction. As the outputs, two matrices are generated. The former contains the distance to voltage instability, total

active/reactive system loading (in PQ buses only) and the smallest eigenvalue of the Jacobian for each loading scenario taken. The latter consists of the minimum MW/MVAr increments in all network buses for reaching voltage instability. Additionally, total active/reactive system loading in the base case and CPU time needed is stored for evaluation purposes. Code settings for solving SDVI problems is shown in Tab. 13.3-1.

Tab. 13.3-1: Settings of the SDVI code

parameter	value
convergence criterion of the Cycled N-R code	1×10^{-8}
maximum number of iterations of the Cycled N-R code	20
maximum number of V-P points in the Cycled N-R code	5000
initial step size of the Cycled N-R code	0.025
divergence criterion of the Cycled N-R code - step size division by	2
maximum number of loading scenarios in the SDVI code	30
final convergence criterion of the SDVI code	1×10^{-8}

Correct SDVI values can be verified only graphically in the 2D parameter space, i.e. when solving simple 2-bus systems with one load (PQ bus). For this purpose, a looped version of the Cycled N-R method was created for examining wide range of load increase directions to voltage instability. In the P-Q plane, the directions are modified by 1 degree within interval between 140 and 370 degrees (the most probable loading region). Critical P/Q values are computed and stored for drawing the fragment of curve *S*. Initial loading point and critical P/Q points obtained by the SDVI code are then drawn together with equal axes for visual evaluation of the shortest distance to instability.

For the evaluation process, five simple 2-bus test systems were prepared - see Tab. 13.3-2. Each of them is defined by passive parameters of the branch, voltage in the slack bus, load and shunt susceptance in the PQ bus. Different initial loading directions were activated to observe the searching process for local minimum distance in more detailed way. Individual graphical outputs are shown in Figs. 13.3-1 to 13.3-5. Initial loading point is projected in green colour, while curve *S* and individually computed critical P/Q points in red and cyan colours, respectively.

Tab. 13.3-2: Input data for 2-bus test systems

test systems	input parameters								
	r [pu]	x [pu]	g [pu]	b [pu]	V_1 [pu]	θ_1 [deg]	P_{L0} [pu]	Q_{L0} [pu]	b_0 [pu]
EPS0002I	0.000000	0.250000	0.0000	0.00	1.0000	0	-0.80	-0.40	0.0000
EPS0002II	0.100000	1.000000	0.0000	0.00	1.0500	20	-0.15	-0.10	0.0000
EPS0002III	0.024793	0.033058	0.0000	0.00	1.0455	0	-0.44	-0.33	0.0000
EPS0002IV	0.009615	0.048077	0.0000	0.02	1.0000	0	-1.80	-0.90	1.0811
EPS0002V	0.006250	0.050000	0.0064	0.96	1.0000	0	-1.00	-0.60	0.0000

As can be seen in Figs. 13.3-1 to 13.3-5, all computed critical P/Q points are lying on the curve *S*. Searching process for local minimum distance always converged relatively fast when needing no more than 15 iterations (i.e. loading scenarios). Local minimum was found successfully in all test cases.
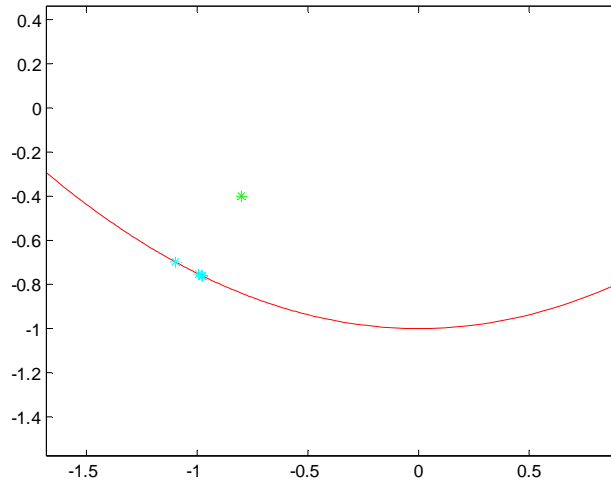
Fig. 13.3-1: Searching process for local minimum (EPS0002I)
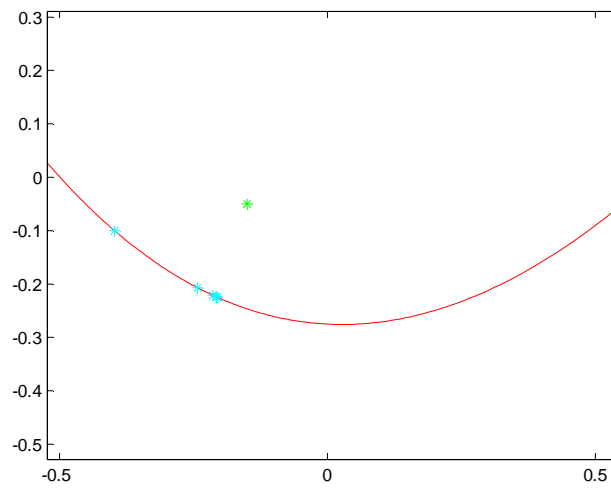
Fig. 13.3-2: Searching process for local minimum (EPS0002II)
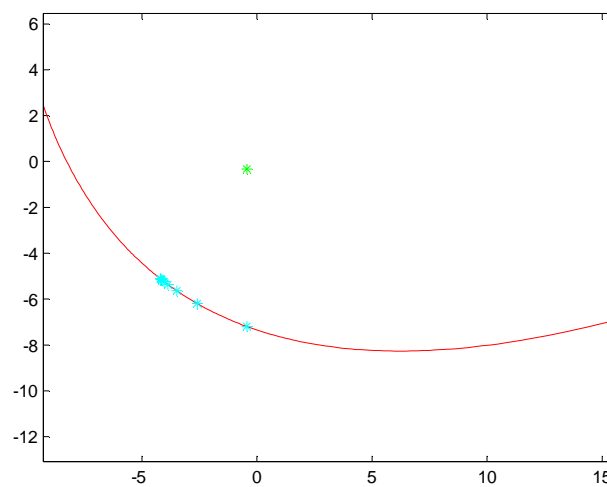
Fig. 13.3-3: Searching process for local minimum (EPS0002III)
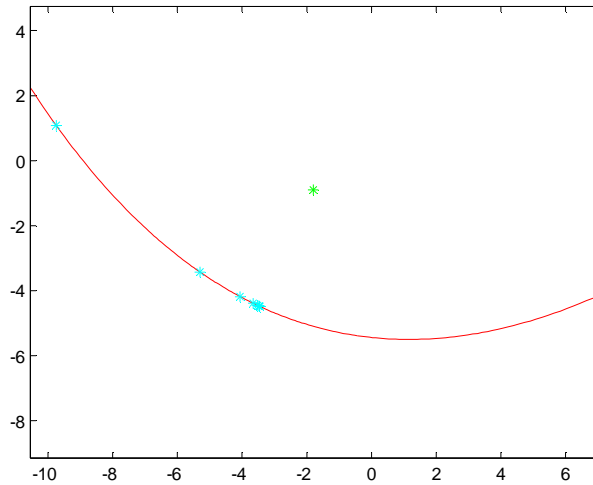
Fig. 13.3-4: Searching process for local minimum (EPS0002IV)
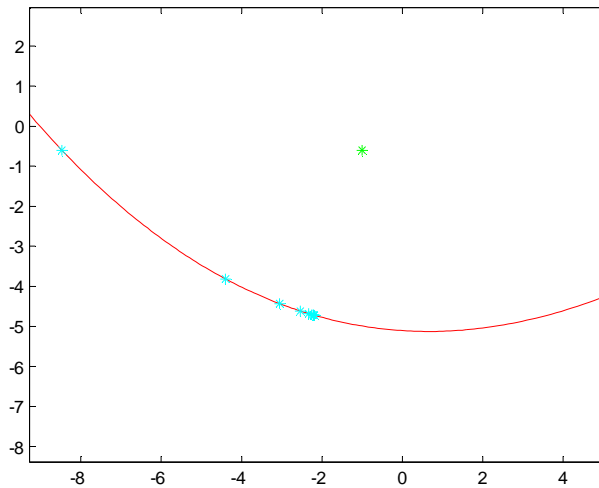
Fig. 13.3-5: Searching process for local minimum (EPS0002V)
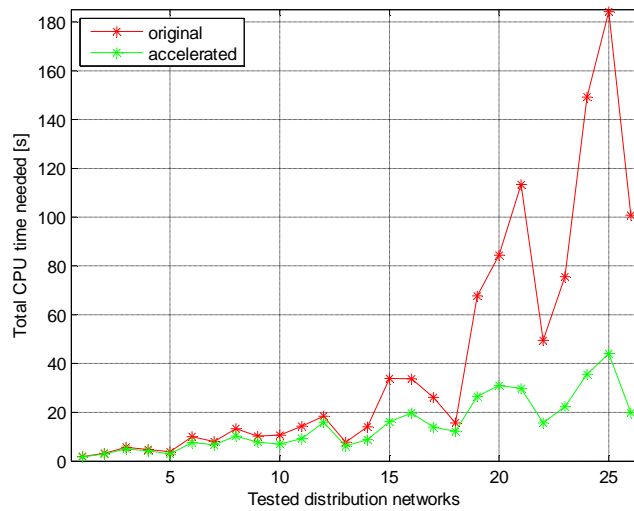
Fig. 13.3-6: Comparison of CPU times for original (eig) and accelerated (eigs) code versions

Next, total of 26 medium-sized and larger distribution power systems between 7 and 794 buses were tested. Except of the Cycled N-R method, the most time-consuming part of the SDVI analysis was the computation of all eigenvalues and left eigenvectors for the singular not-sparse Jacobian (function 'eig') along with locating the smallest eigenvalue. Code upgrades were further implemented to compute only the one key eigenvalue and left eigenvector of the sparse Jacobian (via 'eigs(Jacobi.',1,'SM')') for the new direction vector. When comparing both code versions (eig vs. eigs functions) in terms of CPU time and solution accuracy, significant CPU time savings were achieved by the latter with only slightly lower precision - see Fig. 13.3-6. Time savings ranged between 8.8 percent for smaller and 80.25 percent for larger systems. After the acceleration process, maximum CPU time needed for meeting given convergence criterion of 1×10^{-8} was 44.05 seconds.

Tab. 13.3-3: Results of the SDVI analysis for medium-sized and larger distribution networks

case	all buses	PQ/P/no loads	total P_L (base-case)	total Q_L (base-case)	iter	distance to instability	total P_L (singular point)	total Q_L (singular point)	critical eigvalue	time [s]
EPS7	7	6/0/0	-0.04800	-0.02280	6	0.01771 / 0.01601	-0.07867 / -0.06561	-0.05347 / -0.05484	-2.13e-5 / -3.64e-5	1.778
IEEE13	13	8/0/4	-0.01089	-0.00662	8	0.01612 / 0.01417	-0.04313 / -0.02558	-0.03887 / -0.04011	7.15e-6 / 5.92e-6	2.974
EPS19	19	9/0/9	-1.34100	-0.39900	12	1.26659 / 0.38426	-4.02784 / -1.41973	-3.08584 / -0.77510	1.57e-4 / 9.51e-5	5.049
EPS34	32	8/0/23	-0.00400	-0.00200	9	0.02697 / 0.01134	-0.05794 / -0.01085	-0.05594 / -0.01302	2.68e-5 / 2.55e-5	4.264
IEEE35	35	6/0/28	-0.00349	-0.00226	6	0.00475 / 0.00369	-0.01172 / -0.00820	-0.01048 / -0.00712	-6.79e-6 / 1.07e-5	3.000
EPS114	106	34/0/71	-0.00899	-0.00436	7	0.02065 / 0.00460	-0.09415 / -0.01192	-0.08952 / -0.00953	1.55e-5 / -1.27e-5	7.686
IEEE125	125	85/0/39	-0.03490	-0.01920	6	0.00375 / 0.00338	-0.05935 / -0.04991	-0.04365 / -0.04331	1.28e-6 / -8.29e-7	6.687
EPS128	128	87/0/40	-0.27161	-0.08927	10	0.03680 / 0.00433	-0.51429 / -0.27283	-0.33196 / -0.09403	1.14e-5 / 9.87e-6	10.348
EPS137	119	32/0/86	-0.01900	-0.00920	7	0.02114 / 0.00453	-0.10356 / -0.02206	-0.09376 / -0.01372	1.63e-5 / 9.45e-6	7.821
EPS167	147	35/0/111	-0.02800	-0.01356	6	0.01365 / 0.00277	-0.08511 / -0.03004	-0.07066 / -0.01600	-1.52e-5 / 2.04e-5	7.093
EPS246	201	56/0/144	-0.00800	-0.00388	6	0.01888 / 0.00299	-0.10789 / -0.01013	-0.10377 / -0.00666	-1.60e-5 / -8.54e-6	9.261
EPS272	258	71/0/186	-0.01799	-0.00874	7	0.01335 / 0.00255	-0.09753 / -0.02066	-0.08828 / -0.01145	1.06e-5 / 6.79e-6	15.881
EPS304	207	46/0/160	-0.00499	-0.00241	4	0.01062 / 0.00186	-0.05593 / -0.00653	-0.05335 / -0.00395	-1.08e-5 / 1.16e-5	6.157
EPS323	304	91/0/212	-0.02499	-0.01214	4	0.01512 / 0.00184	-0.12694 / -0.02638	-0.11409 / -0.01373	-1.25e-5 / -1.26e-5	8.752
EPS361	361	0/285/75	-0.59615	0.00000	7	0.01772 / 0.00929	-0.80772 / -0.64784	-0.21157 / -0.05087	2.22e-6 / 3.61e-6	16.167
EPS366	340	93/0/246	-0.03198	-0.01550	8	0.04124 / 0.00718	-0.31319 / -0.03705	-0.29670 / -0.02526	1.64e-5 / -2.64e-5	19.791
EPS392	266	72/0/193	-0.00999	-0.00485	7	0.02036 / 0.00454	-0.13217 / -0.01324	-0.12703 / -0.01196	-1.10e-5 / 1.15e-5	13.936
EPS396	203	43/0/159	-0.00570	-0.00276	8	0.02132 / 0.00456	-0.10454 / -0.00949	-0.10160 / -0.00759	1.65e-5 / 2.13e-5	12.288
EPS535	504	140/0/363	-0.02999	-0.01454	8	0.02941 / 0.00443	-0.27603 / -0.03395	-0.26058 / -0.02061	-1.34e-5 / 1.15e-5	26.484
EPS558	533	151/0/381	-0.04598	-0.02227	9	0.01496 / 0.00618	-0.17592 / -0.05460	-0.15221 / -0.04254	6.11e-7 / -1.37e-5	30.992
EPS682	634	186/0/447	-0.05201	-0.02523	6	0.01757 / 0.00273	-0.22147 / -0.05533	-0.19468 / -0.02900	-1.24e-5 / -2.17e-5	29.853
EPS706	608	147/0/460	-0.02999	-0.01453	4	0.01102 / 0.00116	-0.12443 / -0.03102	-0.10898 / -0.01557	-1.11e-5 / -7.41e-6	15.715
EPS707	657	182/0/474	-0.03403	-0.01647	5	0.01342 / 0.00118	-0.16205 / -0.03496	-0.14449 / -0.01749	-1.12e-5 / 1.22e-5	22.350
EPS760	726	224/0/501	-0.05998	-0.02902	7	0.02679 / 0.00291	-0.34346 / -0.06202	-0.31250 / -0.03284	1.37e-5 / -1.80e-5	35.589
EPS791	752	210/0/541	-0.02498	-0.01208	9	0.01004 / 0.00260	-0.12784 / -0.03105	-0.11494 / -0.01682	-2.03e-6 / -1.44e-5	44.055
EPS794	750	204/0/545	-0.04000	-0.01934	4	0.01458 / 0.00172	-0.18724 / -0.04190	-0.16658 / -0.02128	9.92e-6 / -1.34e-5	19.890

Complete results of the SDVI analysis for tested distribution networks are shown in Tab. 13.3-3. For each system, two rows are presented - first for initial direction (uniform P/Q load increase applied), second for the final (critical) direction. When comparing both initial and critical distances to instability, significant decreases between 9.61 and 91.21 percent can be observed. Comparison of distances to voltage instability is further provided in Fig. 13.3-7 for 25 examined networks.
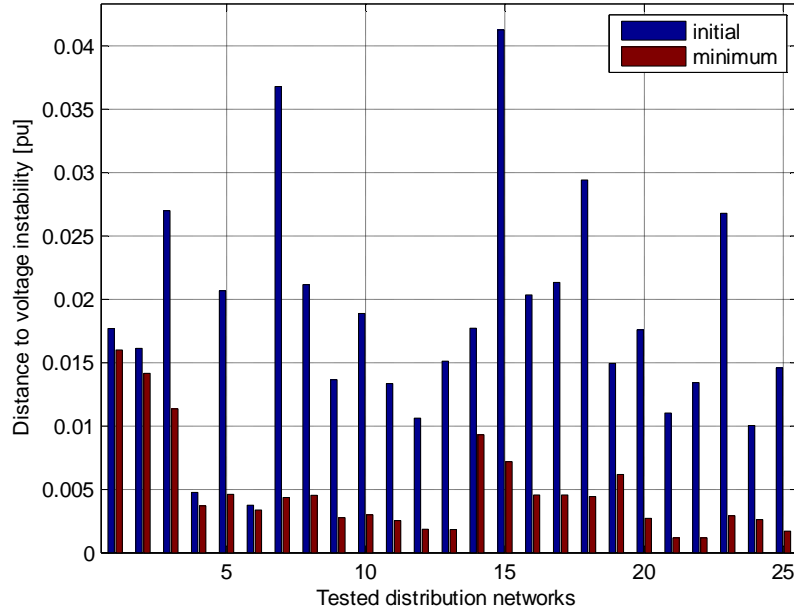
Fig. 13.3-7: Comparison of initial/minimum distances to instability for 25 examined networks

In the studies above, uniform initial system loading was applied. This means that both active/reactive power loads in all network buses were increased equally (i.e. under -135 degrees in the P-Q plane). However, two other initial directions were also tested - only P direction (angle of -180 degrees) and only Q direction (angle of -90 degrees). For five tested systems, alternative critical distances and P/Q increments were found - see Tab. 13.3-4.

Tab. 13.3-4: Alternative shortest distances to voltage instability

case	minimum distance to instability [pu]		
	uniform	only P	only Q
EPS34	0.011340	0.011340	0.011735
EPS128	0.004334	0.004639	0.004334
EPS558	0.006183	0.006183	0.004237
EPS760	0.002908	0.008800	0.002908
EPS791	0.002599	0.002599	0.001165

Both higher and even smaller minimum distances to instability can be obtained when applying different (e.g. only P, only Q) initial loading directions. However, it depends whether such loading scenario is reasonable for such distribution network. For all performed simulations, only uniform loading direction is applied due to simpler input data structure.

13.4 Testing of the Shortest Distance to Voltage Instability - Case Study I.

The 19-bus distribution network [62] of the western part of Czech Republic was tested for finding the minimum distance to instability - see Fig. 13.4-1. It includes the connection to the superior system via the shunt conductance/susceptance in the slack bus.
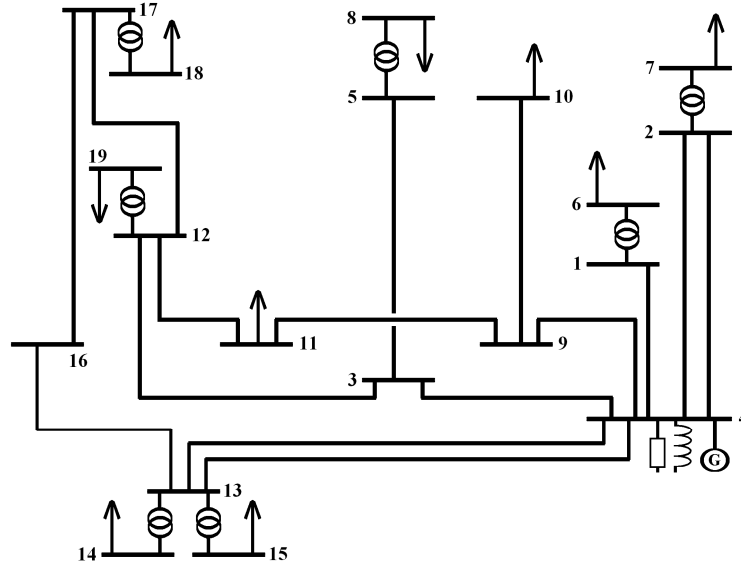
Fig. 13.4-1: Scheme of the 19-bus distribution network (Distribuce Plzeň - Jih)

Tab. 13.4-1: Overview of network buses

bus number	bus name	voltage level [kV]
1	Chlumčany	110
2	Plzeň Jih	110
3	T1	110
4	Přeštice	110
5	Holýšov I	110
6	Chlumčany	22
7	Plzeň Jih	22
8	Holýšov I	22
9	T2	110
10	Holýšov II	110
11	Vranov	110
12	Stříbro	110
13	Domažlice	110
14	Domažlice A	22
15	Domažlice B	22
16	TD	110
17	Tachov	110
18	Tachov	22
19	Stříbro	22

The goal is to find minimum MW/MVAr increments in load buses No. 6, 7, 8, 10, 11, 14, 15, 18 and 19 for the base case of -134.1 MW and -39.9 MVAr to reach voltage instability. Uniform initial load increase was applied for active/reactive power loads. Only P and only Q initial directions were also examined but identical results were obtained. In Tab. 13.4-2, the searching process for finding local minimum distance to voltage instability is presented.

Tab. 13.4-2: Searching process for local minimum distance to voltage instability

loading scenario number	distance to instability	total P_L (singular point)	total Q_L (singular point)	min eigvalue
1	1.26659	-4.02784	-3.08584	1.57e-4
2	0.39126	-1.51583	-0.74903	-1.46e-4
3	0.38566	-1.46315	-0.76480	7.93e-5
4	0.38455	-1.43958	-0.77070	9.69e-5
5	0.38432	-1.42883	-0.77315	1.05e-4
6	0.38427	-1.42390	-0.77422	-1.21e-4
7	0.38426	-1.42163	-0.77470	-1.53e-4
8	0.38426	-1.42058	-0.77493	1.60e-4
9	0.38426	-1.42011	-0.77502	4.87e-5
10	0.38426	-1.41988	-0.77507	1.30e-4
11	0.38426	-1.41978	-0.77509	-1.19e-4
12	0.38426	-1.41973	-0.77510	9.36e-5

As can be seen, initial uniform loading leads to excessively optimistic distance to voltage instability (about 1.2666 pu, i.e. increase of about 268.6842 MW/MVAr). The entire searching process converges relatively quickly where the solution does not change too much after the third loading scenario. Under the critical loading increase, much lower distance to voltage instability is obtained (about 0.3843 pu, i.e. decrease of 69.66 percent). At this point, only increase of 7.87 MW and 37.61 MVAr to the base-case loading leads to instability.
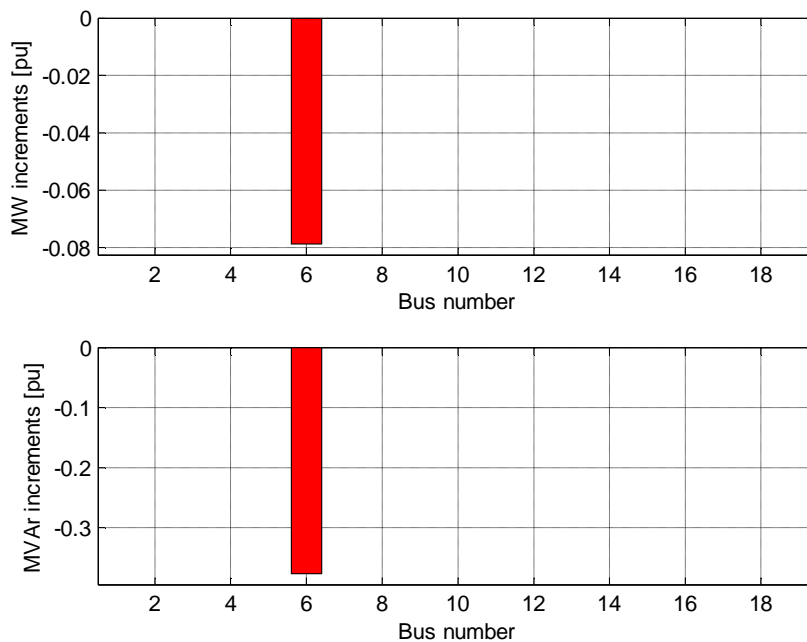
Fig. 13.4-2: Minimum MW/MVAr bus increments

Critical MW/MVAr bus increments for reaching voltage instability are surprisingly bound only with bus No. 6 (Chlumčany 22 kV) which may still withstand such load increase during real operating conditions - see Fig. 13.4-2.

This study supports the fact that it is necessary to focus on finding the minimum distance to instability when evaluating the voltage stability margin of the network. Uniform load increase may provide reasonable but too optimistic results.

13.5 Testing of the Shortest Distance to Voltage Instability - Case Study II.

The 125-bus distribution network [81] containing total of 6 switches for various system operation modes was tested in terms of shortest distance to voltage instability - see Fig. 13.5-1. When looking for the most suitable combination of switched-on/-off system switches in individual reconfiguration schemes by the distribution system operator, it will probably be necessary to include the criterion for uniform (or better minimum) voltage stability margins along with requirements on proper voltage conditions.
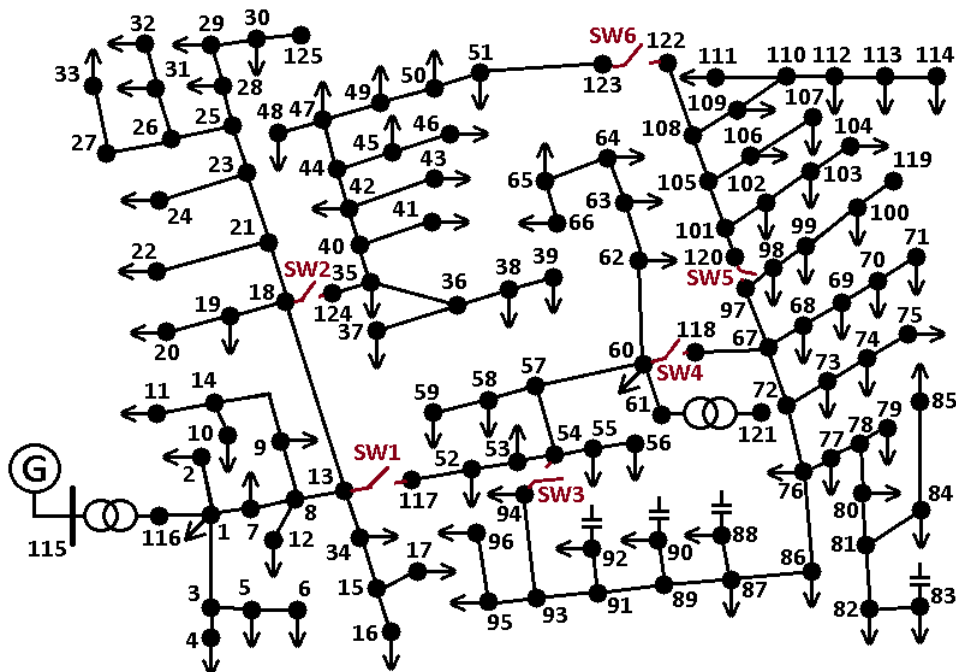
Fig. 13.5-1: The 125-bus distribution power system [81]

The task is to examine all possible combinations of network switches in terms of proper voltage conditions and uniform/minimum voltage stability margins. The former is needed to avoid possible under-/over-voltages in the base-case operation (permitted tolerance is ±10%). The latter is to maximize the uniform/minimum distances to voltage instability when compared to the network conditions before the reconfiguration.

For the modelling of switches, optimum passive parameters must be applied. If too high, significant voltage drops are observed in all the studies. If too small, the N-R method may have serious problems with preserving fair numerical convergence. As applied in [75], the switches should be modelled as standard power lines of an 0.5-meter length with typical reactance value of 0.4 Ω/km.

From all 64 (2^6) combinations of system switches, only 16 of them (9 for radial, 7 for loop network operations) maintain all network buses to be connected to the slack bus No. 115 - see Tab. 13.5-1. For each reconfiguration scenario, the basic load flow is first performed to obtain the minimum voltage magnitude in any of network buses. Then, the searching process for minimum distance to voltage instability is accomplished as in the previous case study.

Tab. 13.5-1: Reconfiguration scenarios for uniform/minimum distance to instability

no.	reconfiguration schemes						system operation mode	min voltage magnitude (base-case)	distance to voltage instability	total P_L (singular point)	total Q_L (singular point)
	SW1	SW2	SW3	SW4	SW5	SW6					
1	1	1	1	1	1	1	loop	0.9270	0.00475	-0.0659	-0.0502
									0.00451	-0.0556	-0.0538
2	1	1	1	1	1	0	loop	0.9237	0.00460	-0.0649	-0.0492
									0.00429	-0.0542	-0.0514
3	1	1	1	1	0	1	loop	0.9172	0.00467	-0.0653	-0.0496
									0.00433	-0.0533	-0.0511
4	1	1	1	0	1	1	loop	0.9185	0.00440	-0.0636	-0.0479
									0.00411	-0.0536	-0.0501
5	1	1	1	0	1	0	radial	0.9001	0.00381	-0.0597	-0.0440
									0.00331	-0.0491	-0.0419
6	1	1	1	0	0	1	radial	0.9165	0.00440	-0.0636	-0.0479
									0.00410	-0.0534	-0.0497
7	1	1	0	1	1	1	loop	0.9156	0.00416	-0.0620	-0.0463
									0.00388	-0.0527	-0.0482
8	1	1	0	1	1	0	radial	0.9077	0.00378	-0.0596	-0.0439
									0.00341	-0.0500	-0.0436
9	1	1	0	1	0	1	radial	0.9156	0.00416	-0.0620	-0.0463
									0.00386	-0.0522	-0.0477
10	1	1	0	0	1	1	radial	0.8185	0.00166	-0.0457	-0.0300
									0.00138	-0.0410	-0.0279
11	1	0	1	1	1	1	loop	0.8619	0.00304	-0.0547	-0.0390
									0.00267	-0.0464	-0.0377
12	1	0	1	0	1	1	radial	0.8021	0.00177	-0.0465	-0.0308
									0.00149	-0.0415	-0.0288
13	1	0	0	1	1	1	radial	0.8351	0.00225	-0.0496	-0.0339
									0.00200	-0.0441	-0.0330
14	0	1	1	1	1	1	loop	0.7265	0.00062	-0.0389	-0.0232
									0.00054	-0.0376	-0.0227
15	0	1	1	0	1	1	radial	0.6651	0.00039	-0.0374	-0.0217
									0.00033	-0.0365	-0.0213
16	0	1	0	1	1	1	radial	0.7265	0.00061	-0.0389	-0.0232
									0.00054	-0.0376	-0.0226
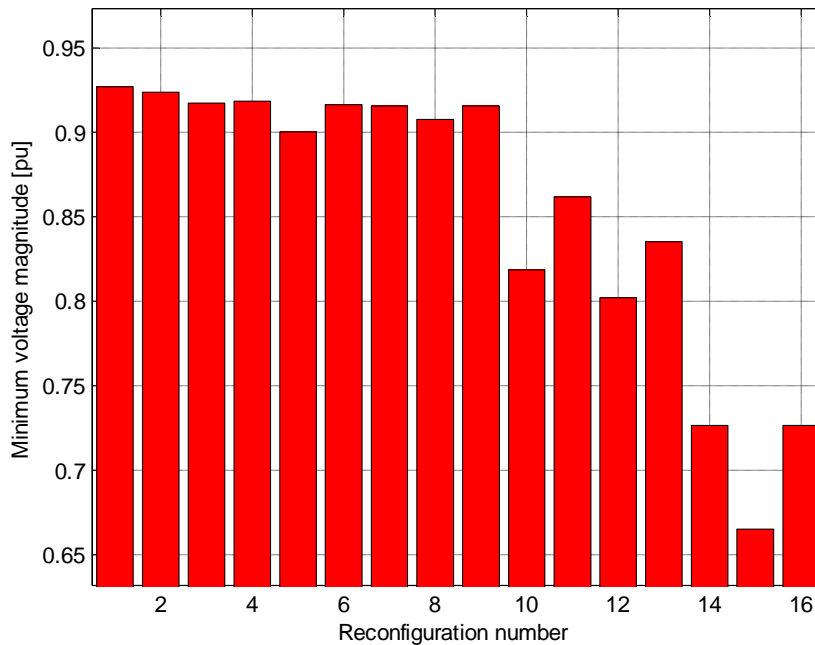
Fig. 13.5-2: Minimum voltage conditions for each system reconfiguration

Let us consider that the system is currently operated using the reconfiguration scheme No. 5. As shown in Fig. 13.5-2, the distribution system operator detects critical

voltage conditions (i.e. lower voltage limit is reached). Within a second, he obtains Fig. 13.5-2 to see which possibilities does he have to handle this problem using the reconfigurations (if no extra compensation devices available). From all reconfigurations, only first nine meet the requirements on voltage magnitudes. In terms of voltage magnitudes, the best reconfiguration scheme is No. 1 and No. 6 for loop and radial network operation, respectively. The choice at this moment remains on the operator, whether the network can be operated also in the looped mode or only in the radial mode.

As the contribution to the problem, improvement of operator's decision-making process can be achieved by including the results of the uniform/minimum distance to voltage instability for each possible system reconfiguration scheme - see Fig. 13.5-3.
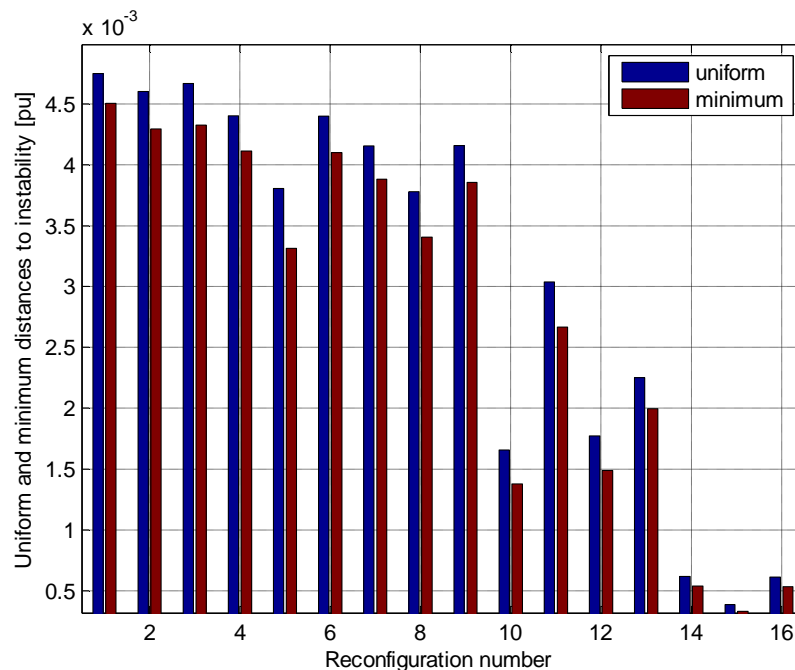
Fig. 13.5-3: Uniform/minimum distances to instability for each system reconfiguration

For the reconfiguration scheme No. 5, visibly lower margins are observed. Now, the operator should look for the best next reconfiguration scheme, i.e. the one with the highest distance to voltage instability. For this example, the conclusions are identical with those from Fig. 13.5-2. Thus, the best option is the reconfiguration scheme No. 1 and No. 6 for loop and radial network operations. However, this may not be valid universally.

Results in Fig. 13.5-3 were obtained by the author-developed SDVI code in approx. 107 seconds (with too strict convergence criterion of 1×10^{-8}). From performed SDVI simulations in previous case studies follows that no significant changes in the solution are achieved after first three iterations. Thus, computation time for this type of analysis would be then pushed below 1 minute. Therefore, applied methodology for voltage stability evaluation (when bound with the reconfiguration problem) is not suitable for real-time decision-making system processes. However, it could be helpful when working with 15-minute forecasted operation schemes of the network and estimated load changes in individual buses (for initial loading increase directions).

14. Testing of Alternative Tools for Load Flow Analyses

In this testing session, comparative load flow studies were performed using the educational GSO version 13 of PowerWorld Simulator [69], free software tool Power System Analysis Toolbox (PSAT) [71] and NEOS Server for Optimization [72] - see Chapters 14.1 to 14.5, respectively. When applied to broad range of load flow studies, they provided vital information whether and under which circumstances they could be reliably used for the verification of results obtained by the author-developed software SimEPS in MATLAB. If not stated otherwise, testings were performed at IntelCore i3 CPU 2.53 GHz/3.8 GB RAM station.

14.1 Comparison of Load Flow Solutions with PowerWorld Simulator

PowerWorld Simulator GSO Version 13 is licensed for educational use and evaluation purposes only. It contains power flow, optimal power flow (OPF) and transient stability toolboxes. For power flow studies, it is capable of solving the cases up to 39 buses. Note: Full version of PowerWorld Simulator can solve the systems up to 100000 buses.

In PowerWorld environment, the user needs to draw the network and specify all network elements with required input data. One of available load flow methods (G-S, N-R, Polar N-R, F-D, DC, Robust solution process) is then activated. Single solution or animated solution output can be obtained including voltage magnitudes, phase angles, slack bus generations, reactive power injections in PV buses, branch power flows and losses, total network losses and others. Due to highly efficient PV-PQ bus type switching logic, var limits in PV buses can be easily included. Nowadays, PowerWorld Simulator has become even more favourite for its interactive environment, transparent graphic interface and highly advanced engine for real-time studies.

In Tab. 14.1-1, the overview of load flow solutions for medium-sized test networks is provided and compared with results of author-developed software in MATLAB environment. Total active/reactive system losses with iteration numbers and CPU times are compared.

Tab. 14.1-1: Comparison of load flow solutions for medium-sized test networks

case	SimEPS - N-R method				PW Simulator GSO version 13			
	ΔP	ΔQ	iter	time [s]	ΔP	ΔQ	iter	time [s]
IEEE9	0.04955	-0.80120	4	0.0156	0.04955	-0.80120	4	0.0180
EPS10	0.04078	0.34497	4	0.0156	0.04078	0.34496	3	0.0180
EPS11I	0.54890	-0.13804	6	0.0156	0.54890	-0.13804	5	0.0230
EPS11II	0.83975	9.07828	8	0.0156	0.83977	9.07830	4	0.0180
IEEE13	0.00019	0.00071	3	0.0156	0.00020	0.00071	3	0.0140
IEEE14	0.13393	0.30122	4	0.0156	0.13393	0.30122	3	0.0150
EPS15	0.12983	-0.17681	4	0.0156	0.12983	-0.17681	5	0.0330
EPS16	0.15012	0.27484	4	0.0156	0.15013	0.27489	6	0.0230
EPS17	0.93979	5.05256	5	0.0156	0.93979	5.05257	5	0.0110
EPS19	0.01562	0.12432	3	0.0156	0.01562	0.12432	3	0.0080
EPS23	0.18297	-1.19279	3	0.0156	0.18297	-1.19279	4	0.0410
IEEE24	0.51246	-0.95132	4	0.0156	0.51246	-0.95132	4	0.0390
IEEE26	0.15764	0.84757	4	0.0156	0.15758	0.83468	4	0.0100
IEEE30	0.17552	0.33039	4	0.0156	0.17552	0.33039	4	0.0090
IEEE35	0.00019	-0.00140	3	0.0156	0.00020	-0.00140	4	0.0450
IEEE37	0.32923	0.22325	3	0.0156	0.32923	0.22326	4	0.0410
IEEE39	0.41592	-0.64442	5	0.0156	0.41594	-0.64441	4	0.0110

All PowerWorld results correspond to the outputs obtained by SimEPS software. In terms of network losses, only minor deviations are visible. These are caused 1) by applying slightly different equivalent schemes for two-winding transformers in PowerWorld Simulator (this effect is especially apparent when off-nominal tap ratios are applied), 2) by the rounding process of passive branch parameters, which is performed defaultly by PowerWorld Simulator on certain digit numbers. Total iteration numbers and CPU times for PowerWorld Simulator are comparable with SimEPS.
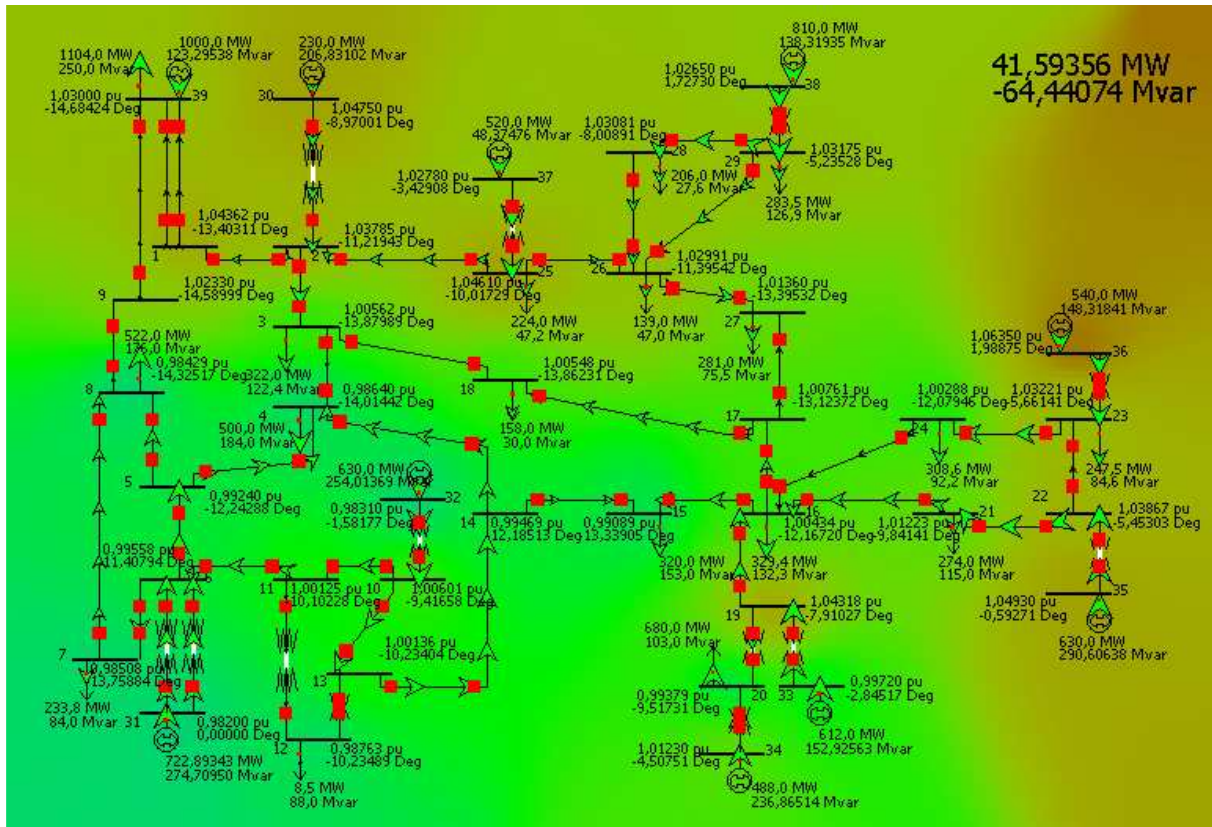
Fig. 14.1-1: Load flow solution of the IEEE 39-bus test network using PowerWorld Simulator

In Fig. 14.1-1, graphical output of PowerWorld Simulator GSO Version 13 is shown when solving the IEEE 39-bus network and providing final bus voltage/angle conditions and active/reactive power bus injections. Power flows are presented only with green arrows in the direction of active power flows. Total network losses are provided in the top-right corner. Contouring is applied to emphasize voltage conditions through the system.

14.2 Comparison of Load Flow and Voltage Stability Solutions with PSAT

PSAT [71] is a Simulink-based open-source library distributed via General Public License (GPL) and designed for electric power system analyses and simulations. Among many others, it contains also the tools for load flow and CLF analyses. All studies must be formulated for one-line network diagram only - either in input data *.m file with required format or in graphical *.mdl file, where the scheme is manually drawn.

When compared to another MATLAB-based open-source tool MATPOWER [70], PSAT is more efficient and highly advanced by providing more analyses, problem variations,

possible outputs and other useful features in its user-friendly graphical interface. MATPOWER does not support most of advanced network devices, entirely omits CLF analysis and has no graphical user interface. Also, it does not consider var limits in PV buses. Incorrect interpretation of reactive power branch losses can be also observed.

In Tab. 14.2-1, comparison between the N-R method in SimEPS and PSAT is provided when solving medium-sized IEEE test power systems. As in Chapter 14.1, total active/reactive system losses are assessed along with iteration numbers and CPU times.

Tab. 14.2-1: Comparison of load flow solutions for medium-sized IEEE test systems

case	SimEPS - N-R method				PSAT			
	ΔP	ΔQ	iter	time [s]	ΔP	ΔQ	iter	time [s]
IEEE9	0.049547	-0.801199	4	0.0156	0.049547	-0.801200	5	0.0533
IEEE13	0.000195	0.000708	3	0.0156	0.000195	0.000708	4	0.0383
IEEE14	0.133933	0.301224	4	0.0156	0.133930	0.301220	4	0.0483
IEEE24	0.512464	-0.951321	4	0.0156	0.512460	-0.951320	5	0.0580
IEEE30	0.175519	0.330387	4	0.0156	0.175520	0.330390	5	0.0667
IEEE35	0.000188	-0.001403	3	0.0156	0.000188	-0.001403	4	0.0517
IEEE39	0.415922	-0.644417	5	0.0156	0.415920	-0.644420	5	0.0550
IEEE57	0.278638	0.063280	4	0.0156	0.278640	0.063280	5	0.0517
IEEE118	1.328735	-5.159017	4	0.0156	1.328700	-5.159000	5	0.0557
IEEE125	0.002070	0.006673	3	0.0156	0.002071	0.006673	5	0.0567

Even larger and more complex power systems were tested and compared with SimEPS to detect any of its possible weaknesses. Unfortunately, several limitations of PSAT were found:

1) Inefficient PV-PQ bus type switching logic is applied. Probably, reverse switching logic is not used and the need for convergence is requested to activate forward switching logic. As a result, unnecessarily more PV buses are being switched permanently to PQ. Furthermore, switching logic completely fails to switch PV buses to PQ for larger systems with high numbers of PV buses.

2) Nominal voltages must be defined in the input data file or the error message 'Divergence - Singular Jacobian' is obtained during the simulation. This seems to be entirely illogical since nominal voltages should not be necessary for 'in per units defined' problems.

3) It seems that no advanced stability techniques are applied for the N-R method in PSAT because of severe numerical oscillations appearing in several studies.

4) PSAT intentionally neglects transformer susceptances and thus causes errors in final load flow results. A column for shunt susceptances is available for power lines only. For transformers, this column is filled with zeros by default.

Under these limitations, load flow results in Tab. 14.2-1 show very good congruity between SimEPS and PSAT. Higher total iteration numbers are needed by PSAT due to missing stability technique(s). Also, CPU times are higher in PSAT due to combining the codes with other analyses and related tool features.

As an example, load flow analysis of the IEEE 14-bus system is performed by PSAT - see Figs. 14.2-1 to 14.2-3.
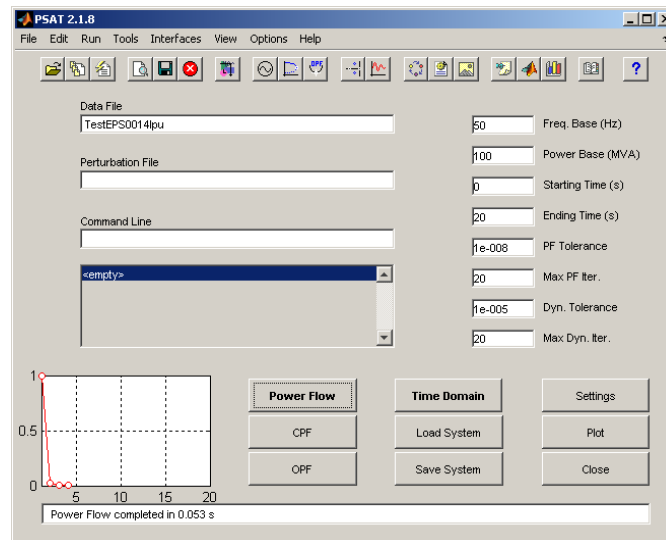
Fig. 14.2-1: GUI in PSAT for load flow analysis of the IEEE 14-bus system
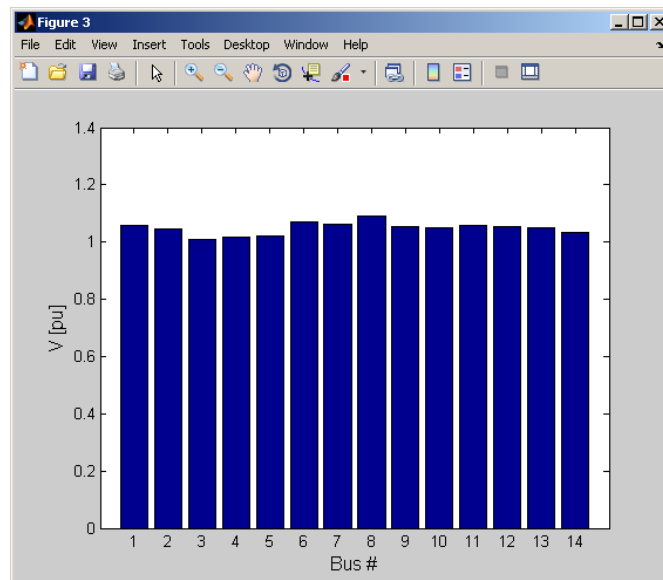
Fig. 14.2-2: Final voltage magnitudes of the IEEE 14-bus power system
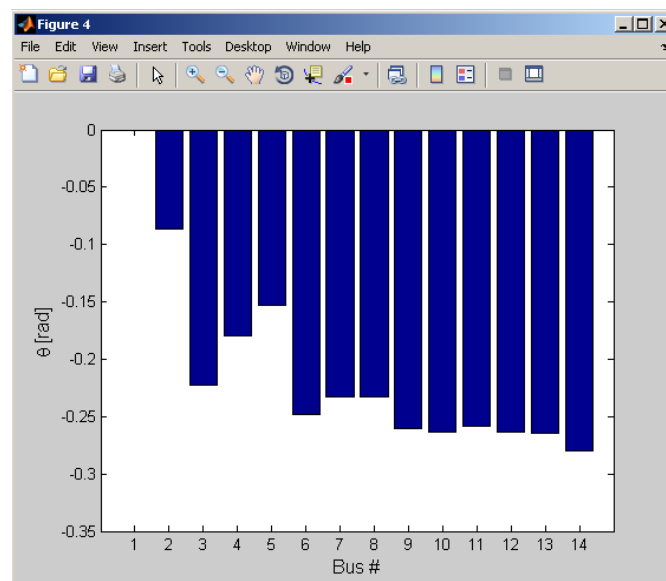
Fig. 14.2-3: Final voltage angles of the IEEE 14-bus power system

For voltage stability studies, PSAT contains the advanced CLF algorithm. Load flow data are extended by two matrices with the sets of PQ/PV buses where the loads/generations are to be increased (various increase rates are possible). After the load flow study, the CLF code is started via a specialized window (Fig. 14.2-4). For better performance, more suitable step size and maximum number of V-P points can be set. Check on voltage/flow/var limits can be also included. PSAT offers two CLF methods - perpendicular intersection (PI) and local parametrization (LP). Three stopping criteria are available: Complete Nose Curve (computing both stable/unstable V-P parts), Stop at Bifurcation (when singular point exceeded) and Stop at Limit (when voltage/flow limit hit).
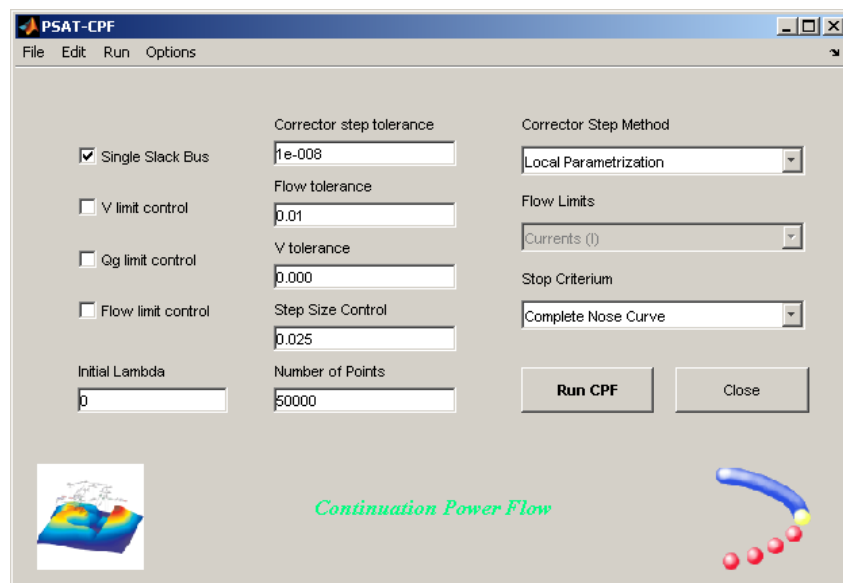
Fig. 14.2-4: Settings of the CLF analysis for solving the IEEE 14-bus power system
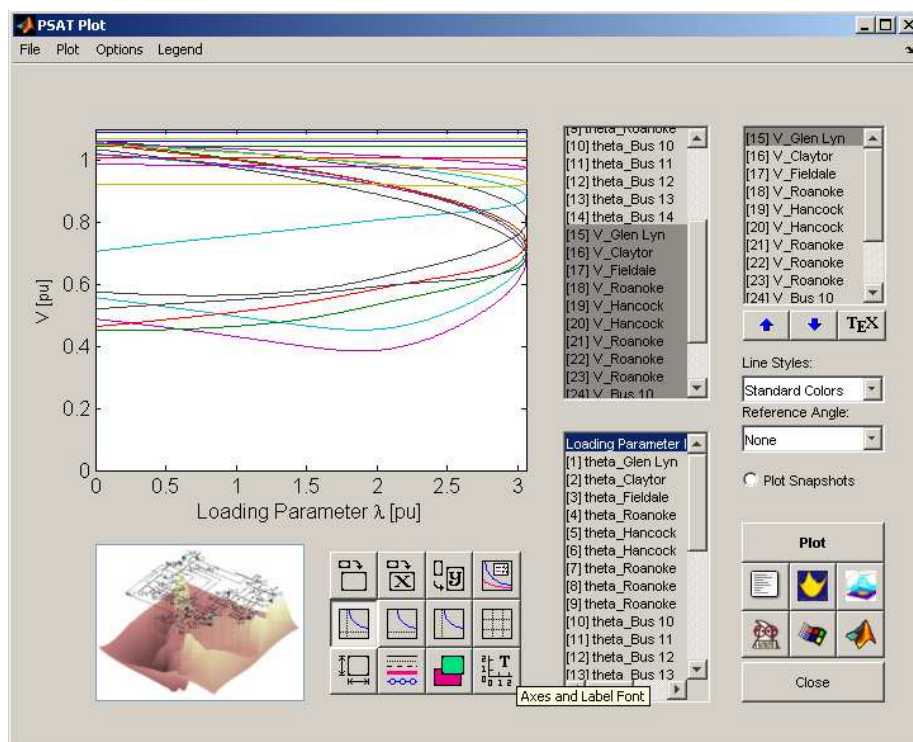
Fig. 14.2-5: Nose curves for all network buses of the IEEE 14-bus test system

Final graphical output of the voltage stability analysis for the IEEE 14-bus power system is shown in Fig. 14.2-5. CLF algorithm in PSAT is defined so that power increases are realized by adding a power increment to the base-case loading, i.e. initial λ is zero. In author-developed Cycled N-R and CLF codes, power increases are performed by multiplying the base-case loading with λ. Therefore, maximum loadability in PSAT must be increased by unity when being compared with the codes from SimEPS.

In Tab. 14.2-2, voltage stability results for medium-sized IEEE test systems are provided by the CLF algorithm (with compromise settings) in SimEPS and compared to those obtained by PSAT (both PI mode with step 0.025 and LP mode with default step 0.5).

Tab. 14.2-2: Voltage stability analysis of medium-sized IEEE test systems - SimEPS vs. PSAT

L+G	SimEPS - CLF			PSAT - PI mode			PSAT - LP mode		
case	λ_{max} [-]	points	time [s]	λ_{max} [-]	points	time [s]	λ_{max} [-]	points	time [s]
IEEE9	2.485382	84	0.2964	2.481220	7	0.2093	2.482000	13	0.3241
IEEE13	4.400577	112	0.3120	4.390420	13	0.3292	4.399570	20	0.4832
IEEE14	4.060252	92	0.3276	4.060100	18	0.4098	4.059420	19	0.4939
IEEE24	2.279398	58	0.2496	2.277550	10	0.2600	2.278670	16	0.4313
IEEE30	2.958814	57	0.2964	2.958550	16	0.8761	2.958250	20	1.5023
IEEE35	2.888950	107	0.3432	2.872940	16	1.1242	2.878420	10	0.2940
IEEE39	1.999202	30	0.2184	1.999110	11	0.2932	1.997840	12	0.3692
IEEE57	1.892089	92	0.4836	1.891920	12	0.9089	1.892090	26	3.9090
IEEE118	3.187128	66	0.5772	3.187100	613	19.1693	3.187120	82	19.7464

Only the networks with given nominal voltages and zero transformer susceptances were tested, logics for var limits were deactivated. For all voltage stability studies, identical power increase rates were considered, only L+G scenario was examined.

Both of PSAT modes showed only average accuracy with satisfiable numbers of V-P points and rather lower computational speed. LP mode was computationally more time-consuming but needed lower numbers of V-P points and usually provided more accurate results. Compromise CLF code provided the best combination of solution accuracy and CPU time requirements in each of the cases. Although higher numbers of V-P points were needed, CPU times were still significantly smaller than those in PSAT due to optimized sparse programming applied.

14.3 Testing of NEOS Solvers for Load Flow Analysis

NEOS Server contains two groups of solvers with input data in AMPL format which could be robust enough to deal with the load flow analysis: Mixed Integer Nonlinearly Constrained Optimization (solvers: Bonmin, Couenne, FilMINT and MINLP) and Nonlinearly Constrained Optimization (solvers: CONOPT, filter, Ipopt, KNITRO, LANCELOT, LOQO, MINOS, MOSEK and SNOPT). To handle binary variables in the PV-PQ bus-type switching logic, one of two approaches is usually taken - 1) strictly respecting 0/1 nature of defined variables, 2) applying continuous approximation of 0/1 variables. Former approach is employed by Bonmin, MINLP and KNITRO solvers. The calculation is then highly accurate but the

calculation time may be too long and time/memory limitations may be exceeded easily even for medium-sized systems. Latter approach (by CONOPT, filter, Ipopt, MINOS, SNOPT and LANCELOT) takes usually less time for computing the results. However, only approximate solutions can be obtained especially for larger networks with high numbers of PV buses.

Wide range of test systems was solved by selected NEOS solvers. All continuous solvers along with Bonmin and MINLP solvers were used with their default settings. In case of KNITRO solver, performance of various option settings was tested and evaluated. KNITRO-A was used with strictly default settings. KNITRO-B applied the active set root node relaxation algorithm along with multistart for obtaining better starting point for the entire optimization. Finally, KNITRO-C also employed the active set root node relaxation algorithm but with significantly increased number of iterations for numerical calculation and with no multistart. For both KNITRO-B and KNITRO-C, the rest of their settings remained default. Additional information for the 'Commands' file of KNITRO solver is shown in Tab. 14.3-1.

Tab. 14.3-1: Option settings for KNITRO solver [73]

version of KNITRO solver	option settings
KNITRO-A	---
KNITRO-B	mip_rootalg=3, ms_enable=1, ms_maxsolves=10
KNITRO-C	mip_rootalg=3, maxit=500000

All tested networks were generated in AMPL format using the author-developed AMPL Builder software in MATLAB environment. Suitable limits for individual variables had to be used - a) if too narrow, infeasibility was frequently observed, b) if too broad, iteration/time/memory constraints were often exceeded. Total active/reactive system losses were compared with those obtained by the N-R method in SimEPS. In Tab. 14.3-2, the evaluation of the results is provided by colour indicators.

Based on the results, the following conclusions can be made. 1) According to the extent of the simulation, the best solvers found were Bonmin and Ipopt. In both of these, exact solutions were obtained for networks up to 300 and 734 buses, respectively. 2) Both CONOPT and filter provided highly reliable and accurate results. Calculation failures were observed only in rare number of problems. In case of filter, the failures can be justified by memory limitations for the largest networks. 3) MINLP solver showed high performance rather for smaller and medium-sized systems. For networks above 50 buses, successful calculation was averted by memory limits. 4) SNOPT and MINOS solvers proved to be robust but highly unreliable when solving even relatively smaller networks. 5) Adjustments of 'Commands' for KNITRO solver had significant impact on its behaviour during the optimization. KNITRO-A provided high number of errors, while KNITRO-B and KNITRO-C minimized these errors to probably tolerable level. Failures in KNITRO solver are definitely caused by weak starting point and/or by ineffective rooting process. 6) LANCELOT solver often presents less accurate results which are primarily caused its performance rather than

127

by the problem size. Nevertheless, deviations of results can be acceptably compared to load flow solutions produced by the N-R method with lower accuracy criterion applied.

case	discrete solvers					continuous solvers					
	Bonmin	MINLP	KNITRO-A	KNITRO-B	KNITRO-C	SNOPT	Ipopt	CONOPT	MINOS	filter	LANCELOT
EPS3I											
EPS4I											
EPS4II											
EPS5I											
EPS5II											
EPS5III											
EPS6I											
EPS6II											
EPS6III											
EPS7I											
EPS7II											
IEEE9I											
EPS10I											
EPS11I											
EPS11II											
EPS11III											
EPS12I											
EPS13I											
IEEE13II											
IEEE14I											
EPS15I											
EPS16I											
EPS17I											
EPS19I											
EPS23I											
IEEE24I											
IEEE26I											
IEEE30I											
IEEE35I											
EPS37I											
IEEE39I											
EPS56I											
IEEE57I											
EPS59I											
EPS59II											
EPS59III											
EPS59IV											
EPS59V											
EPS59VI											
EPS61I											
IEEE118I											
IEEE125I											
EPS128I											
EPS133I											
IEEE162I											
IEEE300I											
EPS361I											
EPS629I											
EPS629II											
EPS734I											
EPS734II											
EPS2383I											

Legend:
- optimal solution found
- infeasible solution
- memory limit reached
- optimal solution found (non-physical)
- iteration limit reached
- optimal solution found (low convergence)
- time limit reached
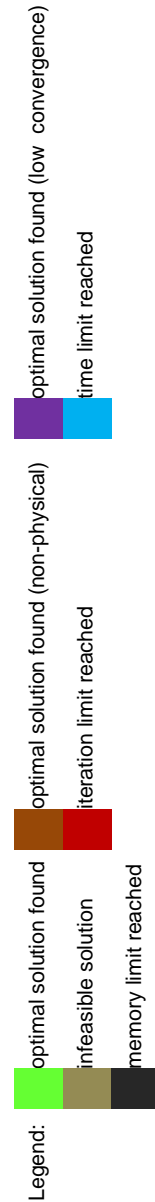
Tab. 14.3-2: Overview of tested NEOS solvers for solving load flow optimization problems

Solvers Couenne, FilMINT, LOQO and MOSEK were excluded from the simulations. Couenne solver provided correct solutions but with too high computation times even for smaller problems. FilMINT solver did not obtain the results at all. LOQO solver often exceeded its iteration limits. MOSEK solver is not designed for solving non-convex problems.

Therefore, it is highly recommended to apply Bonmin, KNITRO-C, filter or Ipopt solvers for solving load flow optimization problems.

14.4 Testing of NEOS Solvers with OLTC Transformers (V/Q/P)

The only useful NEOS solvers for robust solving of V/Q/P control optimization problems are Bonmin, MINLP and KNITRO, i.e. those with precise definition of both binary/integer variables.

Set of IEEE test systems modified by a number of OLTC transformers was tested by each suitable NEOS solver. In the evaluation, total V/Q/P square error was evaluated and compared along with the numbers of PV-to-PQ-switched network buses - see Tab. 14.4-1. Both Bonmin and MINLP solvers were used with their default settings. In case of KNITRO solver, performances of various option settings were tested (versions KNITRO-A, KNITRO-B and KNITRO-C from Chapter 14.3.

Tab. 14.4-1: Overview of NEOS solvers for solving V/Q/P control optimization problems

case	Bonmin		MINLP		KNITRO-A		KNITRO-B		KNITRO-C	
	PV->PQ	VQP_err	PV->PQ	VQP_err	PV->PQ	VQP_err	PV->PQ	VQP_err	PV->PQ	VQP_err
9LTC-1	0/2	1.24e-6	0/2	1.24e-6	0/2	1.24e-6	0/2	1.24e-6	0/2	1.24e-6
9LTC-2	1/2	1.29e-6	0/2	1.41e-6	1/2	1.29e-6	1/2	1.34e-6	1/2	1.29e-6
14LTC-1	2/4	7.48e-7	2/4	7.45e-7	2/4	7.48e-7	2/4	7.48e-7	2/4	7.48e-7
24LTC-1	4/10	1.94e-5	4/10	9.05e-5	4/10	1.90e-5	4/10	1.90e-5	2/10	1.09e-4
30LTC-1	4/5	6.78e-6	4/5	3.05e-5	4/5	5.74e-6	4/5	5.74e-6	4/5	7.75e-6
30LTC-2	3/5	7.83e-6	3/5	2.36e-5	3/5	3.37e-7	3/5	1.40e-7	3/5	1.71e-7
39LTC-1	0/9	1.13e-6	0/9	9.92e-7	0/9	9.95e-7	0/9	1.25e-6	0/9	9.97e-7
57LTC-1	3/6	3.23e-4	---	---	3/6	4.22e-4	3/6	3.22e-4	3/6	4.64e-4

As can be seen from Tab. 14.4-1, tap settings for the lowest V/Q/P square error was frequently obtained by KNITRO-B (in 6 of 8 cases). Slightly worse was solver KNITRO-A with 5 optimal solutions only, while remaining solvers had their successfulness below 60 percent. It is also visible that all applied NEOS solvers mostly switched the identical PV buses to PQ. Although the final V/Q/P square error values were kept inside a satisfiable region, final tap settings obtained by individual NEOS solvers were surprisingly greatly different from each other. MINLP solver showed smaller region of solvable load flow cases with OLTC transformers. Unfortunately, none of the solvers was capable to solve any of V/Q/P control optimization problems for networks larger than 57 buses due to memory limitations.

Higher number of possible solutions for this type of optimization problem follows from the discrete definition of tap magnitudes/angles of OLTC transformers. Therefore, the IEEE 39-bus power system was further tested by chosen NEOS solvers to demonstrate large differences between individual tap solutions - see Fig. 14.4-1 and Tab. 14.4-2.
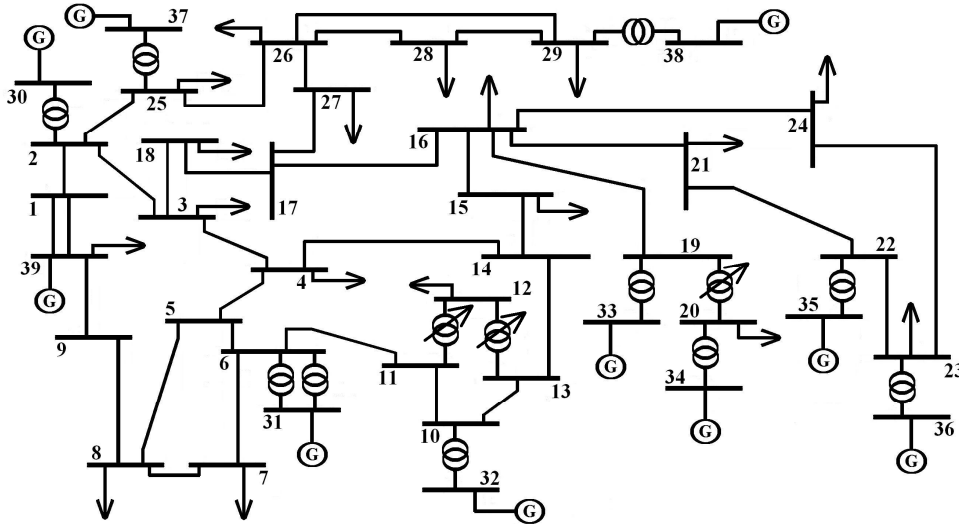
Fig. 14.4-1: Scheme of the IEEE 39-bus power system with 3 OLTC transformers

Tab. 14.4-2: Overview of OLTC transformers in the IEEE 39-bus power system

from-to bus	control bus	tap settings (min/max/step)	voltage target [pu]
12-11	11	0.92/1.08/0.002	1.00
12-13	13	0.92/1.08/0.002	1.00
19-20	20	0.92/1.08/0.002	1.00

Tab. 14.4-3: Final tap solutions of the IEEE 39-bus power system with OLTC transformers

solver	final tap settings			VQP_err
	t_{12-11}	t_{12-13}	t_{19-20}	
Bonmin	0.978	0.966	1.014	1.13e-6
MINLP	0.968	0.962	1.014	9.92e-7
KNITRO-A	0.982	0.978	1.014	9.95e-7
KNITRO-B	0.968	0.962	1.012	1.25e-6
KNITRO-C	1.030	1.026	1.014	9.97e-7

As transparently visible in Tab. 14.4-3, each of applied NEOS solvers obtained markedly different final tap solutions and V/Q/P square error values. Due to very small differences between these errors, all the tap solutions can be considered as correct for real power system operation. No PV bus was switched to PQ by any of NEOS solvers.

From all simulations follows that KNITRO solver with multistart and active set root node relaxation algorithm (KNITRO-B) showed the largest range of solvable V/Q/P control optimization problems, provided the best results in majority of cases and was evaluated as highly robust for this type of optimization problem. Nevertheless, remaining settings of KNITRO solver along with Bonmin and MINLP solvers showed similar performances. In case of the latter one, however, slightly smaller range of solvable problems was observed.

14.5 Testing of NEOS Solvers for Voltage Stability Analysis

As the most promising for singular point localization, solvers Bonmin, MINLP and KNITRO were tested and evaluated. For the latter, its performance for various option

settings was also assessed - see Tab. 14.5-1. Interior/direct (barrier), interior/cg (barrier) and active set algorithm was activated for solvers KNITRO1, KNITRO2 and KNITRO3, respectively. In case of solvers KNITRO4, KNITRO5 and KNITRO6, multistart with a number of starting studies was applied along with sufficiently large maximum number of iterations. However, when the multistart number is too large (say 200), time limit can be reached even for smaller systems. If so, such cases were tested again with another "ms_maxsolves" parameter value.

Tab. 14.5-1: Option settings for KNITRO solver [73]

version of KNITRO solver	option settings
KNITRO1	mip_rootalg=1
KNITRO2	mip_rootalg=2
KNITRO3	mip_rootalg=3
KNITRO4	mip_rootalg=1 ms_enable=1 ms_maxsolves=200 maxit=500000
KNITRO5	mip_rootalg=2 ms_enable=1 ms_maxsolves=200 maxit=500000
KNITRO6	mip_rootalg=3 ms_enable=1 ms_maxsolves=200 maxit=500000

Tab. 14.5-2: Overview of tested NEOS solvers for solving voltage stability problems

case	scenario L									scenario L+G								
	CLF	B	M	K1	K2	K3	K4	K5	K6	CLF	B	M	K1	K2	K3	K4	K5	K6
EPS3I	32.19816									32.19816								
EPS4I	26.22217									26.22218								
EPS4II	4.13120									4.63607								
EPS5I	1.20142									1.20246								
EPS5II	1.79084									1.79084								
EPS5III	2.77174									3.09336								
EPS6I	6.67488									6.67488								
EPS6II	3.41793									4.22602								
EPS6III	1.33722									1.37171								
EPS7I	1.41156									1.28144								
EPS7II	1.93031									1.93031								
IEEE9II	1.30263									1.16205								
EPS10I	2.26676									2.25894								
EPS11I	1.09871									1.09871								
EPS11II	1.23089									1.33688								
EPS11III	42.45786									46.76852								
EPS13I	35.55000									6.84024								
IEEE13II	4.40058									4.40058								
IEEE14I	1.76033									1.77800								
EPS15I	1.35461									1.41159								
EPS16I	1.23434									1.23422								
EPS17I	1.02212									1.01441								
EPS19I	3.75416									3.75416								
EPS23I	2.59173									2.52217								
IEEE24I	1.51091									1.66293								
IEEE26I	2.44857									2.48202								
IEEE30I	1.53690									1.54675								
IEEE35I	2.88896									2.88896								
EPS37I	13.46508									13.46508								
IEEE39I	1.21862									1.53950								
EPS43I	1.01696									1.01696								
IEEE57I	1.40678									1.61684								
EPS59I	1.14462									1.46536								
EPS59II	1.02889									1.23877								
EPS59III	1.06503									1.25177								
EPS59IV	1.14796									1.89259								
EPS59V	1.09888									1.58676								
EPS59VI	1.13517									1.94585								
EPS61I	1.24132									1.25480								
IEEE118I	1.61355									2.08086								

Note: B - Bonmin, M - MINLP, K1-6 - KNITRO

- optimal solution
- optimal solution (non-physical)
- infeasible solution
- iteration limit
- time limit
- memory limit

Broad range of 40 test power systems was tested on voltage stability with both L and L+G scenarios - see Tab. 14.5-2. For verification purposes, author-developed CLF algorithm (high accurate settings) was applied to provide reliable voltage stability solutions. In the evaluation process, maximum loadabilities from the CLF algorithm and tested NEOS solvers were compared. For smaller IEEE test networks, maximum loadability values are fully provided for both scenarios in Tab. 14.5-3 and 14.5-4. As can be seen, correct solutions with high accuracy were obtained in majority of load flow cases.

Tab. 14.5-3: Solution details for selected IEEE test power systems (scenario L)

case	maximum loadability value					
	CLF	Bonmin	MINLP	KNITRO4	KNITRO5	KNITRO6
IEEE9I	1.302632		1.30263	1.30263	1.30263	1.30263
IEEE14I	1.760331	1.76033		1.76033	1.76033	1.76033
IEEE24I	1.51091	1.51091	1.51091			
IEEE26I	2.448574	2.44857	2.44857	2.44857		2.44857
IEEE30I	1.536905	1.5369	1.5369	1.5369	1.5369	1.5369
IEEE37I	13.46508	13.4651	13.4651	13.4651	13.4651	13.4651
IEEE39I	1.21862		1.21862	1.21862		

Tab. 14.5-4: Solution details for selected IEEE test power systems (scenario L+G)

case	maximum loadability value					
	CLF	Bonmin	MINLP	KNITRO4	KNITRO5	KNITRO6
IEEE9I	1.162053	1.16205		1.16205	1.16205	1.16205
IEEE14I	1.777995	1.778		1.778	1.778	
IEEE24I	1.662933	1.66294	1.66294	1.66294	1.66294	
IEEE26I	2.482021	2.48202		2.48202		
IEEE30I	1.546751	1.54675	1.54675	1.54675	1.54675	1.54675
IEEE37I	13.46508	13.4651	13.4651	13.4651	13.4651	13.4651
IEEE39I	1.539505	1.53951	1.53951		1.53951	1.53951

From Tab. 14.5-2 follows: 1) Solver KNITRO4 proved to be the most robust and advanced for this type of optimization problem by producing only 12 infeasible and 7 non-physical solutions for both scenarios together (total of 80 load flow cases). No infeasibility and only 6 non-physical solutions were detected for cases up to 39 buses. 2) Slightly worse solver Bonmin provided 19 infeasible and 8 non-physical solutions in total. Moreover, it was able to successfully solve even some of the largest load flow cases. Also, from all tested solvers it showed the fastest solution progress. 3) Solvers KNITRO3, KNITRO5 and KNITRO6 were slightly worse than those above. Therefore, it is worthy to customize the settings of KNITRO solver for individual optimization problems. 4) Solvers KNITRO1 and KNITRO2 were highly unreliable. Solver MINLP was assessed as the worst solver at all.

Therefore, it is strongly recommended to apply Bonmin and KNITRO solvers with all presented option settings for solving voltage stability optimization problems. With high probability, at least one of these should provide the correct solution which will be identical with the output of the CLF algorithm. Though, more work must be done to tune KNITRO solver for increasing its solution reliability when solving voltage stability optimization problems.

15. Review and Discussion on the Results

In this doctoral thesis, main emphasis was placed on a) numerical improvements of conventional load flow methods, b) voltage/power control possibilities of OLTC transformers in especially larger and excessively complex power systems, c) voltage stability analysis of the networks along with the evaluation of maximum loadabilities, locations of weak network areas and detections of critical scenarios for minimum distance to voltage instability and d) the use of alternative computational tools for load flow analyses. Individual key topics of this doctoral thesis are further evaluated.

Numerical instabilities were often observed especially in the N-R method when solving highly loaded and sparse power systems. Therefore, several stability techniques were applied and further tuned to improve its numerical stability and avoid possible low-convergence and/or divergence scenarios. Furthermore, revival of both G/G-S methods with the proposed PV/PQ bus-type switching logic was realized for obtaining numerically stable, reliable and highly accurate results. Although the CPU time requirements remained relatively high, they were significantly decreased by sparse and vectorized programming and the use of acceleration techniques with optimized settings. In the F-D method, its both versions (XB, BX) were designed and comprehensively tested to find that the XB-type of the F-D method had eventually better numerical performance in terms of calculation speed and total numbers of iterations not only for ill-conditioned power systems but also for distribution networks. Proposed version of the DC load flow method was also successful to locate better approximate solutions than the widely published original DC load flow method.

Due to high convergence/divergence rate, numerical oscillations were often induced in the N-R method when dealing with OLTC transformers. Unfortunately, tuning of the OLTC algorithms for V control in the N-R method was not fully accomplished along with the inclusion of codes for Q/P control. Proposed OLTC algorithms with fair cooperation with var limits in PV buses were realized in the G/G-S methods when producing reliable and much better results including optimal tap settings than the N-R method. Again, increased CPU times and iteration numbers were successfully reduced by acceleration techniques with optimized settings and by vectorized and sparsely programmed codes. No V/Q/P control mechanisms were included into the F-D method.

Both Cycled N-R and CLF methods were sparsely programmed and comprehensively tested to find the most suitable settings for obtaining relatively fast but still reliable and accurate results. Innovative methodology was proposed for locating weak network buses/branches/areas in terms of voltage stability using both VSMI and VSF indices. For a given test system, several corrective strategies were developed, tested and evaluated. Furthermore, the SDVI analysis was developed to assess the minimum distance to voltage instability along with critical MW/MVAr loading scenarios for even larger power systems. However, the PQ-only systems (e.g. distribution networks) could be successfully solved only. Unfortunately, none of these softwares were designed so that real-time calculations of electric power systems would be possible.

Definition of selected optimization problems in AMPL format was not only possible but also highly effective in majority of cases. Suitable NEOS solvers for reliable calculation of load flow, V/Q/P control and voltage stability optimization problems were identified and fully tested on high number of test power systems. Unfortunately, their use was rarely in conflict with permitted requirements of NEOS Server for Optimization on calculation time, memory and maximum size of input data file. Despite of these complications, the NEOS Server proved its suitability, reliability and robustness to deal with these optimization tasks.

15.1 Author's Contribution

One of the Author's contributions to the topic is the tuning of both G-S/N-R methods for decreasing iteration and CPU time requirements and increasing numerical stability, respectively. By these, both G/G-S methods can be still useful for off-line reliability network studies, for output verifications of the N-R method and for simple load flow calculations of especially medium-sized power systems. For the N-R method, stability techniques are strongly recommended to be applied to avoid numerical oscillations and even divergence scenarios under abnormal operating conditions of electric power systems (unplanned generations from renewable power sources, highly loaded networks, etc.).

Voltage control demonstration in the islanded distribution network with strong representation of photovoltaic power sources and broad range of voltage/var compensation devices was provided in this doctoral thesis. It shows that suitable cooperation of the variety of controllable system devices may be shortly essential for stable, reliable and sustainable operation and control of electric power systems with connected renewable power systems. Performed simulation provides new perspective on such wholesale control of the network using the centralized computing centre with real-time running optimizer (Smart Grid concept).

In practical voltage stability analyses, the CLF algorithm is strongly recommended to be applied with its compromise step size settings (as programmed by the Author in MATLAB environment) for the best combination of precision level and CPU time requirements. In the actual version, however, the CLF method can be still applied only for off-line planning and development studies of electric power systems. In such studies, it is suggested to apply the proposed methodology for full-scale voltage stability analysis of the system for locating its voltage/power weak areas using the VSMI/VSF indices. For such areas, a list of potentially highly-effective corrective/preventive strategies can be prepared in advance to improve voltage profiles and avoid black-out and islanding problems. From this list of strategies, only the one which meets both technical/economical criteria should be executed by the operator.

From the SDVI analysis follows that the idea of stressing the system uniformly for evaluating the voltage stability margin is completely wrong. In practice, the system is being stressed in a rather unbalanced way, i.e. P/Q increments are dependent on time period during the day and other internal/external system effects. Therefore, more suitable would be the SDVI approach for finding the minimum distance to voltage instability and critical P/Q increments for evaluating the voltage stability margin. The operator should enter the initial loading scenario for each network bus individually based on measured network data, forecasted system conditions, his personal experience or knowledge about actual power

system operation. Then, practical minimum distance to voltage instability and thus critical voltage stability margin could be obtained.

15.2 Suggestions for Future Work

With respect to actual problems and challenges in electric power system operation and control, each scope of this work can be further developed.

Stabilization process of the N-R method can be further improved in the pre-processing part by using the modified version of the CLF algorithm. Since the CLF method is numerically stable also in the singular point and its surrounding area, it can suitably deal with numerical singularities in the base case for ill-conditioned and badly-converging load flow cases where the standard N-R method may have numerical problems.

Further tuning of OLTC algorithms for the N-R method (including the Q/P control) is necessary to fully accomplish this task. For the F-D method, sensitivity approach seems to be the most suitable due to totally distinct mathematical concept of this load flow method. Potentially, sensitivity factors may be more effective also for the N-R method when avoiding frequent switching of OLTC transformers from the regulated to the fixed mode.

In the CLF algorithm, the step-size control has not been fully covered for the minimization of CPU time requirements. Other procedures, such as local (or arc length) parameterization techniques [5], could offer better step sizes during the calculation and further decrease the CPU times. Furthermore, the Q-limit guided CLF algorithm [60] would be the most robust and advanced for minimizing the numbers of stable V-P points for reaching the bifurcation point. Using these methods, the real-time evaluation of system's voltage stability would be possible.

For the SDVI analysis, the inclusion of PV buses along with their var limits is crucial to extend the use of this method also on broad range of complex power systems. In case of excessively increased problem complexity, optimization techniques (e.g. particle swarm, genetic algorithms, etc.) will be probably necessary to be employed instead.

Further developments of the SimEPS software can be easily accomplished due to its simple and transparent code structure. Moreover, the AMPL Builder can be also perfected especially in following areas:

1] More effective formulation of the voltage stability optimization problem is needed for increasing calculation reliability of selected NEOS solvers.

2] Modification of the V/Q/P control optimization problem by introducing continuous representation of transformer tap settings would ease the calculation by producing exact but idealized solutions. Then, other solvers (filter, Ipopt, etc.) could be also safely applied.

3] Further investigation of user setting possibilities for KNITRO solver could provide even better and more reliable results along with increased calculation speed.

4] Search also for another free web solvers to be downloaded and used would reduce the problems with time/memory limitations of NEOS Server.

5] Voltage stability optimization problem could be further combined e.g. with the reconfiguration problem where optimizing on/off positions of network switches. From NEOS Server, solvers Bonmin and KNITRO should be the best for solving this problem.

16. References

[1] GLOVER, J.D., SARMA, M.S. and OVERBYE, T.J. *Power System Analysis and Design*. 4th ed. CENGAGE-Engineering, 2007. ISBN 0-5345-4884-9.

[2] SAADAT, H. *Power System Analysis*. 2nd ed. McGraw-Hill, 2002. ISBN 0-0728-4869-3.

[3] GRAINGER, J.J., STEVENSON, W.D. *Power System Analysis*. 2nd ed. McGraw-Hill, 1994. ISBN 0-07-061293-5.

[4] KUNDUR, P. *Power System Stability and Control*. McGraw-Hill, 1994. ISBN 0-07-035958-X.

[5] CANIZARES, C., CONEJO, A.J. and EXPOSITO, A.G. *Electric Energy Systems: Analysis and Operation*. CRC Press, 2008. ISBN 978-0-8493-7365-7.

[6] BERGEN, A.R. and VITTAL, V. *Power System Analysis*. 2nd ed. Prentice-Hall, 2000. ISBN 0-13-691990-1.

[7] CROW, M. *Computational Methods for Electric Power Systems*. CRC Press, 2002. ISBN 0-8493-1352-X.

[8] ARRILLAGA, J. and WATSON, N.R. *Computer Modelling of Electrical Power Systems*. 2nd ed. John Wiley & Sons, 2001. ISBN 0-471-87249-0.

[9] AJJARAPU, V. *Computational Techniques for Voltage Stability Assessment and Control*. Springer, 2006. ISBN 0-387-26080-3.

[10] MOHAN, N. *First Course on Power Systems Year 2006 Edition*. MNPERE, 2006. ISBN 0-9715292-7-2.

[11] GROSS, C.A. *Power System Analysis*. 2nd ed. John Wiley & Sons, 1986. ISBN 0471862061.

[12] WOOD, A.J. and WOLLENBERG, B.F. *Power Generation, Operation and Control*. John Wiley & Sons, 1984. ISBN 0-471-09182-0.

[13] CUTSEM, T.V. and VOURNAS, C. *Voltage Stability of Electric Power Systems*. Springer, 2008. ISBN 978-0-387-75535-9.

[14] GUILE, A.E. and PATERSON, W. *Electrical Power Systems*. 2nd ed. Pergamon Press, 1977. ISBN 0-08-021728-1.

[15] YAMAYEE, Z.A. and BALA, J.L. *Electromechanical Energy Devices and Power Systems*. John Wiley & Sons, 1994. ISBN 0-471-57217-9.

[16] WEEDY, B.M. and CORY, B.J. *Electric Power Systems*. 4th ed. John Wiley & Sons, 1998. ISBN 0-471-97677-6.

[17] KUSIC, G.L. *Computer-Aided Power System Analysis*. Prentice-Hall, 1986. ISBN 0-13-164526-9.

[18] BARRET, J.-P., BORNARD, P. and MEYER, B. *Power System Simulation*. Chapman & Hall, 1997. ISBN 0-412-63870-3.

[19] KOLCUN, M., CHLADNÝ, V., VARGA, L., BEŇA, L´., ILENIN, S., LEŠČINSKÝ, P. and MEŠTER, M. *Analýza elektrizačnej sústavy*. PRO, 2005. ISBN 80-89057-09-8.

[20] MERTLOVÁ, J., HEJTMÁNKOVÁ, P. and TAJTL, T. *Teorie přenosu a rozvodu elektrické energie*. ZČU, 2004. ISBN 80-7043-307-8.

[21] FOURER, R., GAY, D.M. and KERNIGHAN, B.W. *AMPL: a modelling language for mathematical programming*. 2nd ed. Brooks Cole, 2002. ISBN 0-89426-232-7.

[22] KOLCUN, M., MÜHLBACHER, J. and HALLER, R. *Mathematical Analysis of Electrical Networks*. BEN, 2004. ISBN 80-7300-098-9.

[23] SONG, Y.H. *Modern Optimisation Techniques in Power Systems*. Springer, 1999. ISBN 0-7923-5697-7.

[24] SHAHIDEHPOUR, M. and WANG, Y. *Communication and Control in Electric Power Systems - Applications of Parallel and Distributed Processing*. John Wiley & Sons, 2003. ISBN 0-471-45325-0.

[25] CHOW, J.H., WU, F.F. and MOMOH, J.A. *Applied Mathematics for Restructured Electric Power Systems - Optimization, Control and Computational Intelligence*. Springer, 2005. ISBN 0-387-23470-5.

[26] IRVING, M. Pseudo-LoadFlow Formulation as a Starting Process for the Newton Raphson Algorithm. In: *Electrical Power and Energy Systems 32.* Vol. 32, No. 8, pp. 835-839. ISSN: 0142-0615.

[27] HECKMANN, W., SORG, A., WEBER, T. and WELLSSOW, W.H. Enhanced AC Power-Flow Solutions for Reliability Analyses. In: *ETEP*. Vol. 11, No. 2, pp. 79-88. ISSN: 2050-7038.

[28] KOH, C.S., RYU, J.S. and FUJIWARA, K. Convergence Acceleration of the Newton-Raphson Method Using Successive Quadratic Function Approximation of Residual. In.: *IEEE Transactions on magnetics.* Vol. 42, No. 4, pp. 611-614. ISSN: 0018-9464.

[29] TRIPATHY, S.C., PRASAD, G.D., MALIK, O.P. and HOPE, G.S. Load-Flow Solutions for Ill-Conditioned Power Systems by a Newton-Like Method. In: *IEEE PES.* Vol. PAS-103, No. 8, pp. 3648-3657. ISSN: 0018-9510.

[30] LAGACE, P.J., VUONG, M.H. and KAMWA, I. Improving Power Flow Convergence by Newton Raphson with a Levenberg-Marquardt Method. In: *IEEE Transactions.* pp. 1-6. ISSN: 1932-5517.

[31] CHAKRAVORTY, J., CHAKRAVORTY, S. and GHOSH, S. A Fuzzy Based Efficient Load Flow Analysis. In: *International Journal of Computer and Electrical Engineering.* Vol. 1, No. 4, pp. 414-418. ISSN: 1793-8163.

[32] GRANVILLE, S., MELLO, J.C.O. and MELO, A.C.G. Application of Interior Point Methods to Power Flow Unsolvability. In: *IEEE Transactions on Power Systems*. Vol. 11, No. 2, pp. 1096-1103. ISSN: 0885-8950.

[33] STOTT, B. and ALSAC, O. Fast Decoupled Load Flow. In: *IEEE Transactions on Power Apparatus and Systems*. Vol. PAS-93, No. 3, pp. 859-869. ISSN: 0018-9510.

[34] ZHAO, J., CHIANG, H.D., LI, H. and JU, P. On PV-PQ bus type switching logic in power flow computation. [online]. 2008, pp. 1-7 [cit. 2010-05-17]. Available on: http://www.pscc-central.org/uploads/tx_ethpublications/pscc2008_128.pdf.

[35] VAN AMERONGEN, R.A.M. A General-Purpose Version of the Fast Decoupled Load Flow. In: *IEEE Transactions on Power Systems*. Vol. 4, No. 2, pp. 760-770. ISSN: 0885-8950.

[36] FAN, J. and BO, Z. Modelling of On-Load Tap-Changer Transformer with Variable Impedance and Its Applications. In: *Proceedings of International Conference on Energy Management and Power Delivery (EMPD)*. pp. 491-494. ISBN: 0-7803-4495-2.

[37] PRADA, R.B., SEELIG, B.H.T., dos SANTOS, J.O.R., PILOTTO, L.A.S. and BIANCO, A. Modelling On-Load Tap Changer Voltage Control and Limits for Network Loading and Voltage Control Effectiveness Assessment. In: *IEEE PowerTech Conference*. pp. 1-6. ISBN: 0-7803-7967-5.

[38] ROMAN, C. and ROSEHART, W. Complementarity Model for Load Tap Changing Transformers in Stability Based OPF Problem. In: *Electric Power Systems Research 76*. Vol. 76, No. 6–7, pp. 592-599. ISSN: 0378-7796.

[39] CUTSEM, T.V. and QUINTANA, V.H. Network Parameter Estimation using Online Data with Application to Transformer Tap Position Estimation. In: *IEE Proceedings of Conference on Generation, Transmission and Distribution*. Vol. 135, No. 1, pp. 31-40. ISSN: 0143-7046.

[40] NAKACHI, Y., KATO, S. and UKAI, H. Coordinated Voltage Control of Transformer Taps with Provision for Hierarchical Structure in Power System. In: *Electrical Engineering in Japan*. Vol. 166, No. 4, pp. 48-55. ISSN: 1520-6416.

[41] OKYERE, H.K., NOURI, H., MORADI, H. and ZHENBIAO, L. STATCOM and Load Tap Changing Transformer (LTC) in Newton Raphson Power Flow: Bus Voltage Constraint and Losses. In: *42nd International Universities Power Engineering Conference (UPEC)*. pp. 1013-1018. ISBN: 978-1-905593-36-1.

[42] HSIAO, Y.-T., LIU, C.-C., CHIANG, H.-D. and CHEN, Y.-L. A New Approach for Optimal VAR Sources Planning in Large Scale Electric Power Systems. In: *IEEE Transactions on Power Systems*. Vol. 8, No. 3, pp. 988-996. ISSN: 0885-8950.

[43] ALLAN, R.N. and ARRUDA, C. LTC Transformers and MVAR Violations in the Fast Decoupled Load Flow. In: *IEEE Transactions on Power Apparatus and Systems*. Vol. PAS-101, No. 9, pp. 3328-3332. ISSN: 0272-1724.

[44] RISTANOVIĆ, P., BJELOGRLIĆ, M. and BABIĆ, B.S. Improvements in Sparse Matrix/Vector Technique Applications for On-Line Load Flow Calculation. In: *IEEE Transactions on Power Systems*. Vol. 4, No. 1, pp. 190-196. ISSN: 0885-8950.

[45] YOUSSEF, R.D. Phase-Shifting Transformers in Load Flow and Short-Circuit Analysis: Modelling and Control. In: *IEE Proceedings of Conference on Generation, Transmission and Distribution*. Vol. 140, No. 4, pp. 331-336. ISSN: 0143-7046.

[46] OKANIK, P., KURTH, B. and HARLOW, J.H. An Update on the Paralleling of OLTC Power Transformers. In: *IEEE Transmission and Distribution Conference*. pp. 871-875. ISBN: 0-7803-5515-6.

[47] ZHU, T.X., TSO, S.K. and LO, K.L. An Investigation into the OLTC Effects on Voltage Collapse. In: *IEEE Transactions on Power Systems*. Vol. 15, No. 2, pp. 515-521. ISSN: 0885-8950.

[48] CHAKRAVORTY, J., CHAKRAVORTY, S. and GHOSH, S. A Fuzzy Based Efficient Load Flow Analysis. In: *International Journal of Computer and Electrical Engineering.* Vol. 1, No. 4, pp. 414-418. ISSN: 1793-8163.

[49] LIN, W.-M., ZHAN, T.-S. and HUANG, C.-H. A Circuit Theory Based Load Flow Tracing Method Considering Counter-Flow Contribution. In: 5th *WSEAS International Conference on Instrumentation, Measurement, Circuits and Systems*. pp. 312-317. ISBN: 960-8457-43-2.

[50] BAKIRTZIS, A.G., KIM, Y.-H. and SAKIS MELIOPOULOS, A.P. Monte Carlo Simulation for Evaluating Retail Wheeling Effects. In: *Electric Power Systems Research 60*. Vol. 60, No. 3, pp. 137-144. ISSN: 0378-7796.

[51] TING, T.O., WONG, K.P. and CHUNG, C.Y. Investigation of Hybrid Genetic Algorithm/Particle Swarm Optimization Approach for the Power Flow Problem. In: *Proceedings of the Fourth International Conference on Machine Learning and Cybernetics*. pp. 436-440. ISBN: 0-7803-9091-1.

[52] EL-ELA, A.A. Fast and Accurate Technique for Power System State Estimation. In: *IEE Conference on Generation, Transmission and Distribution*. Vol. 139, No. 1, pp. 7-12. ISSN: 0143-7046.

[53] POPOVIĆ, D.S. Impact of Secondary Voltage Control on Voltage Stability. In: *Electric Power Systems Research 40*. Vol. 40, No. 1, pp. 51-62. ISSN: 0378-7796.

[54] PROKOP, L. and MISAK, S. Hodnocení provozu fotovoltaické elektrárny. In: *Electric Power Engineering Conference (EPE)*. pp. 1-4. ISBN: 978-80-248-2393-5.

[55] CHEN, M.J., WU, B. and CHEN, C. Determination of Shortest Distance to Voltage Instability with Particle Swarm Optimization Algorithm. In: *European Transactions on Electrical Power*. Vol. 19, No. 8, pp. 1109 - 1117. ISSN: 2050-7038.

[56] CHANG, S.K. and BRANDWAJN, V. Solving the Adjustment Interactions in Fast Decoupled Load Flow. In: *IEEE Transaction on Power Systems*. Vol. 6, No. 2, pp. 801-805. ISSN: 0885-8950.

[57] ŠMON, I., PANTOŠ, M. and GUBINA, F. An improved voltage-collapse protection algorithm based on local phasors. In: *Electric Power Systems Research 78 (2008)*. Vol. 78, No. 3, pp. 434-440. ISSN: 0378-7796.

[58] GONG, Y. and SCHULZ, N. Synchrophasor-Based Real-Time Voltage Stability Index. In: *Proceedings of PSCE conference*. pp. 1029-1036. ISBN: 1-4244-0177-1.

[59] DOBSON, I., CUTSEM, T.V., VOURNAS, C., DEMARCO, C.L., VENKATASUBRAMANIAN, M., OVERBYE, T. and CANIZARES, C.A. *Voltage Stability Assessment: Concepts, Practices and Tools - Chapter 2*. 2002. Power System Stability Subcommittee Special Publication. IEEE Power Engineering Society.

[60] ZHU, P. *Performance Investigation of Voltage Stability Analysis Methods*. London, 2008. Doctoral thesis. Brunel University of West London.

[61] STANIULIS, R. *Reactive Power Valuation*. Lund, 2001. Academic thesis. Department of Industrial Electrical Engineering and Automation at Lund University.

[62] ŠILHÁN, P. *Modelování a řízení přenosové soustavy*. Pilsen, 2008. Doctoral thesis. University of West Bohemia in Pilsen.

[63] SOUKUP, M. *Řízení provozu mikro-sítí napájených OZE*. Pilsen, 2006. Diploma thesis. University of West Bohemia in Pilsen.

[64] SCHMIDT, S. Load flow. In: Sector Energy D SE PTI NC - Siemens AG [online]. 2008 [cit. 2009-11-07]. Available on: http://www.tavanir.org.ir/dm/etozi/download/siemens/Network%20Analysis%20and%20Calculation/06-LoadFlow.ppt.

[65] TATE, Z. Initialization Schemes for Newton-Raphson Power Flow Solvers. [online]. 2008 [cit. 2008-05-28]. Available on: http://grb.physics.unlv.edu/~zbb/files/upload/29UV3GPCVQ WO6ERVE9RABFQ5M.pdf.

[66] PATEL, S.B. System of Super Super Decoupled Loadflow Computation for Electrical Power System. In: US patent No. 20080281474 [online]. 2008 [cit. 2012-06-19]. Available on: http://www.faqs.org/patents/app/20080281474.

[67] CONEJO, A.J. Load Flow. In: Universidad de Castilla-La Mancha [online]. 2011 [cit. 2013-01-15]. Available on: www.uclm.es/area/gsee/Archivos%20Pag-web/docencia/aelect/01 _LoadFlow_R1.pdf.

[68] NEDIC, D. Tap Adjustment in AC Load Flow. In: UMIST [online]. 2002 [cit. 2013-02-20]. Available on: www.ee.washington.edu/research/real/Library/Reports/Tap_Adjustments_in _AC_Load_Flows.pdf.

[69] PowerWorld Simulator 13 GSO version [online]. [cit. 2008-09-29]. Available on: http://www.powerworld.com/.

[70] Homepage of MATPOWER [online]. [cit. 2008-09-30]. Available on: http://www.pserc. cornell.edu/matpower/.

[71] Homepage of PSAT [online]. [cit. 2013-03-03]. Available on: http://www3.uclm.es/ profesorado/federico.milano/psat.htm.

[72] NEOS Server for Optimization [online]. [cit. 2008-09-19]. Available on: http://neos.mcs. anl.gov/neos/.

[73] KNITRO 7.0 User Options for AMPL [online]. [cit. 2010-11-29]. Available on: http://www. ziena.com/docs/QuickRef_KnitroAmpl.pdf.

[74] PSS®E 32.0 Program Operation Manual - revised version 2009 [online]. [cit. 2011-07-17]. Available on: www.siemens.com/power-technologies.

[75] Czech Transmission System Operator ČEPS, a.s. [online]. [cit. 2012-03-10]. Available on: www.ceps.cz.

[76] EGÚ Praha Engineering, a.s. [online]. [cit. 2010-11-23]. Available on: http://www.egu-prg.cz/.

[77] Company OTE, a.s. [online]. [cit. 2012-01-03]. Available on: http://www.ote-cr.cz/.

[78] Photovoltaic Geographical Information System [online]. [cit. 2011-10-30]. Available on: http://re.jrc.ec.europa.eu/pvgis/apps4/pvest.php#.

[79] Brunel Institute of Power Systems (BIPS) [online]. [cit. 2009-05-05]. Available on: http:// www.brunel.ac.uk/sed/ece/research/bips.

[80] IEEE test power systems [online]. [cit. 2008-12-10]. Available on: http://www.ee. washington.edu/research/pstca/.

[81] IEEE PES Distribution Test Feeders [online]. [cit. 2012-02-16]. Available on: http://ewh.ieee.org/soc/pes/dsacom/testfeeders/.

[82] Simplified 14-generator model of the SE Australian Power system [online]. [cit. 2011-11-02]. Available on: http://www.eleceng.adelaide.edu.au/Groups/PCON/PowerSystems/IEEE/ BenchmarkData/Simplified_14-Gen_System_Rev3_20100701.pdf.

17. Appendices

For transparency reasons, several issues were omitted in the main body of the thesis and thus, they are presented in following appendices. Appendix A shows the input data structure of the 5-bus test power system [1] for the author-developed software SimEPS. Appendices B, C and D provide the input data of the network above in AMPL format for load flow, V/Q/P control and voltage stability optimization by NEOS solvers, respectively. Appendix E displays the list of all examined test networks for this doctoral thesis. Remaining test systems were created from these networks for specific purposes such as testings of logics for var limits and tap changing transformers.

Appendix A: Input Data Structure of the 5-Bus Test System in SimEPS
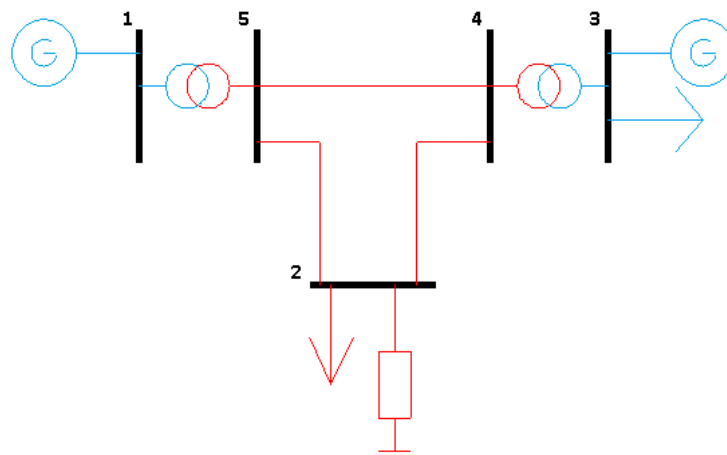

```
M1=[
1 1 5 1 0 0.00150 0.020 0.0 0.00 1.0 30.0 0.0 0.0 0.0 0.0 0.0 400e6
2 1 4 3 0 0.00075 0.010 0.0 0.00 1.0 30.0 0.0 0.0 0.0 0.0 0.0 800e6
3 0 2 4 0 0.00900 0.100 0.0 1.72 0.0  0.0 0.0 0.0 0.0 0.0 0.0 2008
4 0 2 5 0 0.00450 0.050 0.0 0.88 0.0  0.0 0.0 0.0 0.0 0.0 0.0 2008
5 0 4 5 0 0.00225 0.025 0.0 0.44 0.0  0.0 0.0 0.0 0.0 0.0 0.0 2008
];

M2=[
1 1  15   0.0   0.0 1.0   0.0   0.0 0.0 0.0 0.0 0.0 0.0 0.9   1.1
2 2 345 -8.0  -2.8 1.0   0.0   0.0 0.0 0.0 0.0 0.0 2.0 0.95 1.05
3 3  15  -0.8  -0.4 1.05 0.0  -2.8 4.0 5.2 0.0 0.0 0.0 0.9   1.1
4 2 345   0.0   0.0 1.0   0.0   0.0 0.0 0.0 0.0 0.0 0.0 0.95 1.05
5 2 345   0.0   0.0 1.0   0.0   0.0 0.0 0.0 0.0 0.0 0.0 0.95 1.05
];
```

Appendix B: Input Data for the Load Flow Optimization

```
#Parameters:
#   Bus Input Data:
        param F      =   100;
        param v1     =   1.00000000;
        param theta1 =   0.00000000;
        param pl2    =  -8.00000000;
        param ql2    =  -2.80000000;
        param bsh2   =   2.00000000;
        param p3     =   5.20000000;
        param vset3  =   1.05000000;
        param qlow3  =  -2.80000000;
        param qupp3  =   4.00000000;
        param pl3    =  -0.80000000;
        param ql3    =  -0.40000000;
```

```
#    Branch Input Data:
       param g5_1        =   3.72902424;
       param b5_1        = -49.72032318;
       param b5_1_0      =   0.00000000;
       param t5_1        =   1.00000000;
       param fi5_1       =   0.52359878;
       param g4_3        =   7.45804848;
       param b4_3        = -99.44064636;
       param b4_3_0      =   0.00000000;
       param t4_3        =   1.00000000;
       param fi4_3       =   0.52359878;
       param g2_4        =   0.89276857;
       param b2_4        =  -9.91965083;
       param b2_4_0      =   0.86000000;
       param g2_5        =   1.78553715;
       param b2_5        = -19.83930166;
       param b2_5_0      =   0.44000000;
       param g4_5        =   3.57107430;
       param b4_5        = -39.67860331;
       param b4_5_0      =   0.22000000;
#Variables:
#    Bus Variables:
       var p1      >=  -500.0, <=  500.0;
       var q1      >=  -500.0, <=  500.0;
       var v2      >=     0.8, <=    1.2;
       var theta2 >=   -6.28, <=   6.28;
       var qsh2    >=  -500.0, <=  500.0;
       var q3      >=  -500.0, <=  500.0;
       var v3      >=     0.8, <=    1.2;
       var theta3 >=   -6.28, <=   6.28;
       var bl3     >=     0.0, <=    1.0,binary;
       var bu3     >=     0.0, <=    1.0,binary;
       var v4      >=     0.8, <=    1.2;
       var theta4 >=   -6.28, <=   6.28;
       var v5      >=     0.8, <=    1.2;
       var theta5 >=   -6.28, <=   6.28;
#    Branch Variables:
       var p5_1     >=  -500.0, <=  500.0;
       var q5_1     >=  -500.0, <=  500.0;
       var p1_5     >=  -500.0, <=  500.0;
       var q1_5     >=  -500.0, <=  500.0;
       var p4_3     >=  -500.0, <=  500.0;
       var q4_3     >=  -500.0, <=  500.0;
       var p3_4     >=  -500.0, <=  500.0;
       var q3_4     >=  -500.0, <=  500.0;
       var p2_4     >=  -500.0, <=  500.0;
       var q2_4     >=  -500.0, <=  500.0;
       var p4_2     >=  -500.0, <=  500.0;
       var q4_2     >=  -500.0, <=  500.0;
       var p2_5     >=  -500.0, <=  500.0;
       var q2_5     >=  -500.0, <=  500.0;
       var p5_2     >=  -500.0, <=  500.0;
       var q5_2     >=  -500.0, <=  500.0;
       var p4_5     >=  -500.0, <=  500.0;
       var q4_5     >=  -500.0, <=  500.0;
       var p5_4     >=  -500.0, <=  500.0;
       var q5_4     >=  -500.0, <=  500.0;
#    Other Variables:
       var Ploss   >=     0.0, <=   10.0;
       var Qloss   >=  -100.0, <=  100.0;
#Objective Function:
    minimize obj:
       bl3+bu3+0;
#Equality and Inequality Constraints:
s.t.
#    Balance Equations:
c1: p1     = +p1_5;
c2: q1     = +q1_5;
c3: 0      = -pl2+p2_4+p2_5;
c4: 0      = -ql2-qsh2+q2_4+q2_5;
c5: p3     = -pl3+p3_4;
c6: q3     = -ql3+q3_4;
c7: 0      = +p4_3+p4_2+p4_5;
c8: 0      = +q4_3+q4_2+q4_5;
c9: 0      = +p5_1+p5_2+p5_4;
c10: 0     = +q5_1+q5_2+q5_4;
#    Shunt Power Flows:
```

```
c11: qsh2   =  bsh2*v2^2;
#   PV Buses:
c12: v3   <=   vset3+bl3*F;
c13: v3   >=   vset3-bu3*F;
c14: q3   <=   qupp3+bl3*(qlow3-qupp3);
c15: q3   >=   qlow3+bu3*(qupp3-qlow3);
c16: 1    >=   bl3+bu3;
#   Branch Power Flows:
c17: p5_1       = g5_1*(v5/t5_1)^2-g5_1*v5*v1/t5_1*cos(theta5-theta1-fi5_1)-
                  b5_1*v5*v1/t5_1*sin(theta5-theta1-fi5_1);
c18: q5_1       = -(b5_1+b5_1_0)*(v5/t5_1)^2+b5_1*v5*v1/t5_1*cos(theta5-theta1-fi5_1)-
                  g5_1*v5*v1/t5_1*sin(theta5-theta1-fi5_1);
c19: p1_5       = g5_1*v1^2-g5_1*v5*v1/t5_1*cos(theta1-theta5+fi5_1)-
                  b5_1*v5*v1/t5_1*sin(theta1-theta5+fi5_1);
c20: q1_5       = -(b5_1+b5_1_0)*v1^2+b5_1*v5*v1/t5_1*cos(theta1-theta5+fi5_1)-
                  g5_1*v5*v1/t5_1*sin(theta1-theta5+fi5_1);
c21: p4_3       = g4_3*(v4/t4_3)^2-g4_3*v4*v3/t4_3*cos(theta4-theta3-fi4_3)-
                  b4_3*v4*v3/t4_3*sin(theta4-theta3-fi4_3);
c22: q4_3       = -(b4_3+b4_3_0)*(v4/t4_3)^2+b4_3*v4*v3/t4_3*cos(theta4-theta3-fi4_3)-
                  g4_3*v4*v3/t4_3*sin(theta4-theta3-fi4_3);
c23: p3_4       = g4_3*v3^2-g4_3*v4*v3/t4_3*cos(theta3-theta4+fi4_3)-
                  b4_3*v4*v3/t4_3*sin(theta3-theta4+fi4_3);
c24: q3_4       = -(b4_3+b4_3_0)*v3^2+b4_3*v4*v3/t4_3*cos(theta3-theta4+fi4_3)-
                  g4_3*v4*v3/t4_3*sin(theta3-theta4+fi4_3);
c25: p2_4       = g2_4*v2^2-g2_4*v2*v4*cos(theta2-theta4)-b2_4*v2*v4*sin(theta2-theta4);
c26: q2_4       = -(b2_4+b2_4_0)*v2^2+b2_4*v2*v4*cos(theta2-theta4)-g2_4*v2*v4*sin(theta2-
                  theta4);
c27: p4_2       = g2_4*v4^2-g2_4*v2*v4*cos(theta4-theta2)-b2_4*v2*v4*sin(theta4-theta2);
c28: q4_2       = -(b2_4+b2_4_0)*v4^2+b2_4*v2*v4*cos(theta4-theta2)-g2_4*v2*v4*sin(theta4-
                  theta2);
c29: p2_5       = g2_5*v2^2-g2_5*v2*v5*cos(theta2-theta5)-b2_5*v2*v5*sin(theta2-theta5);
c30: q2_5       = -(b2_5+b2_5_0)*v2^2+b2_5*v2*v5*cos(theta2-theta5)-g2_5*v2*v5*sin(theta2-
                  theta5);
c31: p5_2       = g2_5*v5^2-g2_5*v2*v5*cos(theta5-theta2)-b2_5*v2*v5*sin(theta5-theta2);
c32: q5_2       = -(b2_5+b2_5_0)*v5^2+b2_5*v2*v5*cos(theta5-theta2)-g2_5*v2*v5*sin(theta5-
                  theta2);
c33: p4_5       = g4_5*v4^2-g4_5*v4*v5*cos(theta4-theta5)-b4_5*v4*v5*sin(theta4-theta5);
c34: q4_5       = -(b4_5+b4_5_0)*v4^2+b4_5*v4*v5*cos(theta4-theta5)-g4_5*v4*v5*sin(theta4-
                  theta5);
c35: p5_4       = g4_5*v5^2-g4_5*v4*v5*cos(theta5-theta4)-b4_5*v4*v5*sin(theta5-theta4);
c36: q5_4       = -(b4_5+b4_5_0)*v5^2+b4_5*v4*v5*cos(theta5-theta4)-g4_5*v4*v5*sin(theta5-
                  theta4);
#   Total Power Losses:
c37: Ploss  =  +p1+pl2+pl3+p3;
c38: Qloss  =  +q1+ql2+qsh2+ql3+q3;
#End of Input Data
```

Appendix C: Input Data for the V/Q/P Control Optimization

In this case, both transformers were switched to regulated mode as shown below.

```
M1=[
1 2 1 5 5 0.00150 0.020 0.0 0.00 1.0 -30.0 0.9 1.1 0.004  1.01  1.02 400e6
2 3 4 3 0 0.00075 0.010 0.0 0.00 1.0  30.0 0.9 1.1 0.002 -1.3  -1.4  800e6
3 0 2 4 0 0.00900 0.100 0.0 1.72 0.0   0.0 0.0 0.0 0.0    0.0   0.0  2008
4 0 2 5 0 0.00450 0.050 0.0 0.88 0.0   0.0 0.0 0.0 0.0    0.0   0.0  2008
5 0 4 5 0 0.00225 0.025 0.0 0.44 0.0   0.0 0.0 0.0 0.0    0.0   0.0  2008
];

#Parameters:
#   Bus Input Data:
        param F       =  100;
        param v1      =  1.00000000;
        param theta1  =  0.00000000;
        param pl2     = -8.00000000;
        param ql2     = -2.80000000;
        param bsh2    =  2.00000000;
        param p3      =  5.20000000;
        param vset3   =  1.05000000;
        param qlow3   = -2.80000000;
        param qupp3   =  4.00000000;
        param pl3     = -0.80000000;
        param ql3     = -0.40000000;
        param vset5   =  1.01500000;
        param qset3_4 =  -1.35000000;
#   Branch Input Data:
```

```
        param g1_5        =   3.72902424;
        param b1_5        =  -49.72032318;
        param b1_5_0      =   0.00000000;
        param fi1_5       =  -0.52359878;
        param t_step1_5   =   0.00400000;
        param g4_3        =   7.45804848;
        param b4_3        =  -99.44064636;
        param b4_3_0      =   0.00000000;
        param fi4_3       =   0.52359878;
        param t_step4_3   =   0.00200000;
        param g2_4        =   0.89276857;
        param b2_4        =  -9.91965083;
        param b2_4_0      =   0.86000000;
        param g2_5        =   1.78553715;
        param b2_5        =  -19.83930166;
        param b2_5_0      =   0.44000000;
        param g4_5        =   3.57107430;
        param b4_5        =  -39.67860331;
        param b4_5_0      =   0.22000000;
#Variables:
#   Bus Variables:
        var p1       >=   -500.0, <=  500.0;
        var q1       >=   -500.0, <=  500.0;
        var v2       >=      0.8, <=    1.2;
        var theta2   >=    -6.28, <=   6.28;
        var qsh2     >=   -500.0, <=  500.0;
        var q3       >=   -500.0, <=  500.0;
        var v3       >=      0.8, <=    1.2;
        var theta3   >=    -6.28, <=   6.28;
        var bl3      >=      0.0, <=    1.0,binary;
        var bu3      >=      0.0, <=    1.0,binary;
        var v4       >=      0.8, <=    1.2;
        var theta4   >=    -6.28, <=   6.28;
        var v5       >=      0.8, <=    1.2;
        var theta5   >=    -6.28, <=   6.28;
#   Branch Variables:
        var p1_5     >=   -500.0, <=  500.0;
        var q1_5     >=   -500.0, <=  500.0;
        var p5_1     >=   -500.0, <=  500.0;
        var q5_1     >=   -500.0, <=  500.0;
        var t1_5     >=      0.9, <=    1.1;
        var m1_5     >=      225, <=    275,integer;
        var p4_3     >=   -500.0, <=  500.0;
        var q4_3     >=   -500.0, <=  500.0;
        var p3_4     >=   -500.0, <=  500.0;
        var q3_4     >=   -500.0, <=  500.0;
        var t4_3     >=      0.9, <=    1.1;
        var m4_3     >=      450, <=    550,integer;
        var p2_4     >=   -500.0, <=  500.0;
        var q2_4     >=   -500.0, <=  500.0;
        var p4_2     >=   -500.0, <=  500.0;
        var q4_2     >=   -500.0, <=  500.0;
        var p2_5     >=   -500.0, <=  500.0;
        var q2_5     >=   -500.0, <=  500.0;
        var p5_2     >=   -500.0, <=  500.0;
        var q5_2     >=   -500.0, <=  500.0;
        var p4_5     >=   -500.0, <=  500.0;
        var q4_5     >=   -500.0, <=  500.0;
        var p5_4     >=   -500.0, <=  500.0;
        var q5_4     >=   -500.0, <=  500.0;
#   Other Variables:
        var Ploss    >=      0.0, <=   10.0;
        var Qloss    >=   -100.0, <=  100.0;
        var VQPerr   >= 0.00000001, <= 0.01;
#Objective Function:
    minimize obj:
        VQPerr;
#Equality and Inequality Constraints:
s.t.
#   Balance Equations:
c1: p1     = +p1_5;
c2: q1     = +q1_5;
c3: 0      = -pl2+p2_4+p2_5;
c4: 0      = -ql2-qsh2+q2_4+q2_5;
c5: p3     = -pl3+p3_4;
c6: q3     = -ql3+q3_4;
c7: 0      = +p4_3+p4_2+p4_5;
```

```
c8: 0      = +q4_3+q4_2+q4_5;
c9: 0      = +p5_1+p5_2+p5_4;
c10: 0     = +q5_1+q5_2+q5_4;
#   Shunt Power Flows:
c11: qsh2  =  bsh2*v2^2;
#   PV Buses:
c12: v3  <=  vset3+bl3*F;
c13: v3  >=  vset3-bu3*F;
c14: q3  <=  qupp3+bl3*(qlow3-qupp3);
c15: q3  >=  qlow3+bu3*(qupp3-qlow3);
c16: 1   >=  bl3+bu3;
#   Tap-Changing Transformers:
c17: t1_5 = m1_5*t_step1_5;
c18: t4_3 = m4_3*t_step4_3;
#   Branch Power Flows:
c19: p1_5    = g1_5*(v1/t1_5)^2-g1_5*v1*v5/t1_5*cos(theta1-theta5-fi1_5)-
                 b1_5*v1*v5/t1_5*sin(theta1-theta5-fi1_5);
c20: q1_5    = -(b1_5+b1_5_0)*(v1/t1_5)^2+b1_5*v1*v5/t1_5*cos(theta1-theta5-fi1_5)-
                 g1_5*v1*v5/t1_5*sin(theta1-theta5-fi1_5);
c21: p5_1    = g1_5*v5^2-g1_5*v1*v5/t1_5*cos(theta5-theta1+fi1_5)-
                 b1_5*v1*v5/t1_5*sin(theta5-theta1+fi1_5);
c22: q5_1    = -(b1_5+b1_5_0)*v5^2+b1_5*v1*v5/t1_5*cos(theta5-theta1+fi1_5)-
                 g1_5*v1*v5/t1_5*sin(theta5-theta1+fi1_5);
c23: p4_3    = g4_3*(v4/t4_3)^2-g4_3*v4*v3/t4_3*cos(theta4-theta3-fi4_3)-
                 b4_3*v4*v3/t4_3*sin(theta4-theta3-fi4_3);
c24: q4_3    = -(b4_3+b4_3_0)*(v4/t4_3)^2+b4_3*v4*v3/t4_3*cos(theta4-theta3-fi4_3)-
                 g4_3*v4*v3/t4_3*sin(theta4-theta3-fi4_3);
c25: p3_4    = g4_3*v3^2-g4_3*v4*v3/t4_3*cos(theta3-theta4+fi4_3)-
                 b4_3*v4*v3/t4_3*sin(theta3-theta4+fi4_3);
c26: q3_4    = -(b4_3+b4_3_0)*v3^2+b4_3*v4*v3/t4_3*cos(theta3-theta4+fi4_3)-
                 g4_3*v4*v3/t4_3*sin(theta3-theta4+fi4_3);
c27: p2_4    = g2_4*v2^2-g2_4*v2*v4*cos(theta2-theta4)-b2_4*v2*v4*sin(theta2-theta4);
c28: q2_4    = -(b2_4+b2_4_0)*v2^2+b2_4*v2*v4*cos(theta2-theta4)-g2_4*v2*v4*sin(theta2-
                 theta4);
c29: p4_2    = g2_4*v4^2-g2_4*v2*v4*cos(theta4-theta2)-b2_4*v2*v4*sin(theta4-theta2);
c30: q4_2    = -(b2_4+b2_4_0)*v4^2+b2_4*v2*v4*cos(theta4-theta2)-g2_4*v2*v4*sin(theta4-
                 theta2);
c31: p2_5    = g2_5*v2^2-g2_5*v2*v5*cos(theta2-theta5)-b2_5*v2*v5*sin(theta2-theta5);
c32: q2_5    = -(b2_5+b2_5_0)*v2^2+b2_5*v2*v5*cos(theta2-theta5)-g2_5*v2*v5*sin(theta2-
                 theta5);
c33: p5_2    = g2_5*v5^2-g2_5*v2*v5*cos(theta5-theta2)-b2_5*v2*v5*sin(theta5-theta2);
c34: q5_2    = -(b2_5+b2_5_0)*v5^2+b2_5*v2*v5*cos(theta5-theta2)-g2_5*v2*v5*sin(theta5-
                 theta2);
c35: p4_5    = g4_5*v4^2-g4_5*v4*v5*cos(theta4-theta5)-b4_5*v4*v5*sin(theta4-theta5);
c36: q4_5    = -(b4_5+b4_5_0)*v4^2+b4_5*v4*v5*cos(theta4-theta5)-g4_5*v4*v5*sin(theta4-
                 theta5);
c37: p5_4    = g4_5*v5^2-g4_5*v4*v5*cos(theta5-theta4)-b4_5*v4*v5*sin(theta5-theta4);
c38: q5_4    = -(b4_5+b4_5_0)*v5^2+b4_5*v4*v5*cos(theta5-theta4)-g4_5*v4*v5*sin(theta5-
                 theta4);
#   Total Power Losses:
c39: Ploss  = +p1+pl2+pl3+p3;
c40: Qloss  = +q1+ql2+qsh2+ql3+q3;
#   VQPerr-output:
c41: VQPerr  =  (v5-vset5)^2+(-q3_4-qset3_4)^2+0;
#End of Input Data
```

Appendix D: Input Data for the Voltage Stability Optimization

```
#Parameters:
#   Bus Input Data:
        param F      =  100;
        param v1     =  1.00000000;
        param theta1 =  0.00000000;
        param pl_in2 = -8.00000000;
        param ql_in2 = -2.80000000;
        param bsh2   =  2.00000000;
        param p_in3  =  5.20000000;
        param vset3  =  1.05000000;
        param qlow3  = -2.80000000;
        param qupp3  =  4.00000000;
        param pl_in3 = -0.80000000;
        param ql_in3 = -0.40000000;
#   Branch Input Data:
        param g5_1      =  3.72902424;
        param b5_1      = -49.72032318;
        param b5_1_0    =  0.00000000;
```

```
        param t5_1         =  1.00000000;
        param fi5_1        =  0.52359878;
        param g4_3         =  7.45804848;
        param b4_3         = -99.44064636;
        param b4_3_0       =  0.00000000;
        param t4_3         =  1.00000000;
        param fi4_3        =  0.52359878;
        param g2_4         =  0.89276857;
        param b2_4         = -9.91965083;
        param b2_4_0       =  0.86000000;
        param g2_5         =  1.78553715;
        param b2_5         = -19.83930166;
        param b2_5_0       =  0.44000000;
        param g4_5         =  3.57107430;
        param b4_5         = -39.67860331;
        param b4_5_0       =  0.22000000;
#Variables:
#    Bus Variables:
        var p1      >=   -500.0, <=  500.0;
        var q1      >=   -500.0, <=  500.0;
        var v2      >=      0.2, <=   1.5;
        var theta2 >=    -6.28, <=   6.28;
        var pl2     >=   -500.0,  <=  500.0;
        var ql2     >=   -500.0,  <=  500.0;
        var qsh2    >=   -500.0, <=  500.0;
        var q3      >=   -500.0, <= 500.0;
        var v3      >=      0.2, <=   1.5;
        var theta3 >=    -6.28, <=   6.28;
        var bl3     >=      0.0, <=   1.0,binary;
        var bu3     >=      0.0, <=   1.0,binary;
        var pl3     >=   -500.0,  <=  500.0;
        var ql3     >=   -500.0,  <=  500.0;
        var p3      >=   -500.0,  <= 500.0;
        var v4      >=      0.2, <=   1.5;
        var theta4 >=    -6.28, <=   6.28;
        var v5      >=      0.2, <=   1.5;
        var theta5 >=    -6.28, <=   6.28;
#    Branch Variables:
        var p5_1     >=   -500.0, <=  500.0;
        var q5_1     >=   -500.0, <=  500.0;
        var p1_5     >=   -500.0, <=  500.0;
        var q1_5     >=   -500.0, <=  500.0;
        var p4_3     >=   -500.0, <=  500.0;
        var q4_3     >=   -500.0, <=  500.0;
        var p3_4     >=   -500.0, <=  500.0;
        var q3_4     >=   -500.0, <=  500.0;
        var p2_4     >=   -500.0, <=  500.0;
        var q2_4     >=   -500.0, <=  500.0;
        var p4_2     >=   -500.0, <=  500.0;
        var q4_2     >=   -500.0, <=  500.0;
        var p2_5     >=   -500.0, <=  500.0;
        var q2_5     >=   -500.0, <=  500.0;
        var p5_2     >=   -500.0, <=  500.0;
        var q5_2     >=   -500.0, <=  500.0;
        var p4_5     >=   -500.0, <=  500.0;
        var q4_5     >=   -500.0, <=  500.0;
        var p5_4     >=   -500.0, <=  500.0;
        var q5_4     >=   -500.0, <=  500.0;
#    Other Variables:
        var lambda  >=      1.0, <= 200.0;
#Objective Function:
    maximize obj:
        lambda;
#Equality and Inequality Constraints:
s.t.
#    Balance Equations:
c1: p1     = +p1_5;
c2: q1     = +q1_5;
c3: 0      = -pl2+p2_4+p2_5;
c4: 0      = -ql2-qsh2+q2_4+q2_5;
c5: p3     = -pl3+p3_4;
c6: q3     = -ql3+q3_4;
c7: 0      = +p4_3+p4_2+p4_5;
c8: 0      = +q4_3+q4_2+q4_5;
c9: 0      = +p5_1+p5_2+p5_4;
c10: 0     = +q5_1+q5_2+q5_4;
#    Shunt Power Flows:
```

146

```
c11: qsh2  = bsh2*v2^2;
#   PV Buses:
c12: v3  <=  vset3+bl3*F;
c13: v3  >=  vset3-bu3*F;
c14: q3  <=  qupp3+bl3*(qlow3-qupp3);
c15: q3  >=  qlow3+bu3*(qupp3-qlow3);
c16: 1   >=  bl3+bu3;
#   Branch Power Flows:
c17: p5_1     = g5_1*(v5/t5_1)^2-g5_1*v5*v1/t5_1*cos(theta5-theta1-fi5_1)-
                b5_1*v5*v1/t5_1*sin(theta5-theta1-fi5_1);
c18: q5_1     = -(b5_1+b5_1_0)*(v5/t5_1)^2+b5_1*v5*v1/t5_1*cos(theta5-theta1-fi5_1)-
                g5_1*v5*v1/t5_1*sin(theta5-theta1-fi5_1);
c19: p1_5     = g5_1*v1^2-g5_1*v5*v1/t5_1*cos(theta1-theta5+fi5_1)-
                b5_1*v5*v1/t5_1*sin(theta1-theta5+fi5_1);
c20: q1_5     = -(b5_1+b5_1_0)*v1^2+b5_1*v5*v1/t5_1*cos(theta1-theta5+fi5_1)-
                g5_1*v5*v1/t5_1*sin(theta1-theta5+fi5_1);
c21: p4_3     = g4_3*(v4/t4_3)^2-g4_3*v4*v3/t4_3*cos(theta4-theta3-fi4_3)-
                b4_3*v4*v3/t4_3*sin(theta4-theta3-fi4_3);
c22: q4_3     = -(b4_3+b4_3_0)*(v4/t4_3)^2+b4_3*v4*v3/t4_3*cos(theta4-theta3-fi4_3)-
                g4_3*v4*v3/t4_3*sin(theta4-theta3-fi4_3);
c23: p3_4     = g4_3*v3^2-g4_3*v4*v3/t4_3*cos(theta3-theta4+fi4_3)-
                b4_3*v4*v3/t4_3*sin(theta3-theta4+fi4_3);
c24: q3_4     = -(b4_3+b4_3_0)*v3^2+b4_3*v4*v3/t4_3*cos(theta3-theta4+fi4_3)-
                g4_3*v4*v3/t4_3*sin(theta3-theta4+fi4_3);
c25: p2_4     = g2_4*v2^2-g2_4*v2*v4*cos(theta2-theta4)-b2_4*v2*v4*sin(theta2-theta4);
c26: q2_4     = -(b2_4+b2_4_0)*v2^2+b2_4*v2*v4*cos(theta2-theta4)-g2_4*v2*v4*sin(theta2-
                theta4);
c27: p4_2     = g2_4*v4^2-g2_4*v2*v4*cos(theta4-theta2)-b2_4*v2*v4*sin(theta4-theta2);
c28: q4_2     = -(b2_4+b2_4_0)*v4^2+b2_4*v2*v4*cos(theta4-theta2)-g2_4*v2*v4*sin(theta4-
                theta2);
c29: p2_5     = g2_5*v2^2-g2_5*v2*v5*cos(theta2-theta5)-b2_5*v2*v5*sin(theta2-theta5);
c30: q2_5     = -(b2_5+b2_5_0)*v2^2+b2_5*v2*v5*cos(theta2-theta5)-g2_5*v2*v5*sin(theta2-
                theta5);
c31: p5_2     = g2_5*v5^2-g2_5*v2*v5*cos(theta5-theta2)-b2_5*v2*v5*sin(theta5-theta2);
c32: q5_2     = -(b2_5+b2_5_0)*v5^2+b2_5*v2*v5*cos(theta5-theta2)-g2_5*v2*v5*sin(theta5-
                theta2);
c33: p4_5     = g4_5*v4^2-g4_5*v4*v5*cos(theta4-theta5)-b4_5*v4*v5*sin(theta4-theta5);
c34: q4_5     = -(b4_5+b4_5_0)*v4^2+b4_5*v4*v5*cos(theta4-theta5)-g4_5*v4*v5*sin(theta4-
                theta5);
c35: p5_4     = g4_5*v5^2-g4_5*v4*v5*cos(theta5-theta4)-b4_5*v4*v5*sin(theta5-theta4);
c36: q5_4     = -(b4_5+b4_5_0)*v5^2+b4_5*v4*v5*cos(theta5-theta4)-g4_5*v4*v5*sin(theta5-
                theta4);
#   VoltStab-output:
c37: pl2 = pl_in2*lambda;
c38: ql2 = ql_in2*lambda;
c39: pl3 = pl_in3*lambda;
c40: ql3 = ql_in3*lambda;
c41: p3  = p_in3*lambda;
#End of Input Data
```

Appendix E: List of Examined Test Power Systems

case	description	ref.
EPS3I	3-bus distribution system, CZE	[62]
EPS4I	4-bus distribution system, CZE	[62]
EPS4II	4-bus test power system (educational)	[3]
EPS5I	5-bus test power system, USA	[1]
EPS5II	5-bus test power system, USA	[48]
EPS5III	5-bus test power system (educational)	[3]
EPS6I	6-bus distribution network, CZE	[62]
EPS6II	6-bus (Ward-Hale) power system	[7]
EPS6III	6-bus test power system	[12]
EPS7I	7-bus test power system (Case study I.), USA	[1]
EPS7II	7-bus test power system (Case study II.), USA	[1]
IEEE9I	IEEE 9-bus power system, USA	[49]
EPS10I	10-bus test power system	[50]
EPS11I	11-bus (Reduced Mato Grosso) test case, BRA	[32]
EPS11II	11-bus test case	[4]
EPS11III	Klos-Kerner 11-bus test power system, light loading	[51]
EPS12I	12-bus Svenska Kraftnät - Sydkraft area test case, SWE, heavy loading	[61]
EPS13I	13-bus test ill-conditioned power system	[29]

IEEE13II	IEEE 13-bus test feeder, USA	[81]
IEEE14I	IEEE 14-bus test power system, USA, winter season 1962	[80]
EPS15I	15-bus load flow case	[15]
EPS16I	16-bus load flow case	[11]
EPS17I	17-bus (Reduced primary AC system for the South Island of New Zealand) test case, NZ	[8]
EPS19I	19-bus distribution system (Distribuce Plzeň - Jih), CZE	[62]
EPS23I	23-bus test power system	[52]
IEEE24I	IEEE 24-bus reliability test system	[70]
IEEE26I	IEEE 26-bus test power system	[2]
IEEE30I	IEEE 30-bus test power system, USA, winter season 1961	[80]
EPS34I	34-bus test local distribution system, ROM	[76]
IEEE35I	IEEE 35-bus test feeder, USA	[81]
EPS37I	IEEE 37-bus distribution system, USA	[24]
IEEE39I	IEEE 39-bus test power system (New England test system)	[9]
EPS43I	43-bus test ill-conditioned power system	[29]
EPS56I	56-bus simplified transmission system, CZE, estimated heavy loading	[75]
IEEE57I	IEEE 57-bus test power system, USA, winter season 1961	[80]
EPS59I	59-bus simpl. test case, AUS - case A: heavy load - G 23030 MW, L 22300 MW	[82]
EPS59II	59-bus simpl. test case, AUS - case B: medium-heavy load - G 21590 MW, L 21000 MW	[82]
EPS59III	59-bus simpl. test case, AUS - case C: peak load - G 25430 MW, L 24800 MW	[82]
EPS59IV	59-bus simpl. test case, AUS - case D: light load - G 15050 MW, L 14810 MW	[82]
EPS59V	59-bus simpl. test case, AUS - case E: medium load - G 19060 MW, L 18600 MW	[82]
EPS59VI	59-bus simpl. test case, AUS - case F: light load - G 14840 MW, L 14630 MW	[82]
EPS61I	61-bus test case, GBR - South England transmission system	[79]
EPS114I	114-bus test local distribution system, ROM	[76]
IEEE118I	IEEE 118-bus test power system, USA, winter season 1961	[80]
IEEE125I	IEEE 123-bus test feeder, USA	[81]
EPS128I	128-bus test local distribution system, CZE	[76]
EPS133I	133-bus test local distribution system, CZE	[76]
EPS137I	137-bus test local distribution system, ROM	[76]
IEEE145I	IEEE 145-bus test power system, USA, summer season 1990	[80]
IEEE162I	IEEE 162-bus test power system, USA, summer season 1990	[80]
EPS167I	167-bus test local distribution system, ROM	[76]
EPS246I	246-bus test local distribution system, ROM	[76]
EPS272I	272-bus test local distribution system, ROM	[76]
IEEE300I	IEEE 300-bus test power system, USA, summer season 1991	[80]
EPS304I	304-bus test local distribution system, ROM	[76]
EPS323I	323-bus test local distribution system, ROM	[76]
EPS361I	361-bus test local distribution system, GBR	[79]
EPS366I	366-bus test local distribution system, ROM	[76]
EPS392I	392-bus test local distribution system, ROM	[76]
EPS396I	396-bus test local distribution system, ROM	[76]
EPS535I	535-bus test local distribution system, ROM	[76]
EPS558I	558-bus test local distribution system, ROM	[76]
EPS629I	629-bus test case, GBR - Scotland area	[79]
EPS682I	682-bus test local distribution system, ROM	[76]
EPS706I	706-bus test local distribution system, ROM	[76]
EPS707I	707-bus test local distribution system, ROM	[76]
EPS734I	734-bus test case, GBR - Scotland+Wales area	[79]
EPS760I	760-bus test local distribution system, ROM	[76]
EPS791I	791-bus test local distribution system, ROM	[76]
EPS794I	794-bus test local distribution system, ROM	[76]
EPS2383I	2383-bus test case, POL, winter season peak 1999-00	[70]
EPS2736I	2736-bus test case, POL, summer season peak 2004	[70]
EPS2737I	2737-bus test case, POL, summer season off-peak 2004	[70]
EPS2746I	2746-bus test case, POL, winter season off-peak 2003-04	[70]
EPS2746II	2746-bus test case, POL, winter season evening peak 2003-04	[70]
EPS3012I	3012-bus test case, POL, winter season evening peak 2007-08	[70]
EPS3120I	3120-bus test case, POL, summer season morning peak 2008	[70]

18. List of Candidate's Publications Related to the Doctoral Thesis

Conferences:

[1] VELEBA, J., IRVING, M.R. Load Flow Analysis with Voltage and Reactive Power Optimization in Distribution Networks. In AMTEE'09. Pilsen: University of West Bohemia, 2009. pp. 1-7. ISBN: 978-80-7043-821-3.

[2] VELEBA, J., IRVING, M.R. Load Flow Analysis with Voltage and Reactive Power Optimization in Distribution Networks. In Elektrotechnika a informatika 2009. Část 3., Elektroenergetika. In Pilsen: University of West Bohemia, 2009. pp. 83-86. ISBN: 978-80-7043-811-4.

[3] VELEBA, J. Numerical Stability of the Newton-Raphson Method in Load Flow Analysis. In Electric Power Engineering 2010. Brno: University of Technology, 2010. pp. 87-92. ISBN: 978-80-214-4094-4.

[4] VELEBA, J. Stability Algorithms for Newton-Raphson Method in Load Flow Analysis. Pilsen, 2010. ISBN: 978-80-7043-893-0.

[5] VELEBA, J. Acceleration and stability techniques for conventional numerical methods in load flow analysis. In Proceedings of Conference ELEN 2010. Prague: ČVUT, 2010. pp. 1-10. ISBN: 978-80-254-8089-2.

[6] VELEBA, J., BUHAWA, Z. Basic Features of the National Transmission Power System of Libya. In Elektrotechnika a informatika 2010. Část 3., Elektroenergetika. Pilsen: University of West Bohemia, 2010. pp. 85-86. ISBN: 978-80-7043-915-9.

[7] VELEBA, J., NOHÁČOVÁ, L. Assessment of Electric Power System Operation in Terms of Steady-State Voltage Stability. In Proceedings of the 12th International Scientific Conference Electric Power Engineering 2011. Ostrava: VSB - Technical University of Ostrava, 2011. pp. 1-4. ISBN: 978-80-248-2393-5.

[8] VELEBA, J., MARTÍNEK, Z. Flicker Perceptibility Analysis for Photovoltaic Power Sources in Distribution Networks. In Proceedings of the 12th International Scientific Conference Electric Power Engineering 2011. Ostrava: VSB - Technical University of Ostrava, 2011. pp. 1-4. ISBN: 978-80-248-2393-5.

[9] VELEBA, J. Possible steady-state voltage stability analyses of electric power systems. In Proceedings of Intensive Programme "Renewable Energy Sources". Pilsen: Department of Electric Power Engineering and Environmental Engineering, Faculty of Electrical Engineering, University of West Bohemia, 2011. pp. 142-150. ISBN: 978-80-261-0010-2.

[10] VELEBA, J., BUHAWA, Z. Perspectives of large wind power plant installations to the national transmission power system of Libya. In Proceedings of Intensive Programme "Renewable Energy Sources". Pilsen: Department of Electric Power Engineering and Environmental Engineering, Faculty of Electrical Engineering, University of West Bohemia, 2011. pp. 87-94. ISBN: 978-80-261-0010-2.

[11] VELEBA, J. Modelling of LTC Transformers in the Load Flow Analysis by the Gauss-Seidel Method. In Elektrotechnika a informatika 2011 - část třetí - Elektroenergetika. Pilsen: University of West Bohemia, 2011. pp. 79-82. ISBN: 978-80-261-0017-1.

[12] KŘÍŽ, J., PISTORA, M., NOHÁČOVÁ, L., VELEBA, J. Possibilities of Black-Start with Using Renewable Sources Energy. In Proceedings of the 21th International Expert Meeting Power Engineering. Maribor, Slovinsko: Fakulteta za elektrotehniko, računalništvo in informatiko, Univerza Maribor, 2012. pp. 1-7. ISBN: 978-961-248-336-4.

[13] NOHÁČOVÁ, L., MERTLOVÁ, J., VELEBA, J. Nové možnosti pro optimalizaci chodu elektrizační soustavy. In Proceedings of the 13th International Scientific Conference – Electric Power Engineering 2012. Brno: Vysoké učení technické v Brně, 2012. pp. 205-210. ISBN: 978-80-214-4514-7.

[14] VELEBA, J., SÍŤAŘ, V. Possibilities of Voltage Control in Islanded Distribution Systems with Photovoltaic Power Sources. In Proceedings of the 13th International Scientific Conference - Electric Power Engineering 2012. Brno: Vysoké učení technické v Brně, 2012. pp. 727-732. ISBN: 978-80-214-4514-7.

[15] VELEBA, J. Voltage Control of Distribution Networks with Photovoltaic Power Sources. In Renewable Energy Sources 2012. Pilsen: University of West Bohemia, 2012. pp. 49-62. ISBN: 978-80-261-0130-7.

[16] VELEBA, J. Possibilities of Voltage Control in Islanded Distribution Systems with Photovoltaic Power Sources - Overvoltage Scenario. In Elektrotechnika a informatika 2012 - část třetí - Elektroenergetika. Pilsen: University of West Bohemia, 2012. pp. 55-58. ISBN: 978-80-261-0121-5.

[17] VELEBA, J., SÍŤAŘ, V., NOHÁČ, K. Application of Alternative Tools for Basic Load Flow Analysis. In Proceedings of the 14th International Scientific Conference Electric Power Engineering 2013. Ostrava: VSB - Technical University of Ostrava, 2013. pp. 1-6. ISBN: 978-80-248-2988-3.

Reviewed Journals:

[18] VELEBA, J. Application of continuation load flow analysis for voltage collapse prevention. Acta Technica ČSAV, 2012, Vol. 57, No. 2, pp. 143-163. ISSN: 0001-7043.

Book Chapters:

[19] Electrical Substations and Lines. BEN - technická literatura, Prague, 2010, 168 pages. ISBN: 978-80-7300-265-7.

[20] VOSTRACKÝ, Z., VELEBA, J. Distribution Power System of the Czech Republic. In Complex Behavior of the Distributed Generation System. Pitesti : Publishing House of the University of Pitesti, 2010, pp. 465-476. ISBN: 978-606-560-128-4.

[21] VELEBA, J. Theoretical and Practical Solution of Steady/Transient States of Electric Power Systems with Accent on Fault Modelling. Pilsen : University of West Bohemia, 2010, 87 pages. ISBN: -.

[22] VOSTRACKÝ, Z., TAPLAMACIOGLU, M., FATTAHI, F., PORUMB, R., TABATABAEI, N.M., VELEBA, J., KAYTEZ, F., ABBASI, H.S. Case Studies - Implementation Stage of the Distributed

Generation System. In Advances in Energy Research: Distributed Generations Systems Integrating Renewable Energy Resources. New York : Nova Science Publishers, Inc., 2011, pp. 613-665. ISBN: 978-1-61209-991-0.

[23] VELEBA, J., BUHAWA, Z. Perspectives of Large Wind Power Plant Installations to the National Transmission Power System of Libya. In Electric Power Engineering and Ecology - Selected Parts I. Prague : BEN - technická literatura, 2011, pp. 76-86. ISBN: 978-80-7300-417-0.

[24] VELEBA, J. Possible Steady-State Voltage Stability Analyses of Electric Power Systems. In Electric Power Engineering and Ecology - Selected Parts II. Prague : BEN - technická literatura, 2011, pp. 12-22. ISBN: 978-80-7300-418-7.

[25] VELEBA, J. Simulation of Voltage Control of Distribution Networks with Photovoltaic Power Plants. In Electric Power Engineering and Ecology - Selected Parts III. Prague : BEN - technická literatura, 2012, pp. 69-89. ISBN: 978-80-7300-460-6.

[26] VELEBA, J. Stability Algorithms for Newton-Raphson Method in Load Flow Analysis. In Electric Power Engineering and Ecology - Selected Parts IV. Prague : BEN - technická literatura, 2012, pp. 39-45. ISBN: 978-80-7300-461-3.

Research Reports:

[27] NOHÁČ, K., TESAŘOVÁ, M., NOHÁČOVÁ, L., VELEBA, J. TAČR - BIOZE průběžná zpráva za KEE 2011. Pilsen : 2011. 45 pages.

[28] VELEBA, J. Současné trendy modelování elektrizačních soustav. Pilsen : University of West Bohemia, 2012. 135 pages.

[29] VELEBA, J. Možnosti řešení optimalizačních úloh v prostředí NEOS Server for Optimization. Pilsen : University of West Bohemia, 2012. 39 pages.

Invited Lectures:

[30] VELEBA, J. Výpočty chodu sítě - teorie. ČEPS, Prague, 2010.

[31] VELEBA, J. Modelování a vyhodnocování napěťové stability elektrizačních soustav. EGÚ, Prague, 2012.